Itek 73-8220-3
FINAL REPORT
17 APRIL 1973

PHOTOHELIOGRAPH THERMAL CONCEPTS STUDY

VOLUME II

DETAILED ANALYSIS

Prepared for
NATIONAL AERONAUTICS AND SPACE ADMINISTRATION
MARSHALL SPACE FLIGHT CENTER
ALABAMA 35812

Under contract NAS8-28520

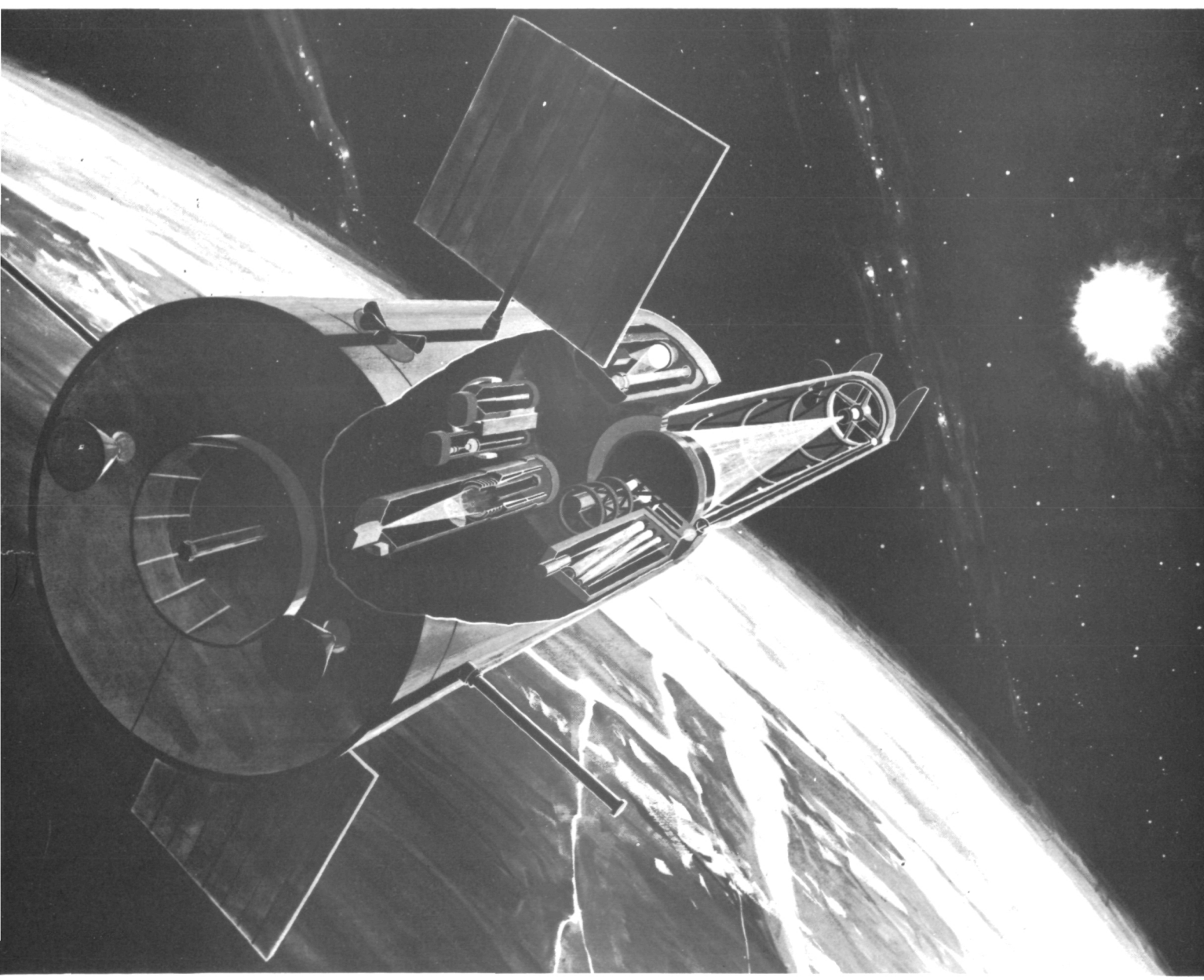

Itek 73-8220-3
FINAL REPORT
17 APRIL 1973

PHOTOHELIOGRAPH THERMAL CONCEPTS STUDY

VOLUME II
DETAILED ANALYSIS

Prepared for
NATIONAL AERONAUTICS AND SPACE ADMINISTRATION
MARSHALL SPACE FLIGHT CENTER
ALABAMA 35812

Under contract NAS8-28520

Itek
Optical Systems Division
10 MAGUIRE ROAD, LEXINGTON, MASSACHUSETTS 02173

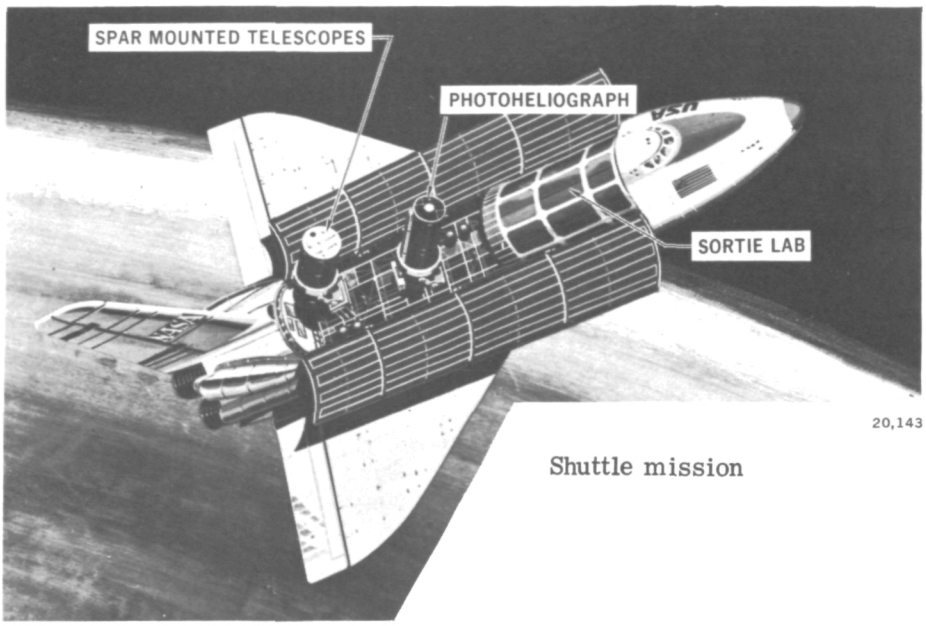

20,143

Shuttle mission

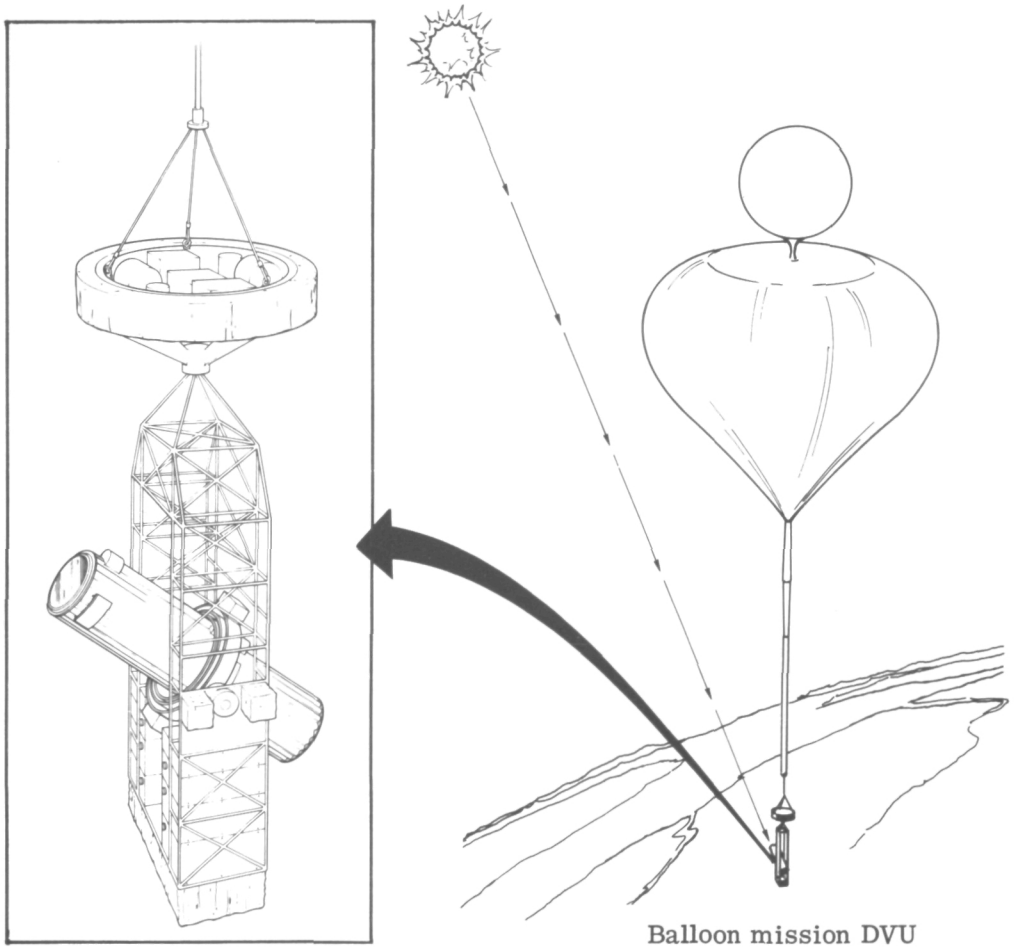

Balloon mission DVU

100-centimeter photoheliographs

PAGE MISSING FROM AVAILABLE VERSION

Pages III + IV

CONTENTS

1. Introduction 1-1

2. 150-Centimeter Photoheliograph for LSO 2-1
   2.1 Background 2-1
   2.2 Baseline Definition Study Summary 2-1
   2.3 Solid Mirror Concept 2-2
   2.4 Insulated Meteoroid Shell 2-2
   2.5 150-Centimeter Analysis Conclusions 2-3

3. 100-Centimeter Photoheliograph for Shuttle Missions 3-1
   3.1 Background 3-1
   3.2 Baseline Thermal Control Concept 3-5
   3.3 Primary Mirror Cooling Analysis 3-9
   3.4 Heat Shield Mirror Cooling Analysis 3-18
   3.5 Secondary Metering Structure 3-22
   3.6 Instrument Structure 3-39
   3.7 Camera Cooling and Control 3-40
   3.8 Thermal Switching Concepts Survey 3-51
   3.9 Selected Baseline 3-57

4. 100-Centimeter Photoheliograph for Balloon Missions 4-1
   4.1 Background 4-1
   4.2 Baseline Thermal Control Concept 4-3
   4.3 Telescope Thermal Control Concepts 4-9
   4.4 Preliminary Telescope Concept Analysis 4-12
   4.5 Detailed Concept Evaluation Analysis 4-14
   4.6 Baseline Concept 4-15

5. Photoheliograph Test Plans 5-1
   5.1 Test Concepts 5-1
   5.2 Breadboard Tests 5-2
   5.3 Subsystem Tests 5-18
   5.4 System Thermal Test 5-23

6. Suggested Additional Effort 6-1
   6.1 100-Centimeter Balloon Program Analysis 6-1
   6.2 Breadboard Testing 6-1

FIGURES

2-1 150-Centimeter Primary Mirror Thermal Model 2-5
2-2 System Thermal Model 2-6
2-3 Photoheliograph Orbits 2-7
2-4 Thermal Resistance Map of Secondary Mirror Subsystem for Sun-Synchronous Orbit 2-9
2-5 Thermal Control System 2-11
2-6 Temperature History for Heat Shield Mirror—Solid Primary, Sun-Synchronous Orbit 2-13
2-7 Temperature History for First Flat—Solid Primary, Sun-Synchronous Orbit . . 2-13
2-8 Temperature History for Second Flat and Secondary Mirror—Solid Primary, Sun-Synchronous Orbit 2-14
2-9 Temperature History for Primary Mirror Face—Solid Primary, Occulted Orbit . 2-14
2-10 Temperature History for Heat Shield Mirror—Solid Primary, Occulted Orbit . . 2-15
2-11 Temperature History for Primary Mirror Face—Cored Primary, Occulted Orbit, Insulated Meteoroid Shell 2-15
2-12 Temperature History for Truss—Cored Primary, Sun-Synchronous Orbit, Uninsulated Meteoroid Shell 2-17
2-13 Temperature History for Truss—Cored Primary, Occulted Orbit, Insulated Meteoroid Shell 2-17
2-14 Truss Temperature Change as a Function of Orbital Time 2-18
3-1 100-Centimeter Photoheliograph in Shuttle 3-2
3-2 Shuttle Cargo Bay Model 3-2
3-3 Gimbal Mounting Assembly Concept 3-3
3-4 Telescope Barrel Model 3-3
3-5 Connection of Mounting Ring to Shuttle Floor 3-6
3-6 Thermal Control Concept 3-7
3-7 Temperature History for Primary Mirror Center Axial Gradient 3-11
3-8 Temperature History for Primary Mirror Middle Axial Gradient 3-11
3-9 Temperature History for Primary Mirror Outer Axial Gradient 3-11
3-10 Radiator Size Versus Temperature 3-12
3-11 Solid Conductor Cold Plate Gradient Analysis 3-14
3-12 Solid Conductor Cooling System Concept 3-14
3-13 Cooling Loop Concept 3-16
3-14 Primary Mirror Cold Plate Fluid Loop Piping Diagram 3-17
3-15 Heat Shield Mirror Heat Pipe Cooling Concept 3-19
3-16 Temperature History for Heat Shield Mirror and First Relay Mirror—Uninsulated 3-20
3-17 Temperature History for Heat Shield Mirror and First Relay Mirror—Insulated . 3-20
3-18 Heat Shield Mirror Fluid Loop Cooling System 3-21

3-19 Heat Shield Mirror Fin Cooling Concept 3-23
3-20 Simplified Thermal Network Radiative Fin Concept 3-24
3-21 Temperature History for Heat Shield Mirror 3-25
3-22 Temperature History for First Relay Mirror 3-25
3-23 Temperature History for Truss Forward Circumferential Gradient—Uninsulated . 3-27
3-24 Temperature History for Truss Center Circumferential Gradient—Uninsulated. . 3-27
3-25 Temperature History for Truss Rear Circumferential Gradient—Uninsulated . . 3-28
3-26 Temperature History for Truss Top Axial Gradient—Uninsulated 3-28
3-27 Temperature History for Truss Middle Axial Gradient—Uninsulated 3-29
3-28 Temperature History for Truss Bottom Axial Gradient—Uninsulated 3-29
3-29 Temperature History for Truss Forward Circumferential Gradient—Insulated . . 3-30
3-30 Temperature History for Truss Center Circumferential Gradient—Insulated . . 3-30
3-31 Temperature History for Truss Rear Circumferential Gradient—Insulated . . . 3-31
3-32 Temperature History for Truss Top Axial Gradient—Insulated 3-31
3-33 Temperature History for Truss Middle Axial Gradient—Insulated 3-32
3-34 Temperature History for Truss Bottom Axial Gradient—Insulated 3-32
3-35 Temperature History for Truss Forward Circumferential Gradient—Uninsulated . 3-33
3-36 Temperature History for Truss Center Circumferential Gradient—Uninsulated. . 3-33
3-37 Temperature History for Truss Rear Circumferential Gradient—Uninsulated . . 3-34
3-38 Temperature History for Truss Top Axial Gradient—Uninsulated 3-34
3-39 Temperature History for Truss Middle Axial Gradient—Uninsulated 3-35
3-40 Temperature History for Truss Bottom Axial Gradient—Uninsulated 3-35
3-41 Temperature History for Truss Forward Circumferential Gradient—Insulated . . 3-36
3-42 Temperature History for Truss Center Circumferential Gradient—Insulated . . 3-36
3-43 Temperature History for Truss Rear Circumferential Gradient—Insulated . . . 3-37
3-44 Temperature History for Truss Top Axial Gradient—Insulated 3-37
3-45 Temperature History for Truss Middle Axial Gradient—Insulated 3-38
3-46 Temperature History for Truss Bottom Axial Gradient—Insulated 3-38
3-47 Instrument Compartment Layout 3-42
3-48 Steady-State Temperature Distribution 3-42
3-49 Instrument Structure Nodal Identification 3-42
3-50 Temperature History for Instrument Compartment—Uninsulated 3-43
3-51 Temperature History for Instrument Compartment—Uninsulated 3-43
3-52 Temperature History for Instrument Compartment—Uninsulated 3-44
3-53 Temperature History for Instrument Compartment—Uninsulated 3-44
3-54 Mounting Configuration 3-45
3-55 Temperature History for Instrument Compartment Wall 3-49
3-56 Thermoelectric Cooling Design. 3-49
3-57 Solid Conductor Cooling Design. 3-50
3-58 Camera Thermal Model Network 3-52
4-1 Air Temperature History 4-2
4-2 Heat Transfer Coefficient Versus Time After Launch Based on a Constant Ascent of 0.304 Kilometer Per Minute 4-2
4-3 System Concept for Avoiding Pluming. 4-5
4-4 100-Centimeter Photoheliograph Balloon Model 4-6
4-5 100-Centimeter Photoheliograph Balloon Model 4-6
4-6 Thermal Control Concept. 4-7
4-7 Phase Change Material Packaging Concept 4-10
4-8 Available Volume for Phase Change Material 4-11
4-9 Temperature History for Window and Earth Shade 4-17
4-10 Temperature History for Outer Shell and Metering Structure 4-17
4-11 Temperature History for Outer Shell and Metering Structure—High ϵ Structure. . 4-18

4-12 Temperature History for Window and Earth Shade—High ϵ Structure 4-18
4-13 Temperature History for Primary Mirror—High ϵ Structure 4-19
4-14 Temperature History for Secondary, Heat Shield, and First Relay Mirrors—High ϵ Structure 4-19
4-15 Temperature History for Outer Shell and Metering Structure—Low ϵ Structure . . 4-20
4-16 Temperature History for Crash Pad, Gondola, and Gimbal—Low ϵ Structure . . 4-20
4-17 Gondola Node Identification 4-21
4-18 System Model Modifications 4-22
4-19 Temperature History for Primary Mirror—Launch Transient 4-23
4-20 Temperature History for Primary Mirror—Launch Transient 4-23
4-21 Temperature History for Primary Mirror—Launch Transient 4-24
4-22 Temperature History for Primary Mirror—Launch Transient 4-24
4-23 Temperature History for Primary, Heat Shield, and First Relay Mirrors—Launch Transient 4-25
4-24 Temperature History for Truss Structure Primary Bay—Launch Transient . . . 4-25
4-25 Temperature History for Truss Structure Secondary Bay—Launch Transient . . 4-26
4-26 Temperature History for Outer Shell—Launch Transient 4-26
4-27 Temperature History for Window—Launch Transient 4-27
4-28 Temperature History for Window—Launch Transient 4-27
4-29 Temperature History for Earth Shade—Launch Transient 4-28
4-30 Temperature History for Gondola—Launch Transient 4-28
4-31 Temperature History for Primary Mirror—Flight Transient 4-29
4-32 Temperature History for Primary Mirror—Flight Transient 4-29
4-33 Temperature History for Primary Mirror—Flight Transient 4-30
4-34 Temperature History for Primary Mirror—Flight Transient 4-30
4-35 Temperature History for Primary, Heat Shield, and First Relay Mirrors—Flight Transient 4-31
4-36 Temperature History for Truss Structure Primary Bay—Flight Transient . . . 4-31
4-37 Temperature History for Truss Structure Secondary Bay—Flight Transient . . . 4-32
4-38 Temperature History for Outer Shell—Flight Transient 4-32
4-39 Temperature History for Window—Flight Transient 4-33
4-40 Temperature History for Window—Flight Transient 4-33
4-41 Temperature History for Earth Shade—Flight Transient 4-34
4-42 Temperature History for Gondola—Flight Transient 4-34
5-1 Primary Mirror Specular Core Breadboard Test 5-3
5-2 Vidicon Camera Cooling Breadboard Test 5-5
5-3 Primary Mirror Heat Rejection System Breadboard Test 5-8
5-4 Heat Shield Mirror Heat Rejection System Breadboard Test 5-11
5-5 Phase Change Material Breadboard Test. 5-14
5-6 Thermal Pluming Breadboard Test 5-16
5-7 Instrument Structure Subsystem Test 5-19
5-8 Photoheliograph System Thermal Test 5-24
5-9 Photoheliograph System Thermal Test Setup 5-25
6-1 Thermal Test System 6-3
6-2 Thermal Pluming Test Facility 6-4

TABLES

2-1	Baseline Thermal Control Requirements	2-4
2-2	Baseline Thermal Control Concepts	2-4
2-3	Subsystem Thermal Loads	2-8
2-4	Summary of Requirements and Initial Results	2-9
2-5	Thermal Control Power Requirements	2-10
2-6	150-Centimeter LSO Baseline Thermal Control Concept	2-10
2-7	Primary Mirror Concept Evaluation	2-10
2-8	Solid Mirror Evaluation—Insulated Meteoroid Shield	2-16
2-9	Average Heater Power	2-16
3-1	Optical System Thermal Loads	3-4
3-2	Estimated Power Dissipation	3-4
3-3	Primary Mirror Temperature Results	3-10
3-4	Properties of FC-78 Coolant	3-16
3-5	Primary Mirror Fluid Loop Cooling System Analysis Results	3-17
3-6	Heat Shield Mirror Fluid Loop Cooling System Analysis Results	3-23
3-7	Shuttle Model Temperature Results	3-26
3-8	Truss Average Temperature Swings and Primary to Secondary Mirror Spacing Change for Half-Orbit	3-41
3-9	Meteoroid Shield/Metering Truss Concept Power Dissipation	3-41
3-10	Instrument Structure Temperature Distribution	3-41
3-11	Instrument Structure Study Motion Analysis for High ϵ Uninsulated Structure	3-45
3-12	21.1 °C Camera Thermal Control Fluid Loop	3-47
3-13	Structural Temperature Distribution	3-53
3-14	100-Centimeter Shuttle Photoheliograph Recommended Baseline	3-57
4-1	Concept Evaluation	4-4
4-2	Proposed Phase Change Materials	4-10
4-3	Balloon Thermal Model Nodal Identification	4-13
4-4	100-Centimeter Photoheliograph Balloon Mission Recommended Baseline	4-16

1 INTRODUCTION

The purpose of this volume is to report on the design details of the Photoheliograph Thermal Concepts Study performed by Itek Corporation for Marshall Space Flight Center under Contract NAS8-28520. Volume I is a summary of the findings reported here.

To begin this report without confusion, we define what we mean by "photoheliograph." A photoheliograph is an instrument system whose purpose is to observe the sun at high resolution in the spectral range from approximately 1100 to 11,000 Å. Basically, it comprises near-diffraction-limited, normal incidence, reflective optics and has a variety of high resolution instruments at the focal plane, including imagery sensors, spectrographs, spectroheliographs, and magnetographs. In addition, it contains subsystems for thermal control, line of sight stabilization, alignment, and electronics, as required for each mission.

The main objective of the Photoheliograph Thermal Concepts Study was to define and compare the performance of thermal subsystem concepts for each of three photoheliograph designs oriented toward unique solar observation missions. These designs and missions may be categorized as:

1. A 150-centimeter photoheliograph for Large Solar Observatory (LSO) missions. This design is intended for multi-year orbital operations as a part of a complement of solar telescopes in a free-flying LSO configuration.
2. A 100-centimeter photoheliograph for Shuttle sorties. This design is intended for observation periods of up to 2 weeks while mounted in the cargo bay of the Shuttle Orbiter vehicle.
3. A 100-centimeter photoheliograph for balloon missions. This design is intended to be a design verification unit (DVU) and precursor to the orbital flight designs. Mission duration is on the order of a single day at an altitude of approximately 24.4 kilometers.

For each of these photoheliograph designs we defined the basic thermal environments, boundary conditions, and applicable thermal control concepts, determined the interactions between concepts and environments; and selected a baseline thermal control concept for the three classes of photoheliographs described here.

A second objective of the Photoheliograph Thermal Concepts Study was the definition of a set of experimental work plans describing the major efforts required to further the detailed design and to confirm analytical performance predictions.

This study is closely related to the recently completed Photoheliograph Definition Study performed by Itek for Marshall Space Flight Center under Contract NAS8-28147. In particular, the definition study furnished the basic configurations of the photoheliograph designs analyzed in this thermal concepts study and most of the data required for the establishment of performance requirements and system operating limitations. The definition study also served to establish the LSO thermal concept baseline, including the lightweight, specular core primary mirror.

The technical approach followed in this study was a straightforward method of defining mission objectives and anticipated boundary conditions at the system level. The system was then analyzed and subsystem concepts were developed. Tradeoff studies of subsystem concepts were conducted, leading to the synthesis of a thermal control system baseline design. The rationale for the baseline system selection and acceptable alternatives is presented.

The analytical efforts were conducted using both hand analysis of selected subsystem concepts and computer models of the entire photoheliograph system as required for particular studies.

In Section 2 of this volume, we report on our studies of the 150-centimeter photoheliograph for the LSO. Results from both the efforts under NAS8-28147 (Photoheliograph Definition Study) and work performed under this contract are discussed.

In Section 3, we report on our studies of the 100-centimeter photoheliograph for Shuttle sorties. These studies resulted in the development of an appropriate thermal baseline that incorporates not only the results of studies of the primary mirror cooling system and main optics support structure, but also defines the scientific instrument structural response as well as the preferred approaches to thermal control of the various on-board sensor systems. Also presented are the results of a thermal switch concepts survey applicable to active control of the Shuttle and LSO photoheliograph designs.

In Section 4, we report on our studies of the 100-centimeter balloon-borne DVU. We discuss the thermal control baseline that has been synthesized from a consideration of the unique characteristics of the balloon mission. Particular emphasis has been placed on the atmospheric phenomena that affect photoheliograph performance, and methods for the reduction or elimination of these effects have been investigated. Some potential mission constraints have been uncovered, and areas requiring further study have been identified.

In Section 5, we discuss a logical series of test plans, leading from breadboard tests to verify system thermal control concepts, through subsystem testing of flight configuration hardware to confirm performance predictions, and culminating in a system thermal test to confirm "as-built" performance. Each test plan is treated as a separate entity with its own requirements, test equipment, concept tradeoffs, and preliminary costing estimate.

In Section 6, we set forth our recommendations for further work in this area.

2. 150-CENTIMETER PHOTOHELIOGRAPH FOR LSO

2.1 BACKGROUND

A significant part of the thermal concept studies for the 150-centimeter LSO photoheliograph were performed under Contract NAS8-28147 (Photoheliograph Definition Study) prior to the award of the Photoheliograph Thermal Concepts Study. These results are briefly summarized below, however, the interested reader is referred to the final report of that program* for a complete discussion of the 150-centimeter photoheliograph baseline studies.

As a result of this prior study, the 150-centimeter photoheliograph analysis constituted a wrapup effort only, directed toward the examination of primary mirror concepts and support structure insulation response. These studies are reported in Sections 2.3 and 2.4, respectively.

2.2 BASELINE DEFINITION STUDY SUMMARY

As one of the initial steps in the thermal control concept definition, the requirements for thermal control on a subsystem level were identified. These baseline requirements guided the interim study effort and serve as a goal for the analytical task. These baseline requirements are presented in Table 2-1. Initial conceptual considerations conducted under Contract NAS8-28147 also led to a preliminary thermal control baseline as indicated in Table 2-2.

The determination of baseline thermal control performance is based on a system thermal model, shown in Figs. 2-1 and 2-2. This model in its basic form consists of approximately 300 nodes with more than 2,500 radiation and 800 conduction connections. Computer simulation of both quasi-steady-state (representing orbital average thermal conditions) and orbital transients was performed. During the initial phases of the program, both a 30-degree inclination occulted orbit and a sun-synchronous orbit were investigated. Fig. 2-3 depicts the orbits.

The other significant environmental parameter input is the incident and absorbed solar loading. Table 2-3 presents the thermal loads calculated for the sun-synchronous orbit described above.

Results of the initial thermal analyses and investigations included the effects of steady-state and orbital transients, the effects of the launch transient, the effects of maintenance shutdown, and the effects of mirror degradation (increase in solar absorbtance). The results of the initial orbital transient studies and their relationship to the baseline requirements are indicated in Table 2-4.

The preliminary conclusions of the 150-centimeter study indicated that the baseline system was operating within the requirements except for the secondary mirror and relay flats, which

---

* Photoheliograph Definition Study, Volume II, Book I, 150-Centimeter Photoheliograph for LSO Mission, Itek Report 73-8212-3 (8 Jan 1973).

were running well below the baseline temperature of 21.1 ± 11 °C (70 ± 20 °F). Analysis of the heat maps and resistance connections show that the connections of the mirror to the cold surroundings are sufficient to keep the mirror temperatures well below the 21.1 ± 11 °C baseline. Therefore, the heat pipes and corresponding cold plates for the above mentioned subsystems were removed, and thermostatically controlled heaters were added to the back of each mirror. The control temperature was set at 21.1 ± 1.1 °C. Fig. 2-4 presents a thermal resistance map of the secondary mirror subsystem in its final configuration, including the added heaters.

The revised baseline model was run in the sun-synchronous and occulted orbits. The computer output from each run confirmed that all subsystems meet the baseline requirements. The average power required to maintain the set-point temperature is shown in Table 2-5.

As part of the revised thermal control, heaters were added to the primary mirror flexure mounts. The mounts were controlled to the same temperature as a local primary mirror faceplate node.

The updated thermal control baseline may be most clearly understood by referring to Fig. 2-5, which is a layout of the entire photoheliograph with the appropriate subsystem elements noted. Item 1 is the lightweight, specular core, primary mirror, which is back cooled by the cold plate/heat pipe (item 2), which rejects the absorbed solar load through the space radiator (item 3). The main support ring (item 4), which establishes the optical reference surface, is held at 21.1 ± 1.1 °C by means of thermostatically controlled heaters. Likewise, the secondary mirror (item 5) and the relay flats (items 6 and 7) are also thermostatically controlled at this temperature. The secondary metering structure is indirectly controlled by the low α/ϵ thermal control finish applied to the external meteoroid shield (item 8). Thermal control of the aluminum heat shield mirror (item 9) is maintained by a direct coupling to a heat pipe/space radiator (items 10 and 11). Table 2-6 summarizes this baseline.

2.3 SOLID MIRROR CONCEPT

As part of the photoheliograph study, a solid ULE mirror was investigated. An 81-node thermal model was made of the 23.6-centimeter-thick mirror. This model was substituted for the baseline mirror model (specular core, lightweight), and the overall system model was computer analyzed in each of the baseline orbits. The thermal control system for the primary mirror was not altered for the solid mirror runs. The temperature gradients, levels, and wavefront errors of the solid and lightweight mirrors are compared in Table 2-7.

The solid mirror runs show that, thermally, there is little difference between the solid and lightweight mirrors. The radial temperature gradients are the same, and the axial gradients differ by only 1.7 °C. The face of the solid mirror runs about 2.8 °C warmer than the lightweight mirror. In order to have equivalent faceplate temperatures, the cold plate temperature for the solid mirror system must be about 2.8 C lower than the cold plate temperature for the lightweight mirror system.

In both cases, the primary mirror wavefront error is within the allowable system error allocation. The large change in error reflects the fact that the solid mirror is much thinner than the specular core mirror and thus more susceptible to thermal bending for identical gradients.

Figs. 2-6 through 2-10 represent typical computer plotted temperature transients for both the sun-synchronous and occulted orbit cases investigated.

2.4 INSULATED METEOROID SHELL

The effect of insulating the photoheliograph meteoroid shell to reduce the structural thermal response characteristics was investigated. The system thermal model was revised to account for multilayer insulation (MLI) between the truss elements and the inner surface of the meteoroid

shell. Since the primary mirror is poorly coupled to the shell through a low emittance finish, the response of the primary was minimal to this change. The overall increase in primary mirror faceplate temperature was 5 °C. This response is shown in Fig. 2-11, which represents a cored mirror in the occulted orbit, and may be compared to Fig. 2-9 for the uninsulated shell. Table 2-8 shows the response of the solid mirror and may also be compared to prior results (see Table 2-7). The significant parameter is the resultant wavefront error, which is within the allowable system error.

The temperature level of the truss structure and the heater power consumed on the main mounting ring were substantially affected by the addition of insulation. The temperature level of the truss structure increased between 15.5 and 32 °C over the entire length. The increase in temperature decreased the ΔT between the main mounting ring and truss structure, resulting in a 50 percent decrease in ring heater power.

Figs. 2-12 and 2-13 represent structural temperature response for the uninsulated and insulated cases, respectively. The reduction in thermal response is more graphically illustrated by Fig. 2-14, which presents normalized orbital temperature changes for both insulated and uninsulated truss nodes.

The thermal power requirements of the insulated and the uninsulated truss systems are given in Table 2-9. As expected, the use of insulation reduces the thermal control power to approximately 50 percent of its previous values. The slight increase in mount thermal control power is the result of the higher ambient temperature of the primary mirror (which the mount tracks).

2.5 150-CENTIMETER ANALYSIS CONCLUSIONS

The results of the analysis indicate the following:

1. The solid mirror concept is acceptable as an alternative to the specular core, lightweight, monolithic design. There is some sacrifice in system performance, but the design as analyzed does meet the thermal error allocations.
2. Insulating the internal surface of the meteoroid shell raises the structural temperature levels significantly (~15.5 to 32 °C) and reduces the normal orbital transient response. Overheating of the primary mirror may present a thermal problem if this concept is pursued.
3. Only the primary mirror and the heat shield mirror require supplementary cooling. The relay flats and the secondary mirror are currently cold biased and require supplementary heating during operation.
4. Degradation of the primary mirror and heat shield mirror reflective coatings by increase in solar absorbtivity result in overheating of the respective mirrors. This phenomenon requires further study both to assess the magnitude of the change in absorbtivity and to determine the final approach toward thermal control to compensate for the increased solar loadings resulting from the degradation.
5. The maintenance operation results in rapid cooldown of the primary and heat shield mirrors when the solar loading is off. Since large temperature changes are clearly undesirable, a method of thermal control that prevents the transfer of heat during maintenance periods is required.

Table 2-1 — Baseline Thermal Control Requirements

Subsystem	Requirements
Primary mirror	0.025λ rms, 3 μm defocus
Secondary mirror and mechanisms	0.005λ rms, 21.1 ± 11 °C (tentative)
Secondary metering structure	0.014λ rms, 15 μm decenter, 3.2 μm defocus, 2-minute observation
Primary mirror mounts	±1.1 °C of local mirror temperature, 0.005λ rms
Heat shield mirror	21.1 ± 11 °C (tentative)
Relay flats	0.005λ rms, 21.1 ± 11 °C (tentative)
Instrument structure	Stability 3.05 μm (2 minutes)

Table 2-2 — Baseline Thermal Control Concepts

Primary mirror	Monolith with high reflectance, specular core, partially open back, cooled from back by cold plate
	Cold plate connected to radiator by heat pipe
Primary mirror mount	Main ring heated 21.1 ± 1 °C
Secondary mirror	Solid mirror, cooled from back by cold plate
	Cold plate connected to radiator by heat pipe
Secondary metering structure	Low α/ϵ meteoroid shield
Heat shield mirror	Solid metal mirror conductively cooled by heat pipe connected to external radiator
Relay flats	Solid mirror same as secondary
Instrument structure	Not addressed

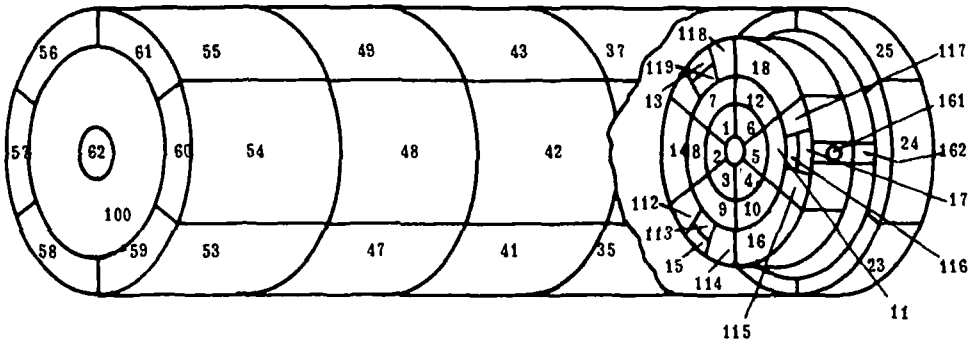

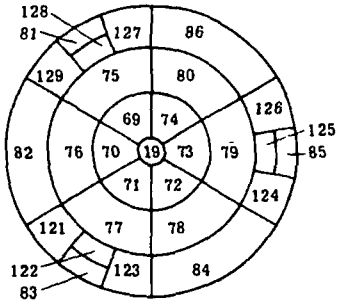

Core

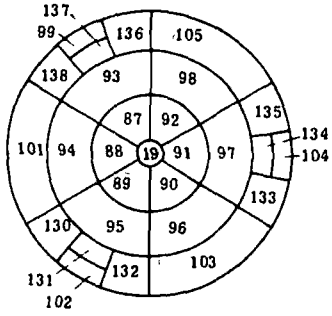

Backplate

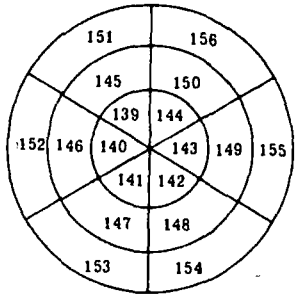

Cold plate

Fig. 2-1 — 150-centimeter primary mirror thermal model

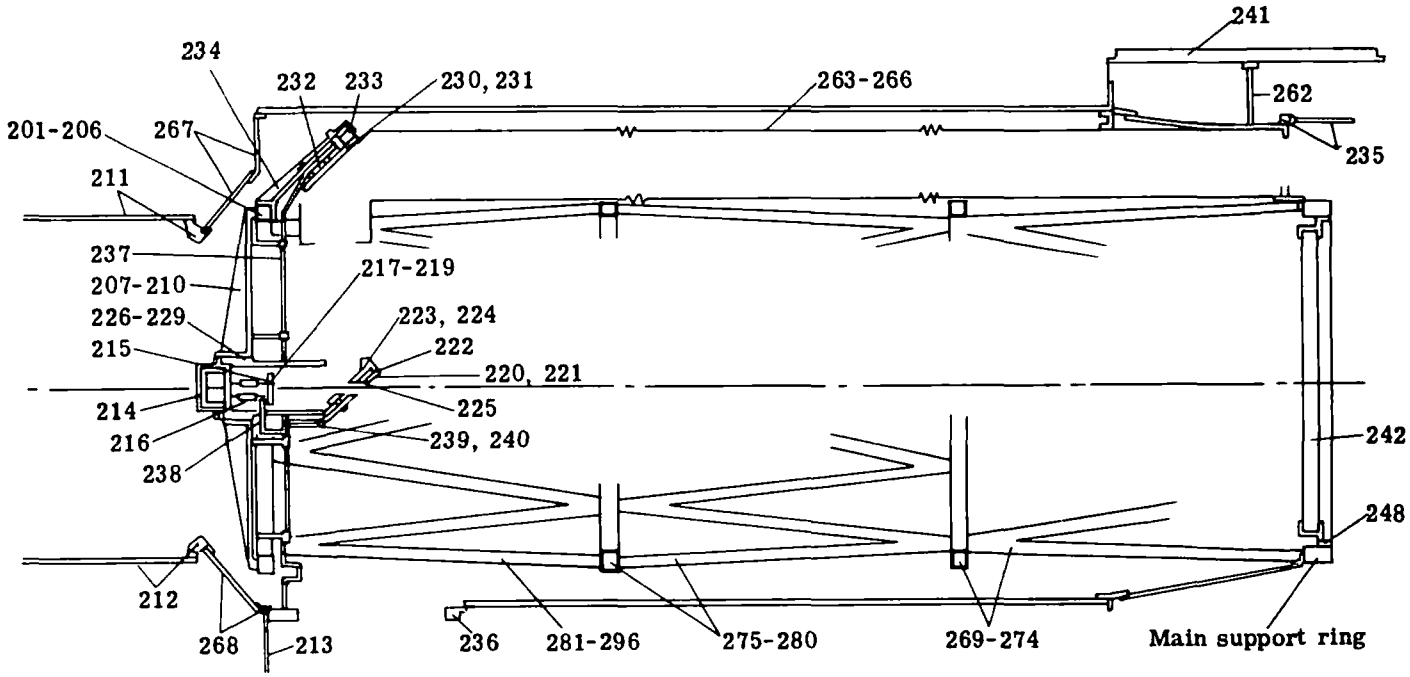

(a) Telescope section

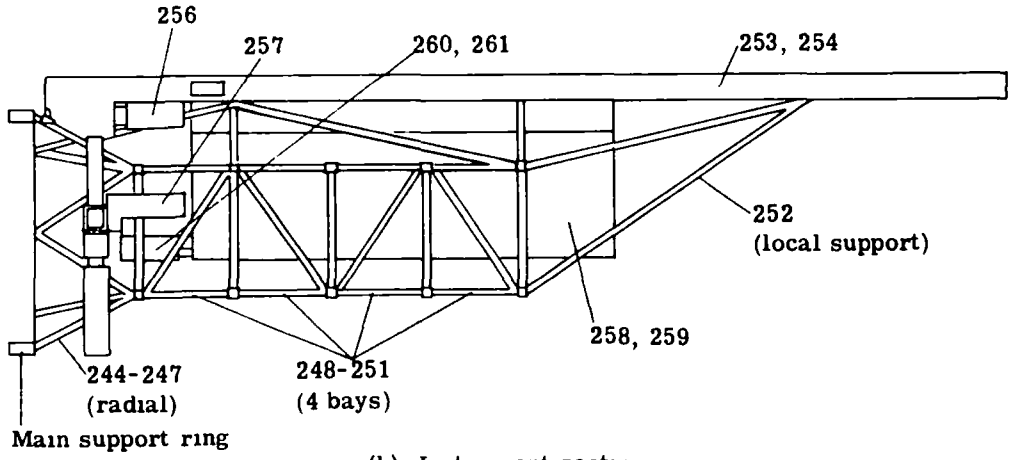

(b) Instrument section

Fig. 2-2 — System thermal model (partial)

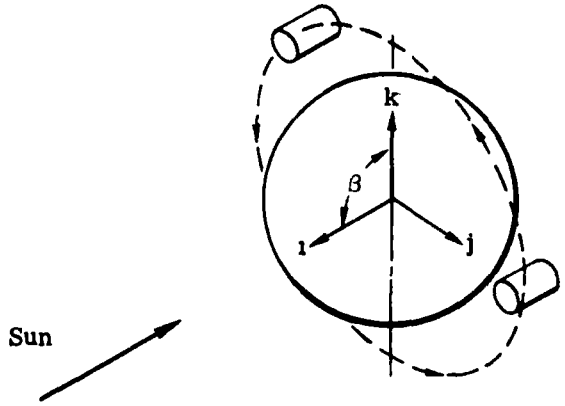

(a) Sun-synchronous orbit: $\imath = 90°$ (polar), $\beta = 90°$

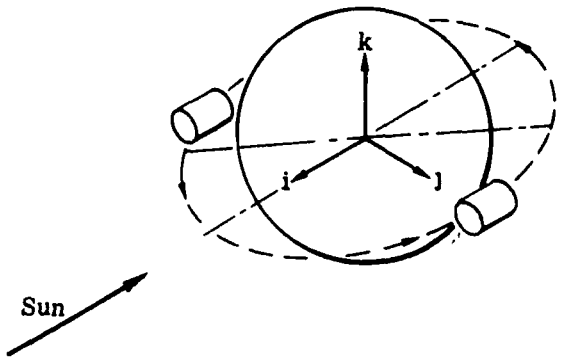

(b) Occulted orbit $\imath = 30°$, $\beta = 0°$

Fig. 2-3 — Photoheliograph orbits (both are 740-kilometer orbits)

Table 2-3 — Subsystem Thermal Loads (Sun-Synchronous Orbit)

Subsystem	Incident Solar, watts	Absorbed Solar, watts	Absorbed Area, watts/cm^2	Power Dissipation, watts
Primary mirror	2,445	a* = 0.12 293	A = 17,900 0.016	—
Secondary mirror and mechanisms	200-arc-second field of view 23.1	a = 0.12 2.78	A = 179 0.015	11.7
Heat and shield mirror	2,150	a = 0.05 106	A = 22.6 4.9	—
First relay and mechanisms	23.1	a = 0.12 2.78	A = 169 0.016	—
Second relay	20.5	a = 0.12 2.46	A = 160 0.0152	11.7
Focal plane	18.2	a = 0.12 2.17	A = 35 0.062	—
Meteroid shield	Earth IR = 0.0242 watts/cm^2 max; albedo = 0	—	—	—
Instrument support structure	—	—	—	Conductive loads from instruments
Instruments	—	—	—	293
Secondary support structure	Earth IR = 0.0242 watts/cm^2 max, albedo = 0; scattered light = 50 watts†	—	—	—

*a = solar absorptance, A = area (square centimeters).
† Environmental loading.

Table 2-4 — Summary of Requirements and Initial Results

Area	Requirement	Result
Primary mirror	0.025λ, 3 μm defocus	0.02λ, 36 μm
Secondary mirror	0.005λ rms, 21.1 ± 11 °C	−21.1 ± 0.5 °C
Secondary metering structure	15 μm decenter 3.2 μm defocus	Negligible decenter 0.25 μm < def < 2.5 μm
Primary mounts	±1 °C of local temperature	21.1 ± 1 °C
Heat shield mirror	21.1 ± 11 °C	24.5 + 0.5 °C
Relay flats	21.1 + 11 °C	−22.2 ± 0.5 °C −35 ± 0.5 °C

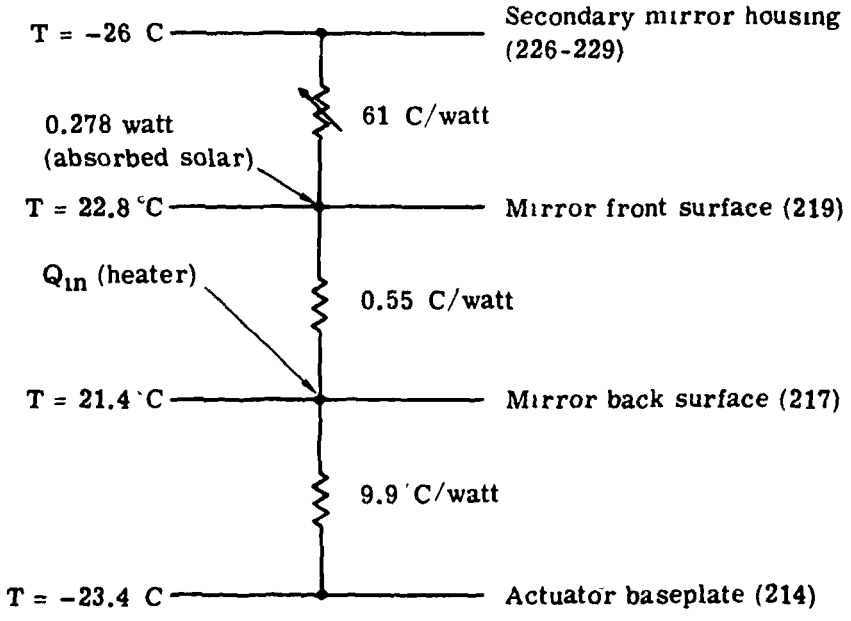

Fig. 2-4 — Thermal resistance map of secondary mirror subsystem for sun-synchronous orbit

Table 2-5 — Thermal Control Power Requirements

	Power Requirements, watts	
	Sun-Synchronous Orbit	Occulted Orbit
Secondary mirror	7	13.5
First relay flat	8.5	15
Second relay flat	13.5	18.5
Mounts	8	5.5
Main ring	56	55.5
Total	93	108

Table 2-6 — 150-Centimeter LSO Baseline Thermal Control Concept

Primary mirror	Monolith with high reflectance, specular core, partially open back, cooled from back by cold plate
	Cold plate connected to radiator by heat pipe
Primary mirror mount	Main ring heated 21.1 ± 1 °C
Secondary mirror	Solid mirror, thermostatically controlled at 21.1 ± 1 °C
Secondary metering structure	Low α/ϵ meteoroid shield, uninsulated
Heat shield mirror	Solid metal mirror conductively cooled by heat pipe connected to external radiator
Relay flats	Solid mirror thermostatically controlled at 21.1 ± 1 °C
Instrument structure	Not addressed

Table 2-7 — Primary Mirror Concept Evaluation (Sun-Synchronous Orbit)

	Solid Mirror		Specular Core Monolith	
Front temperature, °C	33.1		29.8	
Back temperature, °C	~15.8		14.5	
Average temperature, °C	~24.7		22.2	
	ΔT, °C	Wavelength RMS	ΔT, °C	Wavelength RMS
Soak	3.5	0.004	1	0.001
Radial gradient	2.2	0.001	2	0.001
Axial gradient	17.0	0.001	15	0.001
Axial gradient/lateral variation	4.1	0.016	4	0.008
		RSS 0.017		RSS 0.009

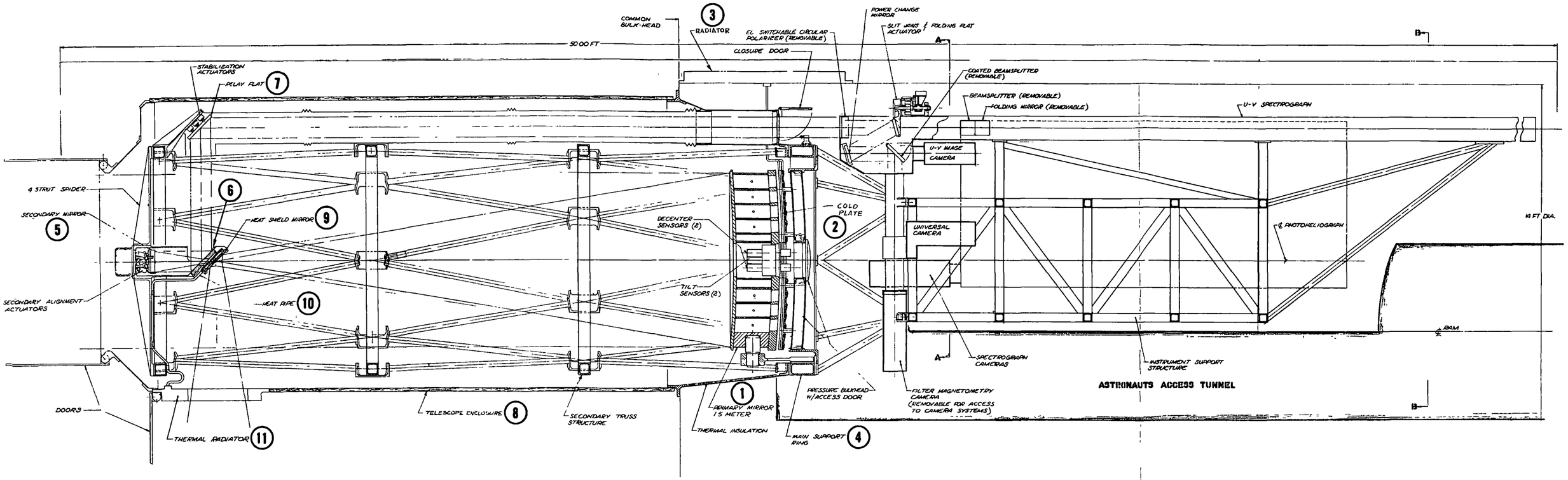

Fig. 2-5 — Thermal control system

Page intentionally left blank

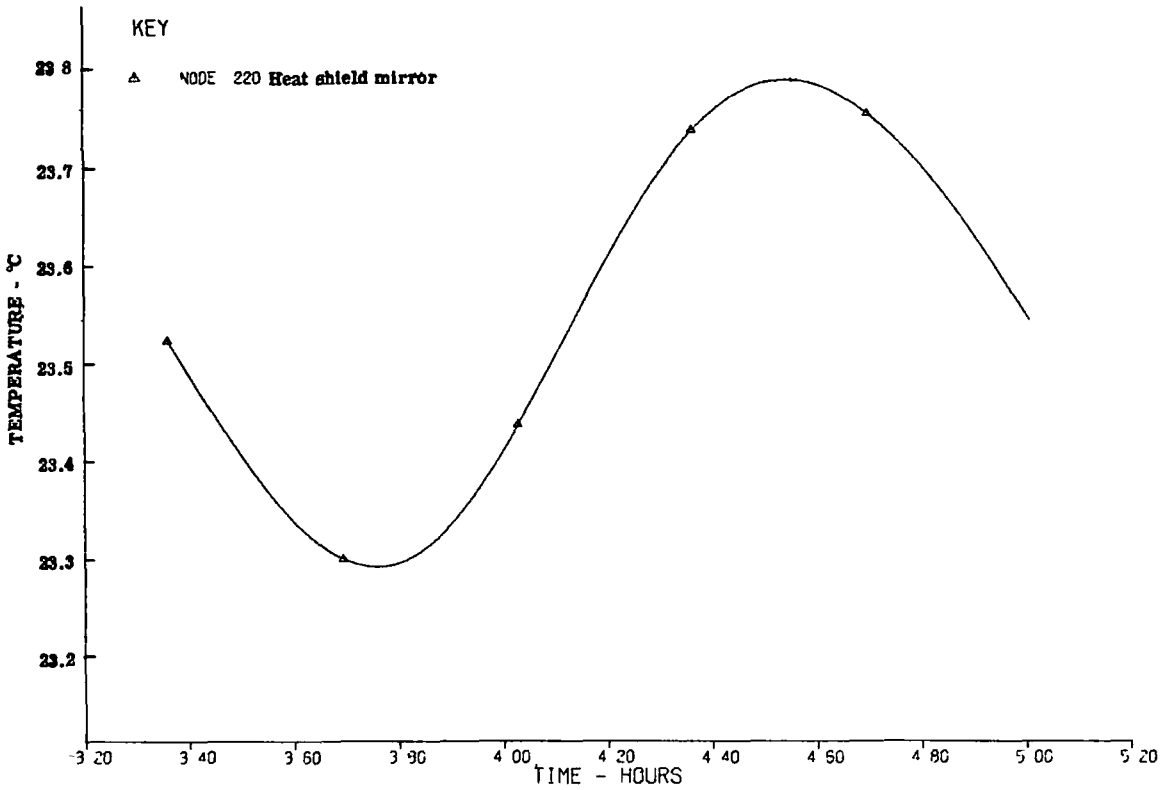

Fig. 2-6 — Temperature history for heat shield mirror—solid primary, sun-synchronous orbit

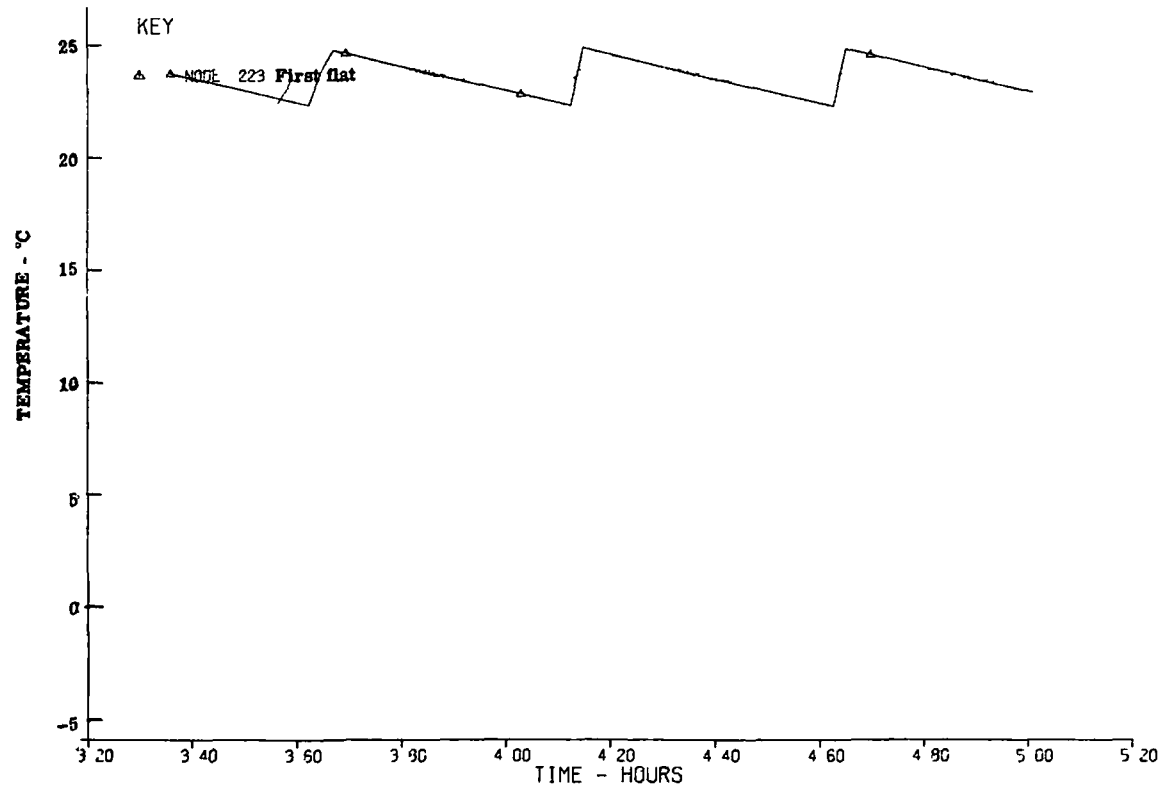

Fig. 2-7 — Temperature history for first flat—solid primary, sun-synchronous orbit

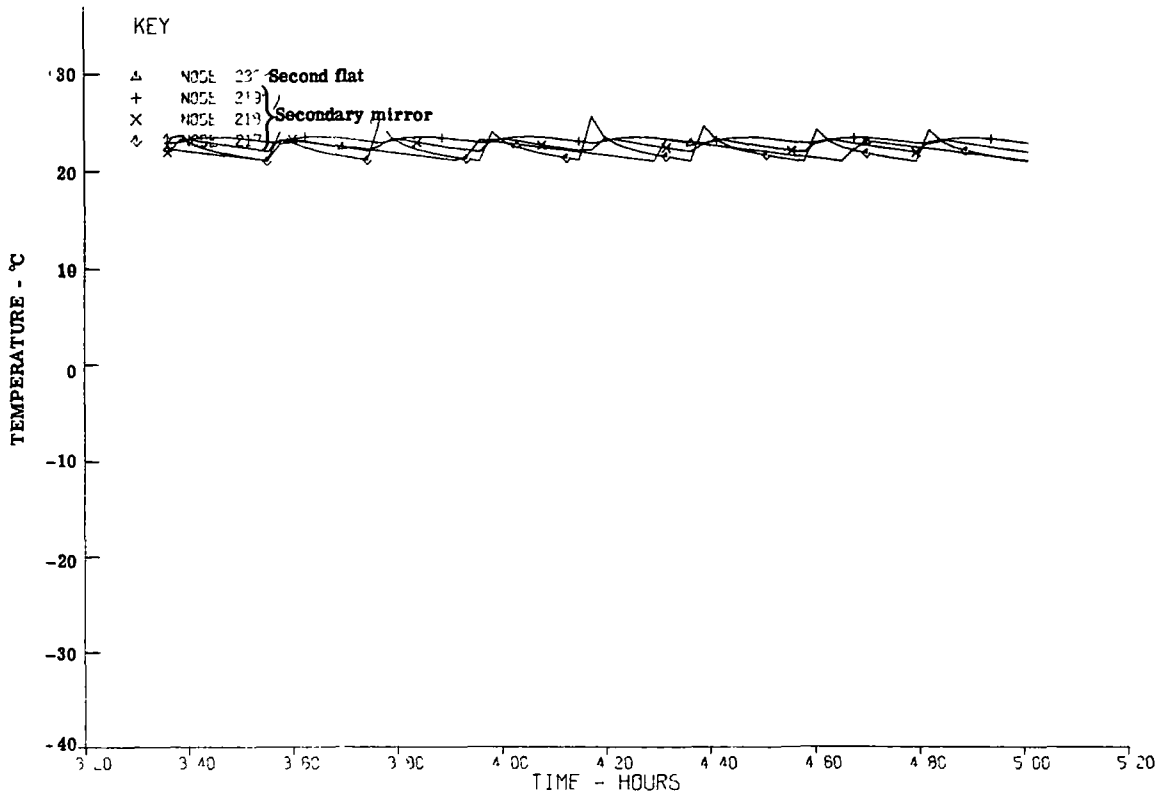

Fig. 2-8 — Temperature history for second flat and secondary mirror—solid primary, sun-synchronous orbit

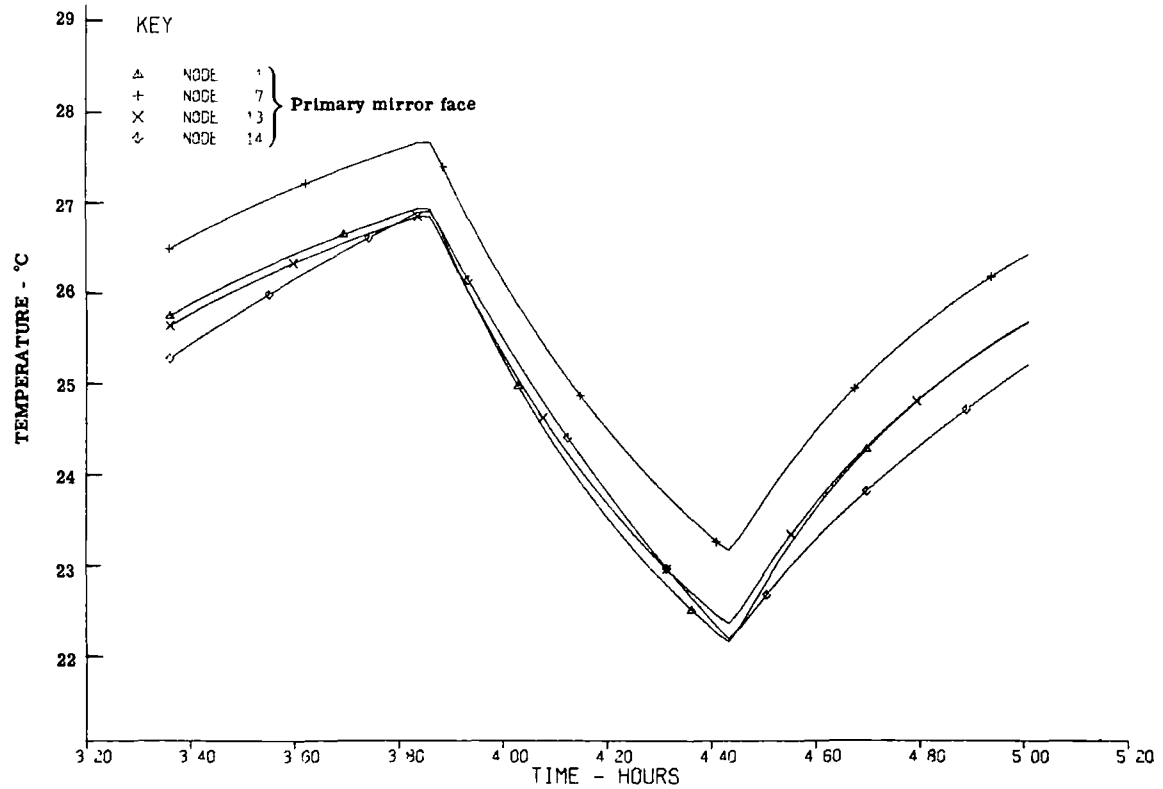

Fig. 2-9 — Temperature history for primary mirror face—solid primary, occulted orbit

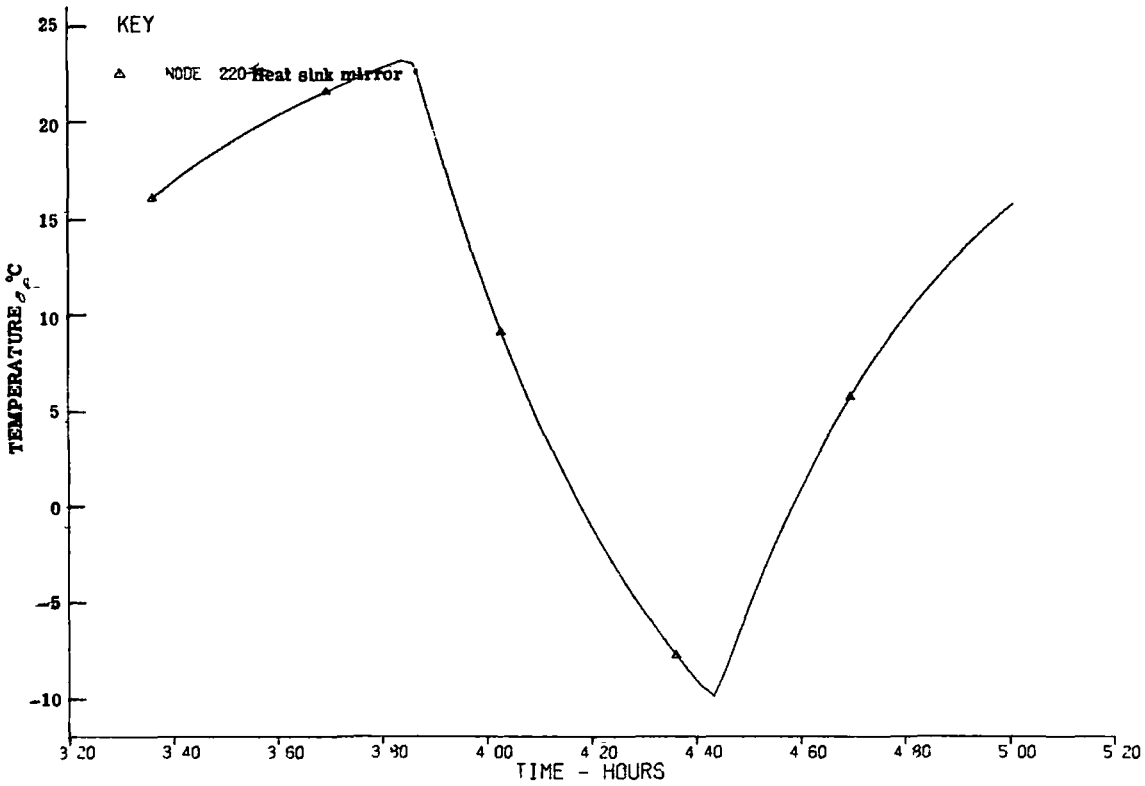

Fig. 2-10 — Temperature history for heat shield mirror —solid primary, occulted orbit

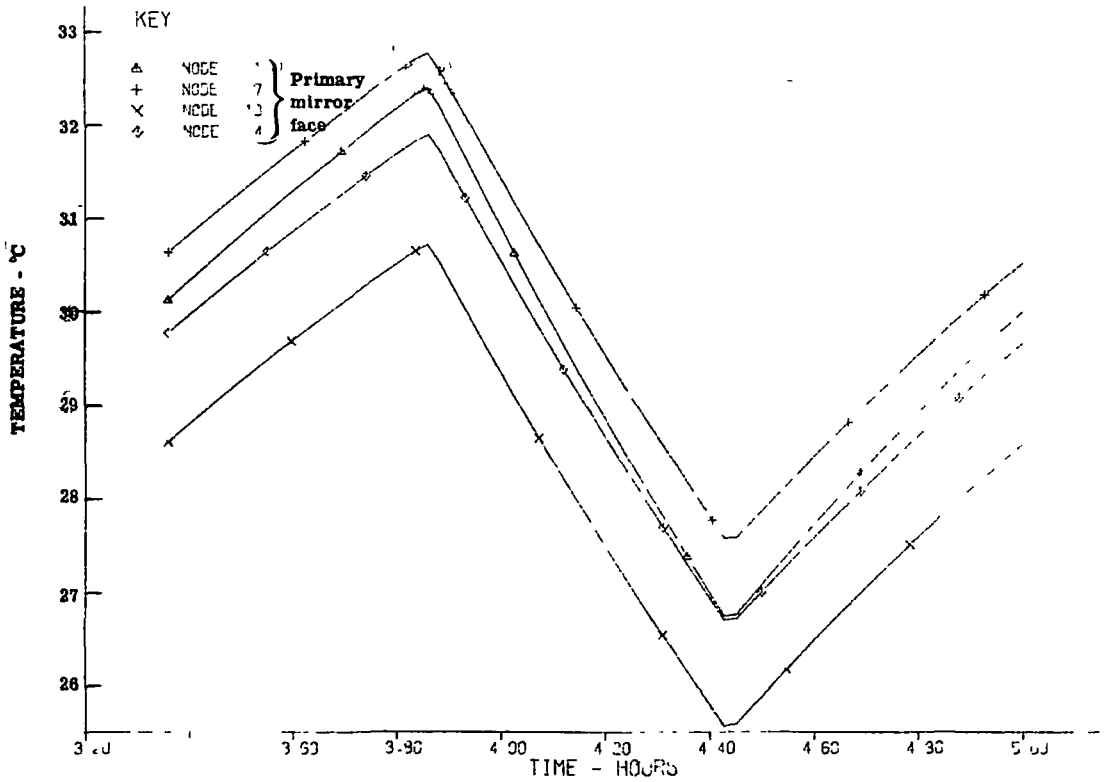

Fig. 2-11 — Temperature history for primary mirror face—cored primary, occulted orbit, insulated meteoroid shell

Table 2-8 — Solid Mirror Evaluation—Insulated Meteoroid Shield

Front temperature, °C	37.5
Back temperature, °C	19.2
Average temperature, °C	28.9

	ΔT, °C	Wavelength RMS
Soak	10	0.010
Radial gradient	4	0.002
Axial gradient	20	0.001
Axial gradient/lateral variation	4	0.016
		RSS 0.020

Table 2-9 — Average Heater Power (Watts)

	Main Ring	Mounts
Insulated meteoroid shield, occulted orbit	26.4	6.65
Insulated meteoroid shield, sun-synchronous orbit	26.4*	8.9
Baseline occulted orbit	55	5.6
Baseline sun-synchronous orbit	56.2	7.9

* Estimated from prior results.

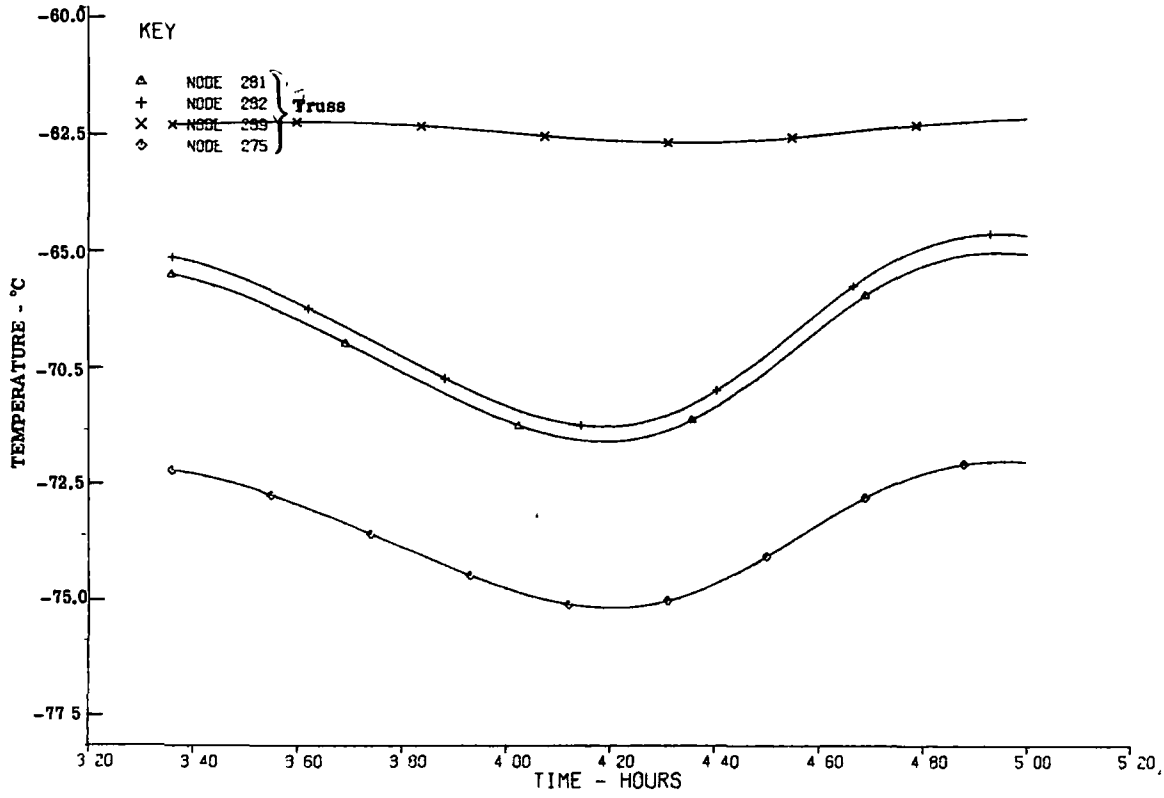

Fig. 2-12 — Temperature history for truss—cored primary, sun-synchronous orbit, uninsulated meteoroid shell

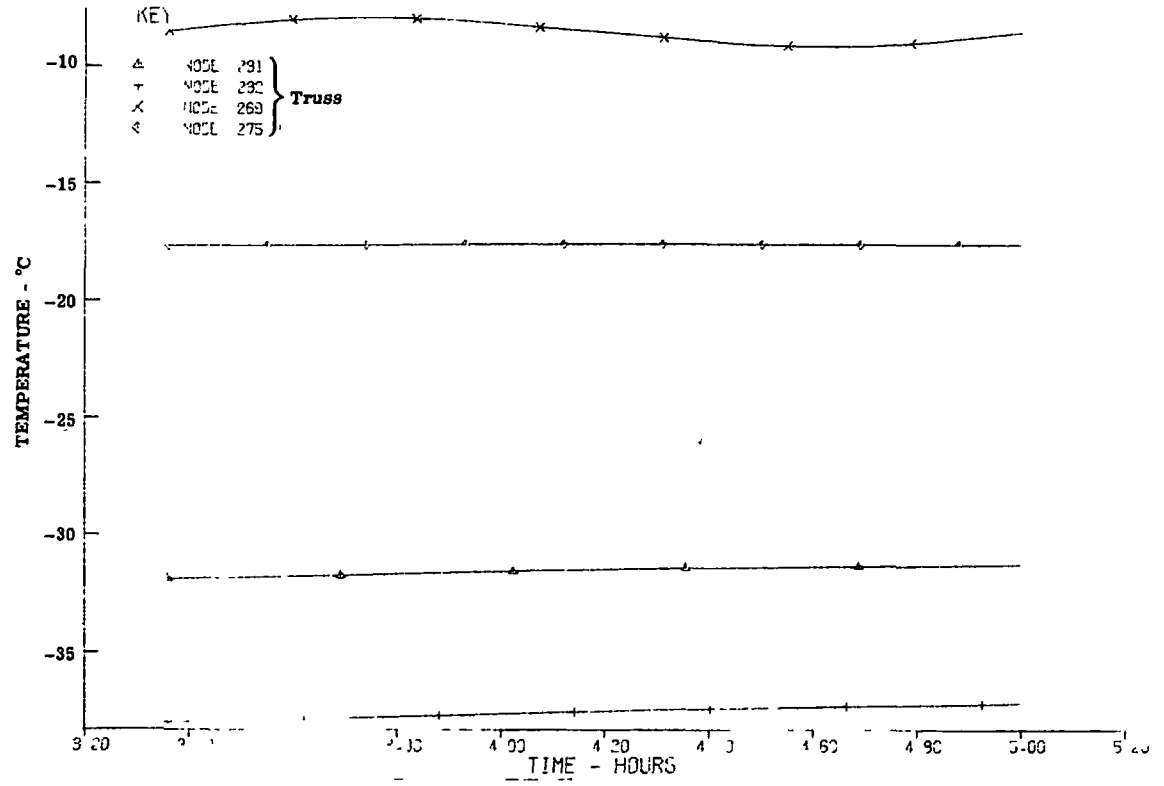

Fig. 2-13 — Temperature history for truss—cored primary, occulted orbit, insulated meteoroid shell

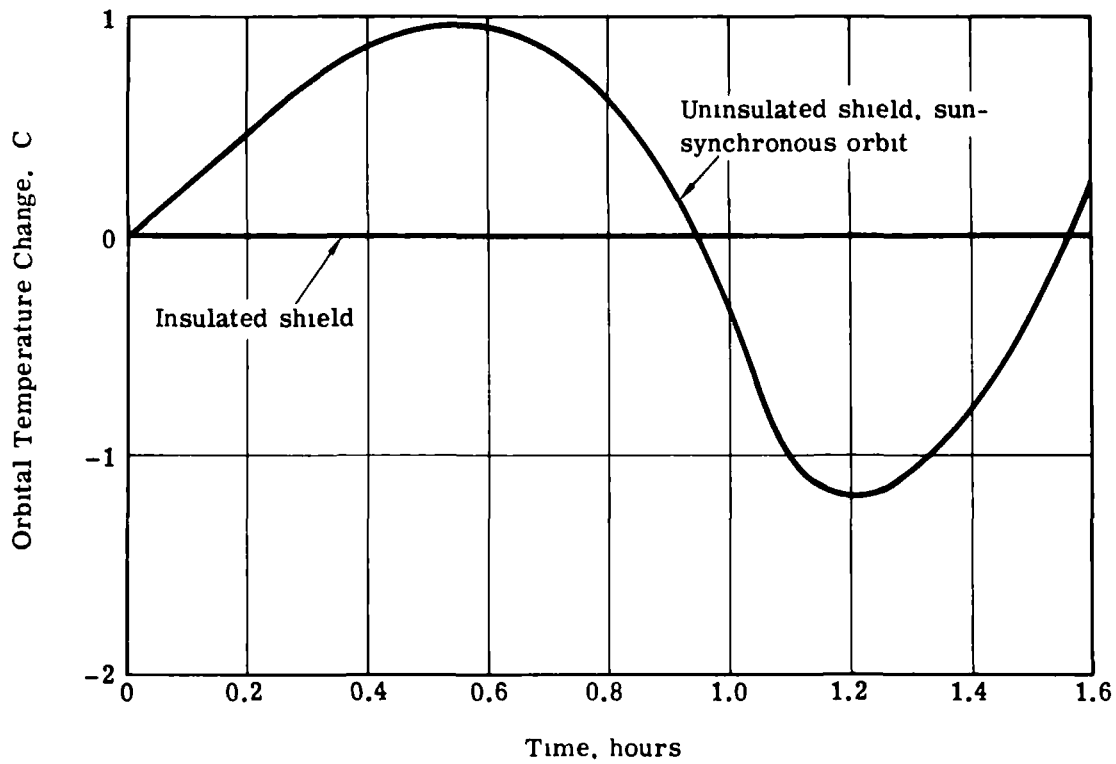

Fig. 2-14 — Truss temperature change as a function of orbital time

3. 100-CENTIMETER PHOTOHELIOGRAPH FOR SHUTTLE MISSIONS

3.1 BACKGROUND

3.1.1 Requirements

A 100-centimeter photoheliograph for operation on Shuttle sorties has been investigated. As for the 150-centimeter LSO photoheliograph, we first established the general design requirements and thermal criteria. The previously developed thermal requirements (see Table 2-1) are in general applicable to the Shuttle mission. However, the allowable primary mirror wavefront error is increased to 0.04 wavelength from the 0.025 wavelength required for the LSO mission.

3.1.2 Environment

The Shuttle mission is based on mounting the 100-centimeter photoheliograph in the cargo bay of the Shuttle Orbiter. Fig. 3-1 is an artist's concept of such an arrangement. Conceptually we have developed a Shuttle bay configuration for the determination of external thermal loads, both directly on the surfaces of the photoheliograph and on the Shuttle cargo bay where they interact with the photoheliograph. Figs. 3-2, 3-3, and 3-4 represent the geometric arrangement of the photoheliograph/Shuttle model configuration.

This configuration was "flown" in an inertial X-POP mode selected to provide continuous solar viewing in order to determine the incident orbital fluxes for the configuration described above. In addition to the external fluxes calculated for the Shuttle flight, we estimated the system optical thermal loads for solar viewing. These loads and the incident energy values are presented in Table 3-1. Both the incident solar loads and absorbed flux (as a function of optical coating) are presented.

Additional thermal loads resulting from normal system operation (e.g., mirror actuators) and from the scientific instruments (cameras, etc.) have been determined. Table 3-2 presents our best estimate of the various nonoptical thermal loads for a Shuttle mission.

3.1.3 Analytical Tools

The basic analytical tool employed in the thermal analysis of the Shuttle-borne photoheliograph was the existing 150-centimeter LSO photoheliograph thermal model. To accomplish the necessary configuration change, the following basic changes were made in the thermal model: the thickness of the solid primary mirror was adjusted, radiation exchange between the Shuttle bay and the photoheliograph surface nodes was added, and a conductive connection representing the gimbal mount was added.

Since the 100-centimeter Shuttle-borne photoheliograph is a smaller instrument than the 150-centimeter LSO photoheliograph, the thickness of the solid primary mirror was reduced from 6 inches to 4 inches (to preserve the present L/D ratio). The radiation exchange between

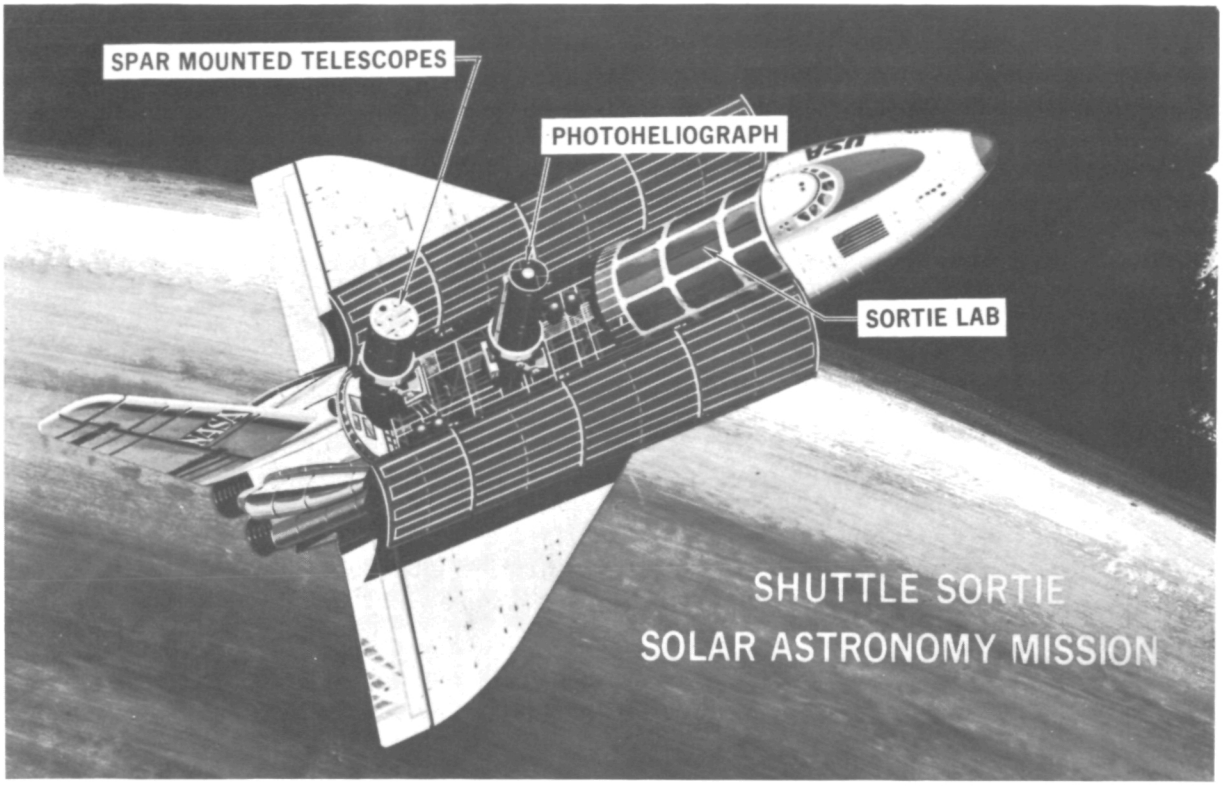

Fig. 3-1 — 100-centimeter photoheliograph in Shuttle

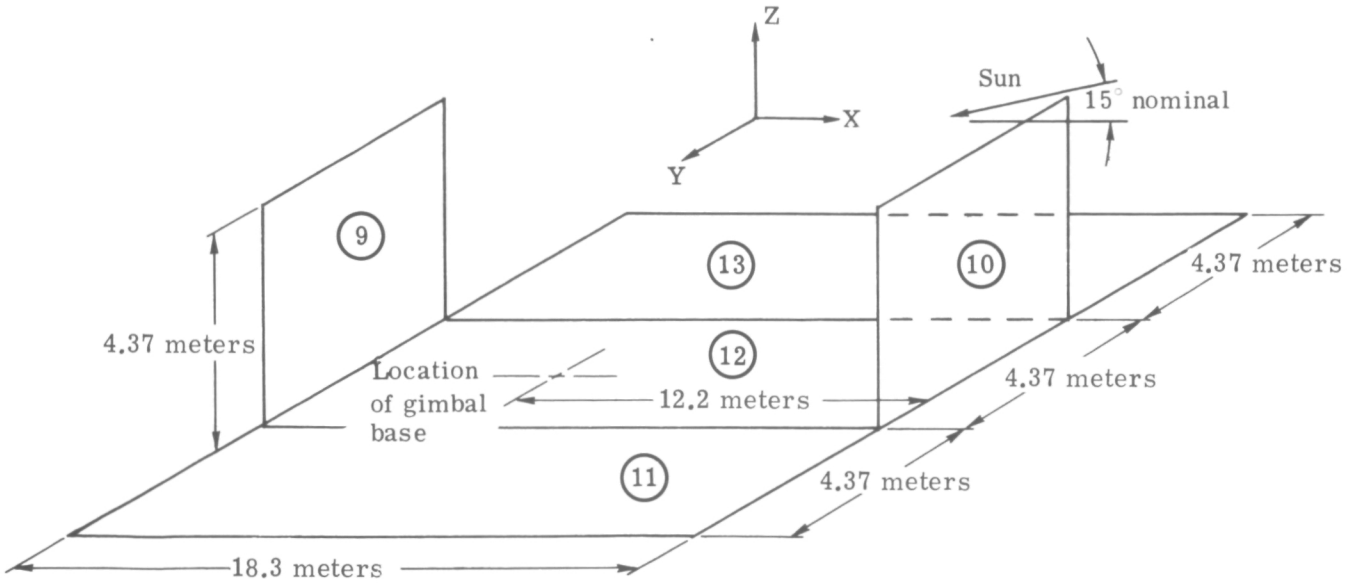

Note: X-POP mode sun-synchronous orbit
X-Z = orbital plane
Surface finish of cargo bay α/ϵ = 0.9/0.9

Fig. 3-2 — Shuttle cargo bay model

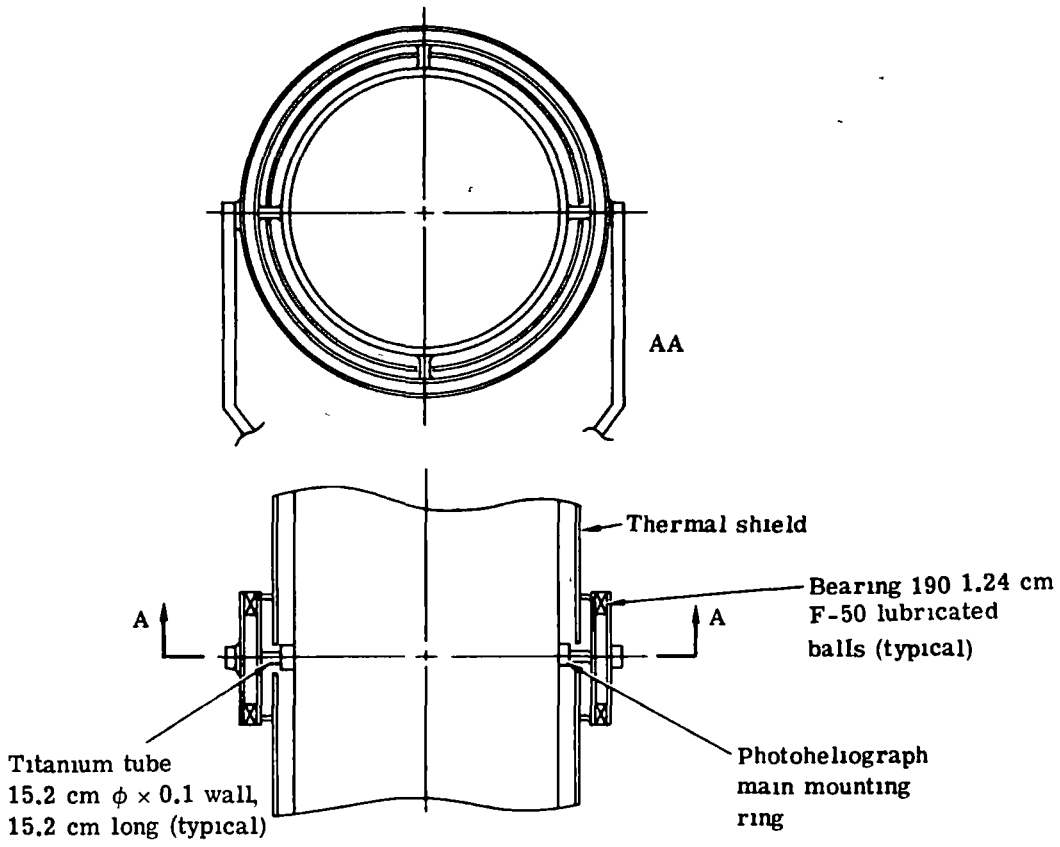

Fig. 3-3 — Gimbal mounting assembly concept

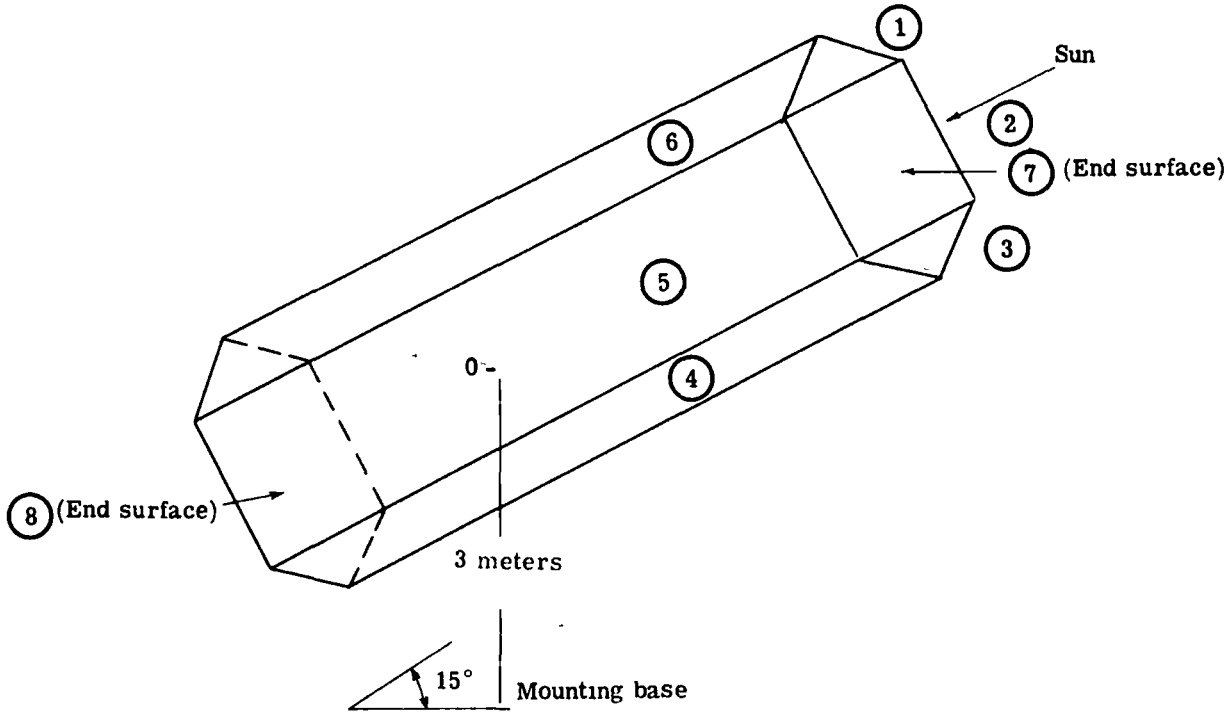

Note: 6 sides, 2 ends for 8 nodes

Fig. 3-4 – Telescope barrel model

Table 3-1 — Optical System Thermal Loads

Location	Incident Load, watts	Absorbed Load, watts
Primary	1,100	132.5 α = 0.12
Secondary (360 arc-sec field of view)	33.4	4.1 α = 0.12
First relay	29.3	3.5 α = 0.12
Second relay	25.5	3.2 α = 0.12
Heat shield	935	48 α = 0.05
At focal plane	22.6	—

Table 3-2 — Estimated Power Dissipation

Source	Load, watts	Duty Cycle, percent	Comments
Alignment sensors	20	2	25 percent at sensor 75 percent at electronics
Alignment actuator	75	6	At secondary mirror
Pointing sensor	30	100	50 percent at image distance 50 percent at electronics
Pointing activator	10	100	At second relay flat
Housekeeping	60	2	At electronics
Data management	16	5	At electronics
Ultraviolet camera train	40	100	
White light camera	15	5	
H-α camera	15	5	
Magnetometer cameras	60	100	
Magnetometer electronics	20	100	
Magnetometer film camera	10	5	
Plane grating spectrometer	30	25	
TV monitor	20	10	
Primary mirror	145		Standby heaters (if required)
Heat shield mirror	50		Standby heaters (if required)

the Shuttle bay and the photoheliograph was determined by calculating nodal view factors based on the 100-centimeter Shuttle configuration to preserve scaling relationships, and these view factors were used to determine the radiation connections between the photoheliograph and the Shuttle bay. The photoheliograph is supported from the main mounting ring by a gimbal assembly this is conductively connected to the floor of the Shuttle bay. Fig. 3-5 depicts how the ring-to-floor connections are made.

3.2 BASELINE THERMAL CONTROL CONCEPT

The baseline thermal control concept for the 100-centimeter Shuttle photoheliograph design is heavily influenced by the established 150-centimeter LSO concept (see Section 2.2). The previously proposed methods for primary and heat shield mirror thermal control by means of cold plates, heat pipes, and space radiators are completely applicable to the Shuttle design. One significant concept change has been made. The primary mirror baseline for the Shuttle sortie design is a solid mirror rather than the lightweight, specular core design baselined for the 150-centimeter LSO photoheliograph. The solid mirror has been selected for the following reasons:

1. The optical performance of the solid mirror meets current requirements.
2. The smaller aperture (relative to the LSO) reduces the solid mirror weight penalty.
3. The cost of a solid mirror blank is significantly lower than that for the specular core, lightweight mirror.

It should be noted that although the solid mirror has been selected as our baseline, the lightweight, specular core mirror could also be used.

Thermostatic control of the main support ring, secondary mirror, and relay flats is also directly transferred from the LSO to the Shuttle concept. A significant effort was made to establish thermal control concepts for those elements of the system that had not been previously addressed and to evaluate alternative approaches to thermal control for those system elements where the baseline was previously established. Specifically, we investigated and selected appropriate thermal control concepts for the scientific instrument complement at two temperature levels (21.1°C and −17.8°C), we evaluated a range of thermal control coatings and selected a passive concept for thermal control of the instrument support structure, we investigated alternative passive and active thermal control concepts for the primary mirror and heat shield mirror; and we evaluated the effects of external shell emittance variation with and without insulation on the secondary support structure.

All of these studies are discussed in the following sections, and our conclusion, the 100-centimeter Shuttle sortie photoheliograph thermal control baseline, is presented.

The major elements of the thermal control baseline may be most clearly understood by referring to Fig. 3-6, which is a layout of the 100-centimeter Shuttle photoheliograph. Incident absorbed solar energy is conducted through the solid primary mirror (item 1) and then radiated to a cold plate (item 2). The absorbed energy is then transferred by heat pipe (item 3) and ultimately rejected by an external radiator (item 4). The main support ring (item 5), the secondary mirror (item 6), and the relay flats (items 7 and 8) are all thermostatically controlled at 21.1 ± 1 °C. The mirror mounts (item 9) are thermostatically controlled at local mirror temperature to reduce induced thermal loads. The secondary metering structure (item 10) is indirectly controlled by the thermal control finish applied to the external shell (item 11). Thermal control of the metal heat shield mirror (item 12) is maintained by direct conduction to a heat pipe (item 13) and ultimately to space by means of an external radiator (item 14). Thermal control of typical scientific data acquisition instruments (items 15 and 16) is accomplished by either direct radiation or conductive coupling (depending on temperature level requirements) to the outer shell of

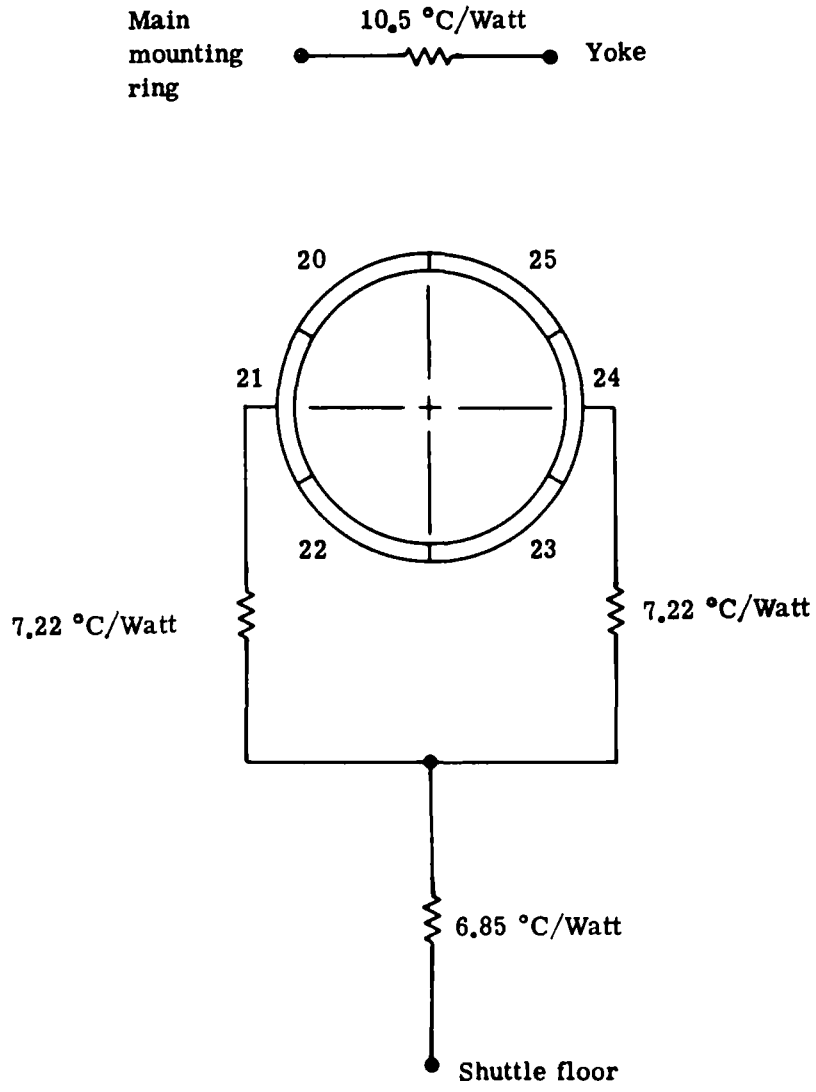

Fig. 3-5 — Connection of mounting ring to Shuttle floor

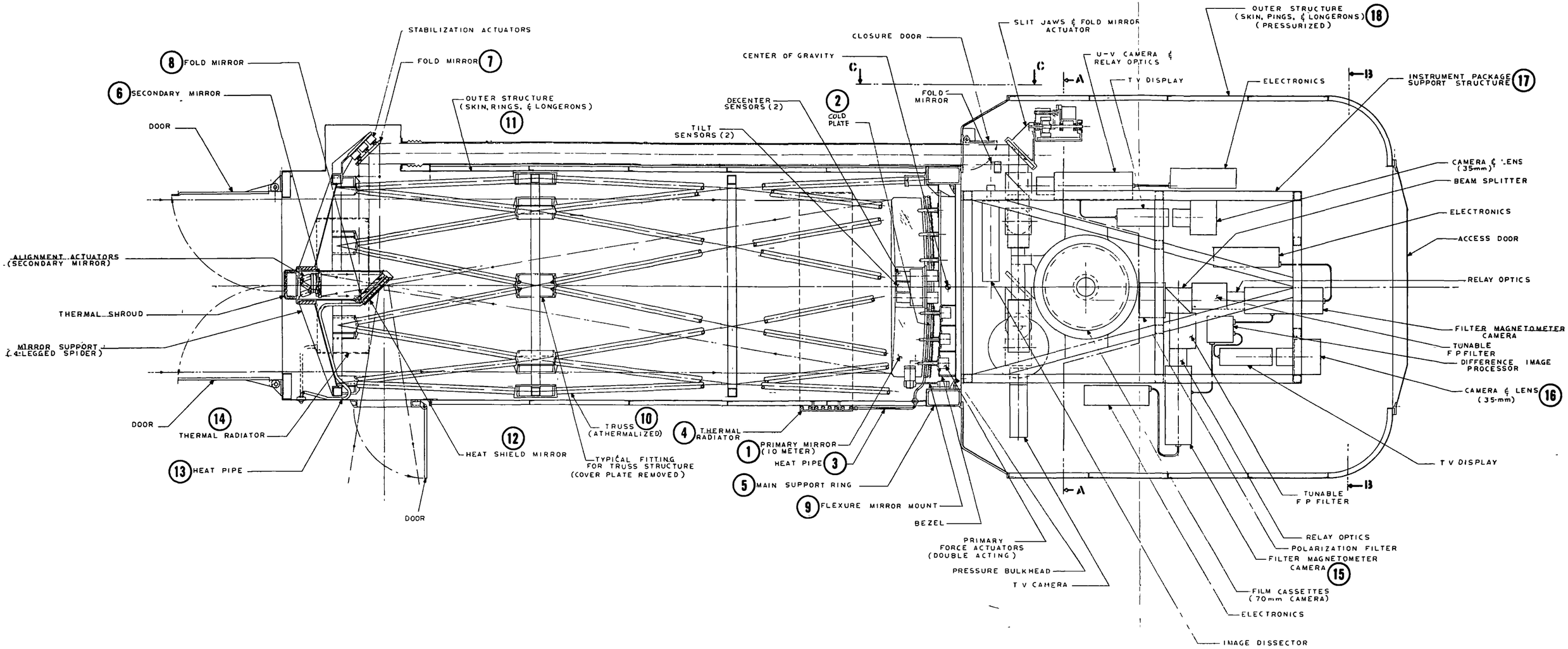

Fig. 3-6 — Thermal control concept

PAGE MISSING FROM AVAILABLE VERSION

the instrument compartment. Passive thermal control of the instrument support structure (item 17) is accomplished by thermal control finishes applied to the outer shell (item 18) of the instrument compartment.

3.3 PRIMARY MIRROR COOLING ANALYSIS

3.3.1 Baseline Primary Mirror Cooling

The baseline primary mirror cooling concept employs a cold plate heat sink located behind the primary mirror and an external radiator mounted to the external surface of the photoheliograph. The radiator and cold plate are linked by means of a heat pipe.

In the course of running the system thermal model, four cases were evaluated for external thermal finishes and meteoroid shell insulation requirements. The response of the primary mirror is presented for these cases in Table 3-3. A preliminary estimate of the wavefront error resulting from these gradients indicates it to be less than 0.025 wavelength for all cases. Figs. 3-7, 3-8, and 3-9 are temperature history plots of the axial temperature distribution at three radial locations for case 3. They are indicative of the orbital performance of the primary mirror.

3.3.2 Alternative Primary Mirror Cooling Concepts

We conducted a detailed investigation of two alternative concepts for primary mirror thermal control. The concepts examined were

1. Solid conductor thermal control
2. Self-contained fluid loop thermal control.

For the investigation we assumed that a solid ULE primary mirror was used and that the mirror thickness was fixed at 10.2 centimeters. This value is identical with the previously reported baseline study. The photoheliograph was also assumed to be in a sun-synchronous inertial orbit. The characteristics of the primary mirror radiator were reviewed and estimates of radiator area versus radiator temperature for the rejection of the primary mirror heat load were made for peak, average, and no incident thermal flux condition. This is plotted as Fig. 3-10. Also plotted on this figure is the cold plate design temperature of -38.4 °C, which corresponds to a mirror faceplate temperature of 21.1 °C. This establishes a lower bound on the required radiator area, which for this system is 15,000 square centimeters.

Solid Conductor

As a first step in the analysis, we evaluated alternative conductor materials. Since we were considering a solid conductor scheme, high conductivity and low weight were required. Two candidate materials were aluminum and copper. Comparing these materials on an equal weight basis, we found that the thermal resistance of aluminum is approximately 2 percent lower than that of copper. Thus, we concluded that an aluminum system will be lighter than a copper system having the same system ΔT.

Having established the basic system material, we considered the three basic components that make up the overall system. For a 100-centimeter photoheliograph, we estimated the solid conductor length as being at least 50.8 centimeters. Since we must allow some excess length for a practical system, the overall solid conductor length was assumed to be 76.2 centimeters. We estimated the characteristics of the solid conductor required as a function of cross-sectional area and concluded that a minimum diameter of 30.5 centimeters is required for the conductor.

Table 3-3 — Primary Mirror Temperature Results

	Case 1 α/ϵ = 0.22/0.88 No Insulation	Case 2 α/ϵ = 0.22/0.88 Insulation	Case 3 α/ϵ = 0.12/0.04 No Insulation	Case 4 α/ϵ = 0.12/0.04 Insulation
Face temperature, °C	31.6	35.3	32.2	35.3
Rear temperature, °C	20	22.6	20	23.1
Radial gradient, °C	0.83	1.22	0.83	1.33

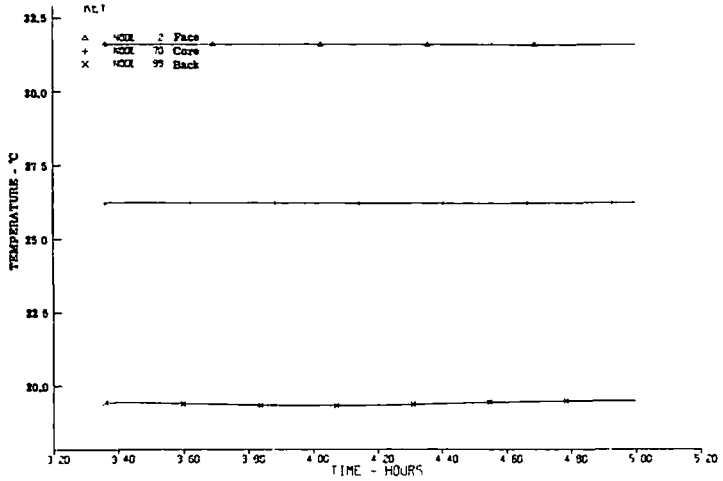

Fig. 3-7 — Temperature history for primary mirror center axial gradient (α/ϵ = 0.12/0.04)

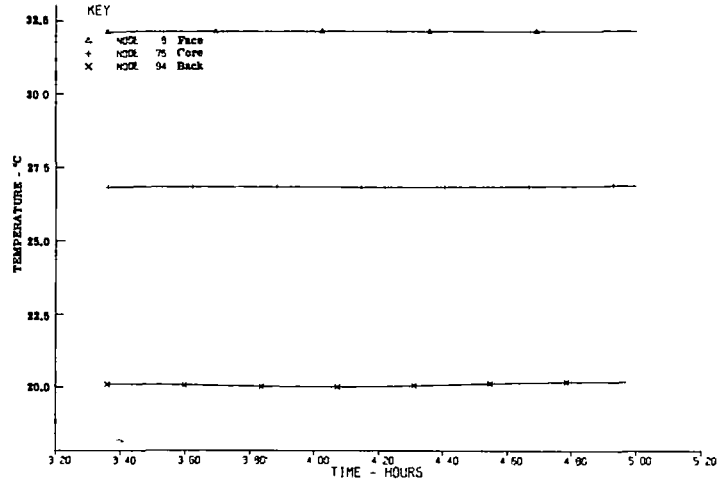

Fig. 3-8 — Temperature history for primary mirror middle axial gradient (α/ϵ = 0.12/0.04)

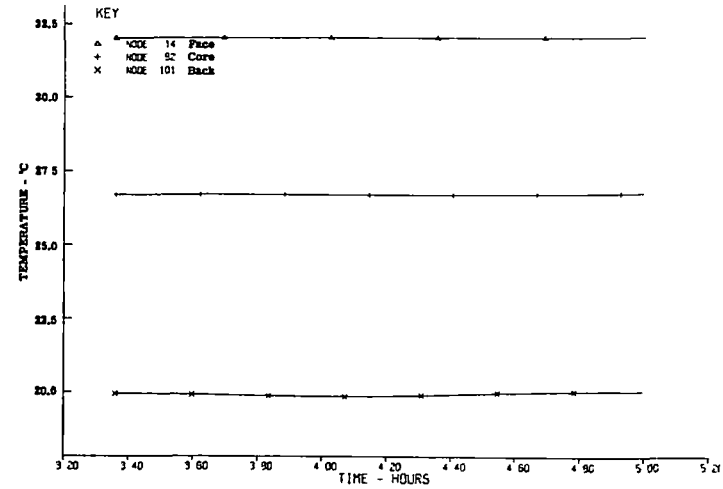

Fig. 3-9 — Temperature history for primary mirror outer axial gradient (α/ϵ = 0.12/0.04)

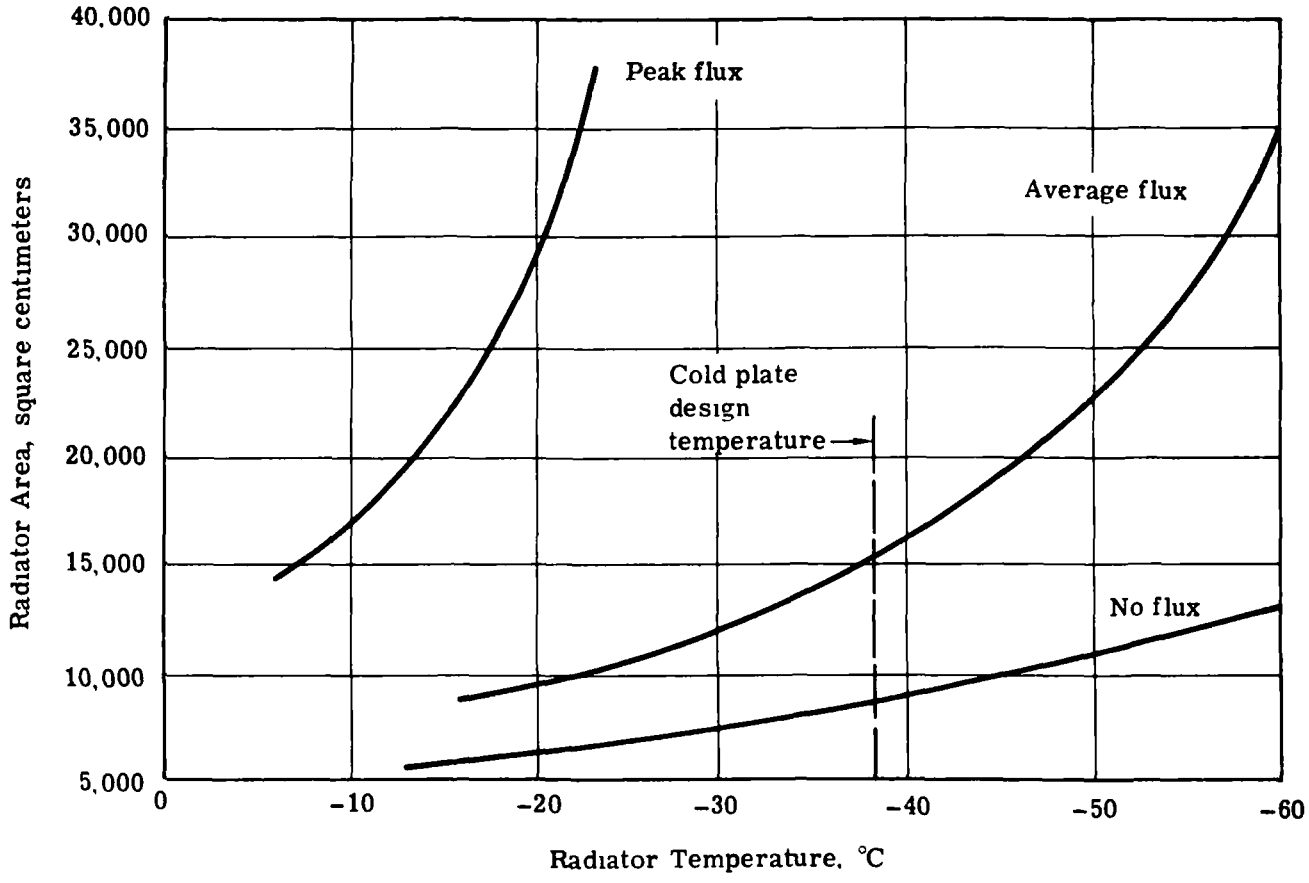

Fig. 3-10 — Radiator size versus temperature (system sized to reject 132 watts)

The results of this conductor sizing study are presented below

Conductor Diameter, centimeters	Conductor Weight, kilograms	Conductor Temperature Drop, °C	Required Radiator Area, square centimeters
15.2	38.5	45.5	47,000
25.4	107	16.6	26,400
30.5	154	11.4	21,600

Once the size of the cold plate/radiator conductor was established, we then established the characteristics of the mirror cold plate. We treated the cold plate as a circular fin of rectangular cross section and solved the appropriate fin equation for temperature distribution as a function of fin thickness. The particular solution is given by Schneider* as

$$\frac{T}{T_0} = \frac{I_0(Nr)K_1(Nr_{2C}) + I_1(Nr_{2C})K_0(Nr)}{I_0(Nr_1)K_1(Nr_{2C}) + I_1(Nr_{2C})K_0(Nr_1)}$$

Fig. 3-11 is a plot of the radial temperature drop calculated from this equation. It is seen that the fin (cold plate) becomes much less effective as the thickness increases beyond 3.8 centimeters. An overall cold plate thickness of 7.6 centimeters was selected for the solid conductor baseline, because thickness increases beyond this point appear to have almost negligible effect on the final cold plate temperature drop.

The final step in the determination of a solid conductor thermal control concept was the establishment of radiator sizing. By referring to Fig. 3-10, we note that the minimum radiator size for a system having the temperature drop calculated above is approximately 23,500 square centimeters. Since there will be some internal temperature drop in the radiator (from the conductor termination to the location on the surface where the transfer of energy to space takes place), we sized the system by assuming an allowable radiator conductive drop, calculating an allowable resistance, and then determining an area. By comparing this assumption with the radiator heat rejection area plot, we can show that the radiator does in fact meet our assumed conditions.

If we assume an allowable temperature drop of −12.2 °C from conductor to edge, we get a radiator resistance of 0.0811 °C/watt. Assuming a 5.1-centimeter-thick radiator, we estimate a radiator area of 28,200 square centimeters. Referring to the radiator area plot (Fig. 3-10), we see that this area will reject the required heat at a temperature of −56.6 °C. Since the actual radiator temperature is somewhat hotter (we neglected losses from the radiator in the sizing analysis), it appears that the system has been slightly overdesigned in terms of radiator thickness and/or area. In summary, we have developed a concept based on a solid conductor approach.

The system is made up of a 7.62-centimeter-thick cold plate immediately behind the primary mirror coupled to a solid 30.5-centimeter-diameter aluminum conductor leading to an external radiator 5.08 centimeters thick and having an overall area of approximately 28,200 square centimeters. The overall design is illustrated in Fig. 3-12, which presents sizes, temperatures, and system weights for the concept.

---

* P. J. Schneider, Conduction Heat Transfer, Addison-Wesley, Reading, Mass., 1955.

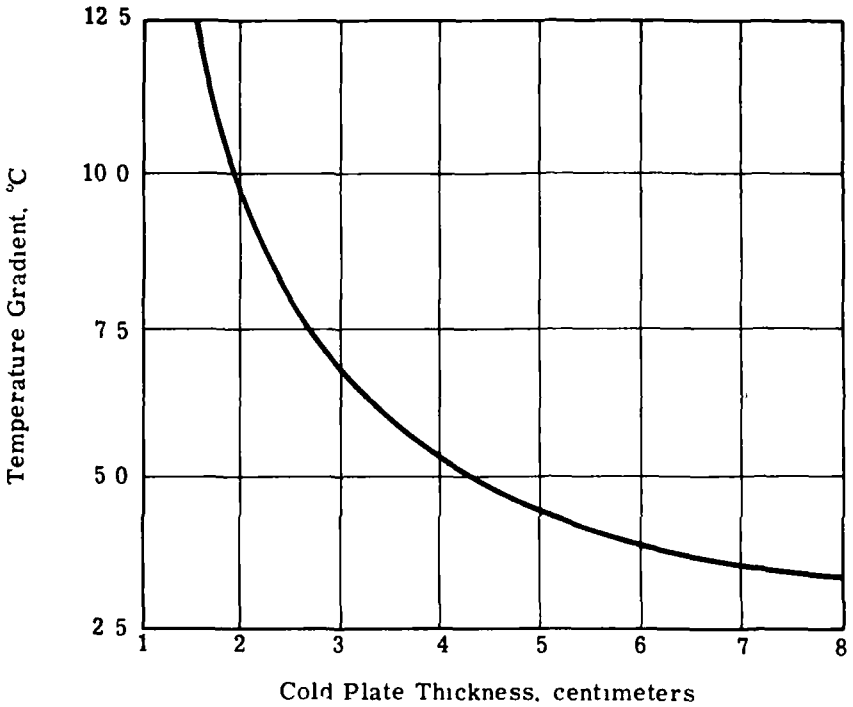

Fig. 3-11 — Solid conductor cold plate gradient analysis

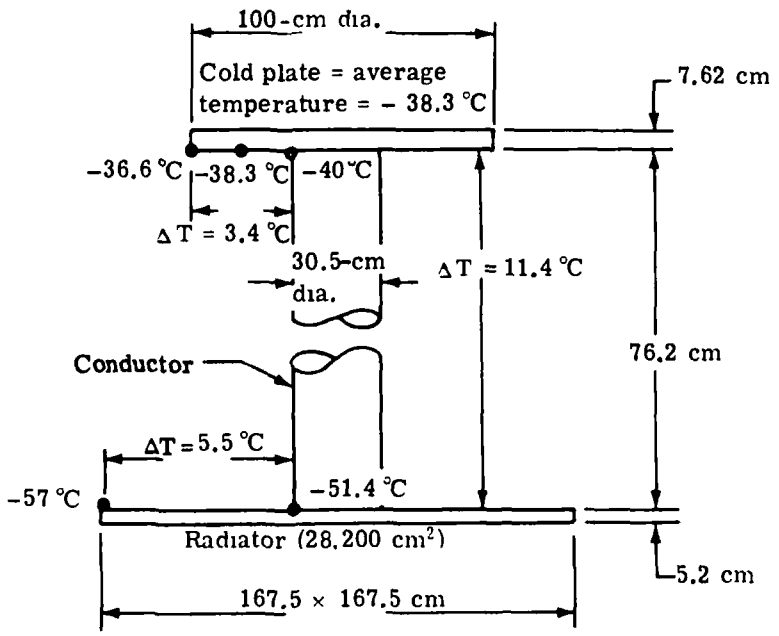

All material is aluminum

Weight, kilograms

Coldplate	=	171
Conductor	=	153.5
Radiator	=	394
Total		718.5

Fig 3-12 — Solid conductor cooling system concept

Self-Contained Fluid Loop

The concept of a self-contained fluid cooling loop for thermal control of the primary mirror had not been evaluated previously for the photoheliograph because the lifetime requirements for an LSO appear to be beyond the state of the art for mechanical pumps. However, for a Shuttle mission of limited duration, the potential for a simple system appeared worthy of investigation, since life-limited components do not affect the design.

The fluid loop thermal control concept is shown schematically in Fig. 3-13. The system consists of a cold plate with integral cooling coils mounted behind the primary mirror, an externally mounted radiator with integral cooling coils, a circulating pump and motor, and an accumulator tank/fill tank. Both heat transfer surfaces are isolated from the fluid lines by flexible couplings to reduce or eliminate induced vibrations. The pump motor is also vibration-isolated from its mounting structure.

Let us first consider the general characteristics of the fluid. Since the primary mirror will be operating at 21.1 °C, the required cold plate temperature is, from Fig. 3-10, approximately −38.3 °C. In general, since the fluid must be colder than the cold plate and since heat will ultimately be rejected from a colder radiator, the fluid selected should have reasonable properties at a level of −45.6 °C. A 60-40 mixture of ethylene glycol and water is one possibility, since its freezing point is approximately −51.1 °C. Evaluation of the fluid properties of this mixture indicated extremely high viscosity, which would result in a high pressure drop system.

As an alternative and more acceptable choice, we selected a fluorinated coolant FC-78 manufactured by the Chemical Division of 3M Company. The physical properties of this fluid are given in Table 3-4. Based on our examination, it appears that the FC-78 coolant is superior in all respects to the ethylene glycol and water mixture and thus we based our design on its use.

Although there are a number of possible geometric arrangements for the cold plate, a helical cooling coil was selected, since for the circular plate, a helical coil can be made that has uniform separation between coils and thus can be analyzed as a simple fin. Such an arrangement has been made and analyzed. The configuration is a 15.2-centimeter helical coil of 0.95-centimeter outside diameter tubing mounted on a 0.318-centimeter-thick aluminum cold plate 100 centimeters in diameter. The cold plate layout is shown in Fig. 3-14.

The design of the radiator is based on the application of the data presented in Fig. 3-10 for the average flux condition. For this condition, a radiator area of approximately 19,750 square centimeters is required to reject the absorbed primary mirror heat with a reasonable temperature drop between cold plate and radiator. The particular radiator configuration selected is an aluminum sheet 0.318 centimeter thick, 160 centimeters long, and 103 centimeters wide. A serpentine coil of 0.95-centimeter outside diameter tubing on a 30.5-centimeter center is mounted on the radiating plate.

Using the above configuration, we conducted a hydraulic and thermal analysis of the system. The results of this analysis are presented in Table 3-5, which also includes an estimate of the total weight of the cooling system.

Since the fluid loop cooling system was sized for steady-state operation, it is of some concern to consider the effect of orbital variations on these temperatures. In particular, a system of this type is sensitive to the variation in energy received (see Fig. 3-10). It does not appear to be possible to design the system for the worst case, and thus the radiator temperature will vary in a cyclical fashion during the orbital period. The most direct method of reducing radiator temperature variation is to provide a temperature controlled fluid bypass around the radiator. Thus, as the radiator changes temperature as a result of variation in orbital position, the mixed fluid temperature may be held closer to the desired temperature by variation in the radiator/bypass fluid ratio.

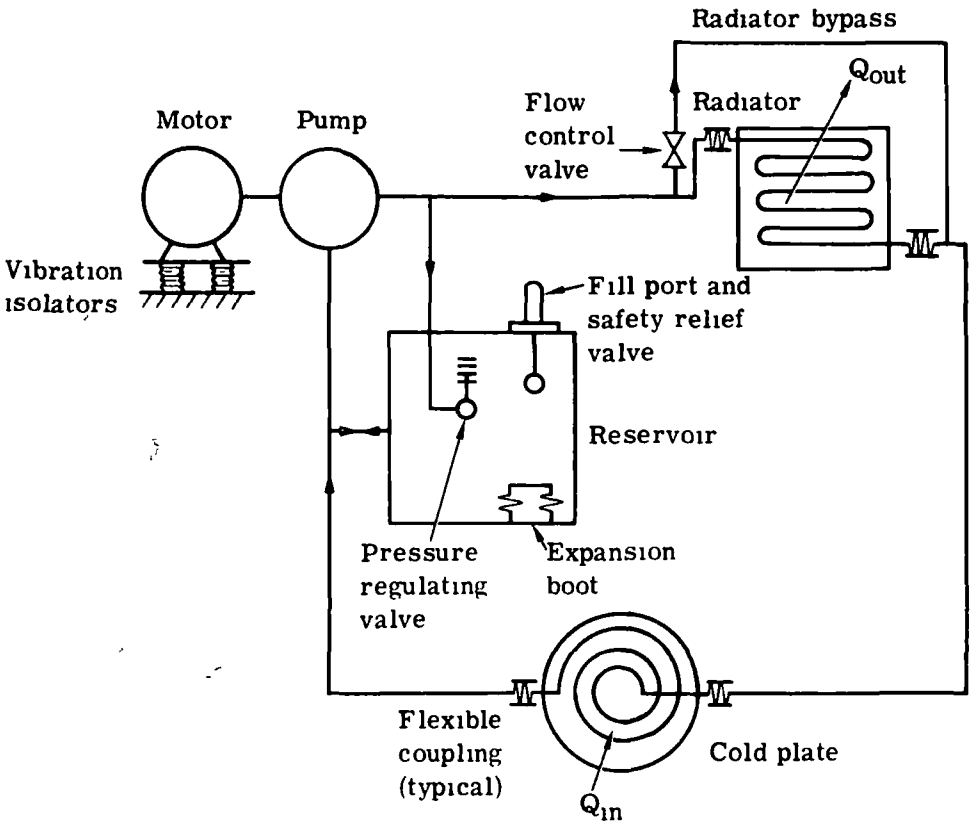

Fig. 3-13 — Cooling loop concept

Table 3-4 — Properties of FC-78 Coolant

Nominal boiling point	37.8 °C
Pour point	−73.4 °C
Density at −53.9 °C	1,900 kg/meter^3
Kinematic viscosity	1.5×10^{-6} meter^2/second
Specific heat	2,140 joules/kg-°C
Thermal conductivity	6.9×10^{-4} watt/cm-°C

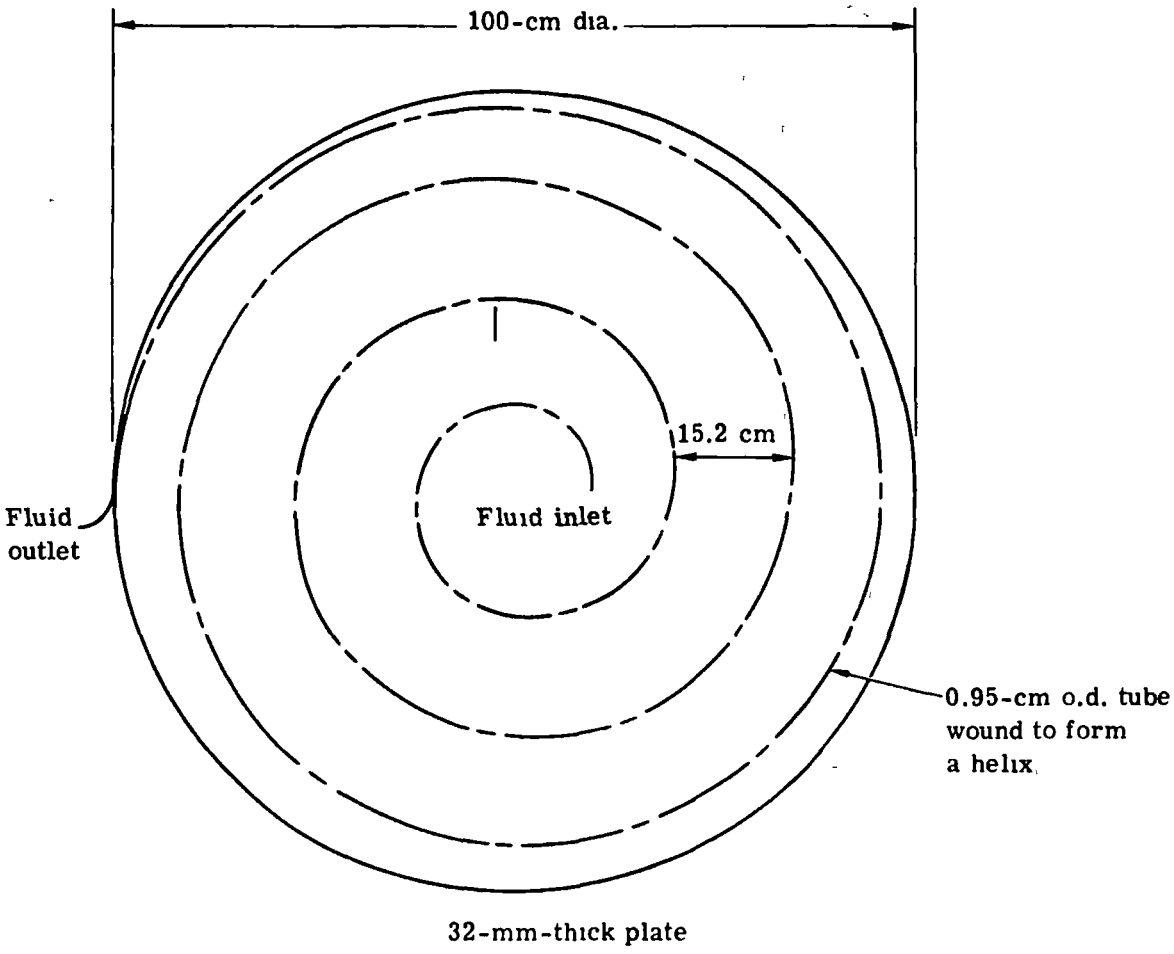

Fig. 3-14 — Primary mirror cold plate fluid loop piping diagram

Table 3-5 — Primary Mirror Fluid Loop Cooling System Analysis Results

Hydraulic	
Mass flow	173.5 kg/hr
Velocity	63.5 cm/sec
Reynolds number	3,600
System pressure drop	44×10^3 newtons/meter^2
Thermal	
Heat transfer coefficient	3.86 10^{-2} watt/cm^2-°C
Bulk temperature rise	3.3 C
Fluid film ΔT	2.36 °C
Cold plate coil ΔT	1.0 °C
Mean cold plate temperature	−37.8 °C
Mean radiator temperature	−45.6 C
System weight	
Increase from baseline	7.08 kg

3.4 HEAT SHIELD MIRROR COOLING ANALYSIS

3.4.1 Baseline Heat Shield Mirror Cooling

As in the case of the primary mirror, the heat shield mirror baseline cooling concept is based on a heat pipe coupled between the external radiator and the internal heat source. For the heat shield mirror, the heat pipe is mounted directly on the rear surface of the mirror. We took this approach because we can achieve better thermal coupling and cause no problems with the system optics. Fig. 3-15 shows the baseline concept.

During the performance of the external thermal finish and insulation parametric study conducted with the previously described system model, heat shield mirror temperatures were calculated. In all cases the mirror temperature remains at or near the baseline value of 21.1 °C with only a minor orbital variation of approximately ± 0.66 °C. This behavior is illustrated by Figs. 3-16 and 3-17 for the low emittance shell, uninsulated and insulated, respectively.

3.4.2 Alternative Heat Shield Mirror Cooling Concepts

We conducted a detailed investigation of two alternative concepts for heat shield mirror thermal control. The concepts examined were·

1. Self-contained fluid loop thermal control
2. Radiative fin thermal control.

Each concept was required to reject the absorbed heat shield mirror thermal load of 48 watts and maintain temperature at 21.1 ± 11 °C. Additional boundary conditions applicable to the study included an uninsulated meteoroid shell with a low emittance external surface finish (α/ϵ = 0.12/0.04).

Self-Contained Fluid Loop

The design of a fluid loop cooling system involves the determination of several interdependent parameters, and a complete parametric study is required to optimize such a system. The intent of this task was not to optimize but rather investigate the feasibility of this thermal control concept as applied to a Shuttle mission, and therefore certain parameters were fixed at the beginning of analysis. These included the type of working fluid, tube size, and coil configuration.

The fluid loop cooling system is shown schematically in Fig. 3-18. The system was required to reject an absorbed thermal load of 48 watts from the heat shield mirror and maintain thermal control at 21.1 ± 11 °C. The system consists of integral cooling coils (0.95 centimeter outside diameter copper tubing) mounted to the heat shield mirror, integral coiling coils mounted to an external radiator, a circulating pump and motor, flow control valves, and a fluid reservoir. To reduce vibrations, both the mirror and radiator are connected to the fluid lines by flexible couplings while the pump and motor are mounted on vibration isolators.

A 40-60 mixture of ethylene glycol and water was chosen as a working fluid. The physical properties of this mixture at 21.1 °C are

Specific heat	3,460 joules/kilogram-°C
Thermal conductivity	0.0052 watt/cm-°C
Dynamic viscosity	0.0028 newton-second/meter^2
Density	1,004.2 kilograms/meter^3

A serpentine coil configuration on a 2.54-centimeter center mounted to the mirror and radiator was chosen for analysis. The radiator was positioned on the underside of the photoheliograph so as to view the Shuttle floor, and thus provide a relatively stable sink. Heat loads on

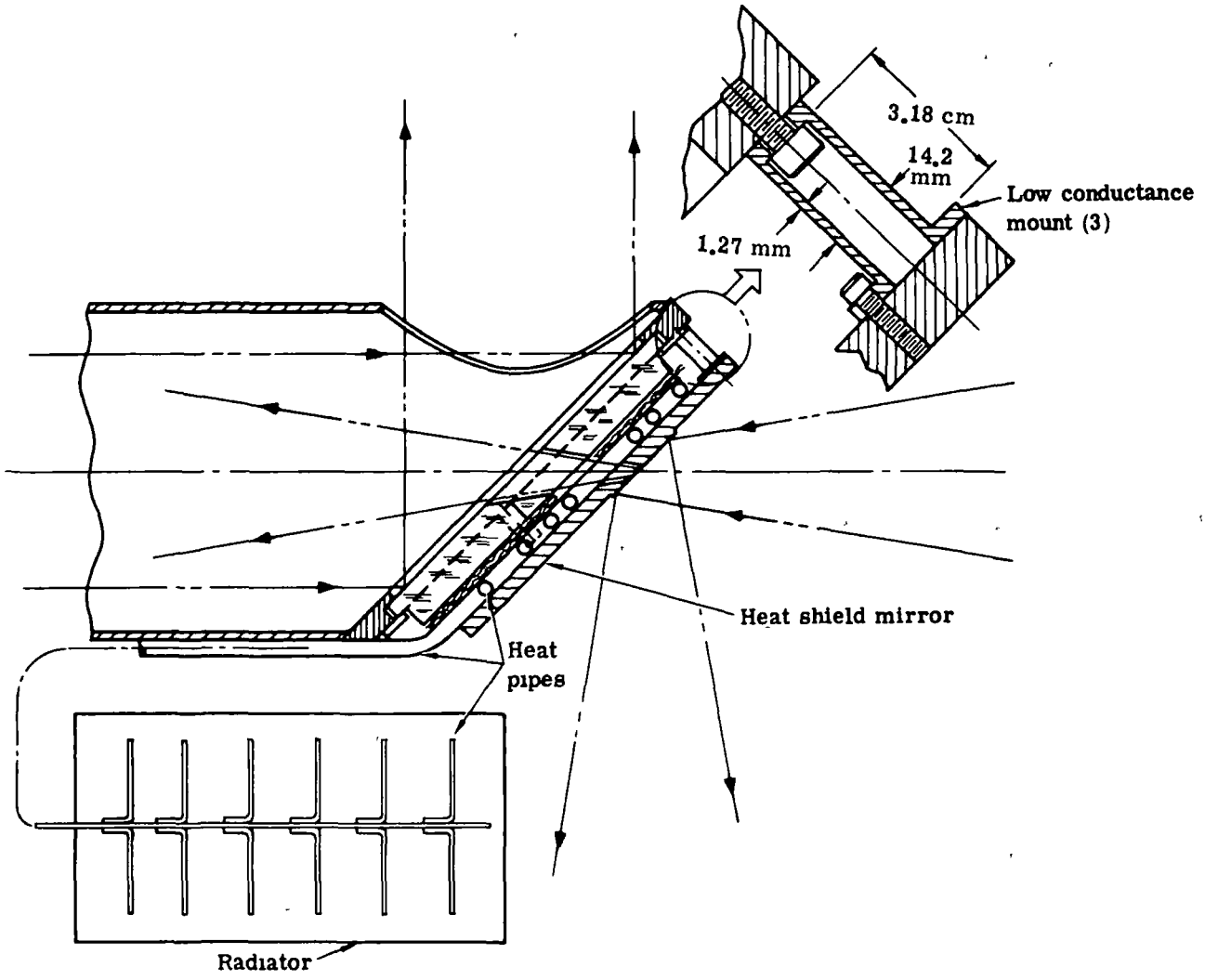

Fig. 3-15 — Heat shield mirror heat pipe cooling concept

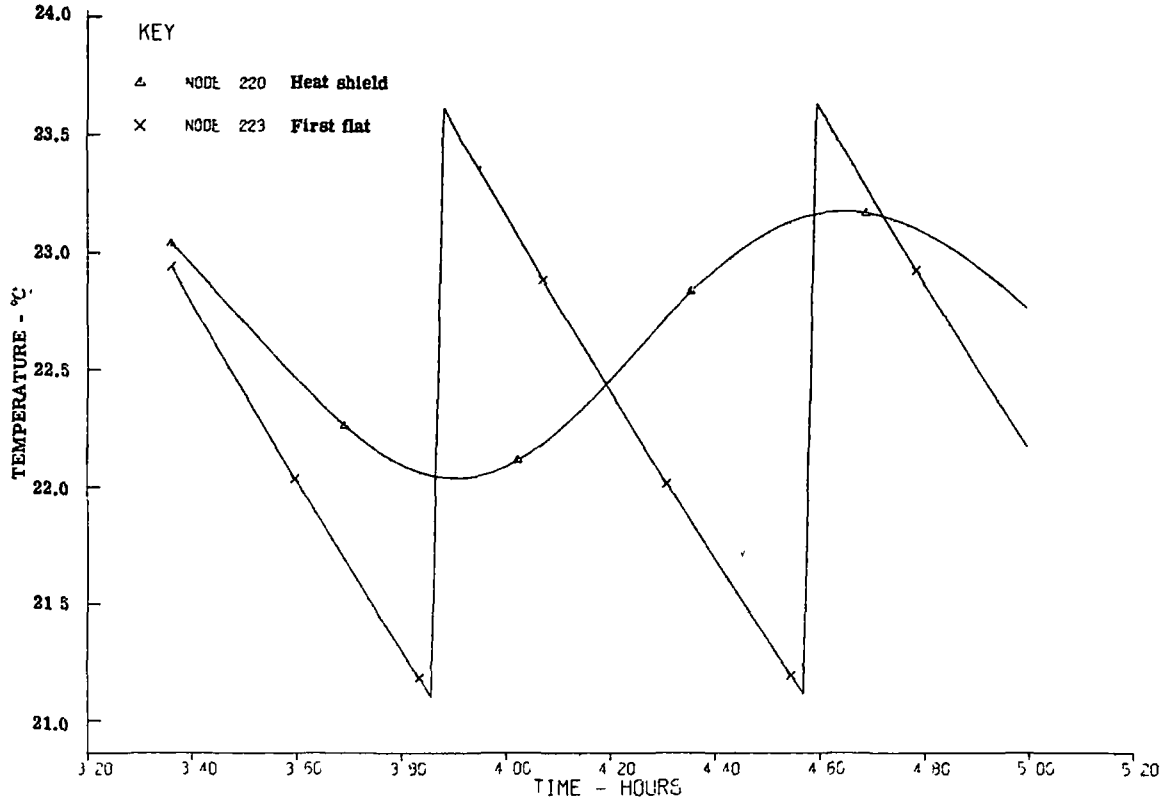

Fig. 3-16 — Temperature history for heat shield mirror and first relay mirror—uninsulated (α/ϵ = 0.12/0.04)

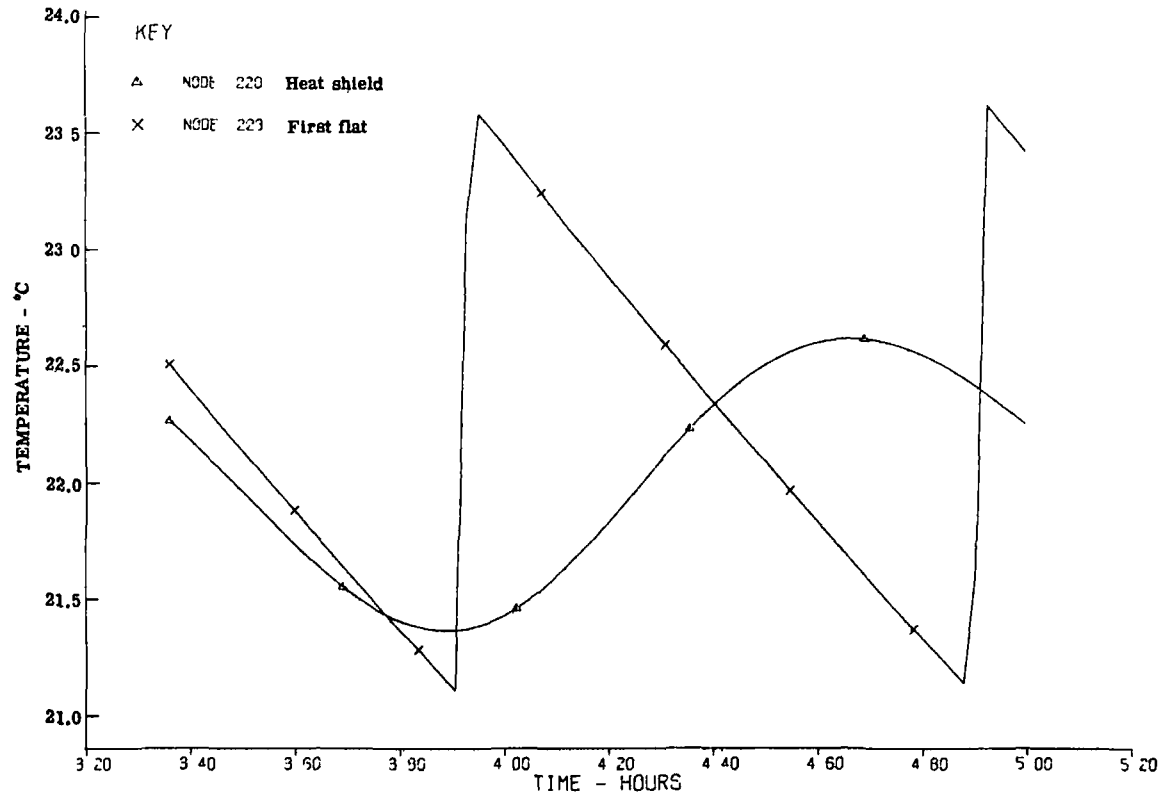

Fig. 3-17 — Temperature history for heat shield mirror and first relay mirror—insulated (α/ϵ = 0.12/0.04)

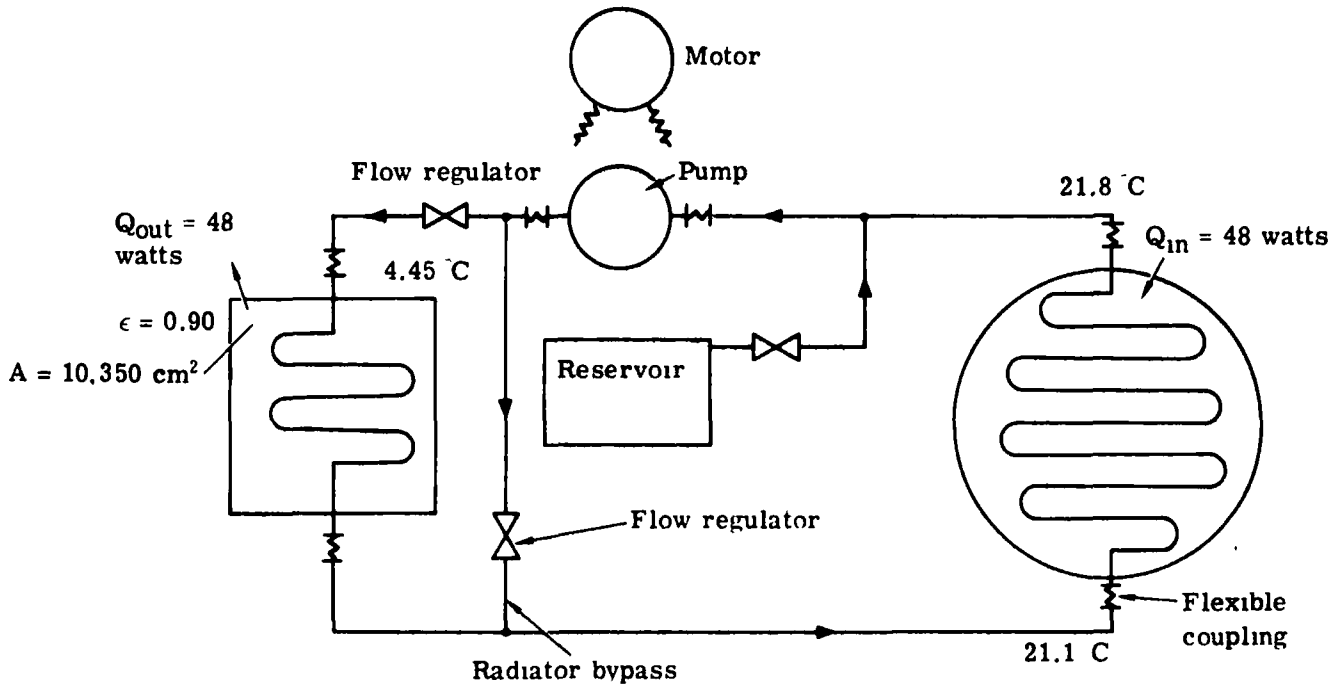

Fig. 3-18 — Heat shield mirror fluid loop cooling system

the radiator from the Shuttle floor and heat loss to deep space were considered in sizing the radiator. A radiator area of approximately 10,350 square centimeters is needed to reject the absorbed heat shield mirror thermal load. The radiator selected is an aluminum sheet 100 by 100 centimeters by 1.57 millimeters thick with an external emissivity of 0.90.

Using the above conditions, we conducted a hydraulic and thermal analysis of the system. The results of this analysis are presented in Table 3-6, including the total weight of the system.

Radiative Fin

We investigated a radiative fin concept as an alternative thermal control system for the photoheliograph heat shield mirror. As shown in Fig. 3-19, the system consists of a cylindrical aluminum fin extending from the heat shield mirror. The purpose of this system is to transfer the absorbed thermal load from the mirror by conduction to this cylindrical fin. Heat rejection from the fin is accomplished by radiation to the interior walls of the vehicle and to deep space. The total external surface area of the fin is approximately 3,760 square centimeters and has a high emittance finish (ϵ = 0.90).

A nodal model was made of the radiative fin system and incorporated into the existing photoheliograph/Shuttle thermal model in accordance with Fig. 3-20. Operation of the thermal model of the photoheliograph radiating fin indicated that the heat shield mirror and the first relay flat (immediately behind it) overheat. Furthermore, overheating also occurs at the secondary mirror. The behavior of the heat shield mirror and the first relay are shown in Figs. 3-21 and 3-22 for the 20-hour time period used in the computer run. We also note that the plotted temperatures have not reached steady state and are still increasing at the conclusion of the 20-hour period.

A review of these results indicates that they are in general agreement with a hand analysis performed concurrently with the operation of the thermal model. Overheating of the heat shield results from the concentrated solar heat load coupled with the thermal resistance of the mirror-to-fin connections. In the case of the first relay, overheating results from an increase in thermal sink temperature from a baseline value of approximately 4.45 °C to approximately 21.1 °C for the radiating fin design, which results in increased temperatures of approximately the same order on the relay flat.

The current radiative fin has been modeled optimistically (high conductivity, high emittance, reasonably thick, and as long as possible). In spite of these conditions, the results indicate heat shield and relay flat temperatures at least 12.2 and 10 °C in excess of the maximum system requirement of 32.2 °C. After examining prior data for a low α, high ϵ, external surface finish that runs colder than the baseline design, we concluded that a maximum component temperature decrease of 5.5 °C is attainable by changing thermal finishes. Even this change will not result in the components meeting our current baseline temperature requirement.

3.5 SECONDARY METERING STRUCTURE

The goal of our efforts in the secondary metering structure area was to evaluate the thermal response of the structure to variations in external thermal control coating both with and without an internal multilayer insulating blanket. Toward this end, the system thermal model was used to evaluate four cases representing a combination of high and low emittance values with and without insulation. All cases were evaluated for the same sun-synchronous Shuttle orbit.

Results of these computer runs in terms of structural temperature response are given in Table 3-7, which tabulates the various circumferential and axial gradients. A more detailed view of the data is presented in Figs. 3-23 through 3-46 for the four cases.

An evaluation of truss temperature response and its effect on the allowable primary to secondary spacing was conducted for three candidate truss material configurations athermalized

Table 3-6 — Heat Shield Mirror Fluid Loop Cooling System Analysis Results

Hydraulic	
Mass flow	70 kg/hr
Velocity	37.8 cm/sec
Reynolds number	1,128
System pressure drop	29.9×10^3 newtons/meter^2
Thermal	
Heat transfer coefficient	4.06×10^{-2} watt/cm^2-°C
Bulk temperature rise	0.69 °C
Fluid film ΔT	2.28 °C
Weight total	6.8 kg

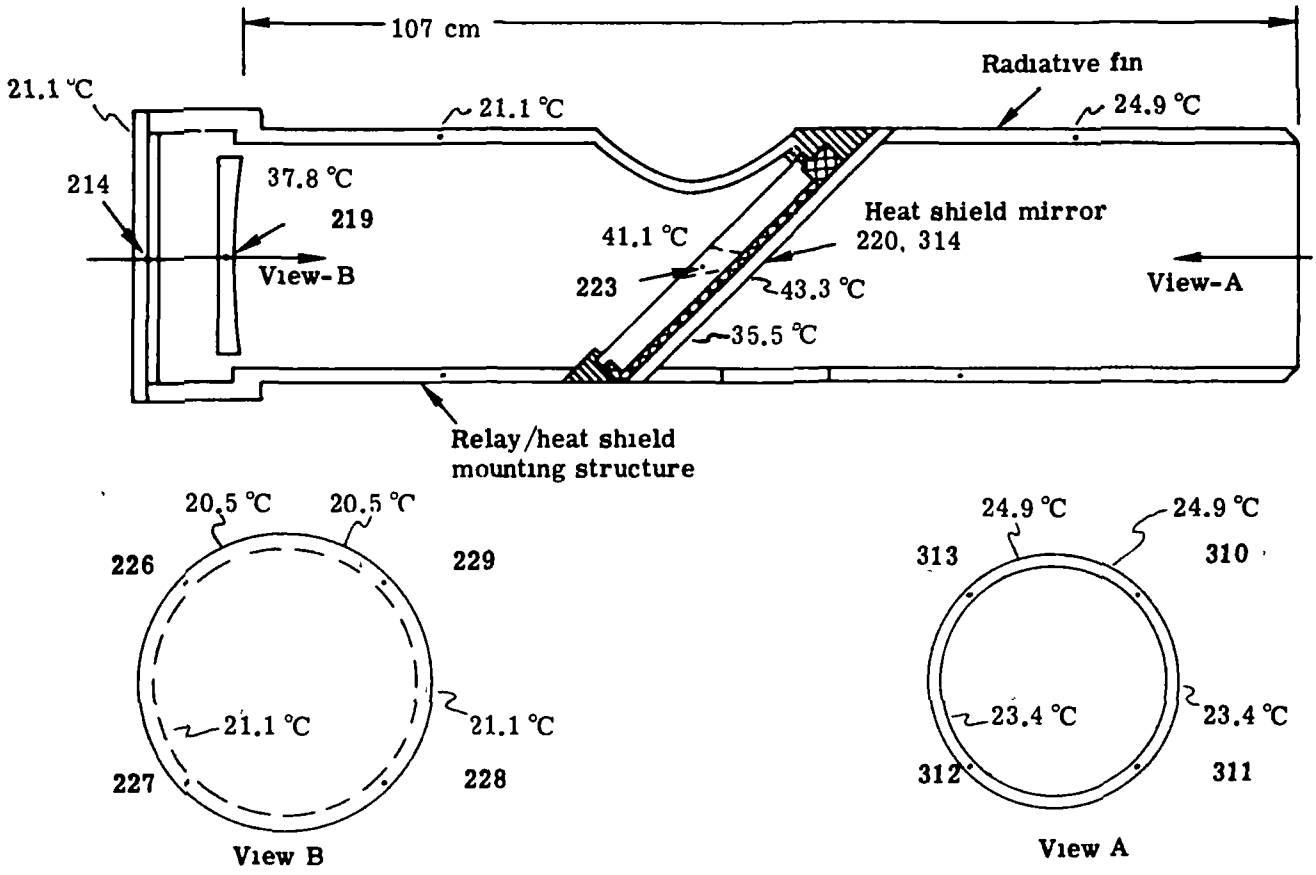

Fig. 3-19 — Heat shield mirror fin cooling concept

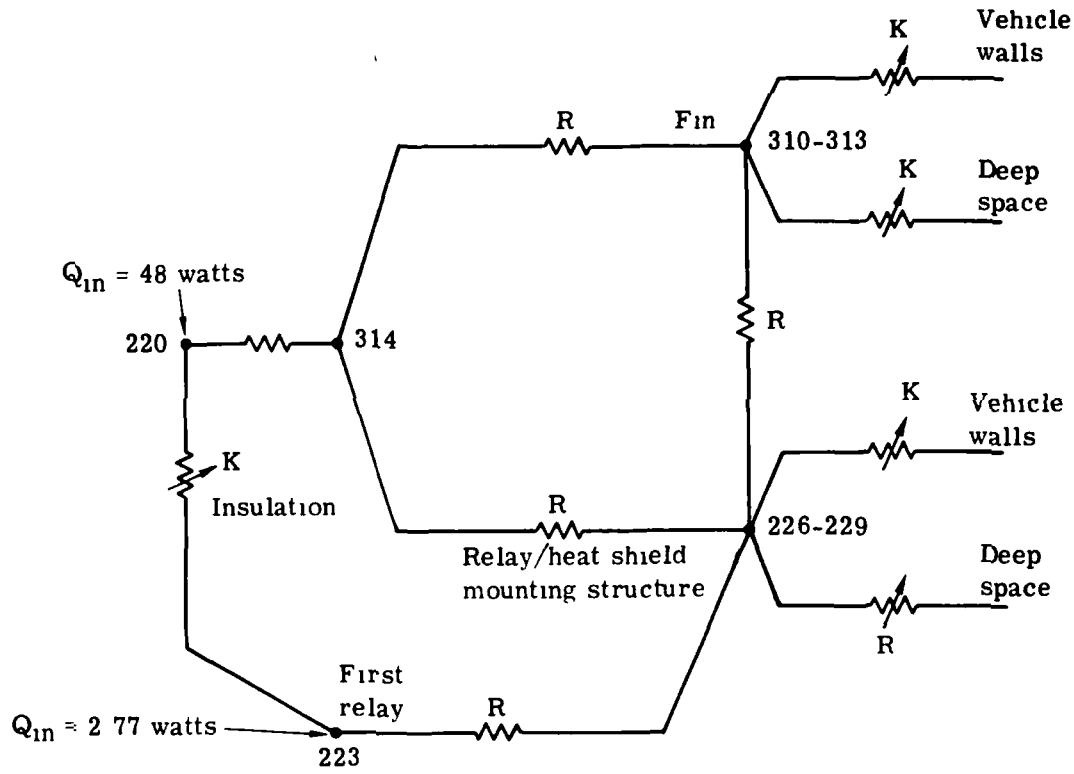

Fig. 3-20 — Simplified thermal network radiative fin concept

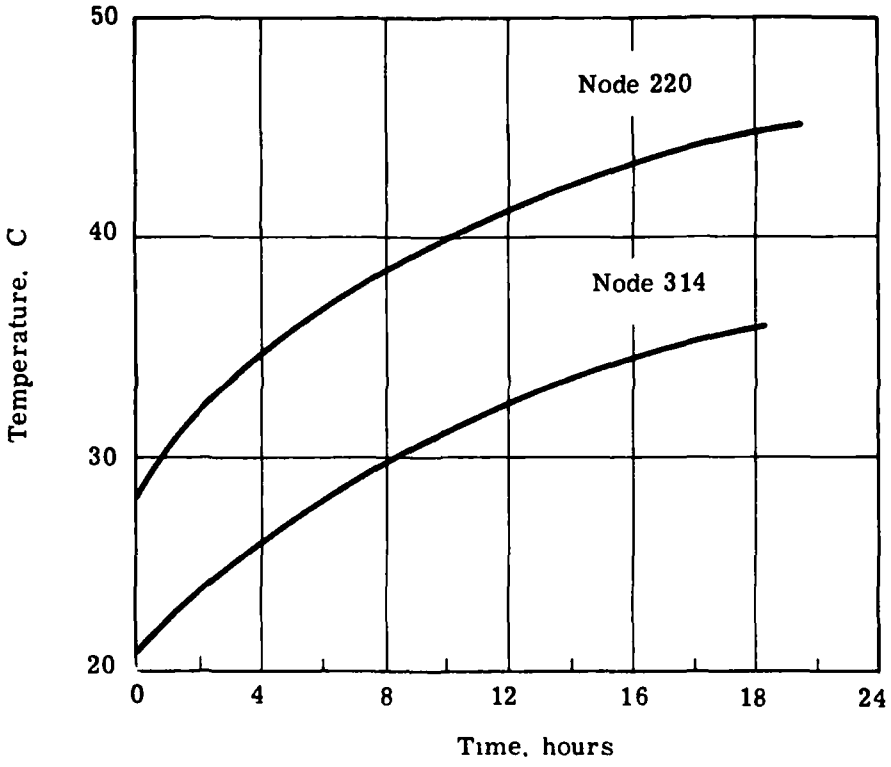

Fig. 3-21 — Temperature history for heat shield mirror

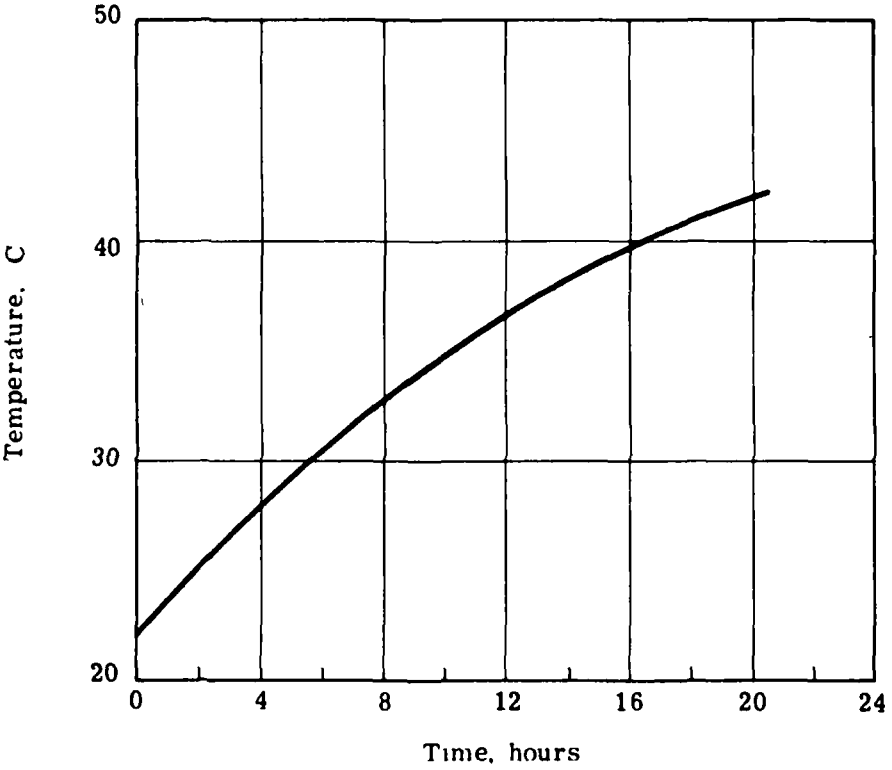

Fig. 3-22 — Temperature history for first relay mirror

Table 3-7 — Shuttle Model Temperature Results

	Case 1 α/ϵ = 0.22/0.88 No Insulation	Case 2 α/ϵ = 0.22/0.88 Insulation	Case 3 α/ϵ = 0.12/0.04 No Insulation	Case 4 α/ϵ = 0.12/0.04 Insulation
Forward circumferential gradient, °C	30.6	1.39	0.61	2.34
Center circumferential gradient, °C	30.6	2.89	1.45	1.9
Rear circumferential gradient, °C	12.8	2.51	2.0	1.45
Top axial gradient, °C	10	10.6	5.0	10
Middle axial gradient, °C	6.1	12.8	7.2	12.2
Bottom axial gradient, °C	11.1	13.3	7.2	13.9

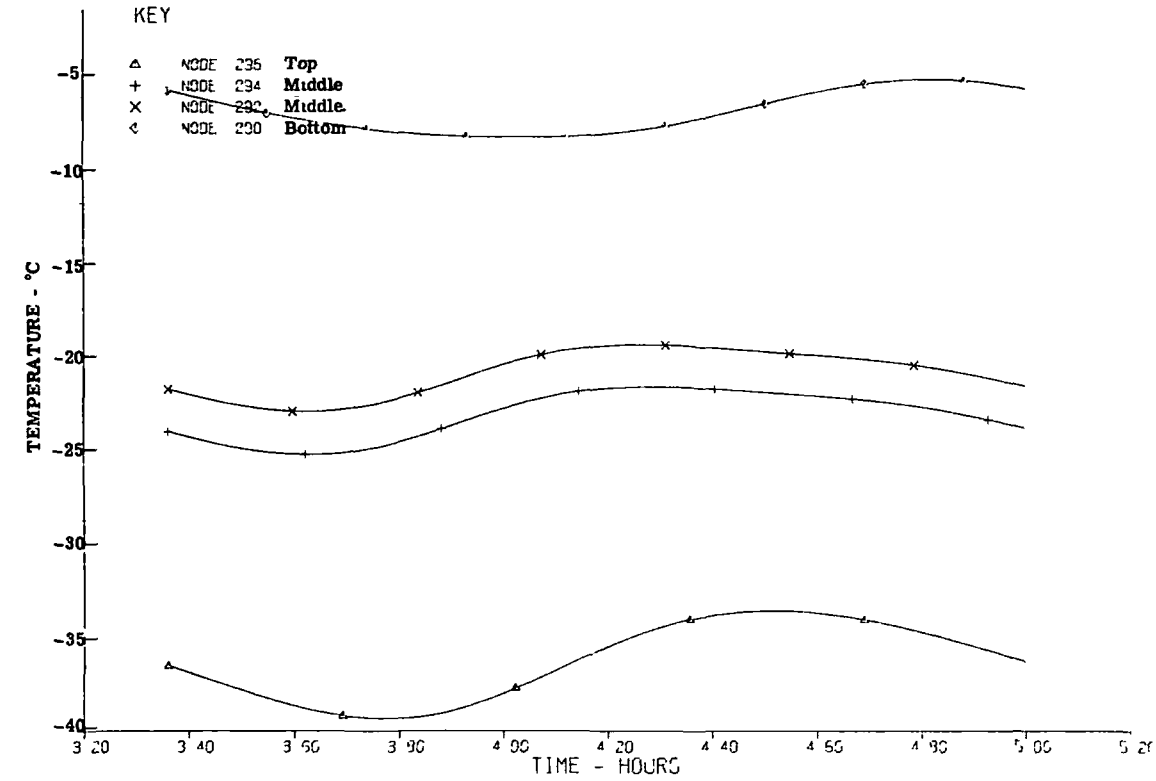

Fig. 3-23 — Temperature history for truss forward circumferential gradient—uninsulated (α/ϵ = 0.22/0.88)

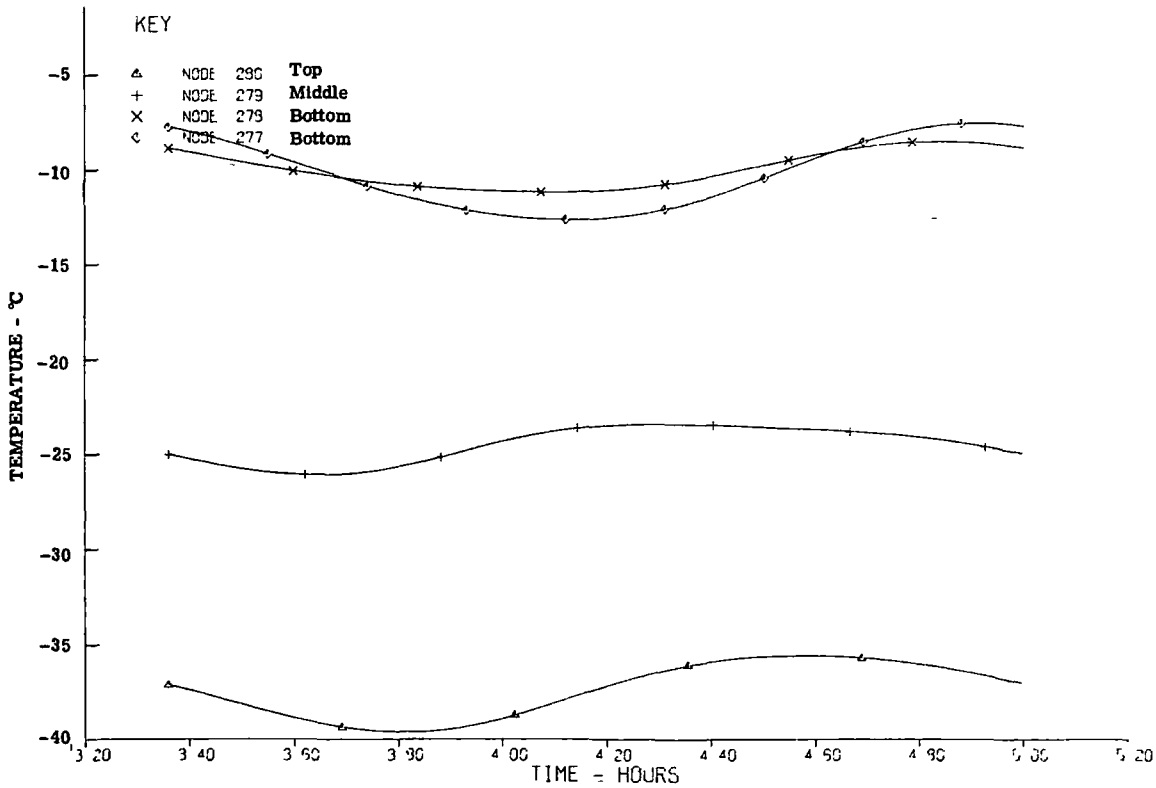

Fig. 3-24 — Temperature history for truss center circumferential gradient—uninsulated (α/ϵ = 0.22/0.88)

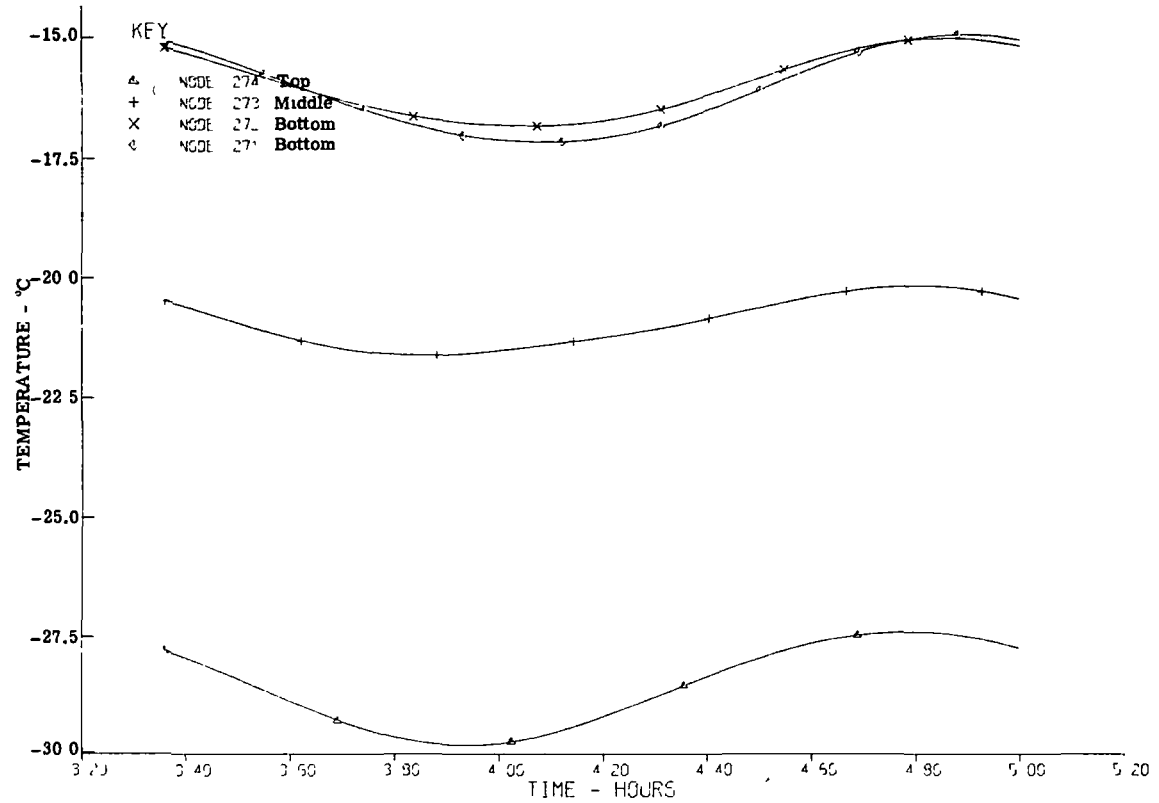

Fig. 3-25 — Temperature history for truss rear circumferential gradient—uninsulated (α/ϵ = 0.22/0.88)

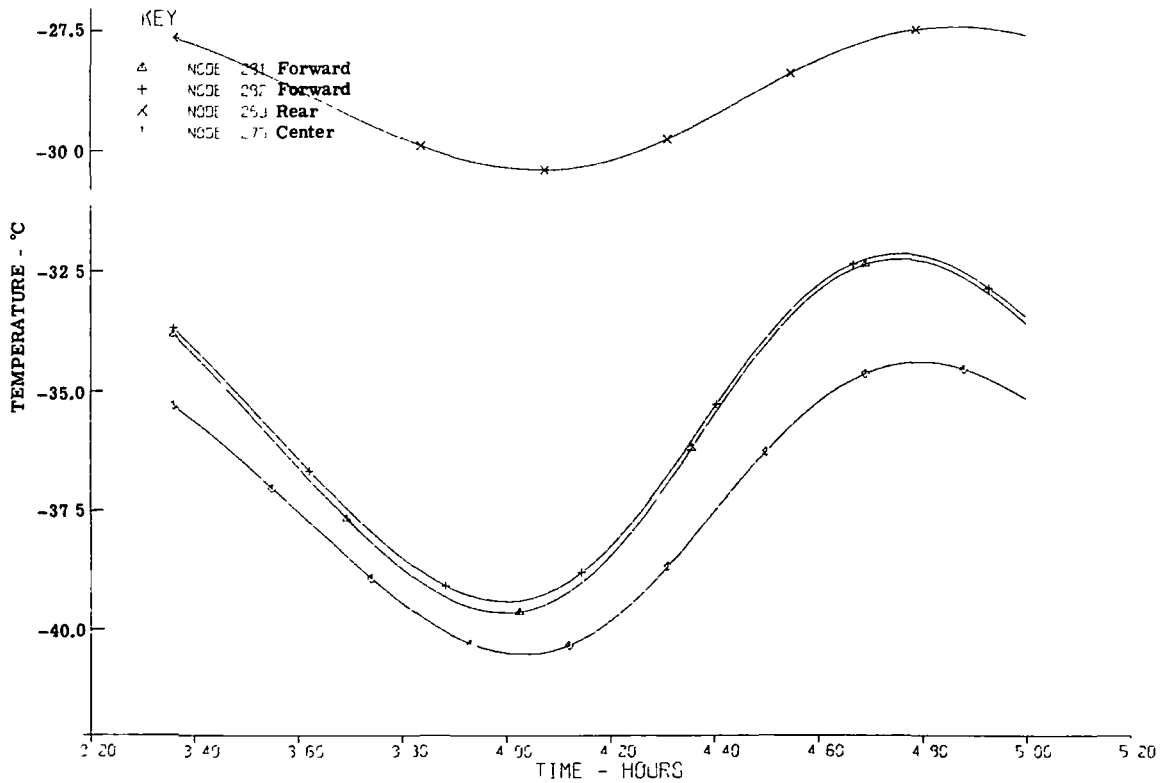

Fig. 3-26 — Temperature history for truss top axial gradient—uninsulated (α/ϵ = 0.22/0.88)

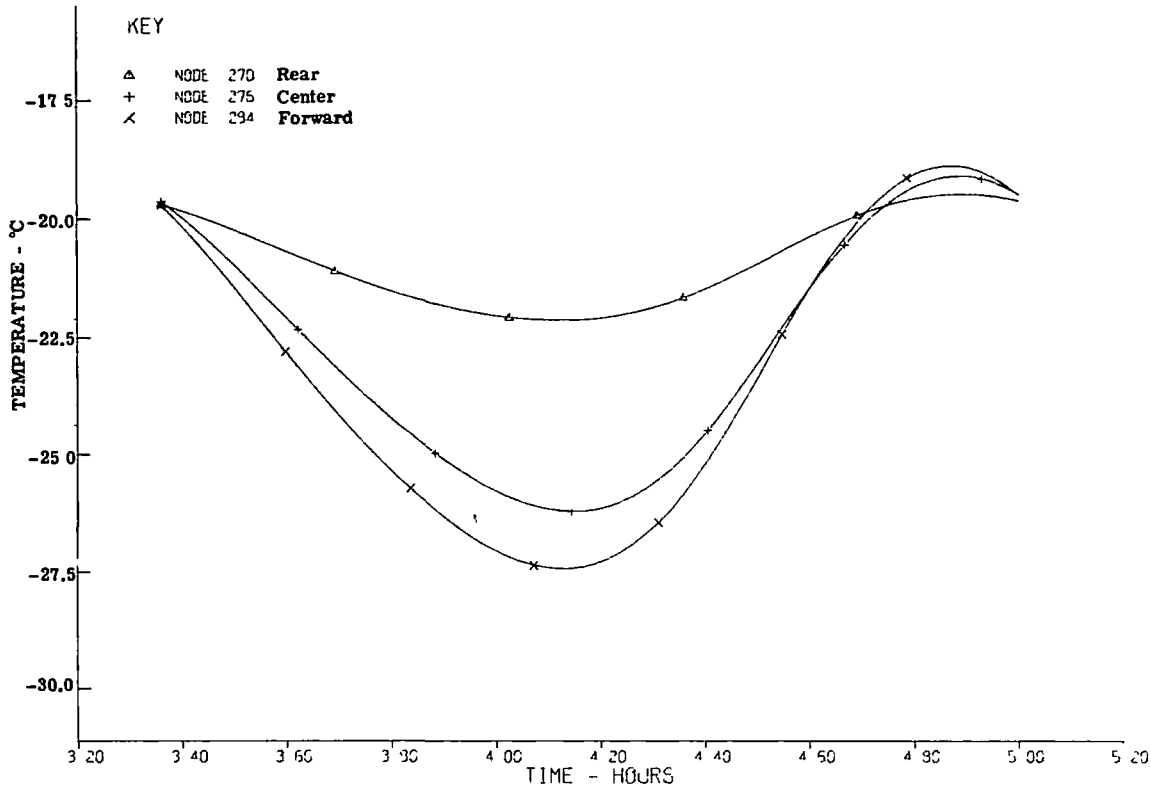

Fig. 3-27 — Temperature history for truss middle axial gradient—uninsulated (α/ϵ = 0.22/0.88)

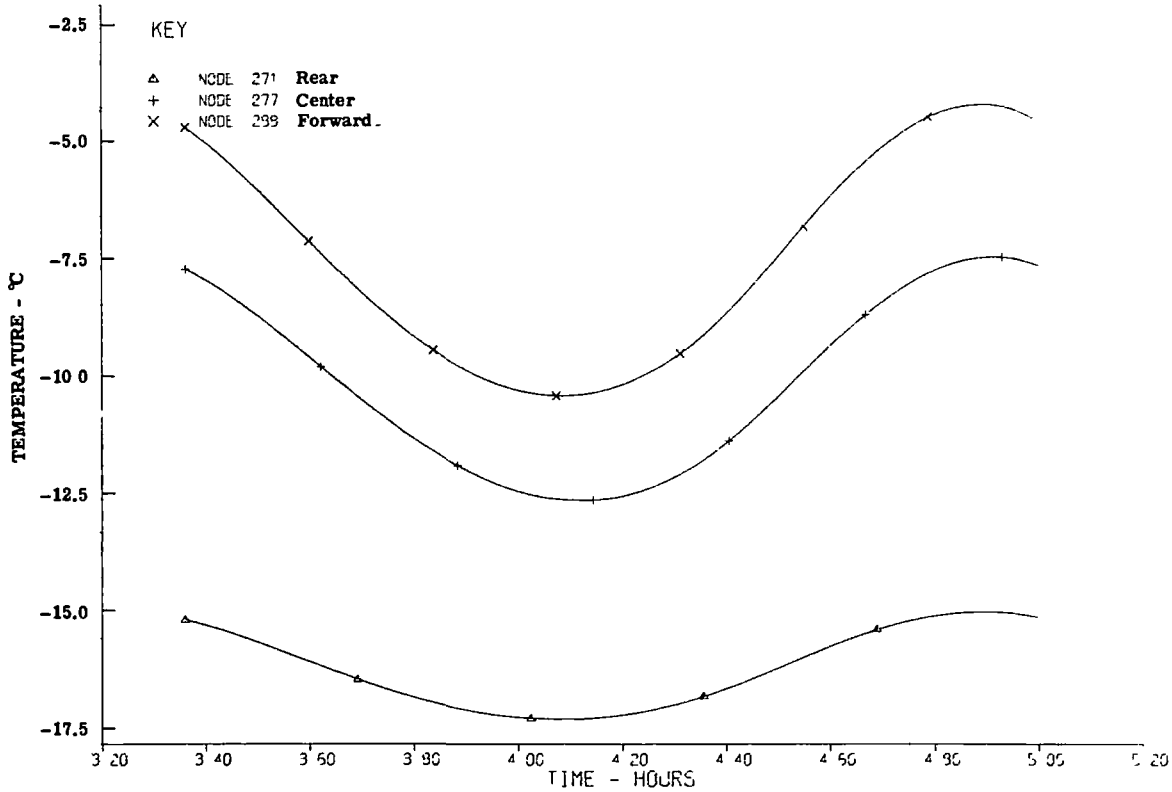

Fig. 3-28 — Temperature history for truss bottom axial gradient—uninsulated (α/ϵ = 0.22/0.88)

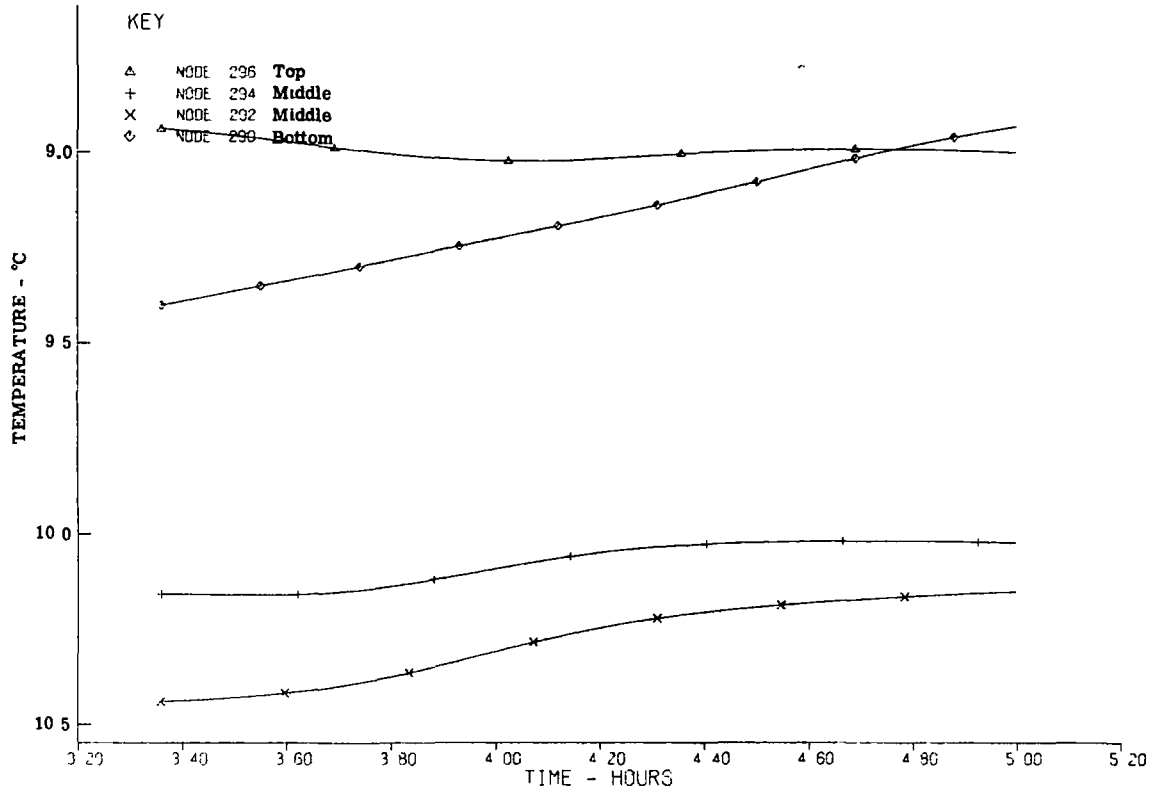

Fig. 3-29 — Temperature history for truss forward circumferential gradient—insulated (α/ϵ = 0.22/0.88)

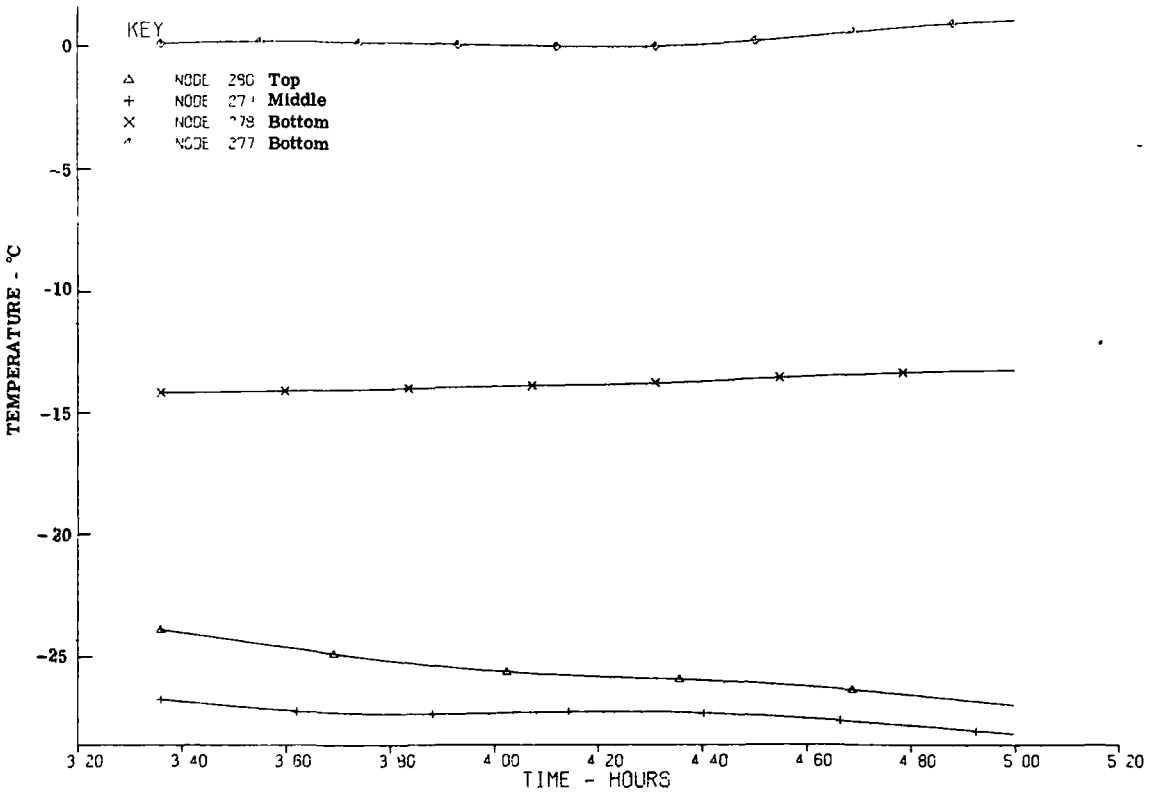

Fig. 3-30 — Temperature history for truss center circumferential gradient—insulated (α/ϵ = 0.22/0.88)

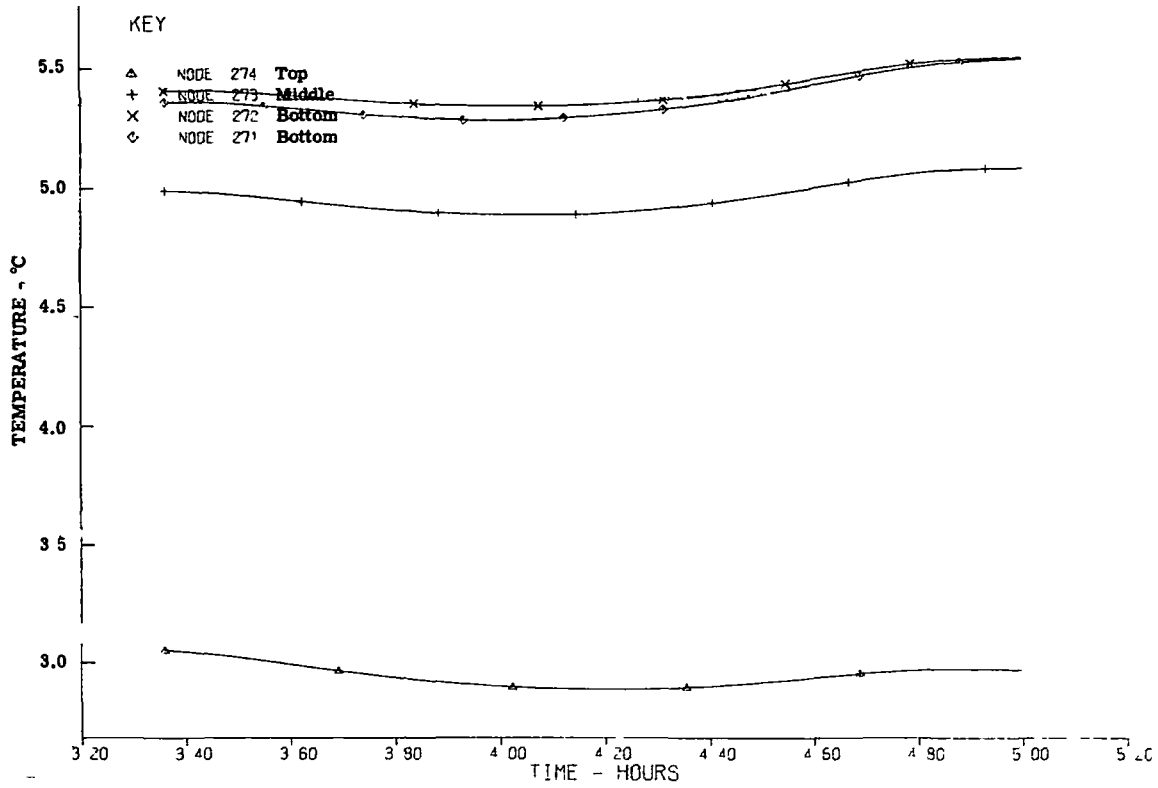

Fig. 3-31 — Temperature history for truss rear circumferential gradient—insulated (α/ϵ = 0.22/0.88)

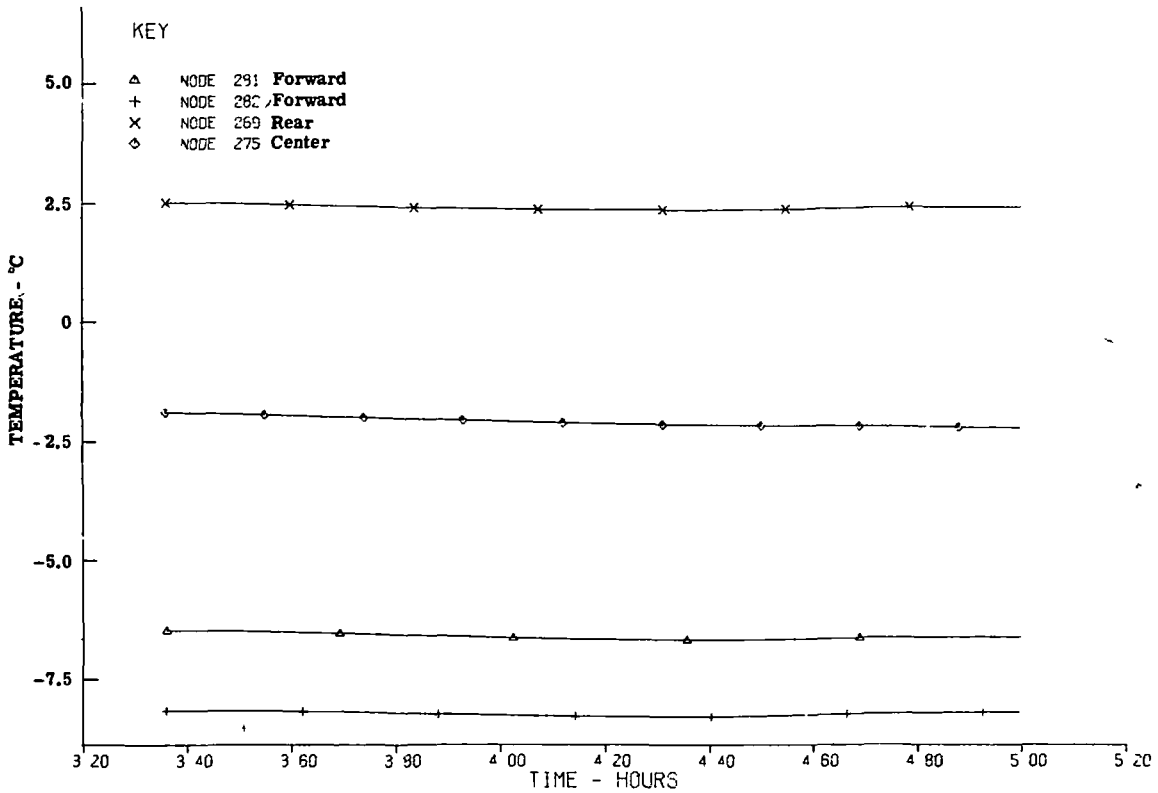

Fig. 3-32 — Temperature history for truss top axial gradient—insulated (α/ϵ = 0.22/0.88)

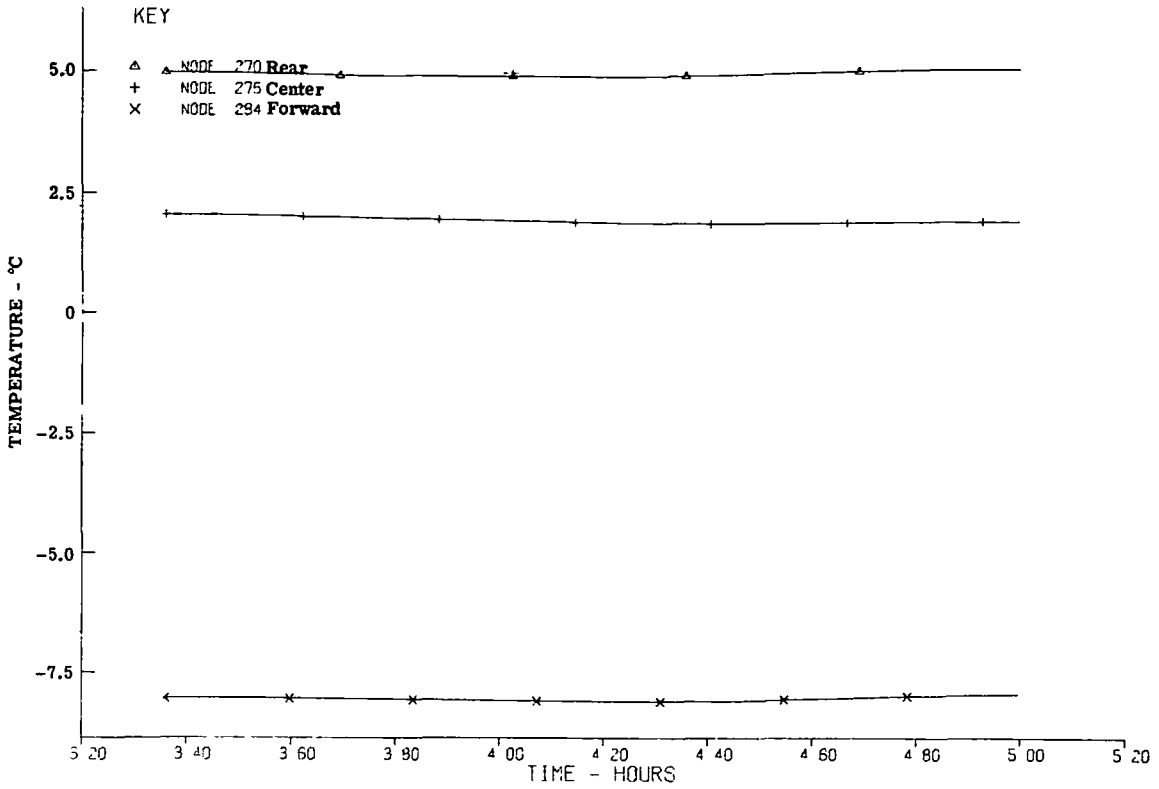

Fig. 3-33 — Temperature history for truss middle axial gradient—insulated (α/ϵ = 0.22/0.88)

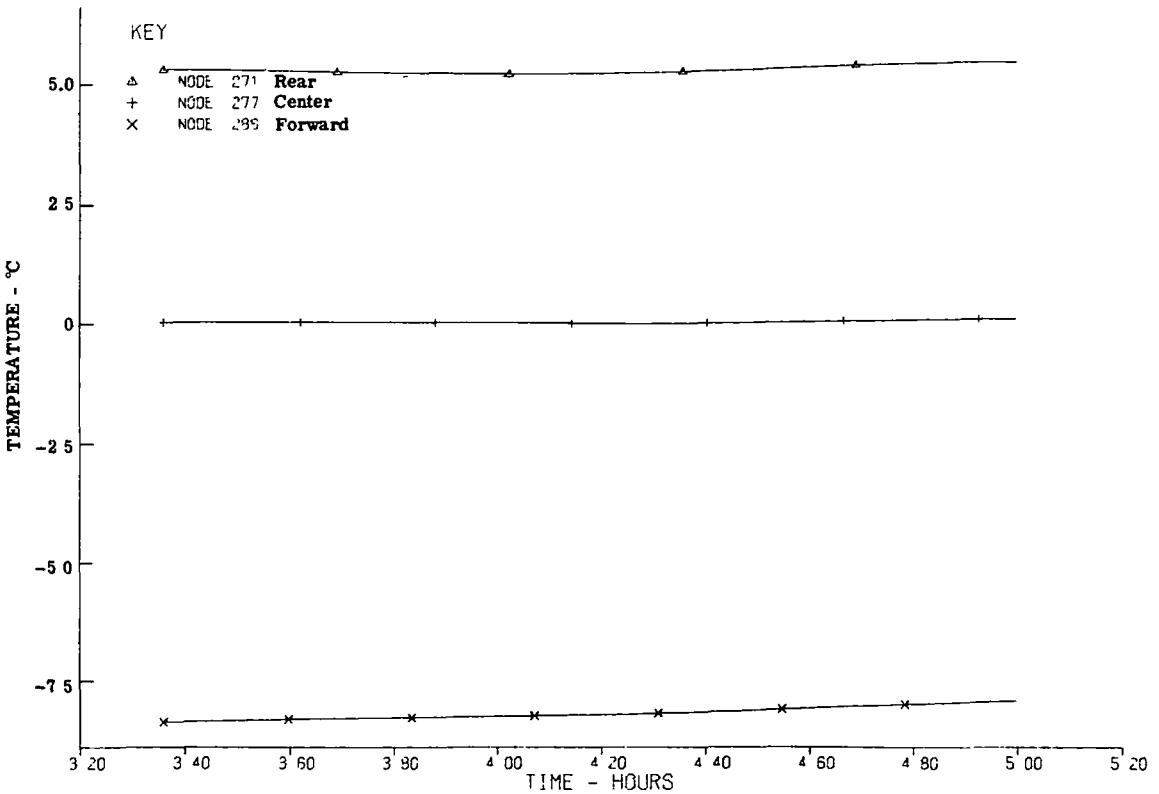

Fig. 3-34 — Temperature history for truss bottom axial gradient—insulated (α/ϵ = 0.22/0.88)

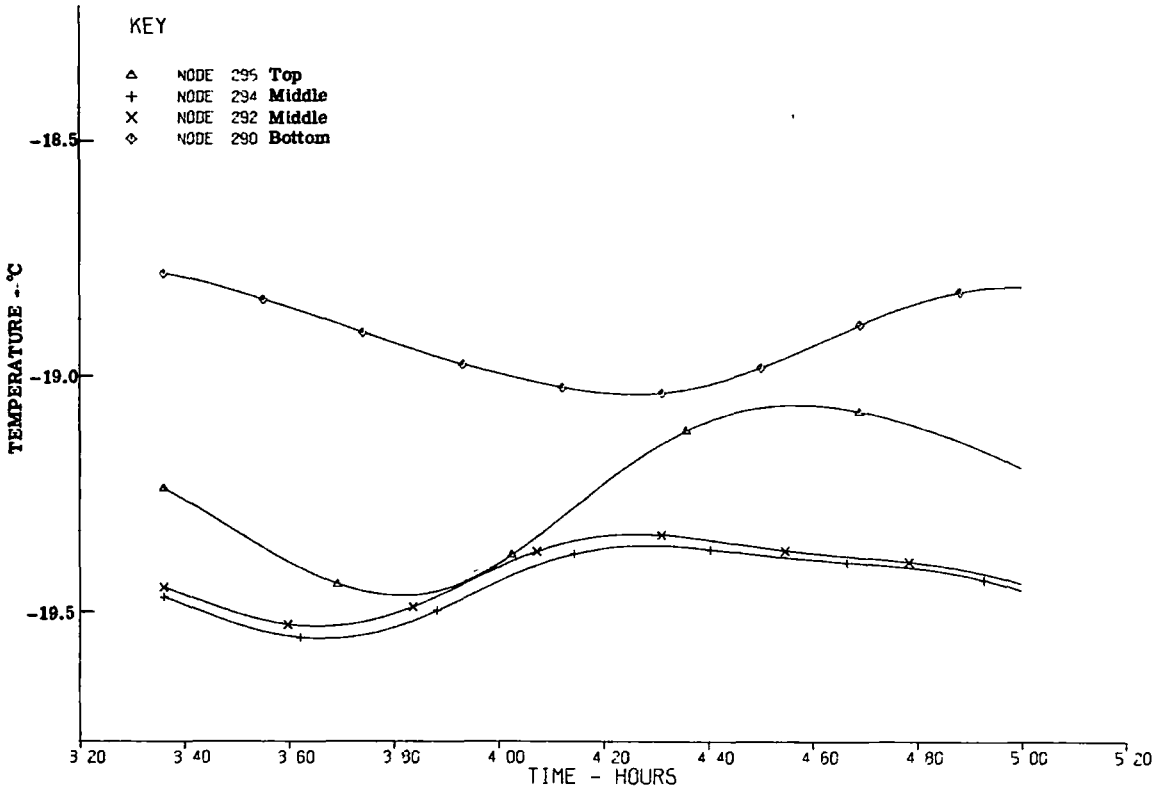

Fig. 3-35 — Temperature history for truss forward circumferential gradient—uninsulated (α/ϵ = 0.12/0.04)

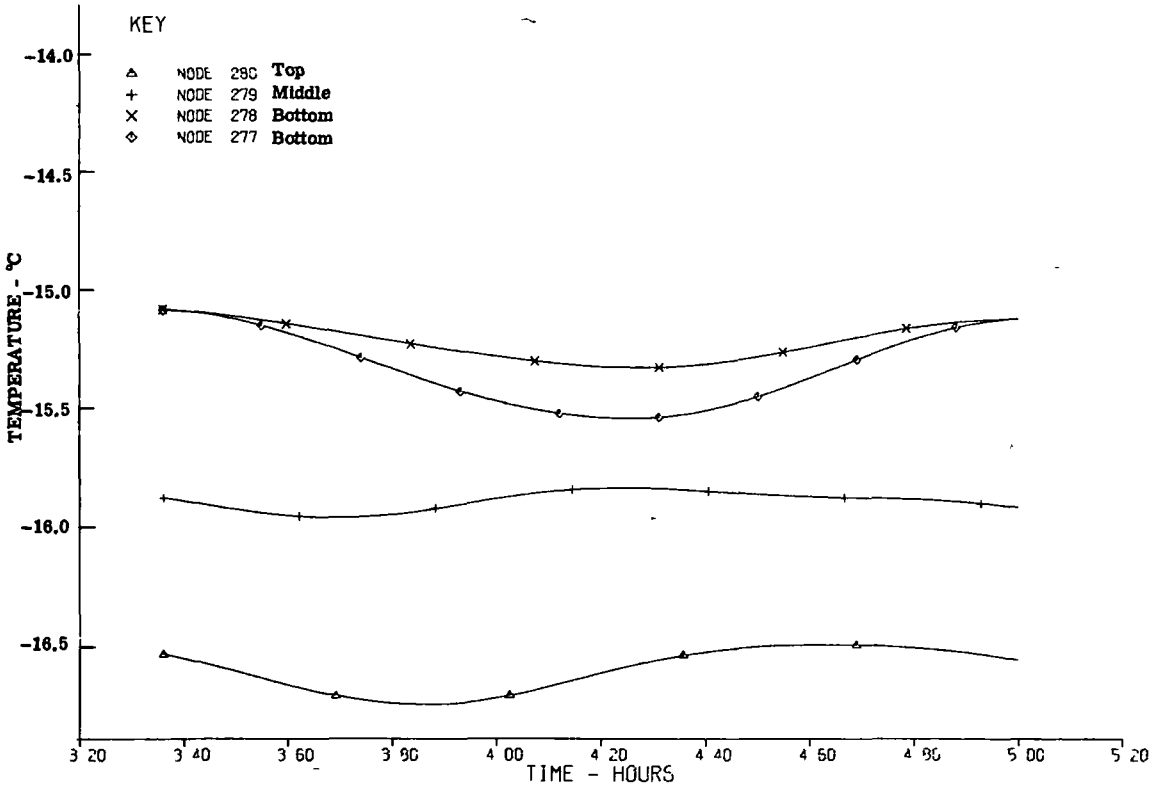

Fig. 3-36 — Temperature history for truss center circumferential gradient—uninsulated (α/ϵ = 0.12/0.04)

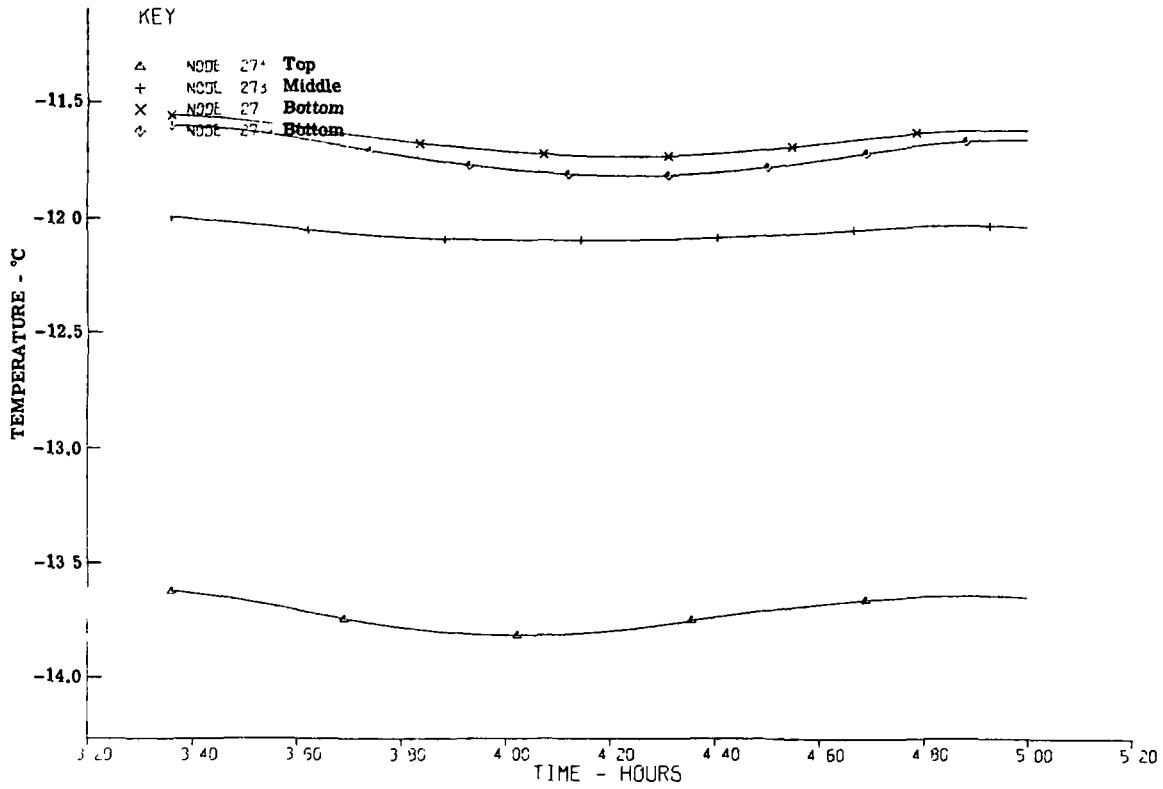

Fig. 3-37 — Temperature history for truss rear circumferential gradient—uninsulated (α/ϵ = 0.12/0.04)

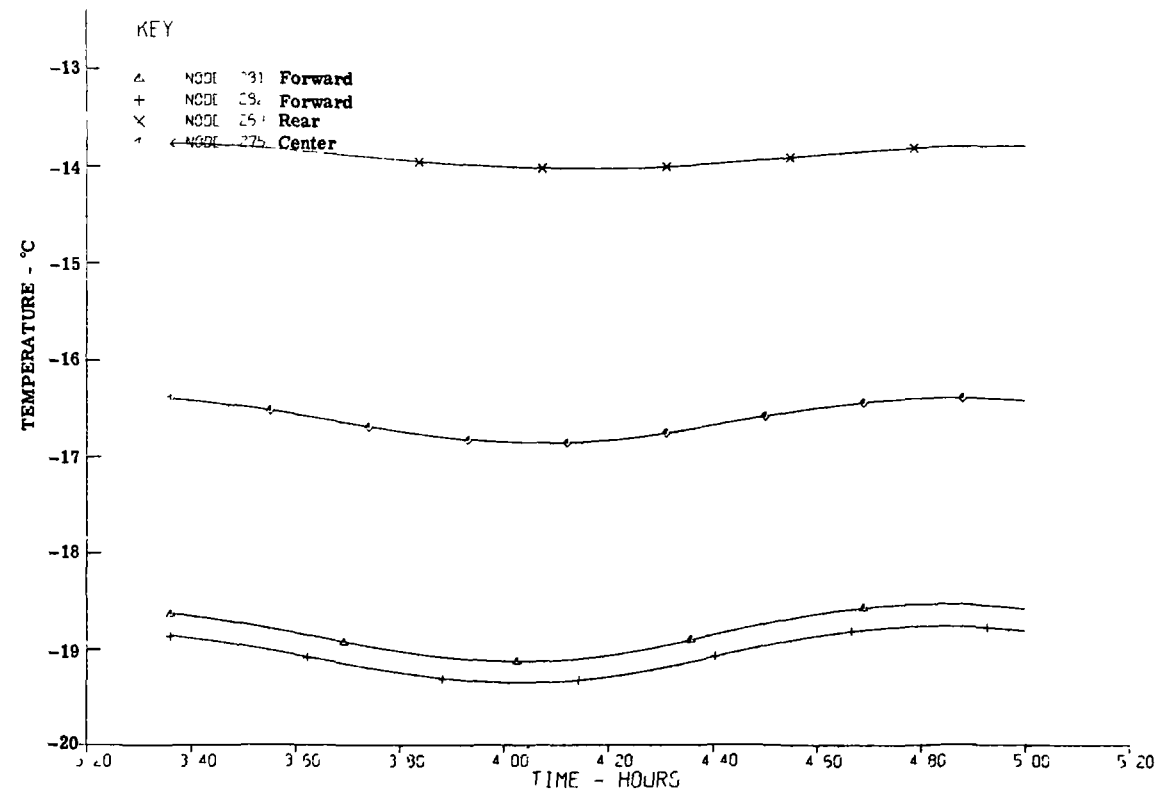

Fig. 3-38 — Temperature history for truss top axial gradient—uninsulated (α/ϵ = 0.12/0.04)

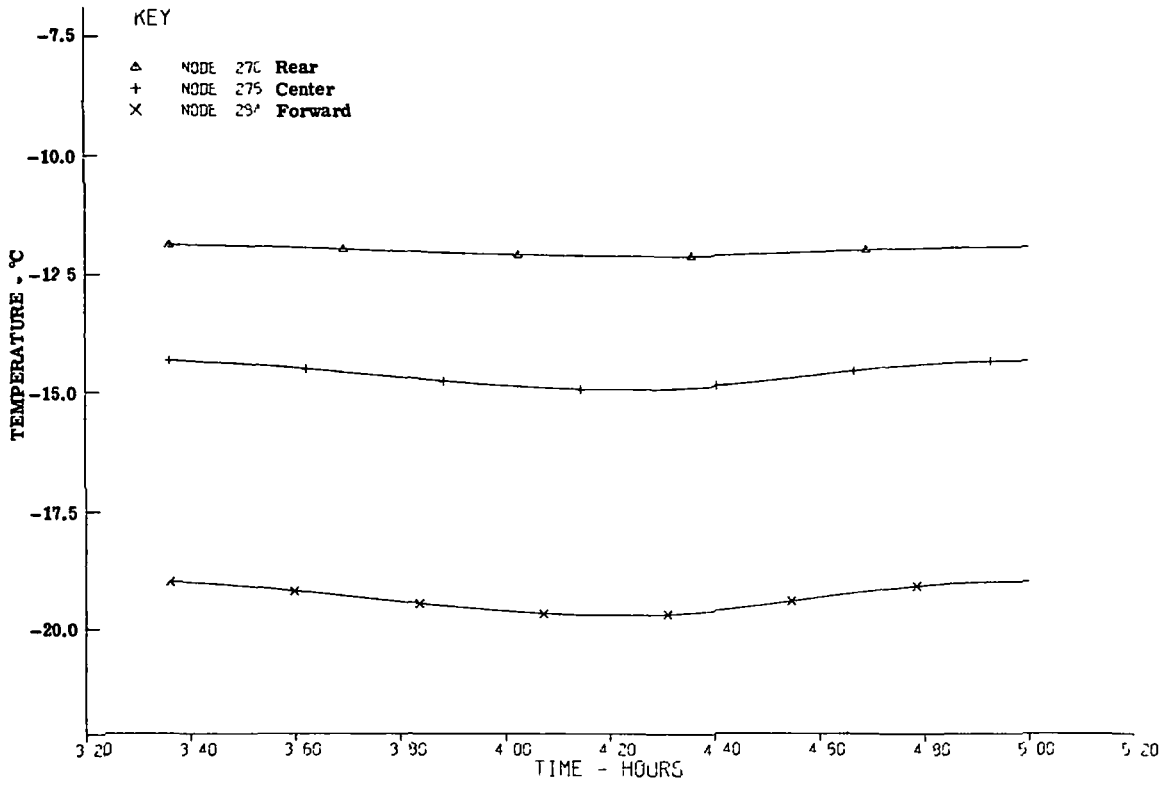

Fig. 3-39 — Temperature history for truss middle axial gradient—uninsulated (α/ϵ = 0.12/0.04)

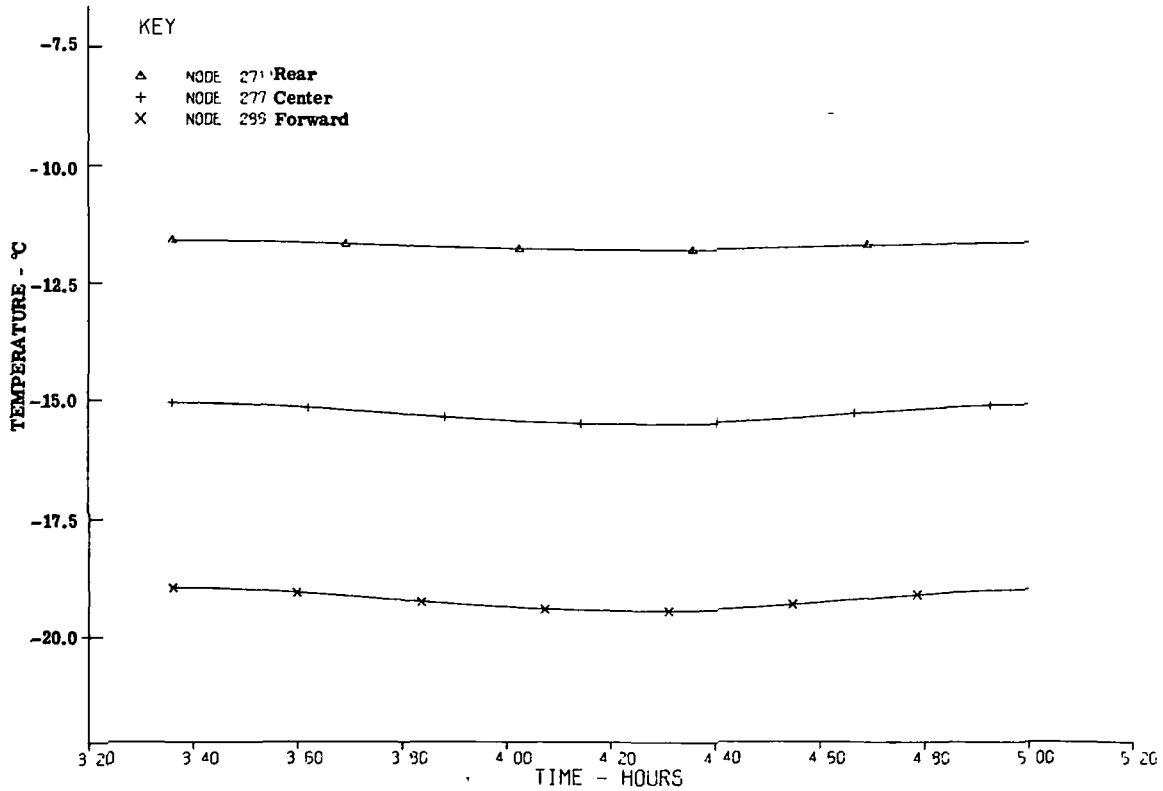

Fig. 3-40 — Temperature history for truss bottom axial gradient—uninsulated (α/ϵ = 0.12/0.04)

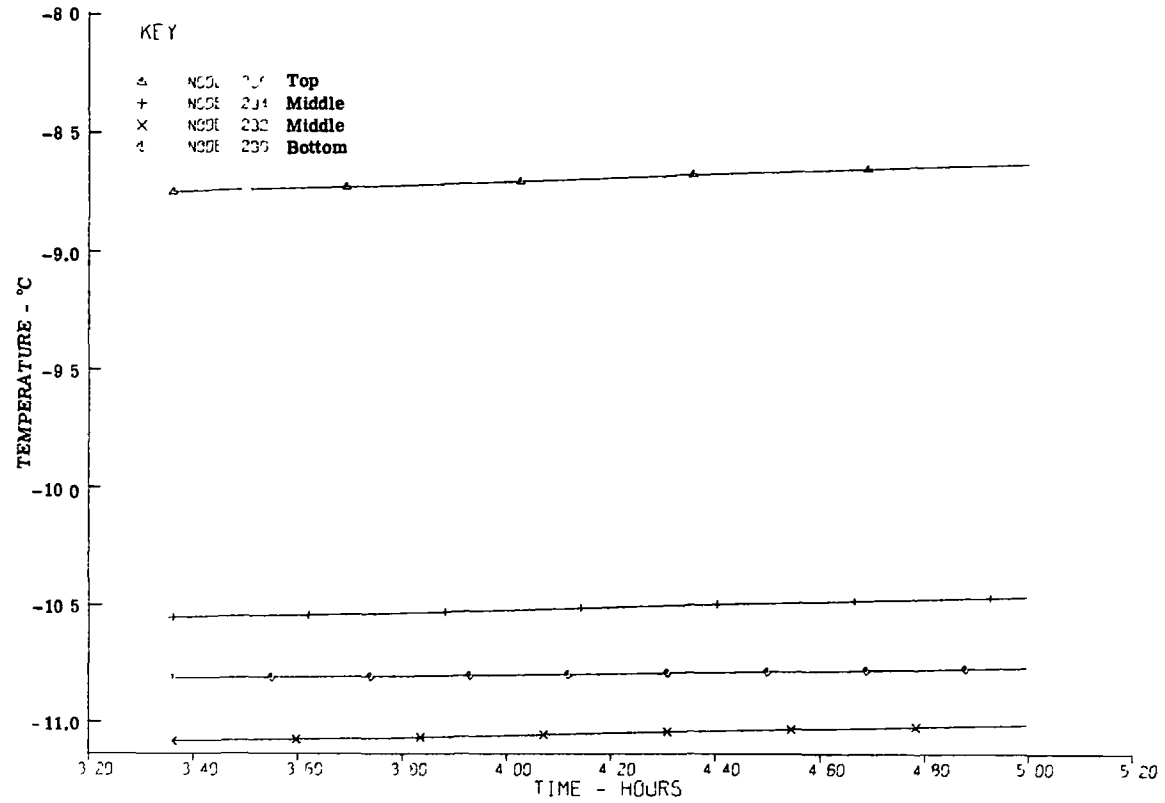

Fig. 3-41 — Temperature history for truss forward circumferential gradient—insulated (α/ϵ = 0.12/0.04)

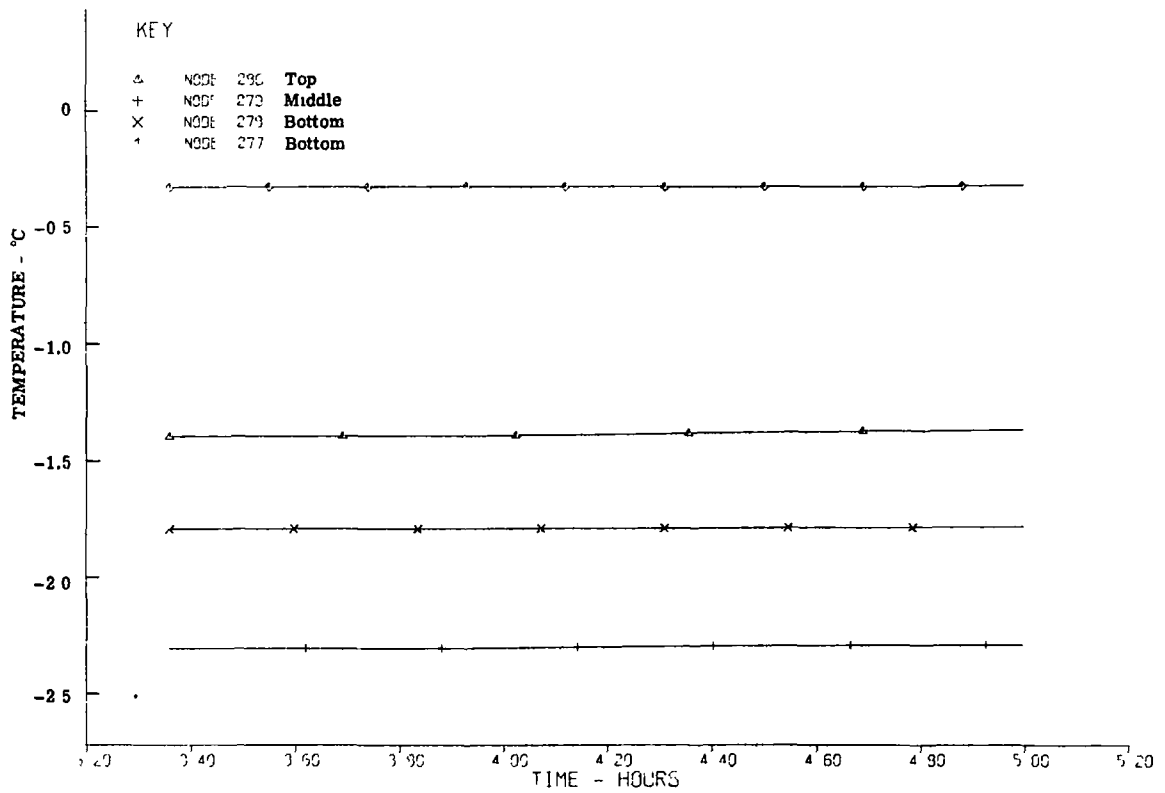

Fig. 3-42 — Temperature history for truss center circumferential gradient—insulated (α/ϵ = 0.12/0.04)

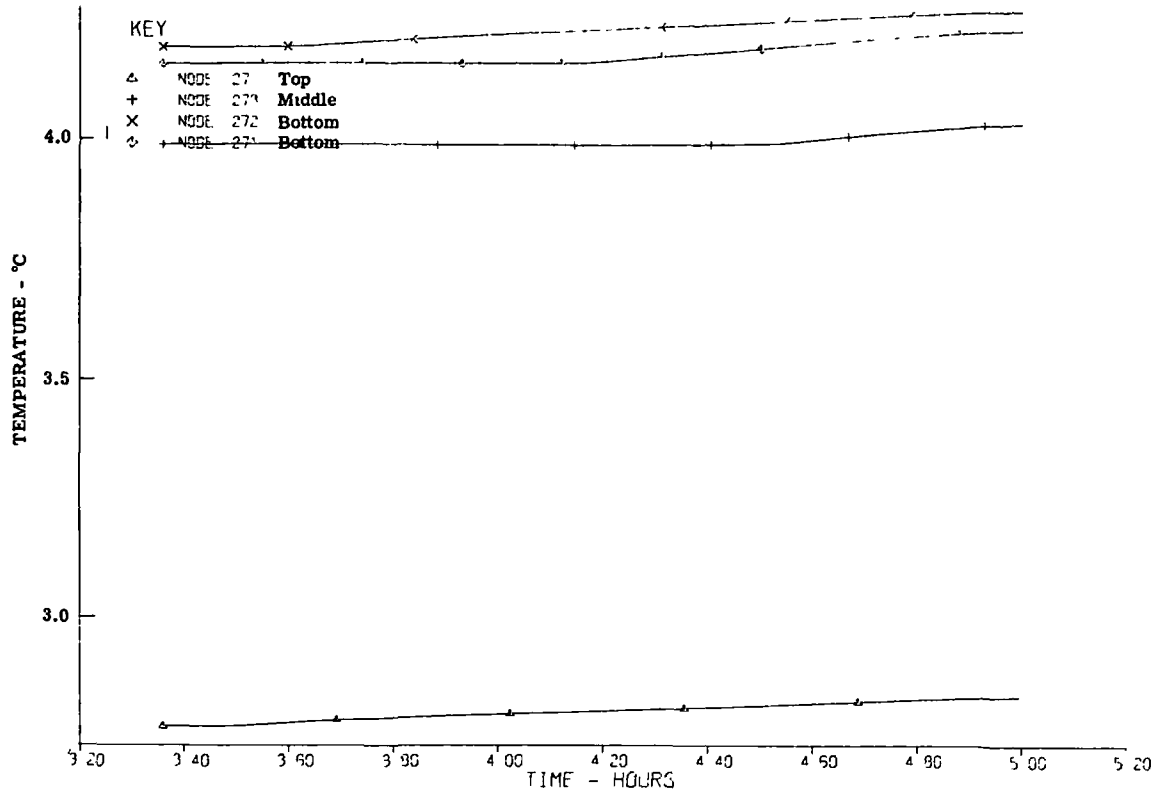

Fig. 3-43 — Temperature history for truss rear circumferential gradient—insulated (α/ϵ = 0.12/0.04)

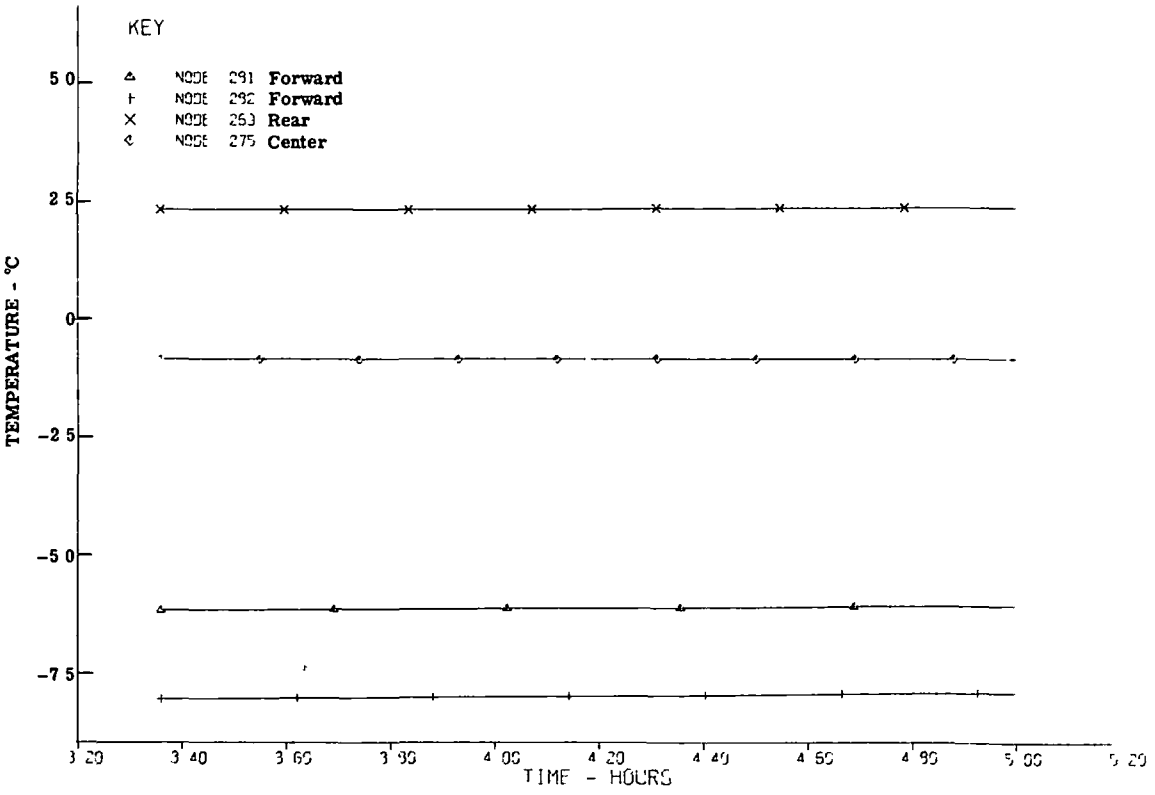

Fig. 3-44 — Temperature history for truss top axial gradient—insulated (α/ϵ = 0.12/0.04)

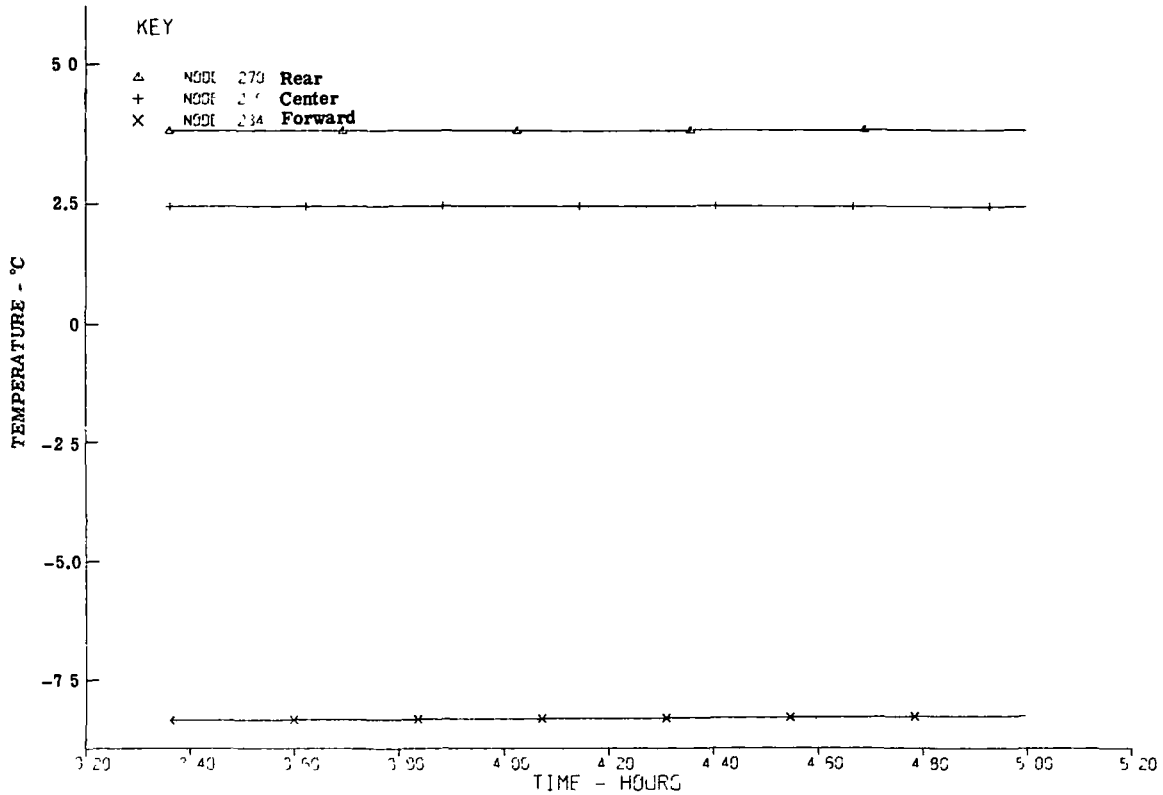

Fig. 3-45 — Temperature history for truss middle axial gradient—insulated (α/ϵ = 0.12/0.04)

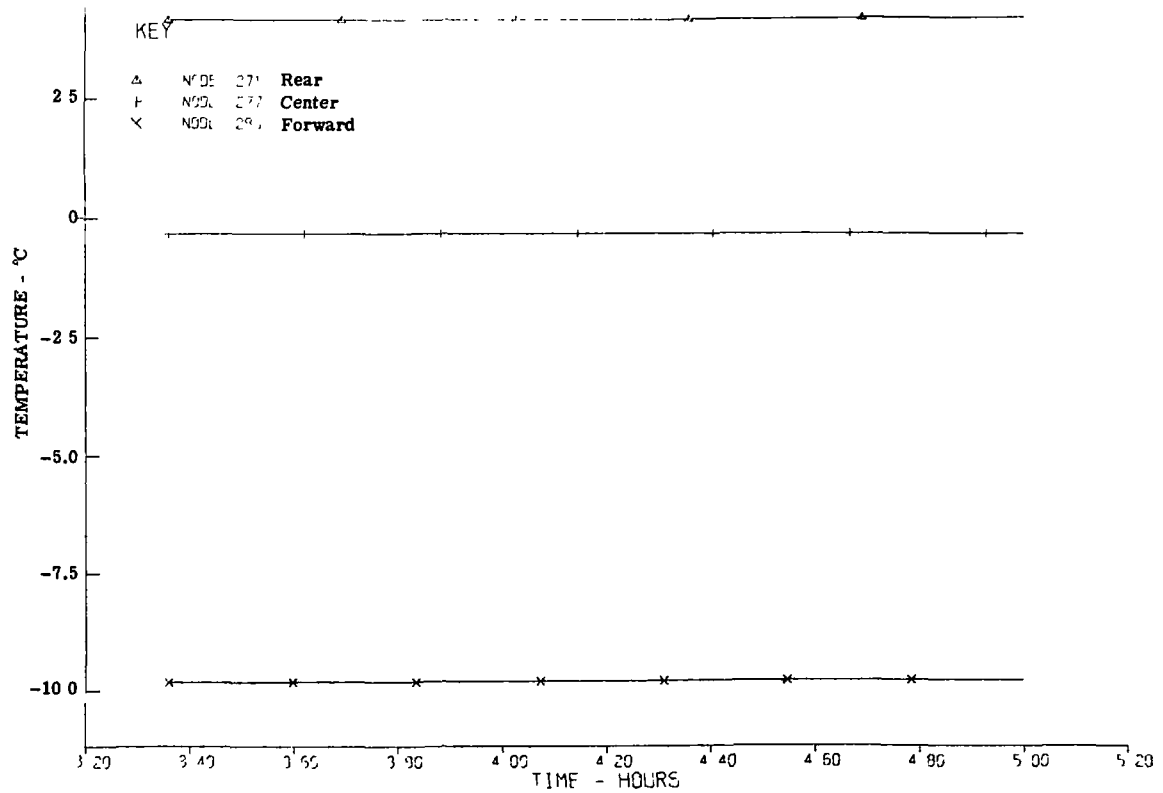

Fig. 3-46 — Temperature history for truss bottom axial gradient—insulated (α/ϵ = 0.12/0.04)

graphite-epoxy composites, and regular graphite-epoxy composites. Results of this evaluation are compared with the allowable orbital transient motion of 3.05 micrometers in Table 3-8. Examination of these results shows that an athermalized graphite-epoxy composite structure meets all requirements under any condition, while the other truss materials may require periodic refocusing, more than twice per orbit under certain circumstances.

Also determined in the course of the structural evaluation was the required thermal control power needed to condition those portions of the system requiring additional heat. The results for all four cases are tabulated in Table 3-9. Characteristically, the insulated systems require less heat; however, the thermal power requirements for even the worst case are not excessive and offer no means for selecting a baseline concept.

3.6 INSTRUMENT STRUCTURE

3.6.1 Instrument Compartment

The instrument compartment structural thermal analysis was directed toward the determination of the structural temperature response as a function of variations in the internal structural emittance and the use of insulation inside the compartment pressure shell. Fig. 3-47 represents the general geometric arrangement of the photoheliograph instrument compartment. A small thermal model of this compartment was constructed for the performance of the parametric studies.

The instrument support structure was assumed to be constructed of graphite-epoxy members. These members are thermally connected to the pressure shell walls by radiation and to the primary ring by conduction. The dominant mode of heat transfer was by radiation, and the following boundary conditions were assumed·

1. Uninsulated pressure shell, high structural emissivity (ϵ = 0.90)
2. Uninsulated pressure shell, low structural emissivity (ϵ = 0.04)
3. Insulated pressure shell, high structural emissivity (ϵ = 0.90)
4. Insulated pressure shell, low structural emissivity (ϵ = 0.04).

Steady-state results for these four cases are given in Table 3-10. Examination of these results clearly shows the influence of the variation in insulation and structural finish characteristics. Also of interest is the temperature distribution of the instrument compartment wall. Fig. 3-48 presents typical data for case 2 above. The interaction between the Shuttle and the photoheliograph is clearly indicated by the circumferential gradient of 41.6 °C.

Although the steady-state temperature distributions are of interest because they indicate the magnitude of the launch-to-operation temperature transient, our major interest is in the orbital transient, since this will directly affect the data acquisition capability of the Shuttle-borne photoheliograph. Typical orbital transient data were collected for all four cases previously described.

Examination of this data indicates, as expected, that the orbital transient temperature variation is proportional to the degree of thermal coupling between the external shell and the instrument structure. For example, the low ϵ uninsulated shell concept exhibits a structural temperature variation of approximately 1.65 °C on the rear members. The insulated shell concepts have structural temperature variations of approximately 0.55 °C and 0.41 °C, depending on the emissivity of the structural member.

Typical data for these analyses are presented in Figs. 3-49 through 3-53. The worst case (high ϵ structure, no insulation) was evaluated to determine the degree of thermal motion. Table 3-11 presents the analytical data and results. It is significant that even this worst case does not

exceed the allowable truss motion. Thus, we can conclude that structural motions during an observation are not a significant problem for the baseline time span.

We can then consider other implications of the design parameters. The use of insulation within the pressure shell results in a pressure shell gradient of 81.1 °C around the wall, while the uninsulated shell has a circumferential gradient of only 41.1 °C. Furthermore, since the uninsulated shell allows internal wall radiation to occur, the main ring heat leakage is approximately 73.2 watts rather than 88 watts, reducing the required heater power somewhat. The effects of the higher shell gradient and increased power consumption have not been assessed in this study. The use of an uninsulated pressure shell offers a significant advantage in the overall design, since it acts as a better heat sink for the various instruments located within the compartment.

3.6.2 Instrument Mount

A preliminary concept was selected for analysis of instrument structure/instrument mount interactions. A typical mounting configuration was chosen on the basis of instrument descriptions supplied by Kollsman Instrument Corporation as typical of the LST. The mount configuration chosen for analysis is shown in Fig. 3-54. This mount contains a bolt, locating pin, and fiberglass epoxy insulating spacer. A brief parametric study was performed to determine the best combination of bolt, pin, and spacer sizes to provide the highest mounting resistance. This study resulted in the following mount specifications·

Item	Material	Thermal Conductivity, watts/cm-°C	Size
Bolt	Titanium	0.0744	12-1.5 × 22.2 mm long
Pin	Titanium	0.0744	6.35 dia. × 22.2 mm long
Spacer	Fiberglass epoxy	0.0026	28.6 ID × 34.9 OD × 15.9 mm long

A typical instrument would contain four mounts, two pinned for positive location and two unpinned. The mounting system thermal resistance of this arrangement was calculated to be 5 °C/watt. To determine the response of the instrument structure through the mount resistance, a 1.1 °C square wave perturbation was assumed on the instrument side of the mount for 10 minutes. The peak temperature rise was estimated for a typical structure node (having a fixed heat capacity) by assuming that all heat flowing across the mount is stored in the adjacent structural node. A temperature increase of the structure was estimated to be 0.32 °C and the resultant thermal growth was found to be less than 10 percent of the allowable value.

3.7 CAMERA COOLING AND CONTROL

3.7.1 21.1 °C Cooling Concepts

The following thermal control concepts were examined for thermal control of the cameras at 21.1 °C:

1. Direct radiation to the compartment walls from the camera
2. Heat pipes
3. Solid conductor
4. Fluid loop cooling system.

Steady-state analysis of each concept was conducted for a single camera, assumed to be in the data integration mode, using LST data for power dissipation and camera configuration. In all cases the thermal flux incident on the camera photocathode was neglected, as were losses from

Table 3-8 — Truss Average Temperature Swings and Primary to Secondary Mirror Spacing Change for Half-Orbit

Condition	Swing, °C	ΔL, centimeters		
		Athermalized Graphite-Epoxy	Graphite-Epoxy	Athermalized Invar
α/ϵ = 0.22/0.88, no insulation	3.9	7.6×10^{-5}	7.6×10^{-4}*	3.8×10^{-4}*
α/ϵ = 0.22/0.88, insulation	0.39	7.6×10^{-6}	7.6×10^{-5}	3.8×10^{-5}
α/ϵ = 0.12/0.04, no insulation	0.55	10.2×10^{-6}	10.2×10^{-5}	5.1×10^{-5}
α/ϵ = 0.12/0.04, insulation	0.055	10.2×10^{-7}	10.2×10^{-6}	5.1×10^{-6}
Requirement	—	3.05×10^{-4}	3.05×10^{-4}	3.05×10^{-4}

* Inadequate.

Table 3-9 — Meteoroid Shield/Metering Truss Concept Power Dissipation (Watts)

Meteoroid Shield/Metering Truss Concept	Case 1 α/ϵ = 0.22/0.88 No Insulation	Case 2 α/ϵ = 0.22/0.88 Insulation	Case 3 α/ϵ = 0.12/0.04 No Insulation	Case 4 α/ϵ = 0.12/0.04 Insulation
Main mounting ring power	23.8	13.8	20.5	13.8
Secondary mirror power	2.7	1.4	2.8	2.2
First relay flat power	3.2	1.7	3.2	2.0
Second relay flat power	2.0	0.8	1.7	1.2
Primary mirror mounts power	2.3	2.3	2.3	1.9
Total power	34.0	20.0	30.5	21.1

Table 3-10 — Instrument Structure Temperature Distribution (°C)

Structure Concept	ϵ = 0.9 No Shell Insulation	ϵ = 0.04 No Shell Insulation	ϵ = 0.9 Shell Insulation	ϵ = 0.04 Shell Insulation
Top temperature (node 9)	-30.8	-8.6	2.3	4.5
Bottom temperature (node 11)	-0.16	2.2	9.7	10.7
Gradient (top to bottom)	-48.4	-28.5	-10.3	-24
Front temperature (node 6)	-14.1	-0.55	8	9
Back temperature (node 18)	8.3	0.0	4.7	5.8
Gradient (front to back)	-40.1	-18.3	-14.5	-14.6

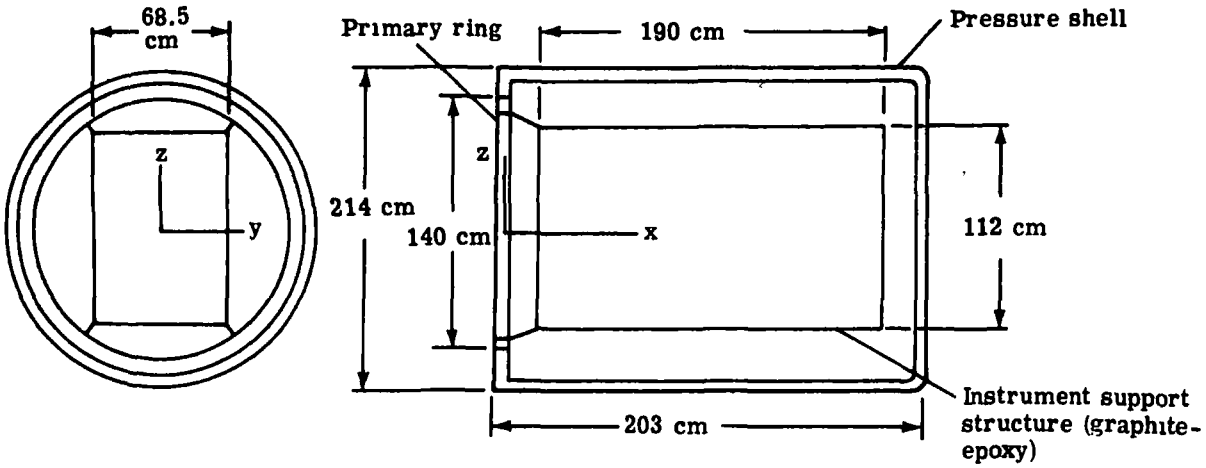

Fig. 3-47 — Instrument compartment layout

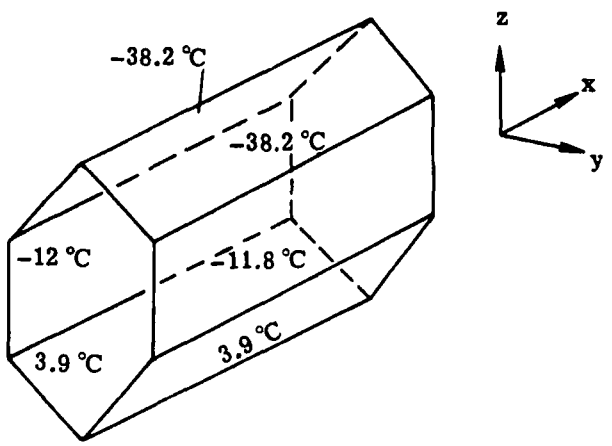

Instrument compartment temperature distribution — uninsulated, low ϵ structure

Fig. 3-48 — Steady-state temperature distribution

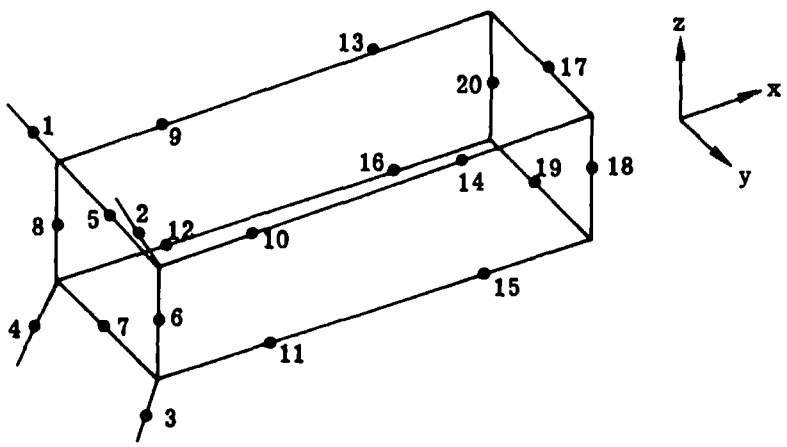

Fig. 3-49 — Instrument structure nodal identification

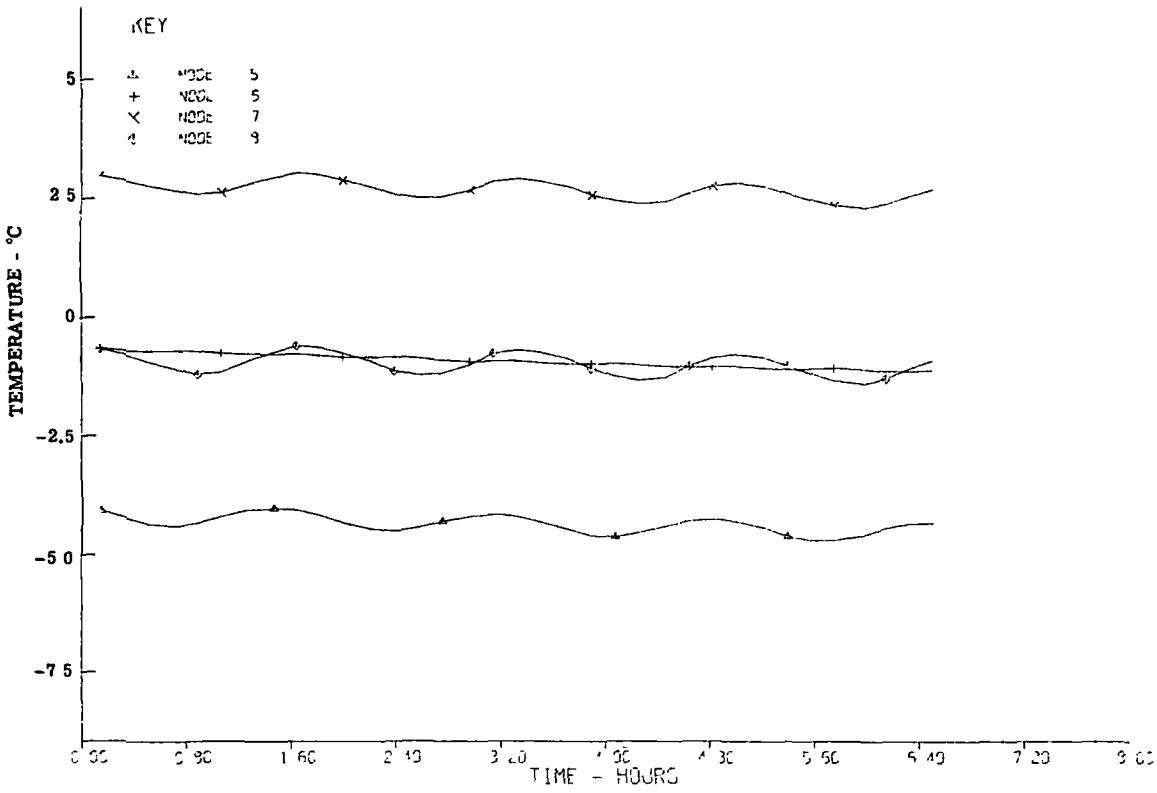

Fig. 3-50 — Temperature history for instrument compartment—uninsulated (α/ϵ = 0.22/0.88)

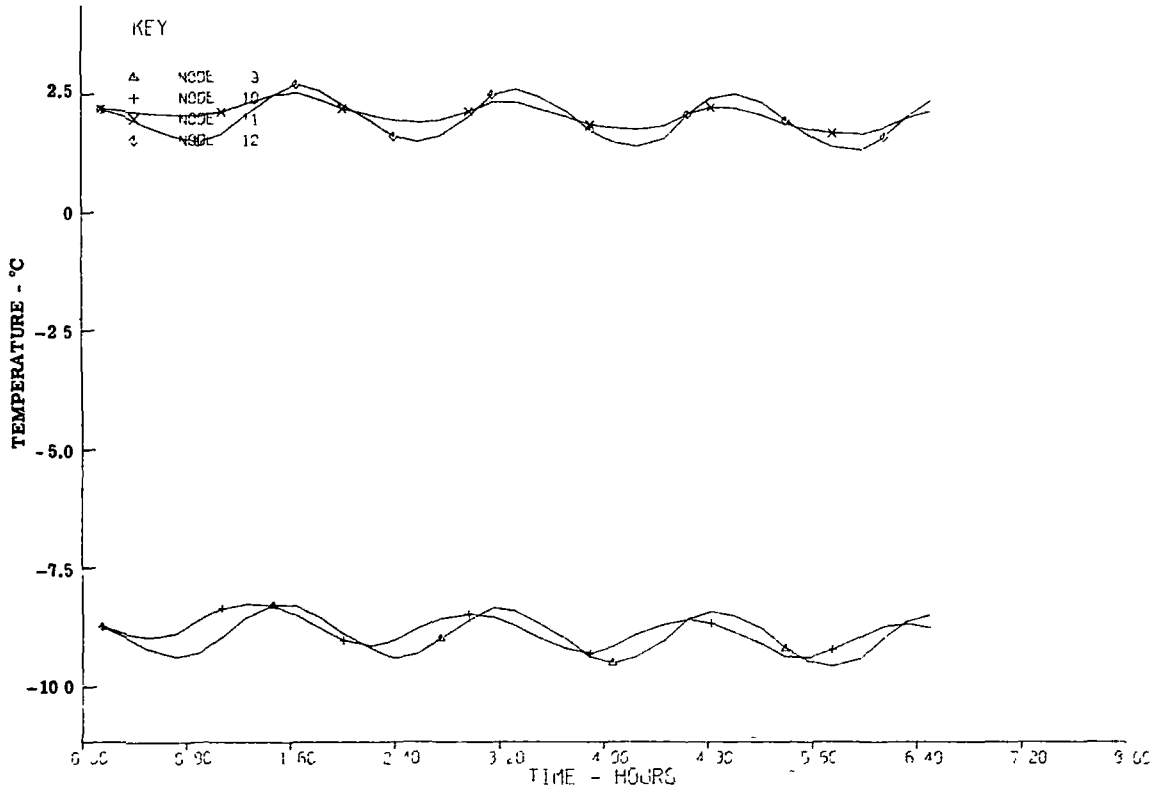

Fig. 3-51 — Temperature history for instrument compartment—uninsulated (α/ϵ = 0.22/0.88)

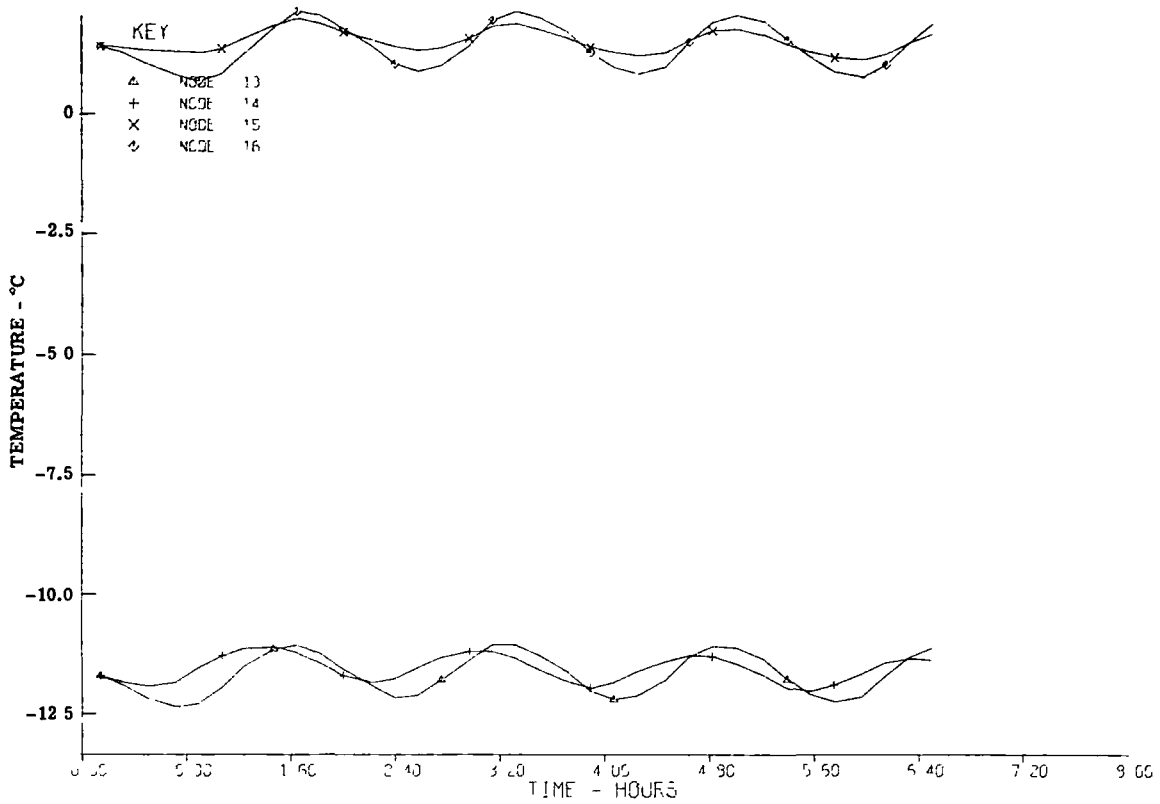

Fig. 3-52 — Temperature history for instrument compartment—uninsulated (α/ϵ = 0.22/0.88)

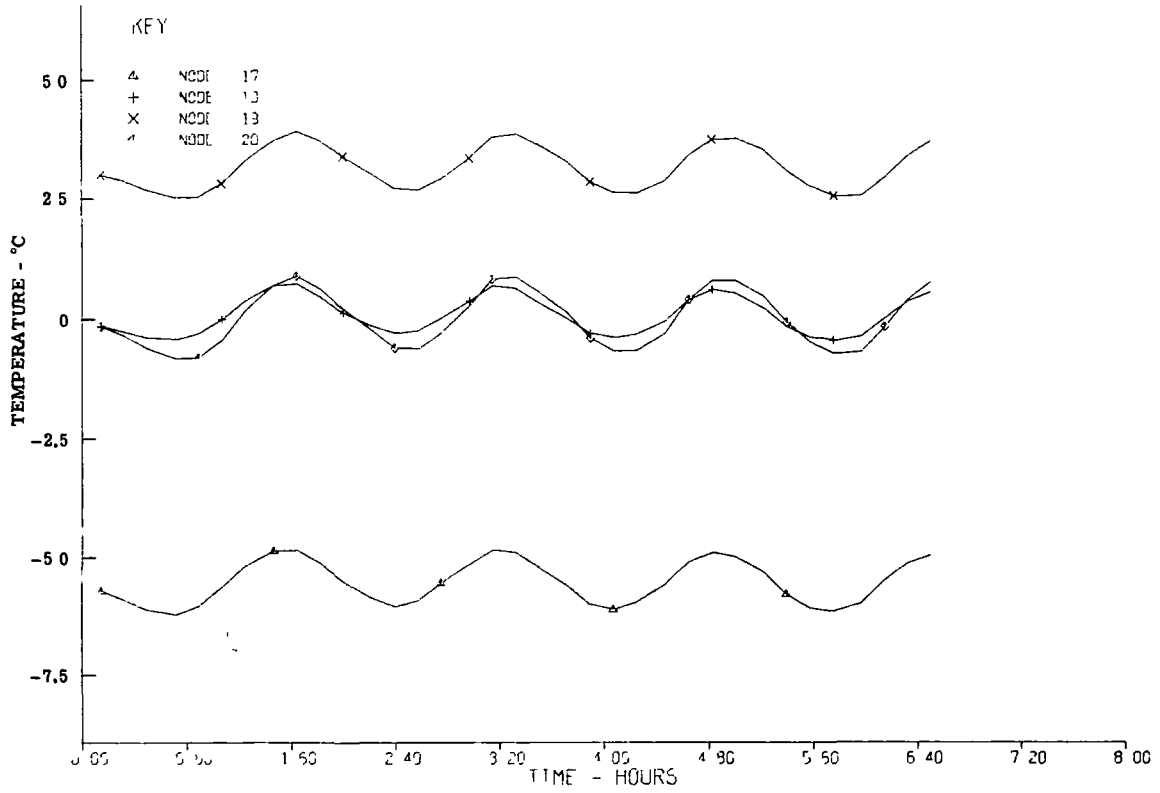

Fig. 3-53 — Temperature history for instrument compartment—uninsulated (α/ϵ = 0.22/0.88)

Table 3-11 — Instrument Structure Study Motion Analysis for High ϵ Uninsulated Structure

Node	$T_{4.25hr}$	$T_{4.50hr}$	ΔT, °C
10	-27.4	-24.2	2.16
11	-1.8	0.83	2.61
14	-26.4	-22.7	2.56
15	-0.9	2.1	2.94
18	8.2	12.8	4.61

For graphite-epoxy composite $\alpha = 0.36 \times 10^{-6}$/°C
Motion in x direction = 1×10^{-6} meter/10 minutes
Allowable motion of truss = 1.5×10^{-6} meter

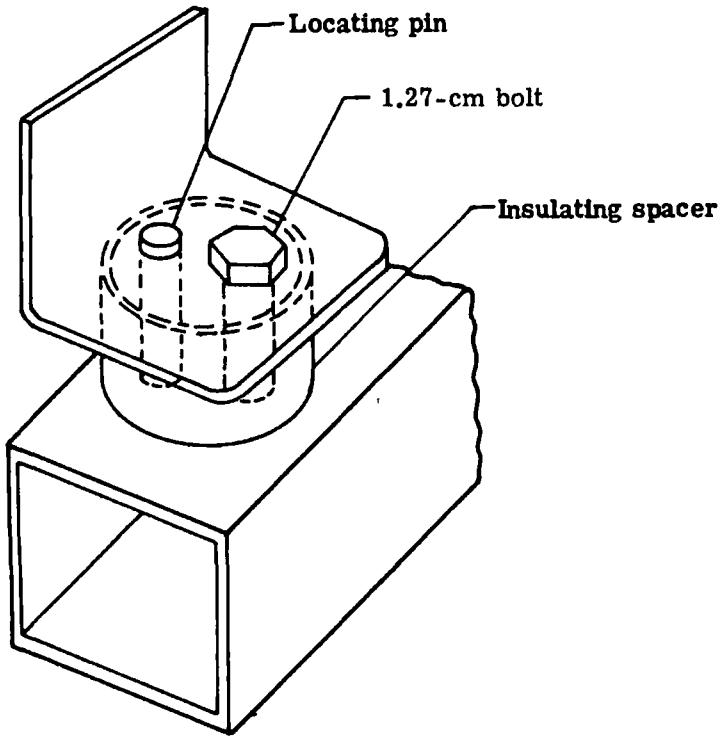

Fig. 3-54 — Mounting configuration

the camera to the instrument mounting interface. Prior analysis (for the LST) determined a realistic camera-instrument interface resistance of 13.9 °C/watt for this connection.

Direct Radiation

The dissipation of 11 watts from the camera by direct radiation to the uninsulated pressure shell walls was investigated. The radiating surface and the cold shell walls were assumed to have an emittance of 0.9. The steady-state temperature distributions of the pressure shell walls were available from the previous analysis (see Fig. 3-48).

The results of this analysis indicated that the method is feasible, however, there is some difficulty in implementation due to the excess cooling capability of the system. It was found that for the initial condition ($\epsilon_{camera} = \epsilon_{wall} = 0.9$, $T_c = 21.1$ °C, $T_{wavg} = -17.8$ °C) approximately 27 watts of makeup heaters are required. This situation may be alleviated somewhat by reducing either the radiating area or the effective emittance of the camera. Of these two methods, a lower emittance appears more feasible The most probable value of emittance for an equilibrium condition is calculated to be approximately 0.27.

Heat Pipe

The use of a heat pipe as a method of conducting waste heat from the camera while maintaining its temperature at 21.1 °C was investigated. In this concept, we assume that the outer shell of the camera is connected directly to the walls of the pressure shell, which acts as a system heat sink. Based on the previously calculated temperature distribution, it appears that low wall temperatures are available and no separate external radiator surfaces are required. Based on the mean wall temperature of −17.8 °C, a thermal resistance of 3.54 °C/watt is required between the camera and the sink to transfer the 11 watts of waste heat.

If we accept some degree of additional complexity, we can assume that the heat pipes are connected to the lower surface of the pressure shell, which results in a smaller gradient (−1.1 °C as opposed to 21.1 °C for the mean wall). Since only 11 watts must be transferred and since the general utility of heat pipes is for the transfer of large quantities of heat at minimum temperature gradients, it appears that the use of heat pipes for this application is not warranted. This conclusion is further confirmed due to the cost, complexity, and general problems associated with a device of this type.

Solid Conductor

A solid copper conductor has been evaluated for transfer of camera waste heat. As in the case of the heat pipe, the waste heat from the camera is rejected directly to the cold walls of the vehicle, where it is radiated to the external environment. Based on an insulated conductor with a mean distance of 91.5 centimeters from the camera to the wall, the overall thermal resistance has been calculated as 3.54 °C/watt. The required conductor area based on a 21.1 °C gradient is 0.66 square centimeter. Although the system heat sink fluctuates approximately 22.2 °C, further analysis indicated that the thermal time constant of this system is sufficiently large (2.07 hours) to dampen these fluctuations by approximately 95 percent. To limit heat loss by radiation from the copper strap to approximately 10 percent of the total heat load, an insulator having an effective emissivity of 0.02 is required, which may be obtained with superinsulation.

Fluid Loop

The final concept considered for 21.1 °C camera thermal control was a fluid loop connecting the camera casing to the cold walls of the instrument compartment. This concept uses a 50-50 mixture of ethylene glycol and water flowing through a 0.635-centimeter line to transfer the camera heat to the external walls. Since the walls are significantly colder than the fluid, only a

minimal heat sink surface area (>1.52 square centimeters) is required to transfer the 11 watts. From a practical standpoint, it appears that a high capacity bypass loop will be required to maintain thermal control with these low heat transfer requirements. Results of this analysis are summarized in Table 3-12.

Table 3-12 — 21.1 °C Camera Thermal Control Fluid Loop

Heat source temperature	21.1 °C
Heat rejected	11 watts
Heat transfer medium	50-50 mixture of ethylene glycol and water
Mass flow rate	10.9 kg/hr
Fluid Reynolds number	166 (laminar)
Heat transfer coefficient	2.52×10^{-2} watt/cm^2-°C
Bulk temperature rise	1.1 °C
Heat sink temperature	+3.9 °C
Required sink area	24.4 cm^2

Summary

Of the four concepts investigated, it appears that two—direct radiation and solid conductors—are worthy of further study. Both heat pipes and fluid loops may be ruled out for the proposed application. It is noted that all methods investigated require additional active control to provide a positive means of thermal control at the set-point. The four concepts are ranked in order below:

1. Direct Radiation. Workable in present concept. No weight penalty to implement. Low cost. Requires makeup heaters to account for wall temperature variation and location. Proven design concept.
2. Solid Conductor. Workable in present concept. Additional 8.25 kilograms weight for conductor. Low cost. Proven design concept. Requires makeup heaters to account for wall temperature variation.
3. Fluid Loop. Workable in present concept. Growth potential for thermal control of multiple instruments. Baseline weight penalty of 3.72 kilograms. Complex system with potential vibration and leakage problems.
4. Heat Pipe. Workable in present concept. Some weight penalty but less than solid conductor. Highest cost based on need to develop and qualify a design. Makeup heaters required on same order of magnitude as solid conductor.

3.7.2 −17.8 °C Cooling Concepts

Since it may be necessary to actively cool the camera vidicon tubes and control their temperature at a low level (−17.8 °C), two cooling concepts for accomplishing this task were investigated:

1. Thermoelectric cooling of camera tube
2. Solid conductor cooling of camera tube.

Both concepts are based on a design concept developed for the LST. In this concept, the camera tube is enclosed within a copper sleeve that is thermally isolated from the camera focus coils by low conductance mounts and ultra-low-emittance surfaces. The copper sleeve is cooled to the desired temperature and the waste heat is rejected at or through the camera outer case, which acts as a radiator or heat dump depending on the cooling method selected.

Thermoelectric Cooling

Thermoelectric cooling of a typical 25- by 25-millimeter format camera was investigated. The camera consists of three major components. the focus coil, the outer casing, and the photocathode tube with cooler shell. In order to establish the required thermal load (to determine pumping requirements), it was necessary to perform a camera heat balance. This heat balance indicated a negligible thermal power input to the tube (0.05 watt). However, for design purposes, we have assumed 2 watts to account for both lead thermal conductance and conduction leaks across the coil/cooler shell interface.

The use of a single-stage thermoelectric module to maintain the tube temperature at −17.8 °C was then investigated to establish the required pumping characteristics. It was found that a module operating at a hot junction temperature of 20 °C and a cold junction temperature of −17.8 °C will pump 2 watts with an efficiency of 26 percent. Thus, a module input power load of 7.7 watts is required for the system.

Since we have now determined the various thermal load outputs from the camera, we must determine if a thermal balance exists between the camera case and the external environment. The total power output from the camera is

9 watts (coils) + 2 watts (tube) + 7.7 watts (T.E. module) = 18.7 watts

It has been found that a camera case temperature of 21.1 °C and mean sink temperature of −17.8 °C requires an emittance of 0.50 for the system to be balanced.

Solid Conductor

Since the estimated thermal heat load from the cooled cameras to the internal shell is approximately 2 watts and since the instrument compartment walls are cold, it appeared to be reasonable to investigate the use of a solid conductor for passively cooling the camera tubes.

A review of the orbital temperature history of the instrument compartment established that the wall temperature cycles between −48.4 °C and −26.1 °C (see Fig. 3-55). Therefore, the design was based on the maximum temperature, and a copper conductor area of 6.17 square centimeters is required. Since the sink temperature is varying, we estimated the maximum heater power required to maintain the cameras at −17.8 °C during the orbital period. This maximum power was calculated to be 5 watts.

An alternative approach may be the use of mechanical switching to provide thermal control.

Summary

The two −17.8 °C cooling concepts have been examined and both appear to be acceptable. These concepts are shown in Figs. 3-56 and 3-57, which illustrate the basic arrangement, general thermal features, and estimated heat flows for each. An estimate of system weights for both concepts is also given.

Based on our evaluation of the two alternative methods for providing camera thermal control at −17.8 °C, it is recommended that the solid conductor concept be chosen for the system baseline. This choice is based primarily on the simplicity of the system and the potential lower cost of this approach, since it requires no hardware qualification program for coolers and controls.

It should be noted that the analysis conducted for the solid conductor concept was based on a nominal camera location. In a practical design the cameras will be positioned at various locations on the structure, and therefore the actual system weights (which reflect the conductor length) will vary depending on the actual location with respect to the cold walls of the instrument compartment.

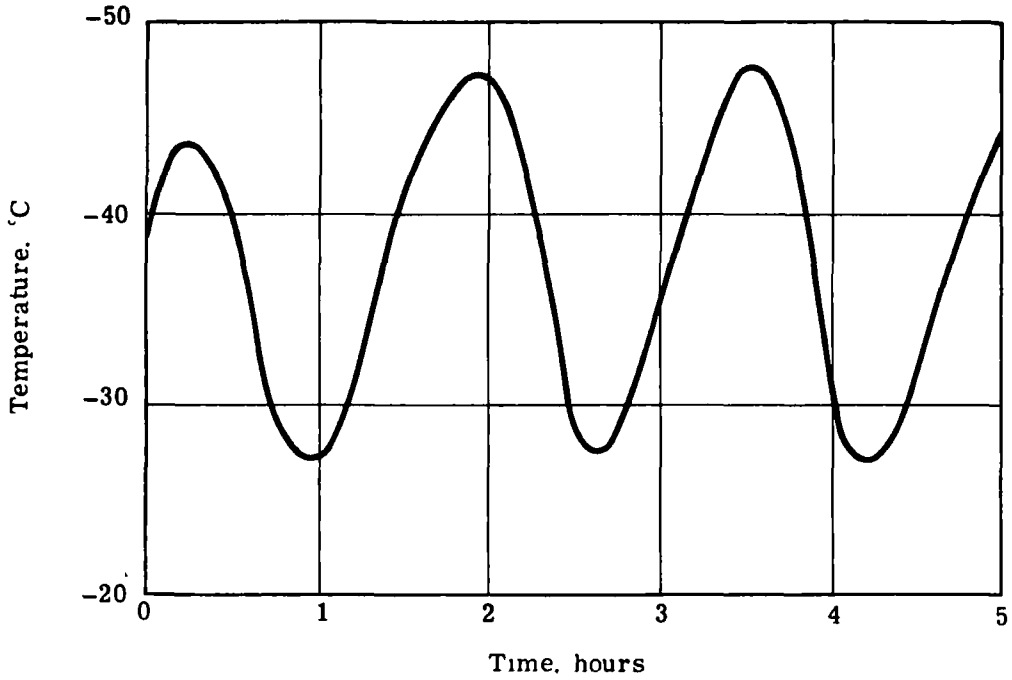

Fig. 3-55 — Temperature history for instrument compartment wall

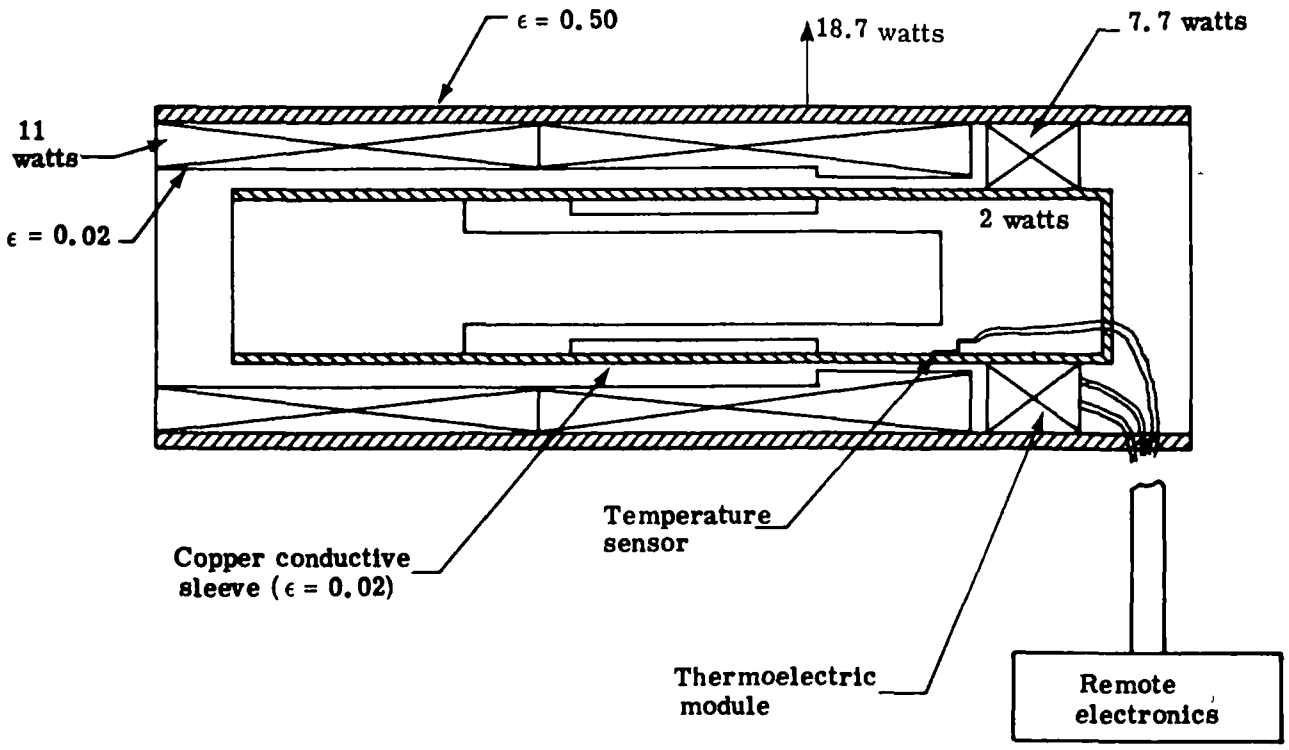

Fig. 3-56 — Thermoelectric cooling design (estimated system weight 2.67 kilograms)

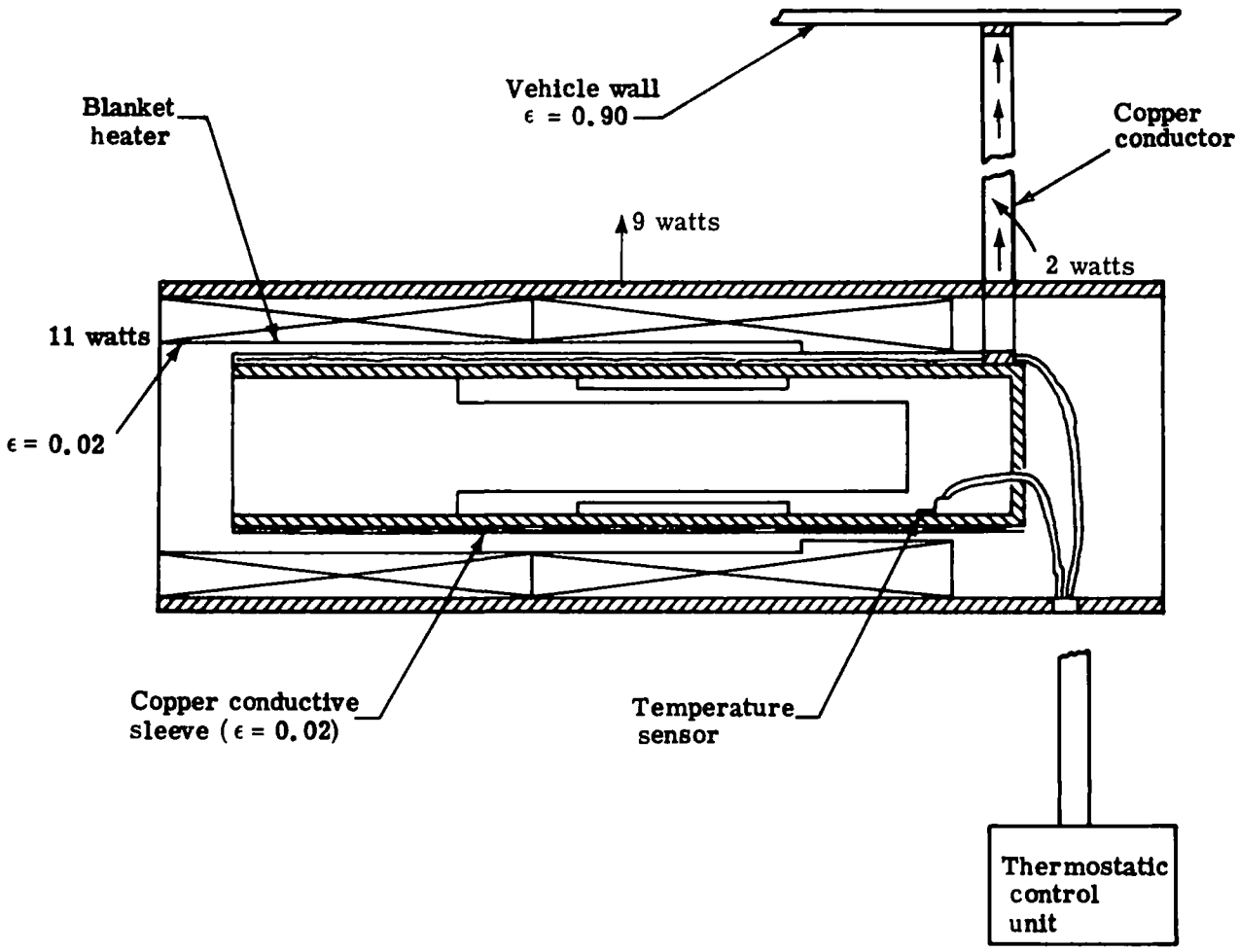

Fig. 3-57 — Solid conductor cooling design (estimated system weight 8.8 kilograms)

The performance of the solid conductor cooling concept was evaluated with the instrument compartment thermal model (see Section 3.6.1). A typical cooled camera was modeled and mounted on the instrument structure. The nodal network required to effect this change is shown in Fig. 3-58.

Examination of the orbital transient temperatures indicates that the orbital variations are essentially identical with the previous values, however, the temperature levels have changed (especially on node 10), reflecting the constant power output of the camera and the associated thermal leak into the structure. These temperature level changes are indicated in Table 3-13.

3.8 THERMAL SWITCHING CONCEPTS SURVEY

3.8.1 Background

A literature search and survey of thermal switching concepts was conducted as a part of the Photoheliograph Thermal Concepts study. The goal of this task was to review and document concepts that have been used for thermal control of spacecraft systems and/or spacecraft that have been flown. A bibliography is given in Section 3.8.7.

We have identified two general classes of conditions where thermal switches can meet a real need. These are system cooldown during orbital maintenance and long term degradation of optical coatings on the primary and heat shield mirrors. In the first case, we have shown that unless the heat transfer from the back of the primary is modulated during maintenance operations (when the normal solar loading is "off"), the primary mirror cools down drastically in a short time (about 16 hours). In the second case, an increase of 25 percent in the absorbtance of the optical coating of the primary and heat shield mirrors results in an increase of system temperature of approximately 25 °C, which results in temperature levels above the current design limitation.

The basic concepts that have been studied are

1. Louvers
2. Mechanical thermal switches
3. Heat pipe thermal switches
4. Variable conductance heat pipes.

Each of these concepts is reviewed below.

3.8.2 Louvers

The use of louvers for thermal control of spacecraft or spacecraft components is a proven technique that has been used for a variety of programs including Mariner, OGO, Pegasus, Nimbus, and ITOS (TIROS). In general, these louver systems have been used to control the temperature of electronic components and/or heat sinks. The general temperature requirement is on the order of 21.1° ± 11 °C.

Characteristically, a louver system consists of a number of lightweight, low emittance, movable blades covering the surface to be controlled and separated from it to reduce conductive heat transfer. The interior surface of the louver may be either specular or diffuse, while the exterior is usually given a specular, low emittance surface finish.

Two types of motion actuators have been used. One is based on the bimetallic spring principle (Mariner, OGO, Pegasus) where the bimetallic element is thermally coupled to the surface to be controlled (radiator) and also to the actuating arm of the louver. Temperature changes in the radiator are translated into torques on the louver actuating arm and result in changes of the louver blade angle. The other technique is based on a low boiling fluid such as Freon expanding a bellows, which in turn drives a rack and pinion arrangement (Nimbus) to position the louvers. The advantage of this system is that temperature control may be based on something other than the space radiator.

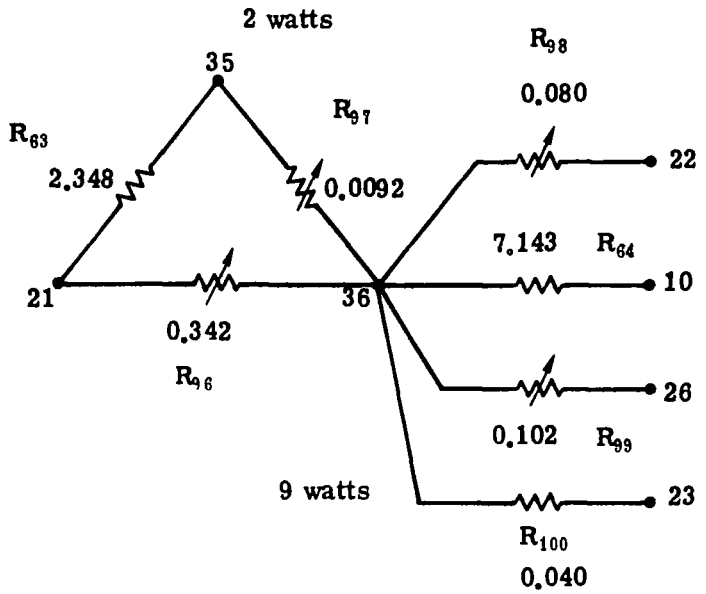

Notes

1. Resistors are labeled to be incorporated in model.
2. The following nodes are used

Node	Description
10	Instrument structure
21	Compartment wall
22	Compartment wall
23	Compartment wall
26	Compartment wall
35	Cooler wall (internal)
36	Camera case (outer)

Fig. 3-58 — Camera thermal model network

Table 3-13 — Structural Temperature Distribution (°C)

Node Number	Without Camera	With Camera
5	−3.9	−1.4
6	−0.55	1.9
7	3.1	4.2
8	−0.55	0.55
9	−8.6	−7.2
10	−8.6	−1.7
11	2.2	3.3
12	2.2	3.05
13	−11.7	−10.8
14	−11.7	−9.5
15	1.45	1.9
16	1.45	1.9
17	−5.5	−4.7
18	0.0	0.83
19	3.05	3.3
20	0.0	0.55

For a typical louver control system, the single significant parameter of interest is the effective emittance, ϵ^*, of the radiating surface as a function of blade opening angle. Plamondon† has calculated values of ϵ^* for a number of radiator emittance values. The peak values of ϵ^* representative of fully open blades are.

ϵ_s	ϵ^*
0.5	0.41
0.75	0.56
0.85	0.61
0.95	0.66

Nimbus test data for a 0.9 radiating surface appear to confirm this analysis with a value of $\epsilon^* \approx 0.58$. On the other hand, Pegasus test data for a 0.75 radiating surface yields $\epsilon^* \approx 0.72$. Although there is considerable disparity between test and experimental data in the fully open position, there is good agreement between test and analysis for blade angles up to approximately 45 degrees.

We conclude that there is sufficient data to consider the louver concept as an acceptable approach for thermal control of the photoheliograph.

3.8.3 Mechanical Thermal Switches

The only uses of thermal switches discovered during this investigation were on Surveyor and Viking. In both cases, the switch does not operate in space but is designed primarily for extraterrestrial ground operation on the moon and mars, respectively.

The Surveyor switch is designed to maintain battery and electronics compartment temperatures in a range of −17.8 to 51.6 °C during the lunar cycle. The switch concept is based on an internal conductive coupling driven by bimetallic strips to an externally mounted radiator integral with the switch assembly. Reported switch conductance is 0.263 watt/°C, and it weighs 0.27 kilogram. Unit conductance as a function of actuation pressure was experimentally determined to be 0.081 to 0.095 watt/cm^2-°C.

The significant problems associated with this switch were sticking contacts, which were ultimately solved by processing changes, and contamination (by foreign material) of the contact area resulting from the particular design concept. It is reported that on one occasion an eyelash trapped between contacts resulted in failure of the switch.

The Viking thermal switch is designed to control the temperature of the Lander baseplate using waste heat from the RTG's. Control is specified over the range of 10 °C (minimum conductance = 0.0263 watt/°C) to 2.2 °C (maximum conductance = 2.07 watts/°C). The operating mechanism is a Freon-12 filled bellows assembly mounted on the Lander baseplate, which drives an actuator linkage mechanism to the mechanical contactor. Switch weight is on the order of 2.73 kilograms (0.91 kilogram actuator, 1.82 kilograms contactor and mount).

3.8.4 Heat Pipe Thermal Switches

Martin Marietta has also designed and fabricated a heat pipe thermal switch, which has not flown. The thermal switch concept is based on mechanically varying the condenser volume by means of an actuated bellows and thus control the fluid pumped to the evaporator section of the heat pipe.

---

†See the bibliography in Section 3.8.7.

Reported results for this design were operating conductance of 5.15 watts/°C and nonoperating conductance of 0.138 watt/°C. The investigator points out that the operating conductance was lower than desired and the nonoperating conductance higher than desired, both conditions attributable to departure from optimum design conditions (hardware problems).

A thermal diode design has been developed by Grumman for use on the ATS-F satellite. This design utilizes the principle of excess liquid blockage, i.e., the heat pipe is filled with excess liquid, which during normal operation, collects at the cold (condenser end) and which is sufficient to completely fill the hot end when the heat flow is reversed. The particular diode was designed to provide heat input to a simulated cold plate under the following conditions:

1. Normal operation·

   Q = 20 watts, ΔT = 7.7 °C

2. Diode operation

   Q = 1.4 watts, ΔT = 144 °C

An experimental model of the diode was built, and test results exceeded the above specification requirements for both modes of operation.

It should be noted that this scheme requires a heat pipe configuration that is strongly influenced by the ratio of evaporator and condenser areas, since the reversed mode must completely flood the normal evaporator.

Another diode scheme examined by Grumman but not implemented utilized a liquid trap technique at the evaporator. During diode operation in the reversed mode, the trap fills with liquid and starves the condenser. The concept was rejected because of size and weight limitations of the required reservoir.

3.8.5 Variable Conductance Heat Pipes

A number of heat pipe designs of interest here are variable conductance heat pipes for precision temperature control of spacecraft components rather than the "isothermalizer" heat pipes proposed by the OAO-C structure.

The concept of a variable conductance heat pipe is based on the implementation of techniques that interfere with normal heat pipe operation. The most common approach is to use noncondensable gas blockage of the condenser area of the heat pipe. Blockage control may be either passive (i.e., gas-vapor interface is dependent solely on system operational heat loads and temperatures) or active by means of an external feedback loop.

Both actively and passively controlled variable conductance heat pipes have been proposed, analyzed, and built. In general, these heat pipes have been applied to the transfer of heat from electronics boxes or compartments to external radiators. Grumman and TRW have both designed, fabricated, and tested passively controlled heat pipes for OAO-C electronics cooling. Interestingly, the approach taken for the transfer of approximately 30 watts at a hot temperature of 15.5 °C to 23.9 °C is completely different. Grumman's design is based on a cold gas reservoir heat pipe using ammonia as the working fluid. TRW, on the other hand, uses a hot gas reservoir heat pipe with methanol as the working fluid. Both designs, however, appear to have met the heat transfer requirements outlined above.

Active feedback control of heat pipes has been considered by Dynatherm, who have outlined two methods of achieving active control (change in excess gas volume and independent temperature control of excess gas volume). The first scheme is similar in some respects to the Martin heat pipe thermal switch. The second scheme has been further developed by Lockheed, and an experimental verification of a practical configuration has been completed.

The Lockheed concept uses an acetone-N_2 heat pipe to provide ±1.1 °C source thermal control over a time-varying source power input (20 watts for 80 minutes, 70 watts for 20 minutes) while the sink temperature changes (same period, sink temperature ±16.7 °C). Reported test results indicate source temperature variations are held to within ±0.55 °C with this arrangement.

3.8.6 Conclusions

Based on this survey, we can conclude the following·

1. Acceptable methods of thermal control by means of louvers or variable conductance heat pipes are available and the use of such devices is understood and reasonably predictable.
2. The degree of thermal control possible with a variable conductance heat pipe is much greater than that attainable with louvers.
3. In general, the demonstration of heat pipe space performance in a 1-g environment may not be possible and ground test compromises may be required.
4. Mechanical thermal switches are potential problems from both weight and handling standpoints.
5. Thermal diodes (unidirectional heat pipes) may be used and can provide large (≪30) variations in conductance.

3.8.7 Bibliography

1. Schnapf, A., Design and Orbital Performance of ITOS-1 (TIROS-M), RCA Government Engineering (No Date).
2. Russell, L., and Linton, R., Experimental Studies of the Pegasus Thermal Control Louver System, Progress in Astronautics and Aeronautics, Vol. 20, pp. 709-724.
3. London, A., Shutter System Design for the Nimbus Spacecraft, Progress in Astronautics and Aeronautics, Vol. 20, pp. 725-757.
4. Christensen, E., Ranger and Mariner Temperature Control Experiences, Progress in Astronautics and Aeronautics, Vol. 18, pp. 797-810.
5. Plamondon, J., Analysis of Movable Louvers for Temperature Control, Journal of Spacecraft and Rockets, Vol. 1, No. 5: pp. 492-497.
6. Heated Bimetal Spring Flips Sun Flap, Machine Design, p.113 (Apr 16, 1970).
7. Deal, T., The Surveyor Thermal Switch, JPL Technical Memorandum 33-355, pp. 93-99.
8. 83709713605 VLC Thermal Control Subsystem Design Criteria, MMC-Denver Division.
9. Viking Program Briefing, MMC-Denver.
10. Gorman, D., Heat Pipe Thermal Switch Final Report, Report D-71-48781-005, MMC-Denver Division.
11. Edelstein, F., and Hemback, R., Design, Fabrication, and Testing of a Variable Conductance Heat Pipe for Equipment Thermal Control, AIAA paper 71-422.
12. Kirkpatrick J., and Marcus, B., A Variable Conductance Heat Pipe Flight Experiment, AIAA paper 71-411.
13. Ekern, W., and Hollister, M., Performance of a Precision Thermal Control System Using Variable Conductance Heat Pipes, AIAA paper 72-270.
14. Swerdling, B., et al., Development of a Thermal Diode Heat Pipe for the Advanced Thermal Control Flight Experiment (ATFE), AIAA paper 72-260.
15. Biernert, W., Brennan, P., and Kirkpatrick, J., Feedback Controlled Variable Conductance Heat Pipes, AIAA paper 71-421.

3.9 SELECTED BASELINE

The end product of the analyses described in Sections 3.3 through 3.7 is the recommended thermal control baseline for the 100-centimeter Shuttle photoheliograph shown in Table 3-14. The elements of this baseline concept are described below.

The solid primary mirror has been selected for this design primarily because it is a low cost element that will meet our established optical performance requirements. The lightweight, specular core concept is an acceptable alternative offering a lower weight backup at higher cost.

The cold plate/heat pipe/space radiator has been selected as the primary mirror heat rejection system because of its simplicity and low weight. A fluid loop cooling system that effectively replaces the heat pipe is an acceptable alternative concept, although it results in an increase in system weight and requires a more complex heat transfer system.

Passive thermal control of the secondary metering structure is provided by an uninsulated, low ϵ coated external shell that has been selected because of the reduced structural temperature response, as well as the lower gradients developed. By constraining the structure material to an athermalized graphite-epoxy composite, a high ϵ thermal coating may be used as an alternative thermal control finish.

The heat shield mirror is actively cooled by means of a heat pipe/space radiator system selected for low weight and simplicity. As in the case of the primary mirror heat rejection system, and with identical reasoning, a fluid loop cooling concept may be employed.

The secondary mirror, relay flats, and main support ring are actively held at 21.1 °C by thermostatically controlled electric heaters, which is a simple approach to maintaining a constant temperature.

The instrument support structure and external shell are passively controlled by a low α, high ϵ thermal finish and internally insulated structural members. This combination has been selected because of its lower thermal response to orbital perturbations that induce sensor motions.

Thermal control of both 21.1 °C and −17.8 °C instruments has been selected after an examination of available concepts. The concepts chosen (direct radiation for 21.1 °C and conductive strap for −17.8 °C) were selected because of their simplicity and lower costs. Acceptable alternatives are available for both set-point values.

Table 3-14 — 100-Centimeter Shuttle Photoheliograph Recommended Baseline

Primary mirror	Solid
Primary mirror cooling	Cooling plate, heat pipe, thermal switch, radiator
Meteoroid shield/metering truss	α/ϵ = 0.12/0.04, no insulation or meteoroid shield, ϵ = 0.9, metering truss
Heat shield mirror	Heat pipe, thermal switch, radiator
Secondary and relay mirrors	21.1 °C thermostatic control
Meteoroid shield/instrument structure	α/ϵ = 0.22/0.88, meteoroid shield, ϵ = 0.04, instrument structure
21.1 °C instrument control	Radiation cooling with makeup heaters
−17.8 °C instrument control	Solid conductor cooling strap

4. 100-CENTIMETER PHOTOHELIOGRAPH FOR BALLOON MISSIONS

4.1 BACKGROUND

4.1.1 Requirements

The thermal studies of the balloon-borne 100-centimeter photoheliograph were directed toward the generation of a thermal control concept compatible with the balloon missions. The major portion of our effort addressed the significant change in environment induced by the operation in air. Prior experiments, in particular Stratoscope II, have shown that convective effects even at altitude significantly degrade optical performance. Thus, in addition to the normal thermal control requirements, which are the same as those of the 100-centimeter Shuttle telescope, we must develop a system that is insensitive or immune to natural convection effects that degrade optical performance.

4.1.2 Environment

The major environmental feature of interest for the balloon-borne photoheliograph is the presence of an atmosphere during operation. The nominal system mission is defined as up to 1 day's operation at an altitude of 24.4 kilometers. At this elevation, the normal air pressure is approximately 3,320 newtons/meter^2, which is sufficient to force us to consider convective heat transfer. The general mission profile assumed was that proposed originally in our Stratoscope III study, i.e., an ascent to the 24.4-kilometer altitude at a nominal rate of 0.3 kilometer per minute. The ambient air temperature and external heat transfer coefficients used for this analysis were furnished by NASA/MSFC for the above study. These are shown in Figs. 4-1 and 4-2, respectively.

The external solar loading was conservatively applied at a 1 sun value of 0.138 watt/cm^2, no solar attenuation by the atmosphere was assumed.

4.1.3 General Thermal Control Concepts

Two general approaches to the thermal control of the balloon-borne telescope are possible. We can run the system at the normal optics temperature of 21.1 °C or we can run the optics at ambient air temperature. A cold system presents a certain degree of risk in terms of mirror figure change and/or coefficient of expansion nonuniformities. On the other hand, the potential convective currents that compromise performance are eliminated. A hot system acts in this opposite manner. However, with a hot system we have another option, that of running the optical system within an enclosure.

At first glance, this does not appear to provide any relief from the convective effects problem. We have considered two alternatives that do offer some relief, one using helium gas as the filler medium and the other employing a vacuum. If the enclosure window can be made to run cold

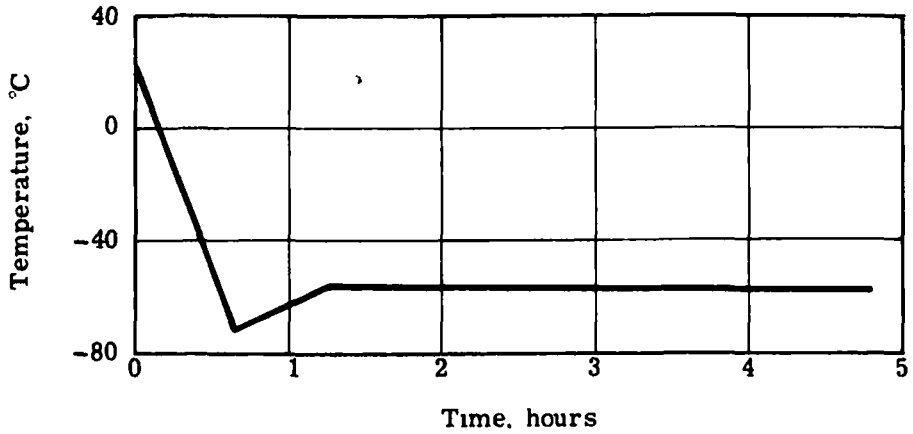

Fig. 4-1 — Air temperature history (MSFC data from Stratoscope II)

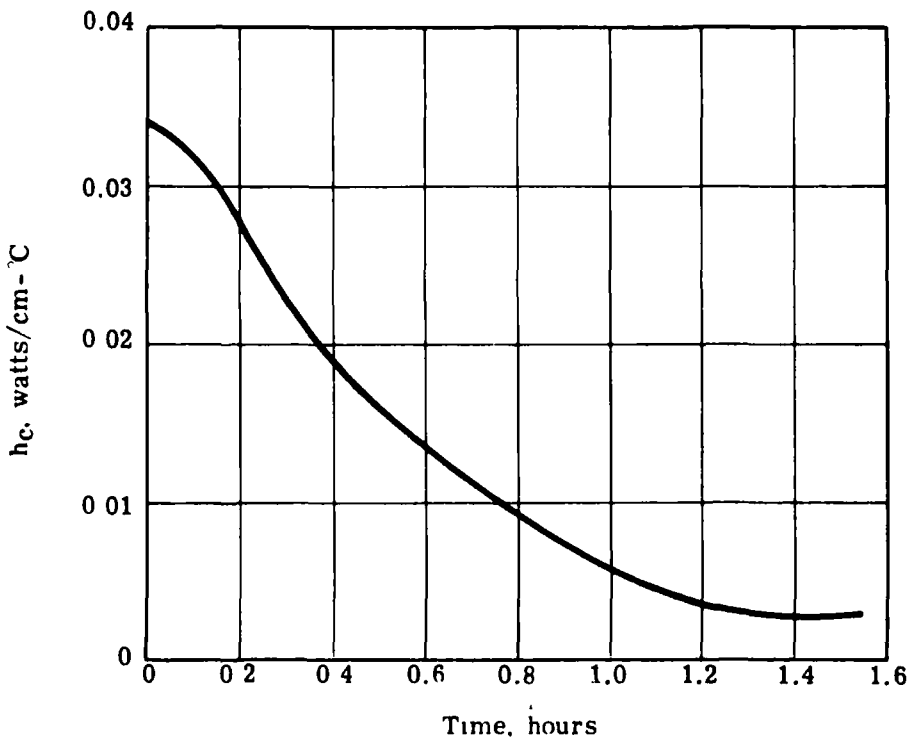

Fig. 4-2 — Heat transfer coefficient versus time after launch based on a constant ascent of 0.304 kilometer per minute (MSFC data from Stratoscope II)

(at ambient temperature), either the vacuum concept or the helium-filled enclosure will provide a satisfactory optical system.

All four thermal concepts have been evaluated for their overall system impact and the results are given in Table 4-1. As a result of this evaluation process, we have directed our effort toward the definition of a vacuum enclosed, "hot" telescope.

The fundamental problems still remaining to be addressed are methods or mechanisms by which·

1. The telescope is cooled prior to operation
2. Thermal control is achieved during observation
3. Thermal convection currents (pluming) are prevented from compromising performance.

The basic concept to be employed is passive cooling of the exterior of the telescope coupled with selective thermal finishes to reduce external radiative loading. An earth shade will be employed to prevent the aperture window from viewing the "warm" earth. A similar approach was used for the preconditioning of Stratoscope III except that no earth shade was required for night operation. The final telescope concept is shown in Fig. 4-3.

4.1.4 Analytical Tools

The balloon concept described above was evaluated by means of both a simple model (Figs. 4-4 and 4-5) and the system thermal model. Due to the complexity of the photoheliograph model, a simple 26-node thermal model incorporating the major design characteristics was made. Sufficient detail was used in this model to identify the major structural features of the photoheliograph for the identification of major performance characteristics.

In addition to the simple model, the photoheliograph system model was reconfigured for the balloon mission.

Where feasible, hand analyses were conducted to establish viable approaches such as the primary mirror and heat shield mirror (discussed in subsequent sections).

4.2 BASELINE THERMAL CONTROL CONCEPT

The key features of the baseline thermal control concept have evolved from the nature of the balloon mission, which is uniquely different from the previously discussed LSO and Shuttle flights. The short mission duration coupled with the ambient atmosphere result in a baseline concept tailored to the balloon flight. The basic features of this design concept are illustrated in Fig. 4-6.

The solid primary mirror (item 1) is used without cooling in an adiabatic configuration. The main support ring (item 2), the secondary mirror (item 3), and the relay flats (items 4 and 5) are all thermostatically controlled at 20.5 ± 1.1 °C. The metering truss (item 6) is indirectly controlled by the thermal control finishes applied to the outer shell/vacuum tank (item 7). This outer shell is also configured to passively obtain and maintain a temperature at least as low as the external ambient air temperature during the mission.

The heat shield mirror (item 8) is thermally controlled by means of a phase change material (item 9) which melts at less than 32.2 °C, storing the absorbed thermal load on this (item 8) element. An aperture window (item 10) required for the vacuum tank concept is thermally controlled by radiation exchange with the earth shade (item 11) at the same low temperature level as the outer shell.

Specific design details of these concepts are discussed in Sections 4.3 through 4.5.

Table 4-1 — Concept Evaluation

	21.1 C Mirror Telescope in Vacuum	21.1 °C Telescope in Helium Gas	-56.8 °C Telescope in Atmosphere	-56.8 °C Telescope in Helium Gas
Thermal problem (ability to n eet requirements)	+	– (pluming at boundary)	– (pluming at mirrors)	–
Design verification adequacy	+	–	–	–
Weight	– (vacuum tank)	– (enclosure)	+	– (enclosure)
Reliability	– (vacuum failure possible)	– (contamination)	+	+
Refurbishment complications	+	+	– (water condensation)	+
Settling time to operating temperatures	– (must control setting of truss)	+	– (requires preconditioning)	– (requires preconditioning)
Overall evaluation	+	–	–	–

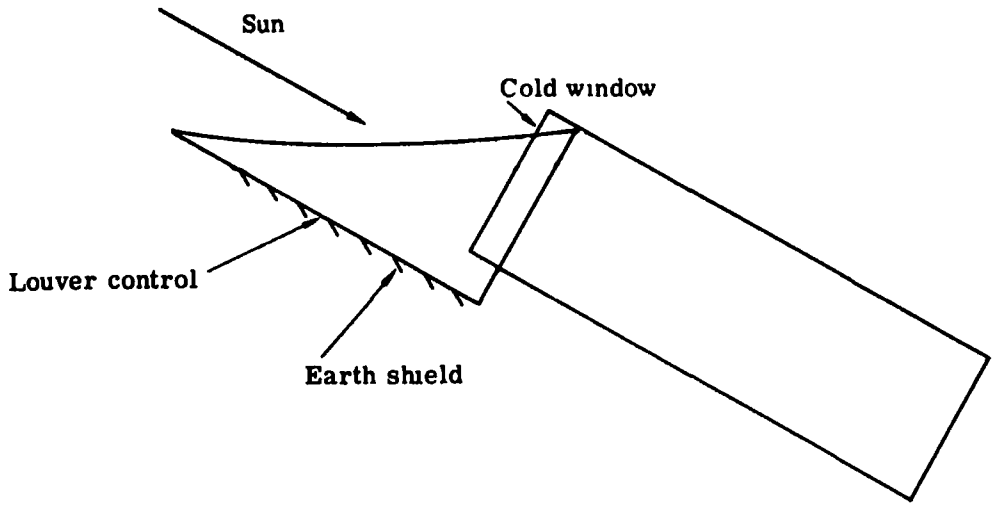

Fig. 4-3 — System concept for avoiding pluming

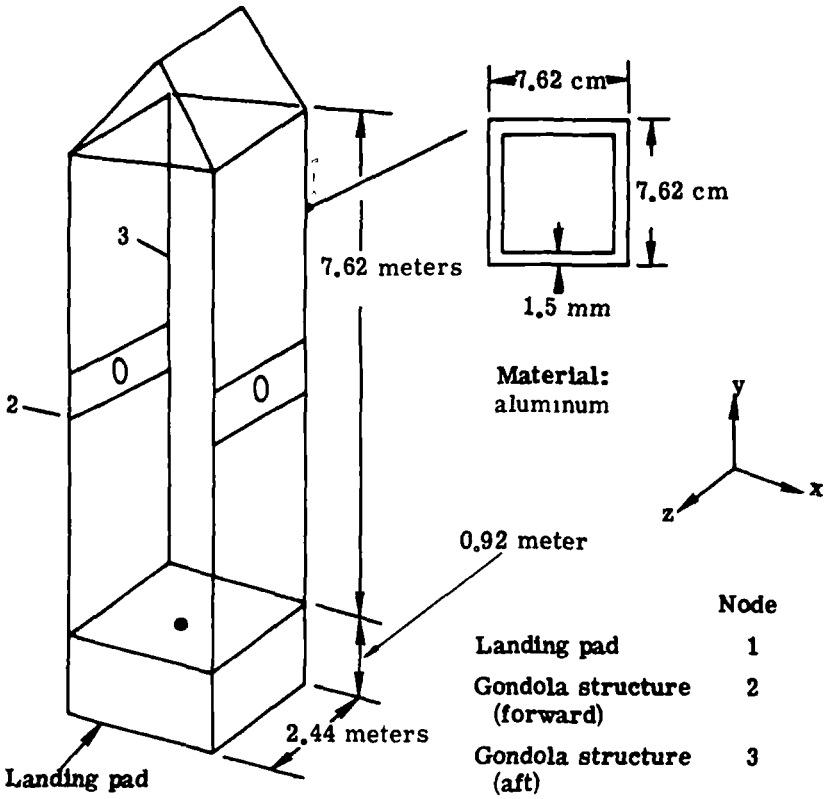

Fig. 4-4 — 100-centimeter photoheliograph balloon model

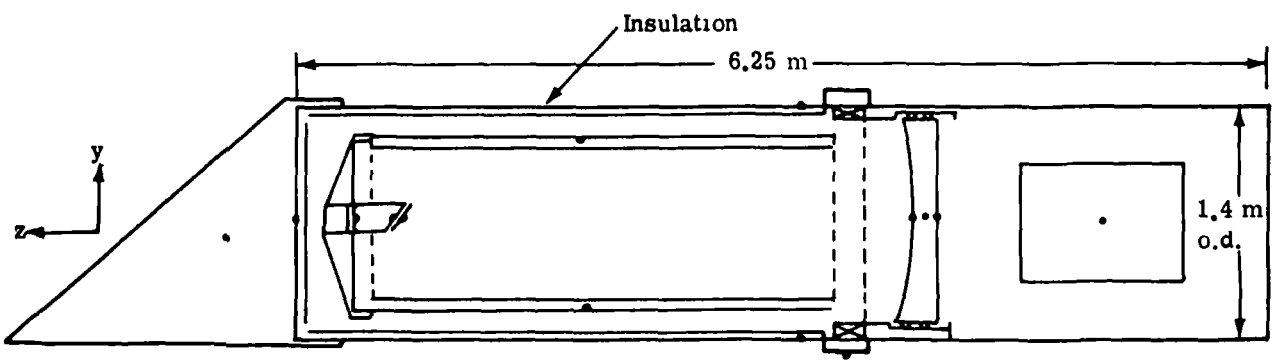

	Node		Node
Earth shade	4	Secondary	12
Outer shell (top)	5	Heat shield	13
Outer shell (bottom)	6	First relay	14
Primary (front)	7	Window	15
Primary (middle)	8	Gimbal	16
Primary (back)	9	Instrument package	17
Metering structure	10		
Metering (bottom)	11		

Fig. 4-5 — 100-centimeter photoheliograph balloon model

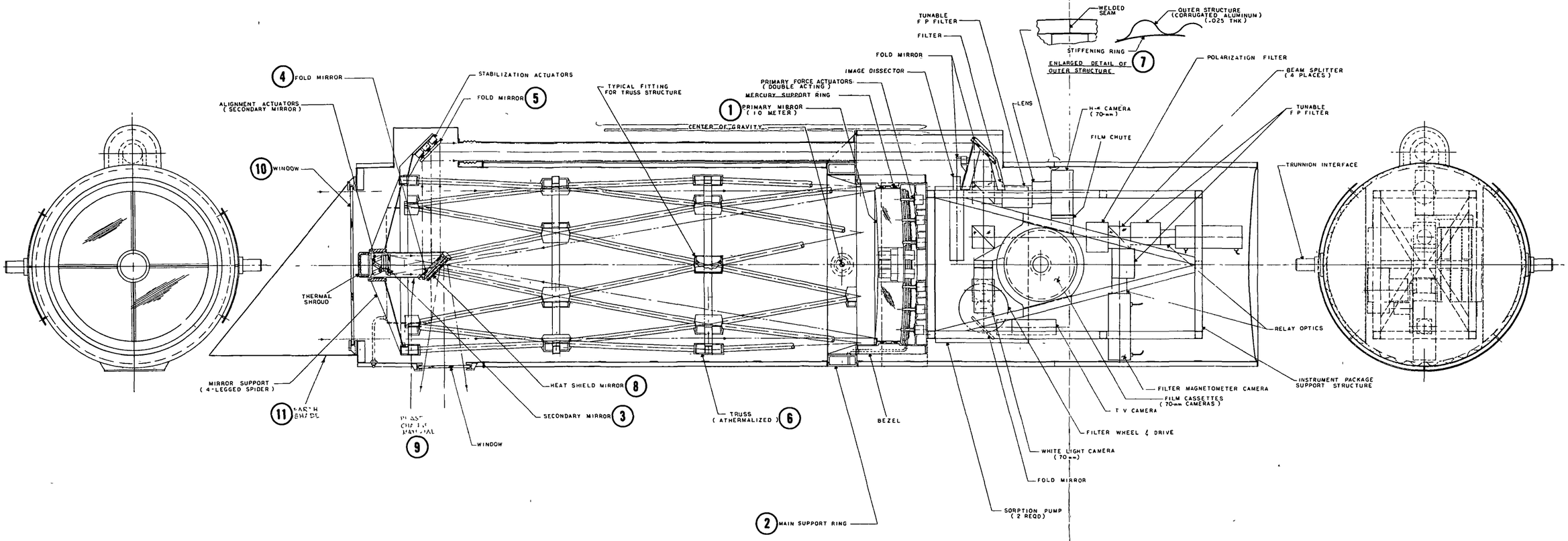

Fig. 4-4 — Thermal control concept

Page intentionally left blank

4.3 TELESCOPE THERMAL CONTROL CONCEPTS

4.3.1 Primary Mirror

Based on the change in mission characteristics, the primary mirror thermal control concepts were reviewed again. Clearly, a cold plate coupled to an external radiator is usable. However, since we are now considering a 1-day mission, an adiabatic primary may also be feasible. A preliminary analysis of the concept was conducted, assuming a one-dimensional transient heating condition, and the results appeared favorable. For a 10-centimeter-thick solid ULE mirror (L/D = 0.1), an axial gradient of approximately 5.5 °C was predicted. Mirror temperature rise is obviously dependent on observation time, and although this might ultimately result in a mission constraint, the elimination of cold plate, heat pipe, and radiator for this mission was considered desirable. Furthermore, the force actuator concept can be significantly simplified if the thermal control hardware behind the mirror is not present.

Accordingly, the baseline concept of an adiabatic primary mirror was selected for further study.

4.3.2 Heat Shield Mirror

As in the case of the primary mirror, the change in mission time resulted in a reevaluation of heat shield mirror thermal control concepts. Two alternative approaches suggest themselves based on the short duration of the observation period. The first is the radiative fin concept investigated for the Shuttle photoheliograph. If we examine the temperature history plots in Figs. 3-21 and 3-22, we note that after 10 hours observation, the peak heat shield mirror temperature is 40.5 °C and the relay flat is 35 °C. For a balloon mission, these temperatures may be somewhat lower, since the outer shell temperatures are lower. Also a mission time constraint might be imposed that would reduce the peak temperature levels accordingly.

A second approach to the thermal control problem is the use of phase change materials to store the absorbed solar energy of the heat shield mirror. A literature search was conducted and three materials were found that may be considered candidates for this concept. They are polyethylene glycol, lithium nitrate trihydrate ($LiNO_3 \cdot 3H_2O$), and n-octadecane ($C_{18}H_{38}$). Each material was selected because of its high heat of fusion or hydration and because its transition temperature was less than 32.2 °C. The significant properties of each are given in Table 4-2.

Each candidate material is required to store the absorbed solar load of 86 watts. Assuming a 10-hour observation period, the mass of phase change material required is 11.5 kilograms, 5.5 kilograms, or 6.9 kilograms, respectively. Based on material densities, the resultant volumes for material are 10,400 cubic centimeters, 3,110 cubic centimeters, and 8,780 cubic centimeters. Based on these considerations, we have eliminated polyethylene glycol from further consideration. Although lithium salt appears very favorable, it has been reported to be corrosive to container materials, and thus we have also dropped it from further consideration at this time.

Having selected a material, we then developed an appropriate packaging concept. The basis for the proposed concept is the radiative fin geometric arrangement. As shown in Fig. 4-7 a double-wall cylindrical container is provided to support the heat shield and first relay mirrors. Additional volume is provided between the mirrors. Fig. 4-8 presents a plot of the available volume as a function of annular or mirror separation distance. For the n-octadecane, a mirror separation of 3.8 centimeters and an annular thickness of 1.9 centimeters are required.

We recognize that certain problems remain to be solved prior to the utilization of phase change material for this application. The most significant are determining a method of enhancing the low conductivity of the organic material to ensure its effectiveness and determining the compatibility of the phase change material with the structural materials used in the photoheliograph.

Table 4-2 — Proposed Phase Change Materials

Material	Transition Temperature, °C	Heat of Fusion, joules/kg
Polyethylene glycol	22.2	1.47×10^5
$LiNO_3 \cdot 3H_2O$	29.8	2.97×10^5
$C_{18}H_{38}$	28	2.42×10^5

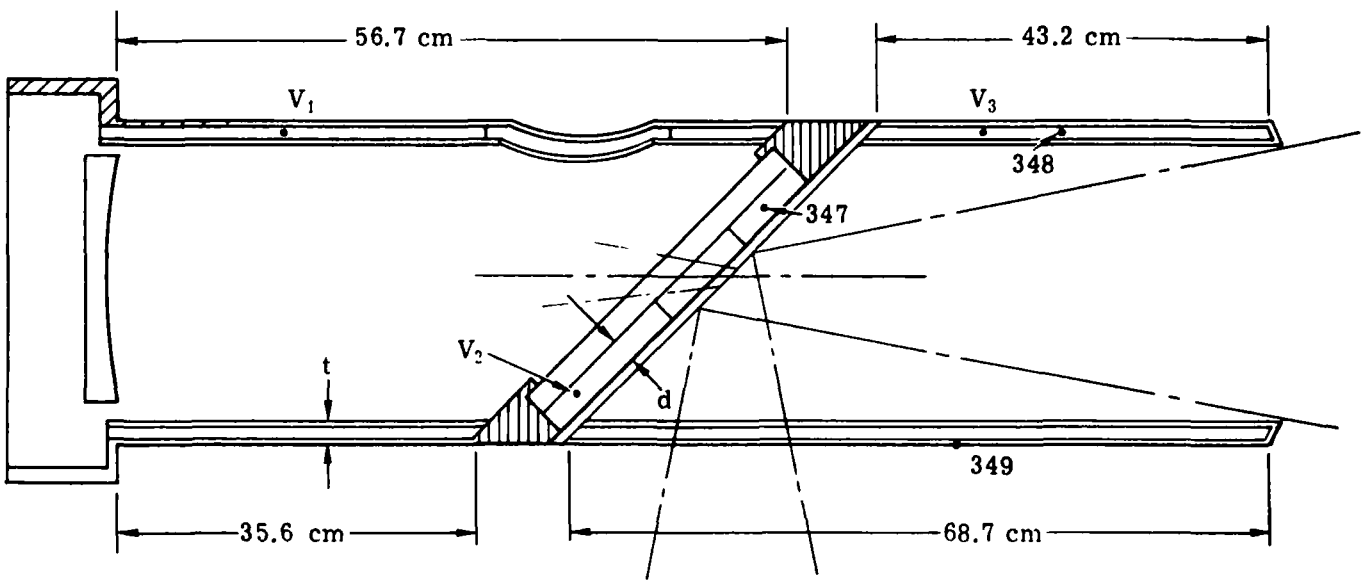

Fig. 4-7 — Phase change material packaging concept

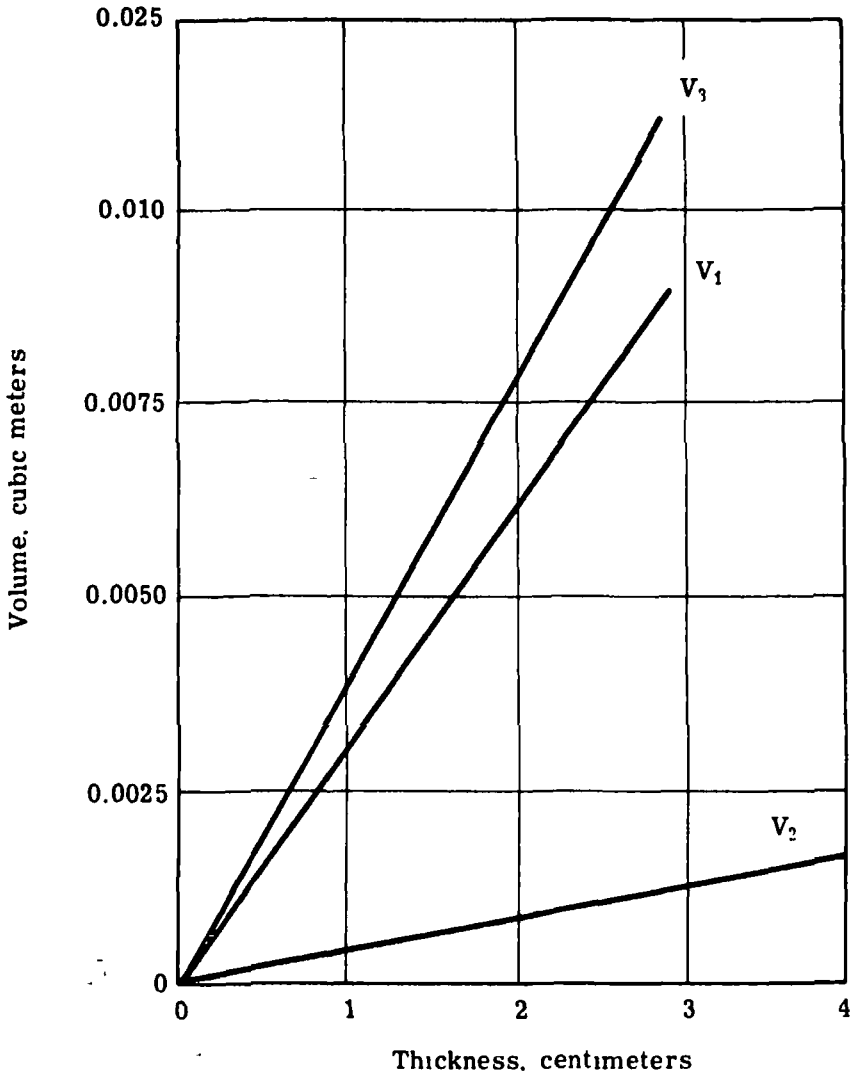

Fig. 4-8 — Available volume for phase change material

At this time we propose the phase change material as the baseline concept with the radiative fin as an alternative backup concept.

4.3.3 Truss Structure

The basic truss structure is radiatively coupled to the vacuum tank/shell walls. These walls are thermally black as is the truss structure. Since external thermal transients are minimal, no problems are anticipated from truss temperature transients.

4.3.4 Instruments

Instrument thermal control is not considered to be a problem. The walls of the instrument compartment are adequate heat sinks for the proposed instrument complement. Prior studies of the Shuttle mission have provided suitable methods for thermal control.

4.4 PRELIMINARY TELESCOPE CONCEPT ANALYSIS

Preliminary evaluation and investigation of telescope operation was conducted using the simple model described in Section 4.1.4. Complete characteristics of the model are given in Table 4-3.

The first run of the simple model was made to evaluate the launch transient and to determine system cooldown time. Particular boundary conditions for the launch included no solar energy and the telescope positioned horizontally. Results of this run are presented in Figs. 4-9 and 4-10. The data indicates that approximately 6 hours is required for the window to reach ambient temperature, however, the bottom of the outer shell did not reach ambient temperature during the time period (16.25 hours) investigated.

Having determined the system cooldown characteristic, we proceeded to modify the model boundary conditions to simulate an entire balloon mission. At the 6-hour point, solar loads were applied to the aperture window and all internal optics, albedo inputs to the lower half of the outer shell, and gondola structure were applied, and the instrument power dissipation was initiated.

Using a 15.2-centimeter-thick primary and a high emittance truss structure, we ran a simulated mission of 10 hours observation. Results of this run are presented in Figs. 4-11 through 4-14. Operation appears to have very little effect on the window and earth shade. The behavior of the primary mirror is illustrated in Fig. 4-13, which not only indicates the development of an axial gradient of approximately 8.3 °C but also the probability of mirror overheating at the conclusion of the 10-hour observation period. The rate of temperature increase is approximately 2.8 °C per hour. Fig. 4-14 illustrates the behavior of the secondary mirror and first relay flat. The large temperature increase of the first relay mirror results from the high resistance mounting connection between mirror and structure.

A second case evaluated with the simple model was directed toward the possible use of low emittance structures. The structural emittance was reduced to 0.04 from the original value of 0.9 while all other boundary conditions remained constant. Virtually no temperature change in truss structure was noted (see Fig. 4-15). Typical gondola structure temperatures are illustrated in Fig. 4-16.

No attempt was made to model the phase change material concept due to the complexity of the concept, and the heat shield mirror was arbitrarily fixed at 21.1 °C throughout the mission.

In general, the simple model results were as expected and did confirm that the surface finishes, primary mirror, truss structure, and instrument sections operated as expected. The performance of the gondola demonstrates that careful design will be required to avoid interactions with the telescope assembly during operation.

Table 4-3 — Balloon Thermal Model Nodal Identification

Node Number	Description	Material	Surface Properties	Notes
1	Gondola crash pad	Styrofoam	α_S = 0.25, ϵ = 0.88 white paint	Consider alternative for sun side of pad
2	Gondola structure, sun side	Aluminum 6061	α_S = 0.25, ϵ = 0.88	Consider alternative α_S = 0.05, ϵ = 0.02
3	Gondola structure, shade side	Aluminum 6061	α_S = 0.25, ϵ = 0.88	α_S = 0.25, ϵ = 0.88
4	Earth shade	Aluminum 6061	ϵ = 0.9 inside α_S = 0.05, ϵ = 0.02 outside	
5	Outer shell, top	Aluminum 6061	ϵ = 0.9 outside ϵ = 0.9 inside	
6	Outer shell, bottom	Aluminum 6061	ϵ = 0.9 inside ϵ = 0.02 outside α_S = 0.05	Alternative outside ϵ = 0.88, α = 0.25 white paint
7	Primary mirror, front	ULE	Aluminum α_S = 0.12 ϵ = 0.04	Sides insulated ϵ = 0.01
8	Primary mirror	ULE	—	Sides insulated ϵ = 0.01
9	Primary mirror, back	ULE	ϵ = 0.01 adiabatic Alternative ϵ = 0.9 cooled	Sides insulated ϵ = 0.01
10	Metering structure, top	Graphite-epoxy	ϵ = 0.9	
11	Metering structure, bottom	Graphite-epoxy	ϵ = 0.9	
12	Secondary	ULE/Cer-Vit	ϵ = 0.04, α_S = 0.12	
13	Heat shield mirror	Aluminum	ϵ = 0.05, α_S = 0.05	
14	First relay mirror	ULE/Cer-Vit	α_S = 0.12, ϵ = 0.04	Alternative α_S = 0.05, ϵ = 0.02
15	Window	BK-7	ϵ = 0.9, α_S = 0.04	Assume 4 percent absorbed
16	Gimbal	Titanium + steel	α_S = 0.25, ϵ = 0.88	
17	Instrument package	Graphite-epoxy, copper, aluminum	ϵ = 0.9	Constant power output Q = 163 watts

4.5 DETAILED CONCEPT EVALUATION ANALYSIS

In order to confirm the findings of the preliminary analyses conducted, the photoheliograph system thermal model was modified to conform to the balloon mission. Additional nodes representing the gondola, window, earth shade, and gimbal were added to the model. These nodes are shown in Figs. 4-17 and 4-18. Furthermore, all surface finishes were adjusted to conform to the previously described simple model values. The phase change material concept was also employed as described in Section 4.3.2.

As before, an initial transient run was made to establish the launch transient. The previously described boundary conditions (see Section 4.4) were applied. A time period of 6 hours, based on our initial analysis, was selected. Results of the initial transient run are given in Figs. 4-19 through 4-30.

Figs. 4-19 through 4-23 present the cooldown characteristics of the primary mirror, the heat shield mirror, and the first relay flat. Examination of the data indicates the development of an axial gradient of approximately 0.55 °C and a radial gradient of 0.28 °C. The latter is illustrated in Fig. 4-22, where nodes 88 and 91 represent the center and nodes 93 and 98 represent the middle ring. The first relay flat is held at temperature while the heat shield mirror is uncontrolled.

Typical truss structural nodes and outer shell nodes are presented in Figs. 4-24, 4-25, and 4-26. The behavior of these nodes may be compared to the prior simple model results shown in Fig. 4-11. Truss temperature diametral gradients of 5.5 to 6.6 °C are developed as a result of the 16.6 °C gradient of the outer shell. Of significance is the fact that predicted temperatures at the end of the 6-hour transient for the bottom of the outer shell range from −67.8 to −65.6 °C, below the ambient air temperature of −56.1 °C. We can conclude from this result that the shell will not contribute to "thermal pluming."

Examination of the calculated window temperatures, illustrated in Figs. 4-27 and 4-28, indicates that the window temperature is below the ambient air. The temperature distribution of the aperture window is, however, much greater than desired. For example, window temperatures range from −71 to −57.6 °C with a peak diametral gradient of 7 °C and center to edge gradient ranging from 0.8 to 3.9 °C. Since these conditions may result in performance degradation, active thermal control of the window is probably required. This may be accomplished either by providing zoned heaters to either the window bezel or the circumference of the window, or by thermally decoupling the window from the bezel by a high thermal resistance mount, or both. In any case, it is obvious that the thermal design of the window is critical and additional study in greater depth is required.

The launch transient final temperatures were determined and used as the initial temperatures for an observation period investigation. The results of the observation period thermal study are presented in Figs. 4-31 through 4-34 for the face, center, and back of the mirror. Evaluation of the test data indicates that after 10 hours of observation, the mirror face temperature is approximately 37.8 °C. Axial gradients in the primary range from 6.4 to 6.7 °C, and a radial gradient of approximately 0.33 °C exists. Review of the mirror data indicates an average temperature rise of 1.8 °C per hour. In terms of system performance, mirror heating is clearly dependent on observation time, since after approximately 4 hours, the final face-to-back gradient has developed. Examination of thermal sensitivity estimates indicates that level changes of the order of 14 to 16.7 °C result in the maximum allowable error. Thus it appears that a 10-hour observation is the maximum that can be allowed. It is possible to extend the observation time by roughly 10 percent by changing the mirror material from ULE to Cer-Vit, since this would increase the heat capacity by approximately this amount.

Fig. 4-35 illustrates the response of the heat shield mirror (node 220), which obviously overheats during observation. We predict that the mirror will reach the phase change material melt

temperature of 28.4 °C in approximately 1.25 hours. The characteristics of the system model do not reflect any enhancement of thermal conductivity to the phase change material and as a result, mirror temperature continues to rise. The study and development of conductivity enhancement techniques and their incorporation into the system model was not undertaken. However, several methods such as the use of aluminum honeycomb, wire mesh, and metallic inserts are all conceptually feasible. We suggest that the use of phase change material thermal control be investigated both analytically and experimentally.

Truss and shell temperature response is shown in Figs. 4-36, 4-37, and 4-38. Some temperature rise during observation is evident. However, the increases are minimal and in general starting gradients are slightly increased or unchanged.

Examination of the transient behavior of the aperture window in Figs. 4-39 and 4-40 and in the computer data generated during the observation period indicates a temperature rise of from 2.8 °C at the center to approximately 6.6 °C at the edges. The maximum diametral gradient has increased to 8.45 °C. However, the radial gradients have decreased to a maximum of 1.95 °C (at the end of 10 hours of observation). Our previous comments regarding active thermal control of the window and additional study are applicable.

Figs. 4-41 and 4-42 present earth shade and gondola temperatures, respectively. Earth shade performance is satisfactory, and the gondola structure clearly demonstrates that the interactions between gondola and telescope, with respect to thermal pluming, must be considered.

4.6 BASELINE CONCEPT

Based on the evaluations and analyses described in this section, we recommend the thermal control baseline outlined in Table 4-4. The major elements of this baseline concept are discussed below.

The solid primary mirror is considered to be a key element in the thermal control baseline for the 100-centimeter balloon system. As a result of the short mission duration, we have established that a solid mirror has sufficient heat capacity to maintain optical performance without external cooling. The adiabatic "cooling" concept results in a much simpler system for primary mirror thermal control.

Likewise, the heat shield mirror thermal control baseline is based on a variation of the adiabatic concept. We propose the use of phase change material for the storage of absorbed solar energy. An alternative concept based on the radiative fin cooling scheme (see Section 3.4.2) is possible for the short duration mission requirement.

The secondary metering structure is passively controlled by means of a high emittance surface finish and no insulation. Consideration of the mission indicates that this simple approach will provide satisfactory performance.

The baseline thermal concept for the outer shell is established by the need to provide passive cooling to the ambient air temperature level during launch and to maintain this level during the observation period. A thermal finish pattern that provides for a high emittance is used on the upper half of the cylindrical shell, while a low emittance surface is used on the lower half. The high ϵ surface maximizes heat loss to space, while the low ϵ surface minimizes heat gain from the "hot" earth. Heat transfer within and across the outer shell is maximized by a high ϵ internal finish.

A similar rationale applies to the earth shade with respect to thermal control coatings selected for the baseline.

The thermal baseline for the aperture window is established by radiation exchange with the earth shade and with space. The earth shade also acts as a shield to prevent albedo and earth

infrared radiation from reaching the window directly. Active thermal control of the window at the ambient air temperature level is provided by bezel heaters. The gradients in the window are far too large for good optical performance. Further analysis directed at reducing the gradients to the 0.55 to 1.65 °C range is necessary.

Table 4-4 — 100-Centimeter Photoheliograph Balloon Mission Recommended Baseline

Primary mirror	Solid
Primary mirror cooling	Adiabatic
Outer shell	Top ϵ = 0.9, bottom α/ϵ = 0.05/0.02, no insulation
Metering structure	High ϵ, no insulation
Heat shield mirror	Phase change material
Earth shade	Inside ϵ = 0.9, outside α/ϵ = 0.05/0.02
Window	Active bezel control at −57 °C
Secondary, relays, and main support ring	21.1 °C active control
Instrument structure and instruments	Same as Shuttle

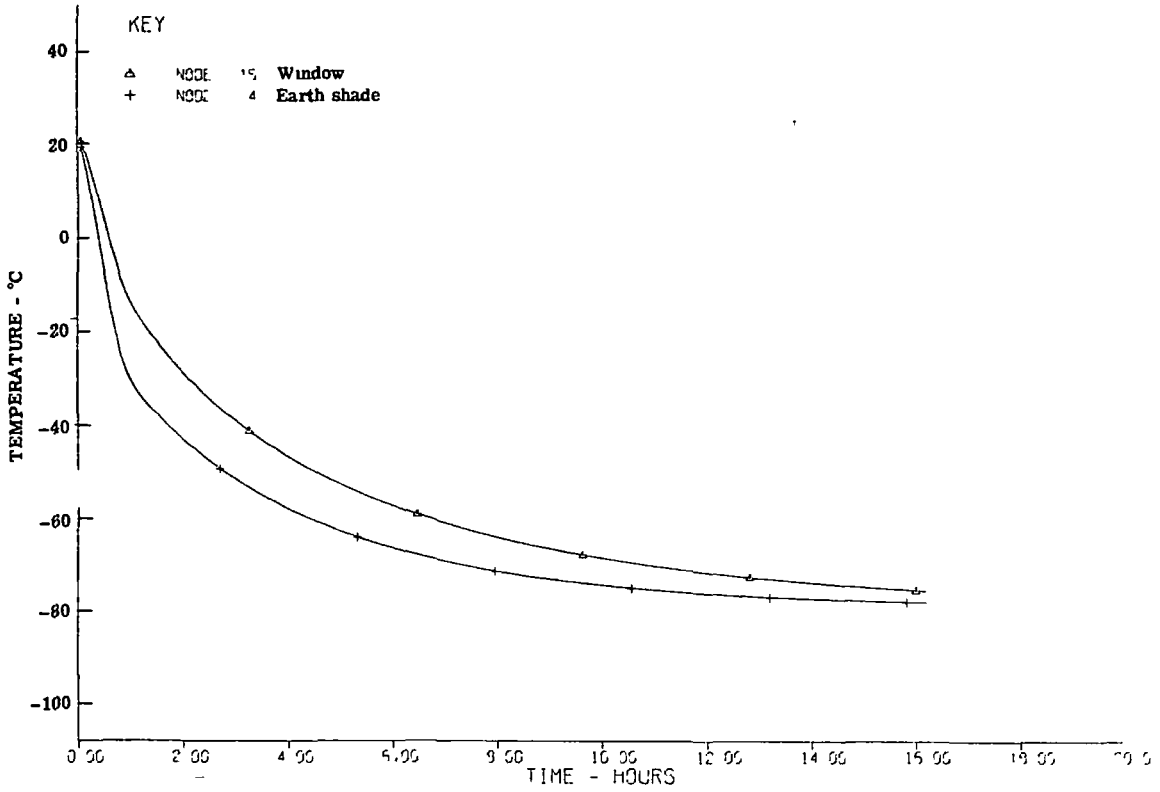

Fig. 4-9 — Temperature history for window and earth shade

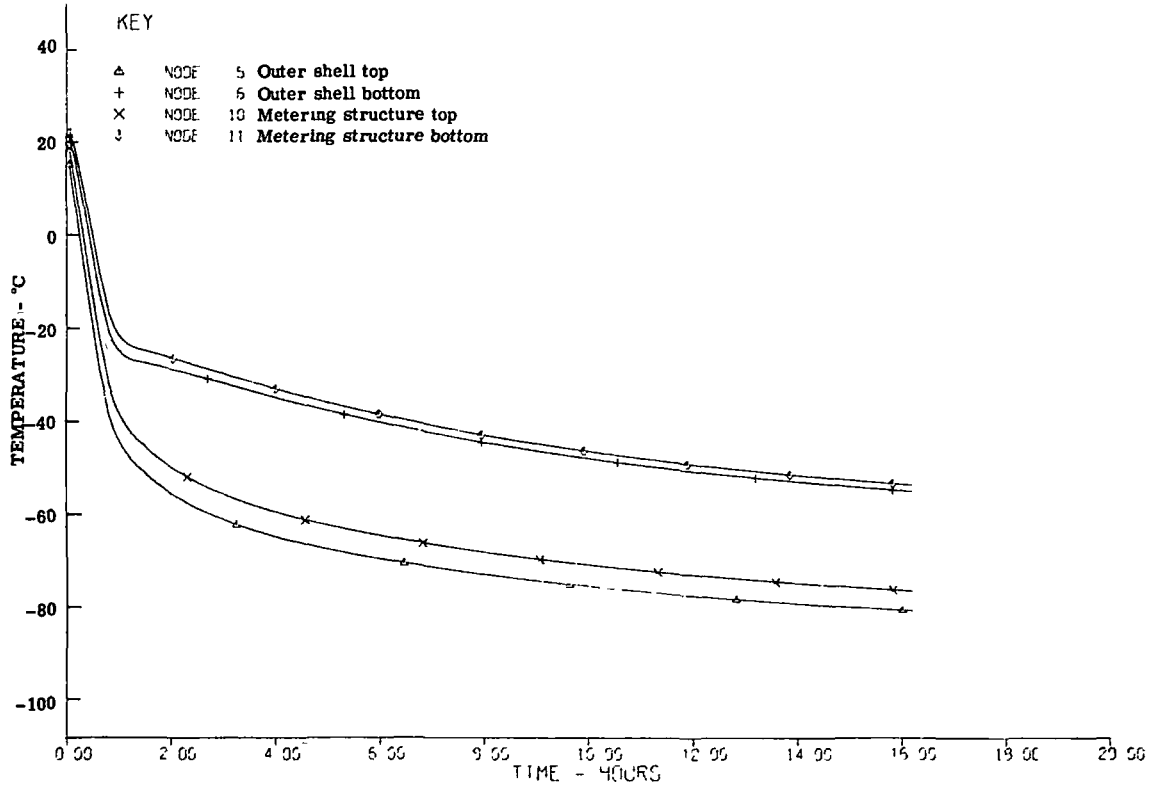

Fig. 4-10 — Temperature history for outer shell and metering structure

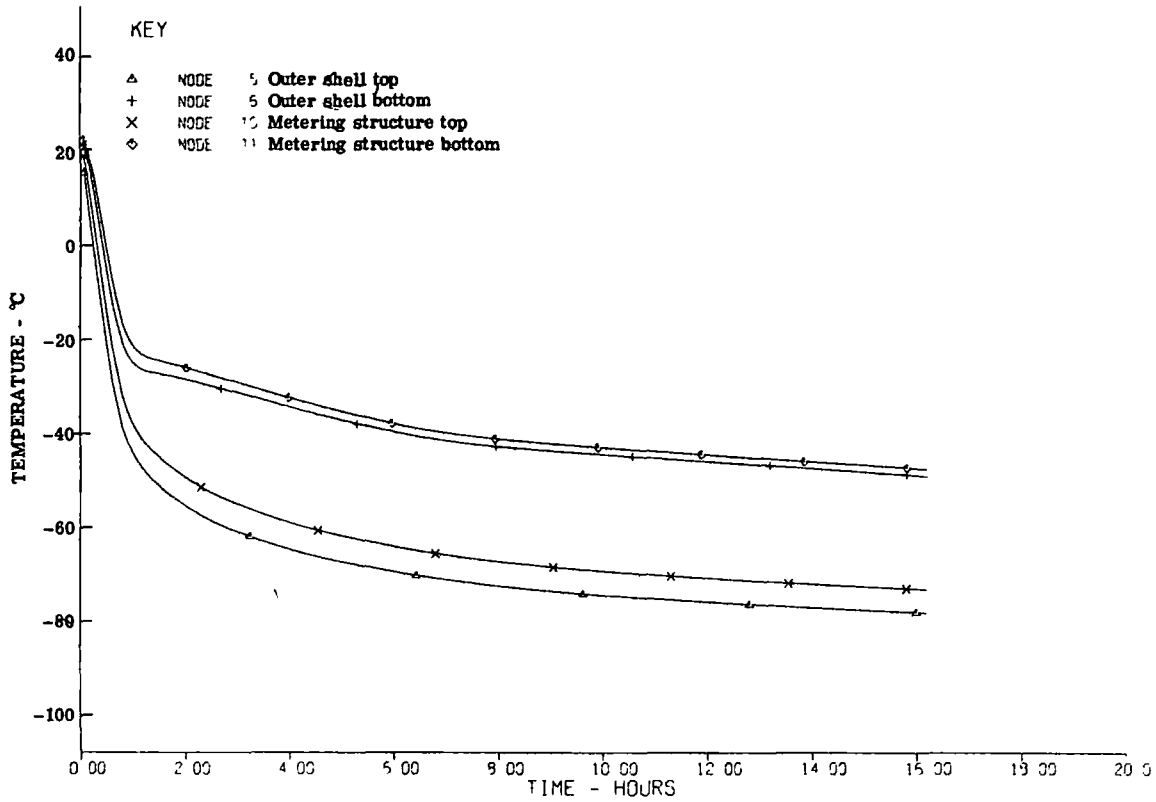

Fig. 4-11 — Temperature history for outer shell and metering structure—high ϵ structure

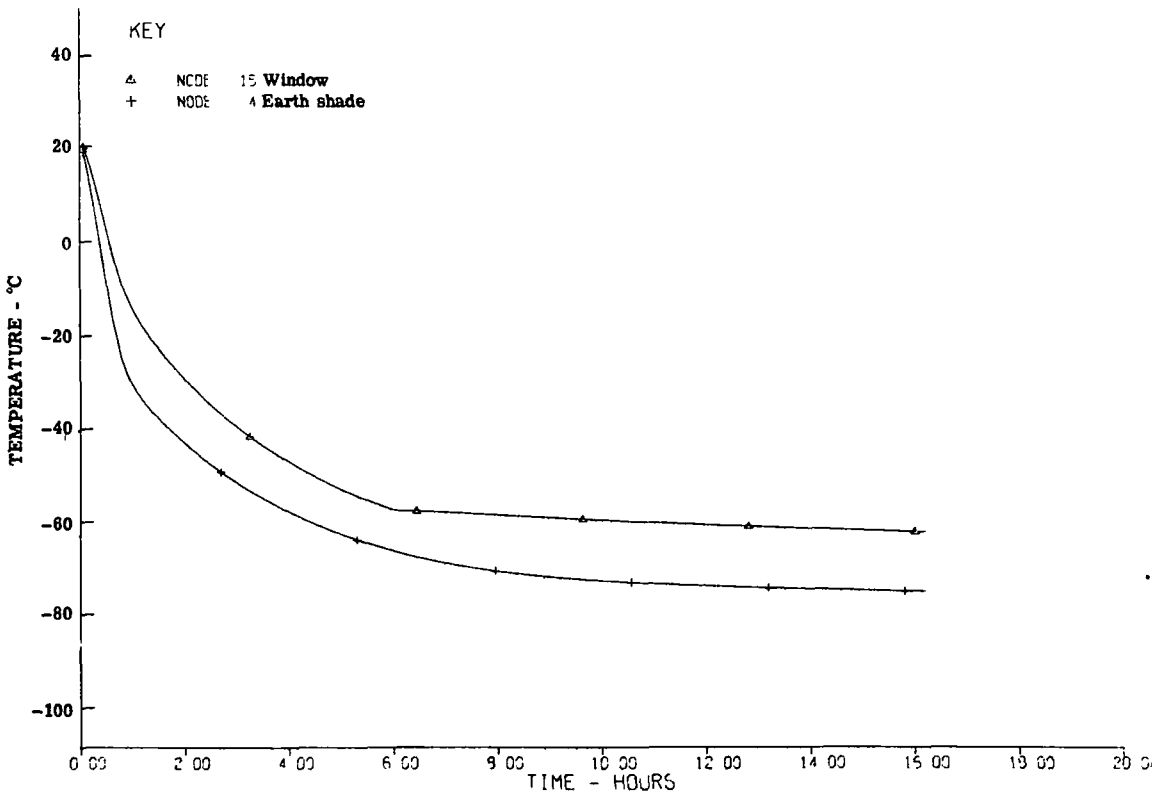

Fig. 4-12 — Temperature history for window and earth shade—high ϵ structure

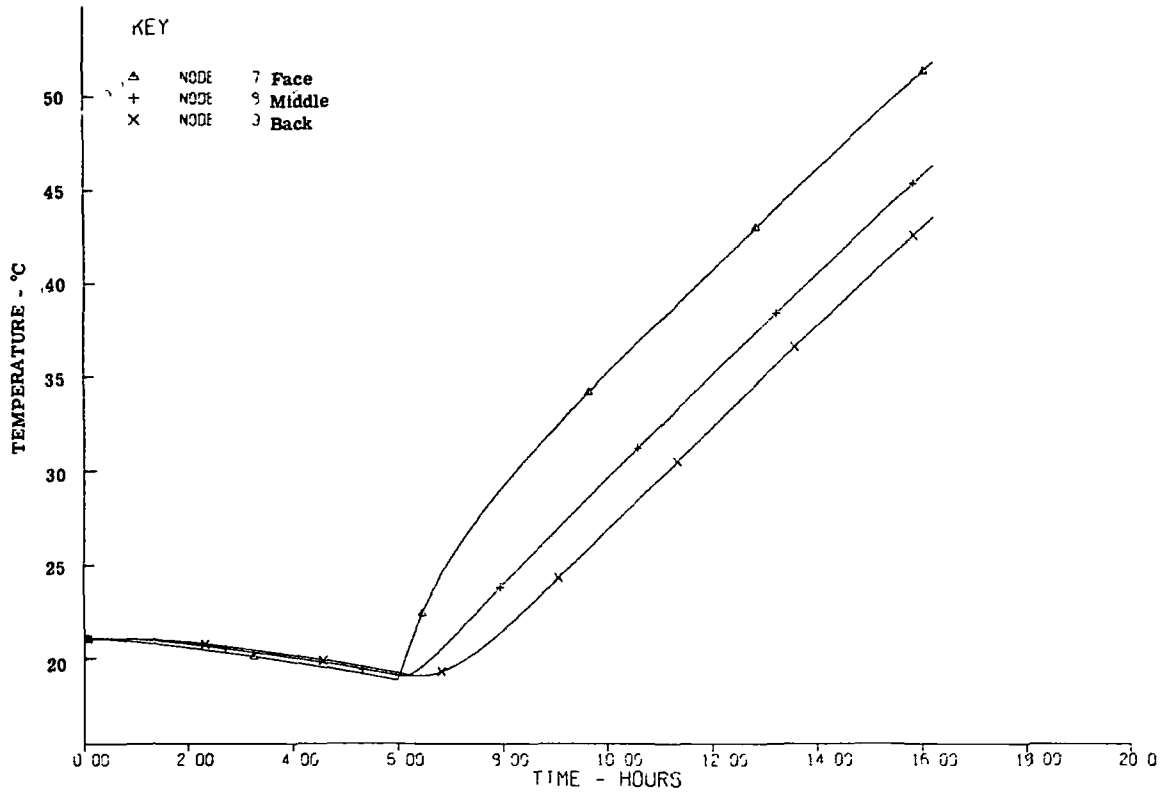

Fig. 4-13 — Temperature history for primary mirror—high ϵ structure

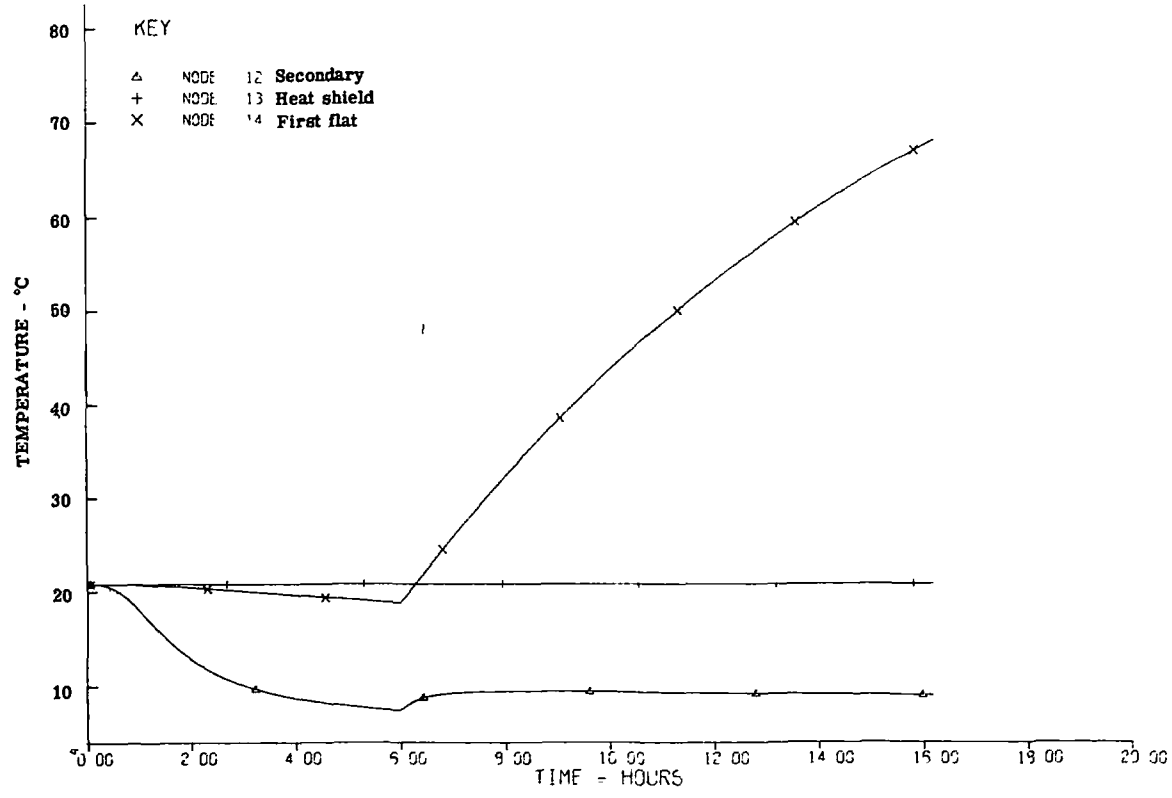

Fig. 4-14 — Temperature history for secondary, heat shield, and first relay mirrors—high ϵ structure

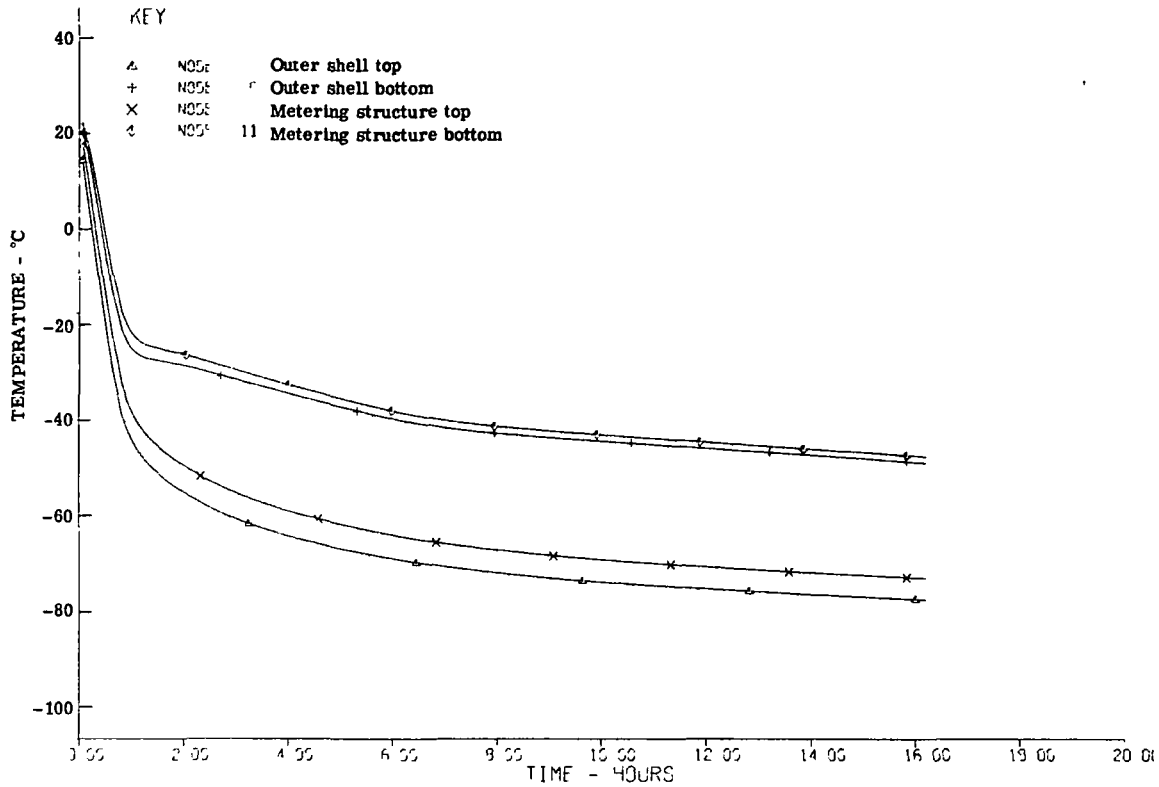

Fig. 4-15 — Temperature history for outer shell and metering structure—low ϵ structure

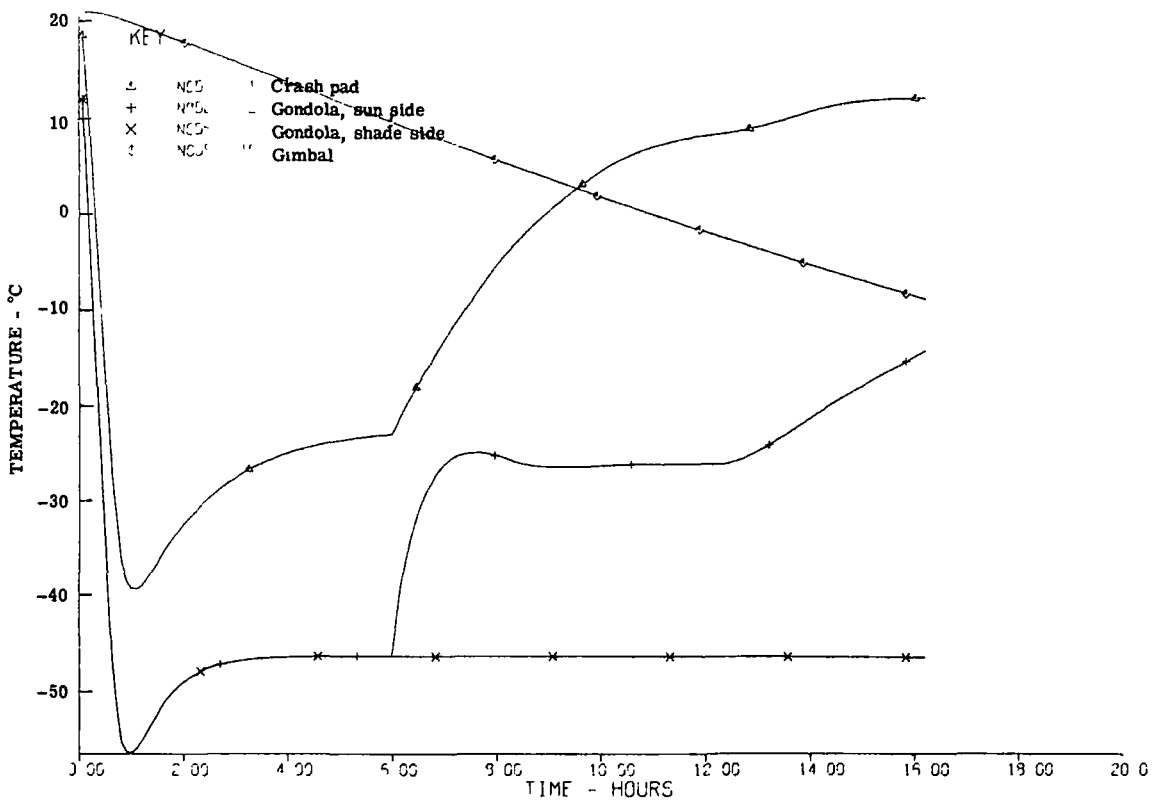

Fig. 4-16 — Temperature history for crash pad, gondola, and gimbal—low ϵ structure

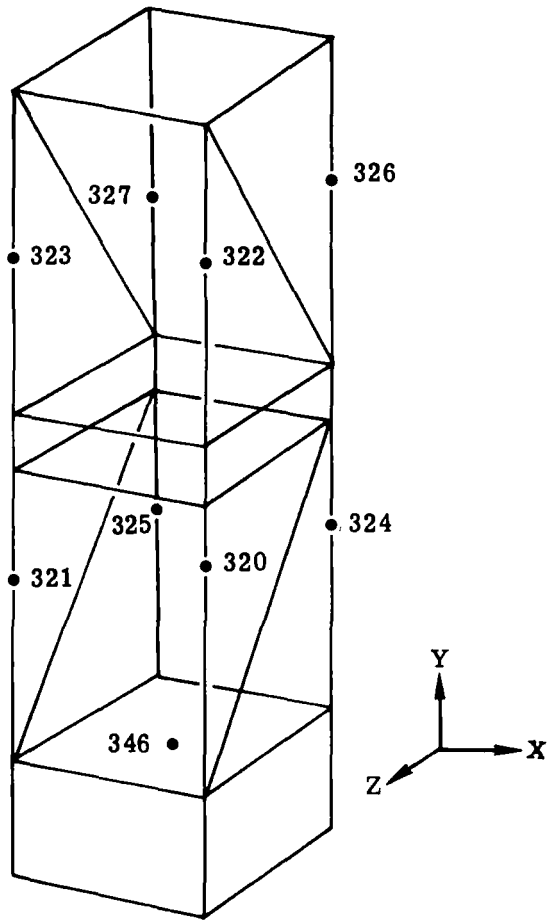

Fig. 4-17 — Gondola node identification

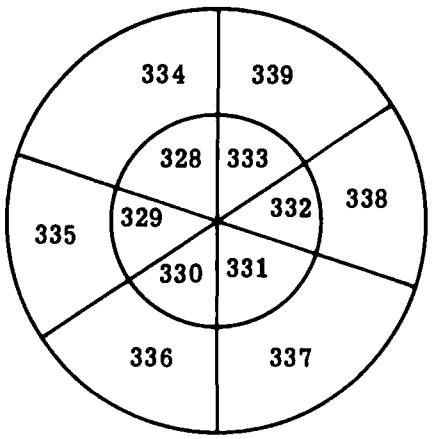

(a) Window nodes

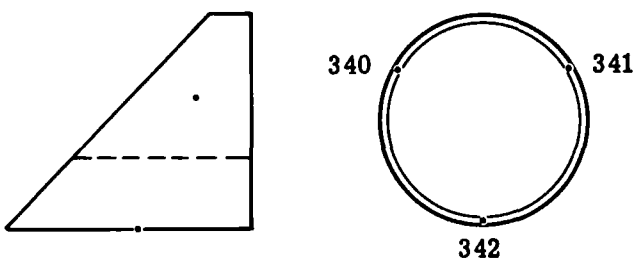

(b) Earth shade nodes

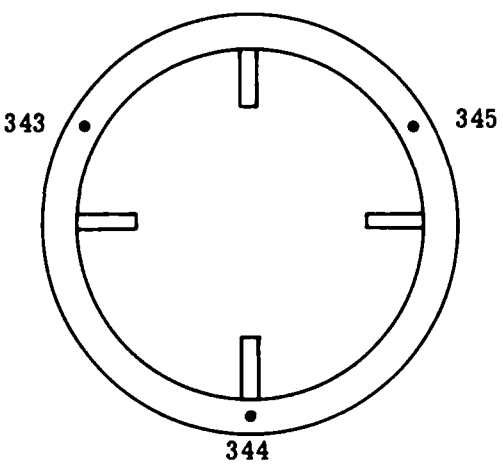

(c) Gimbal nodes

Fig. 4-18 — System model modifications

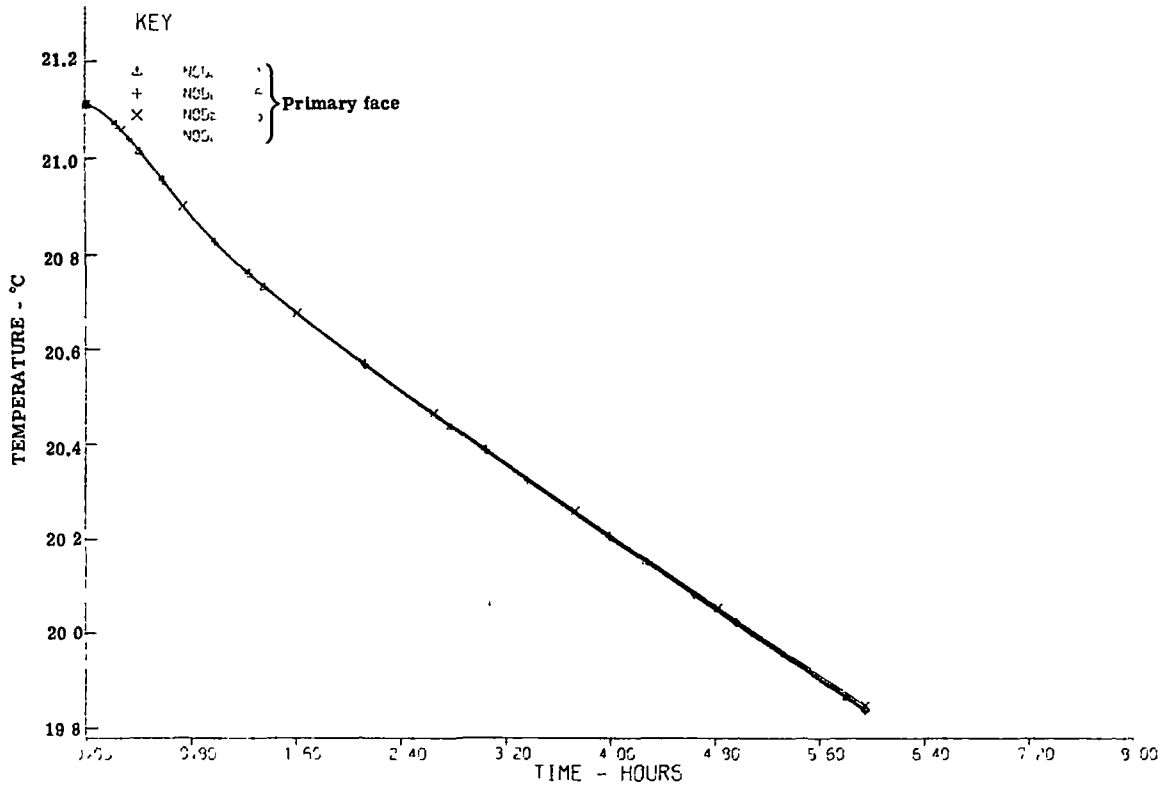

Fig. 4-19 — Temperature history for primary mirror—launch transient

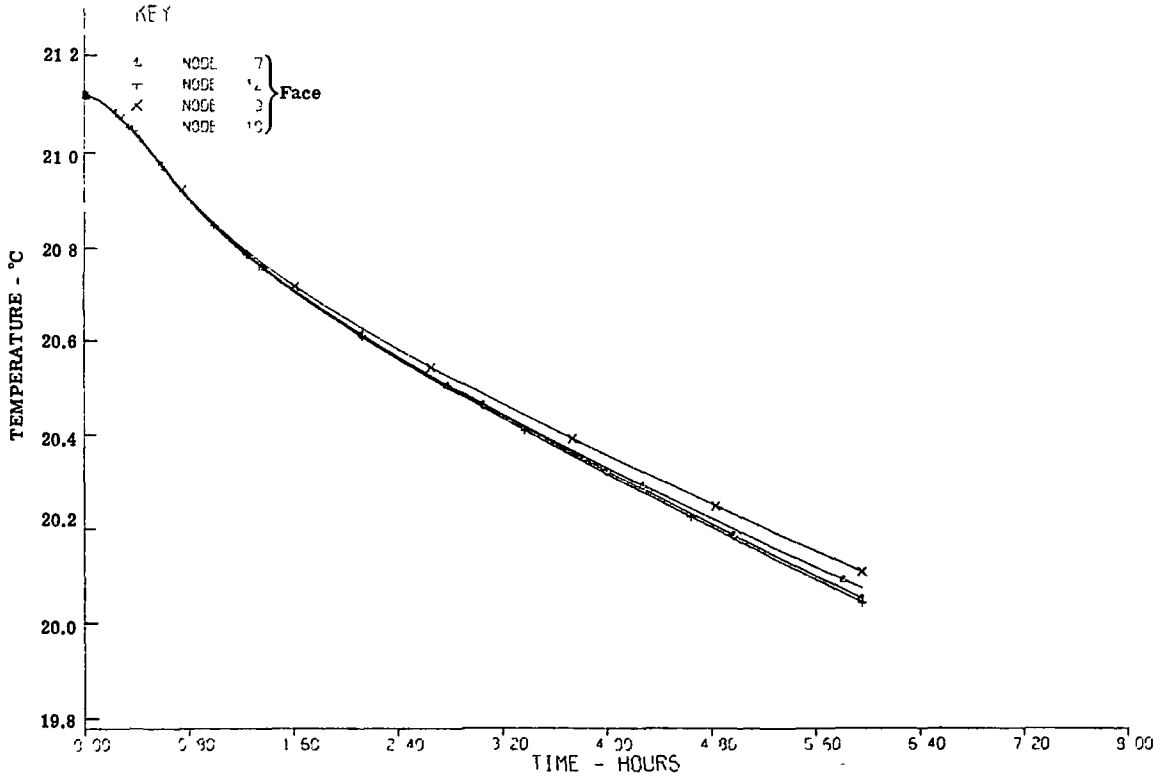

Fig. 4-20 — Temperature history for primary mirror—launch transient

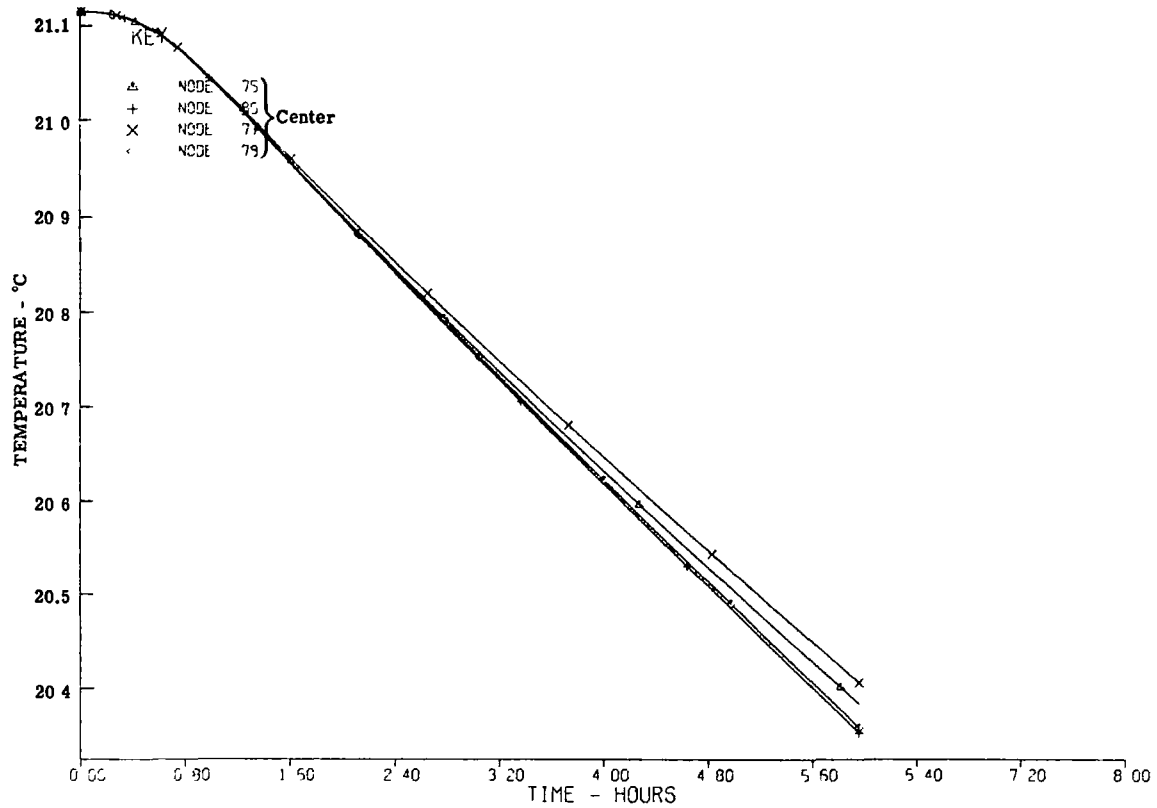

Fig. 4-21 — Temperature history for primary mirror—launch transient

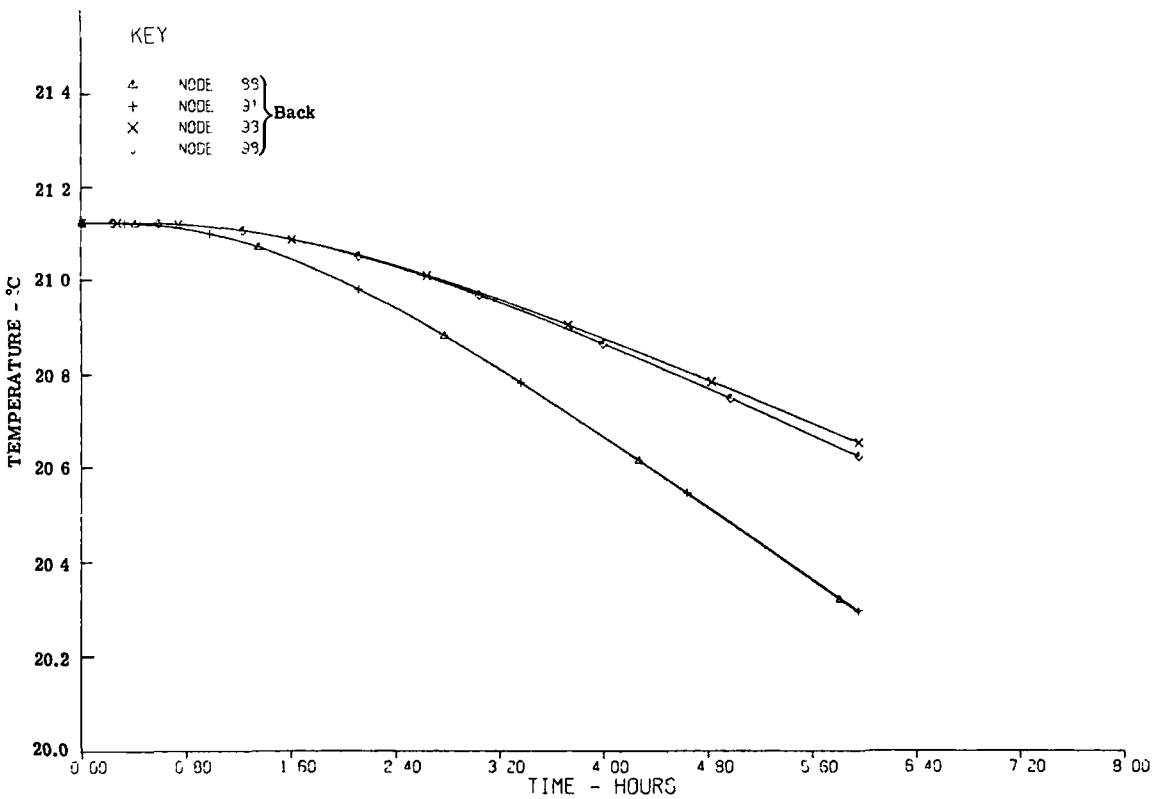

Fig. 4-22 — Temperature history for primary mirror—launch transient

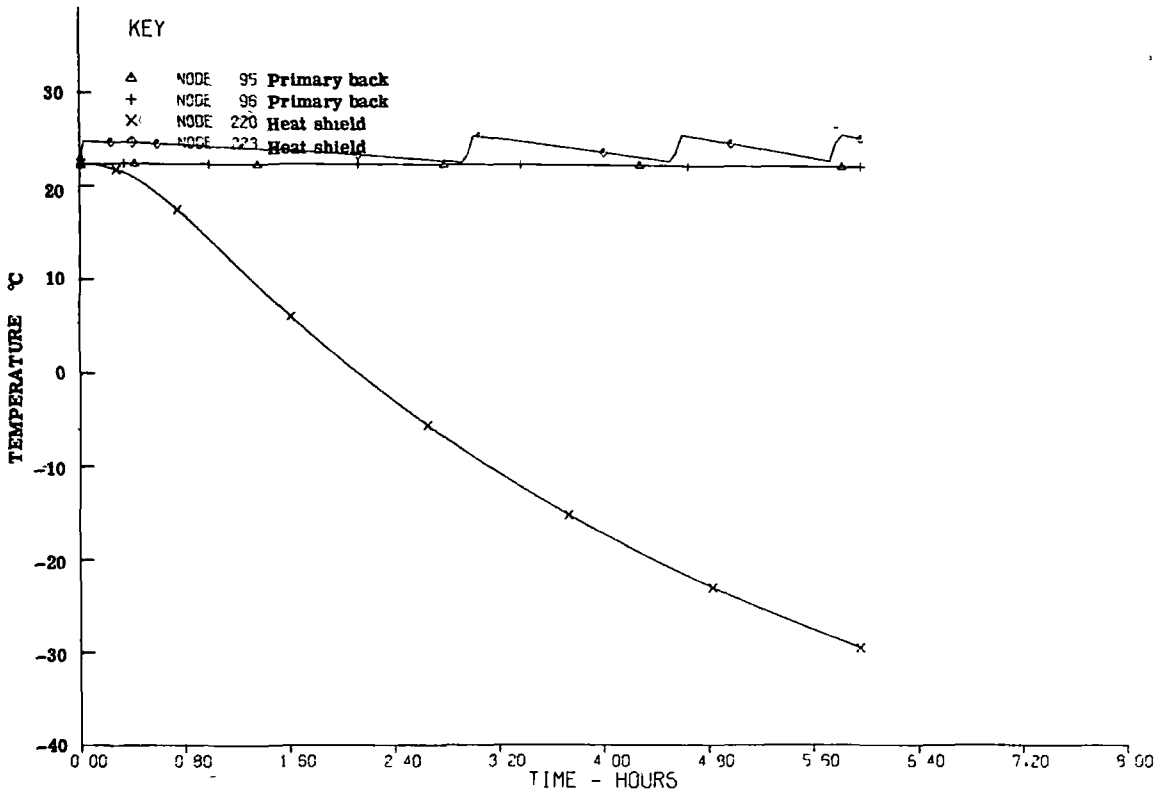

Fig. 4-23 — Temperature history for primary, heat shield, and first relay mirrors—launch transient

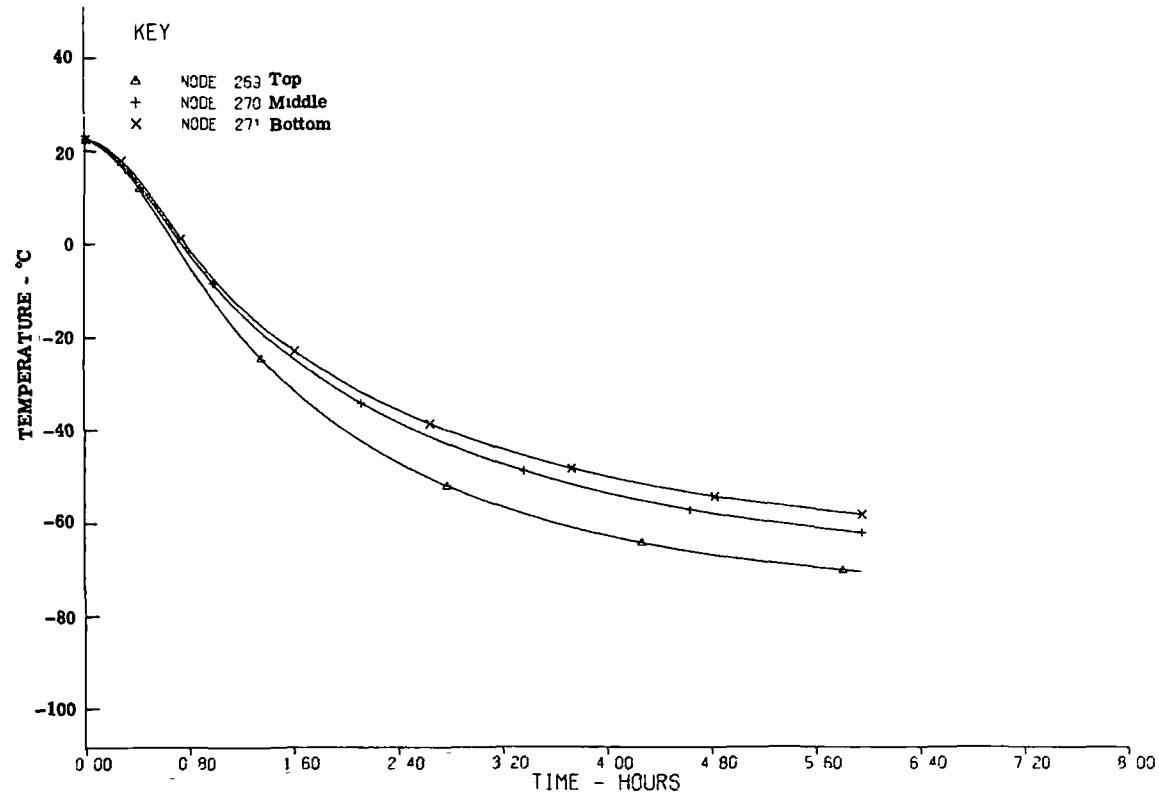

Fig. 4-24 — Temperature history for truss structure primary bay—launch transient

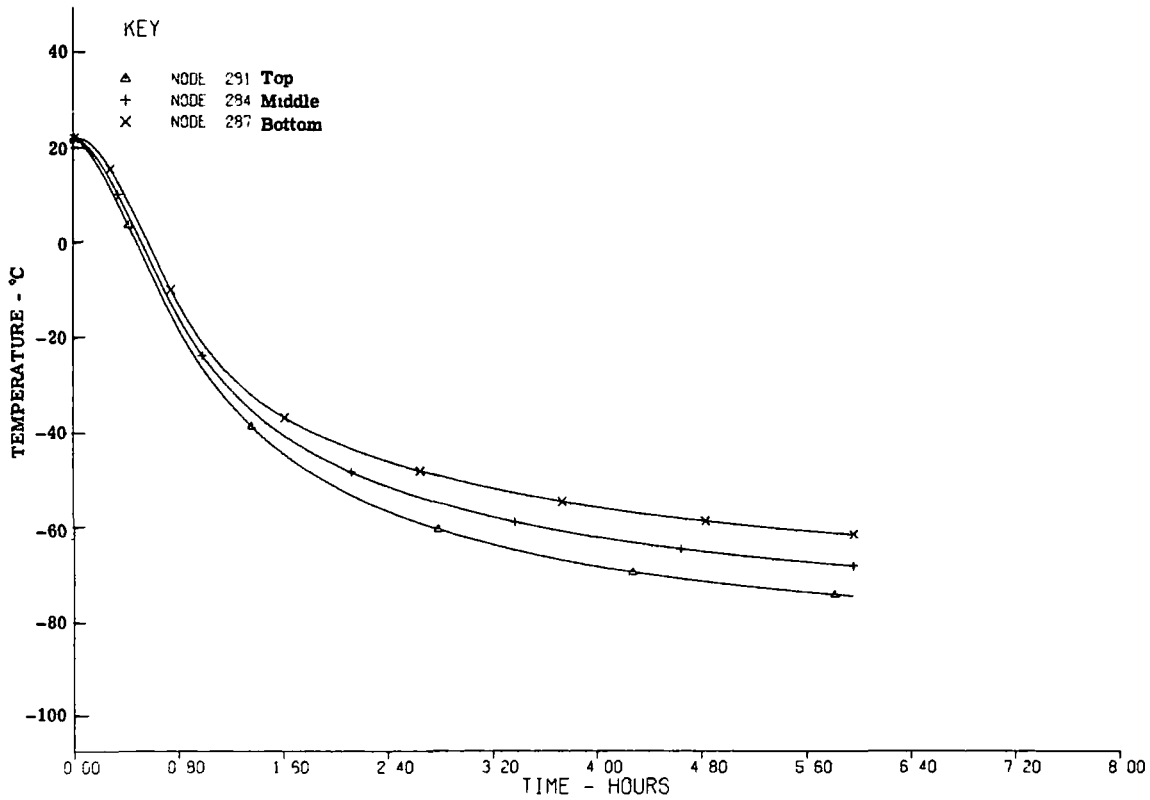

Fig. 4-25 — Temperature history for truss structure secondary bay—launch transient

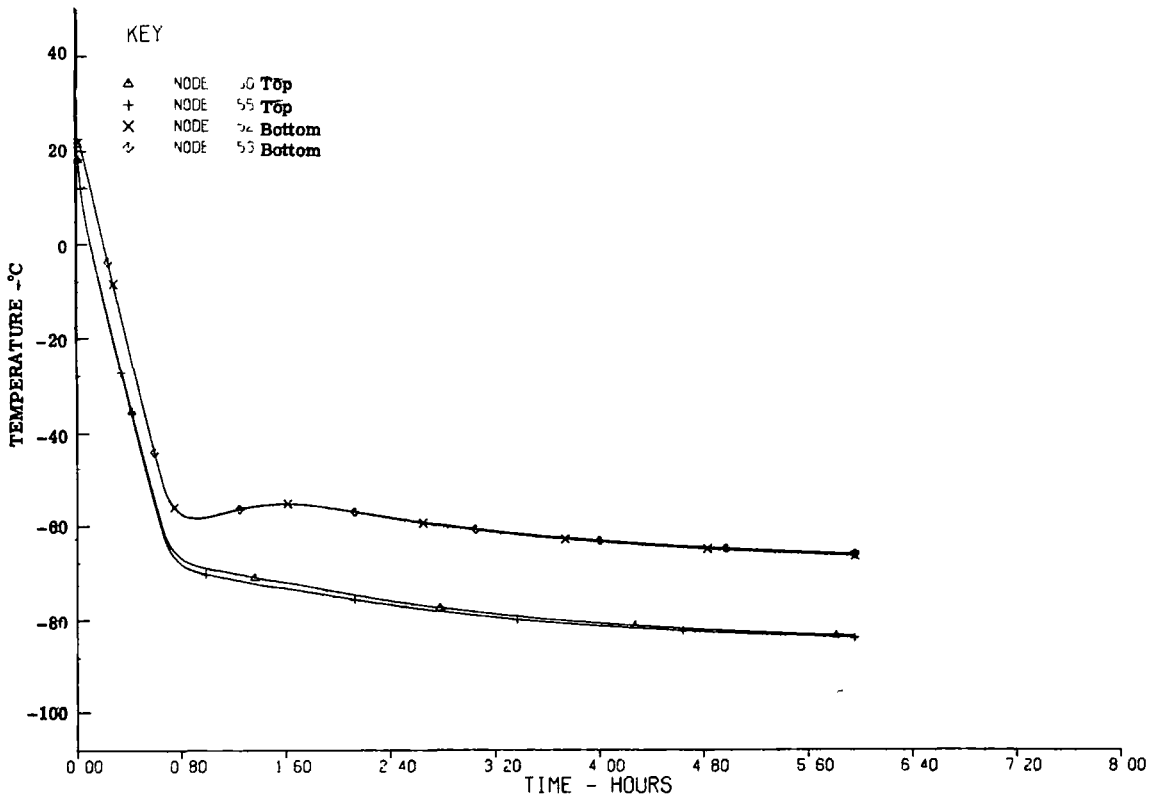

Fig. 4-26 — Temperature history for outer shell—launch transient

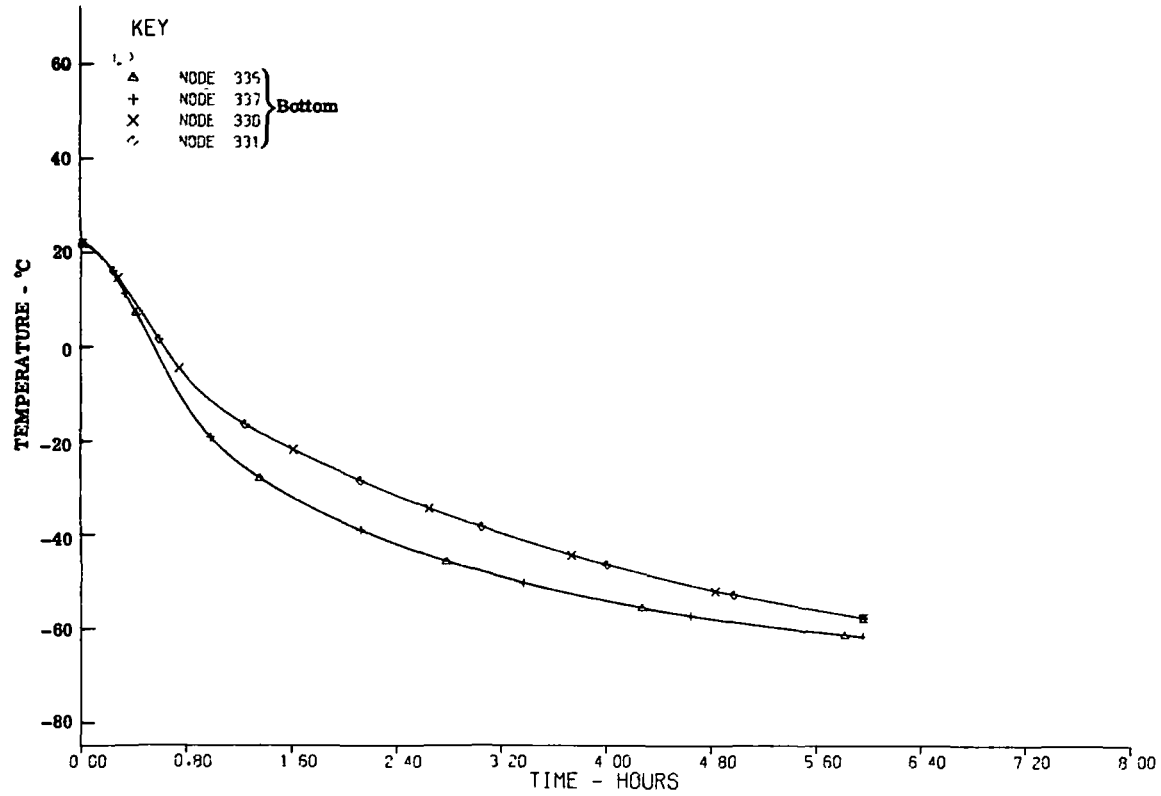

Fig. 4-27 — Temperature history for window—launch transient

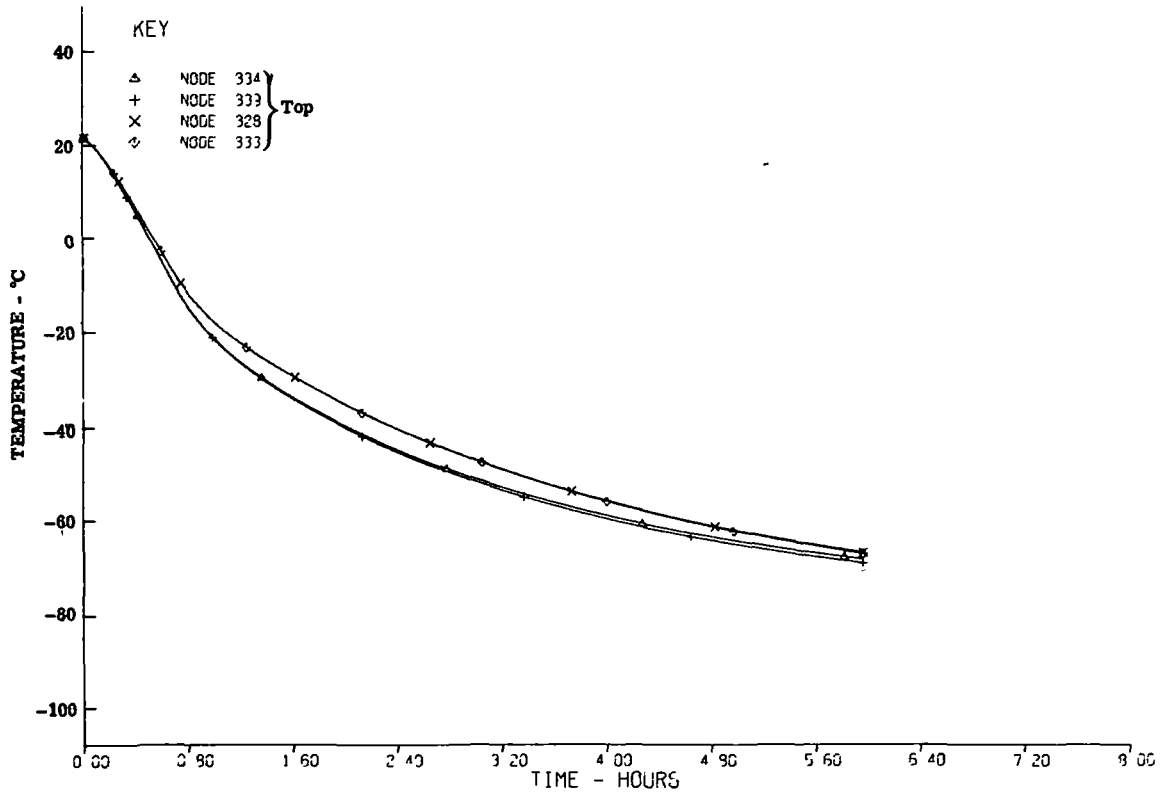

Fig. 4-28 — Temperature history for window—launch transient

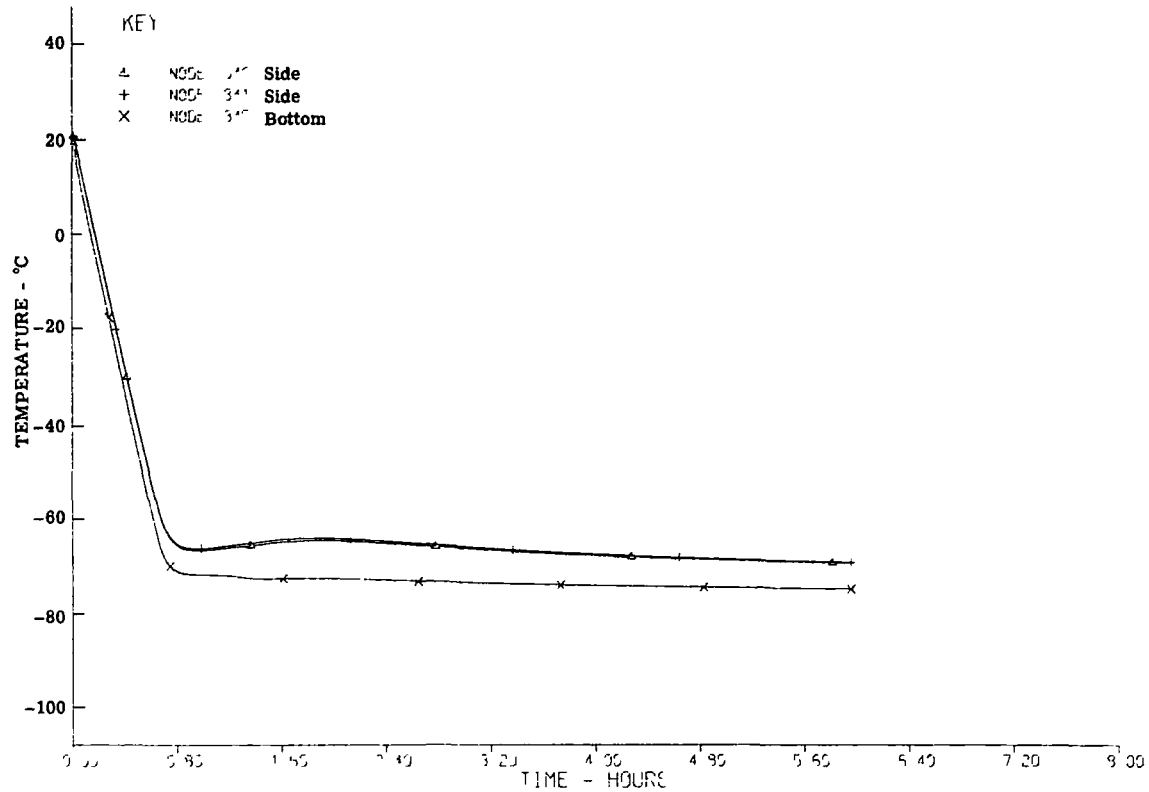

Fig. 4-29 — Temperature history for earth shade—launch transient

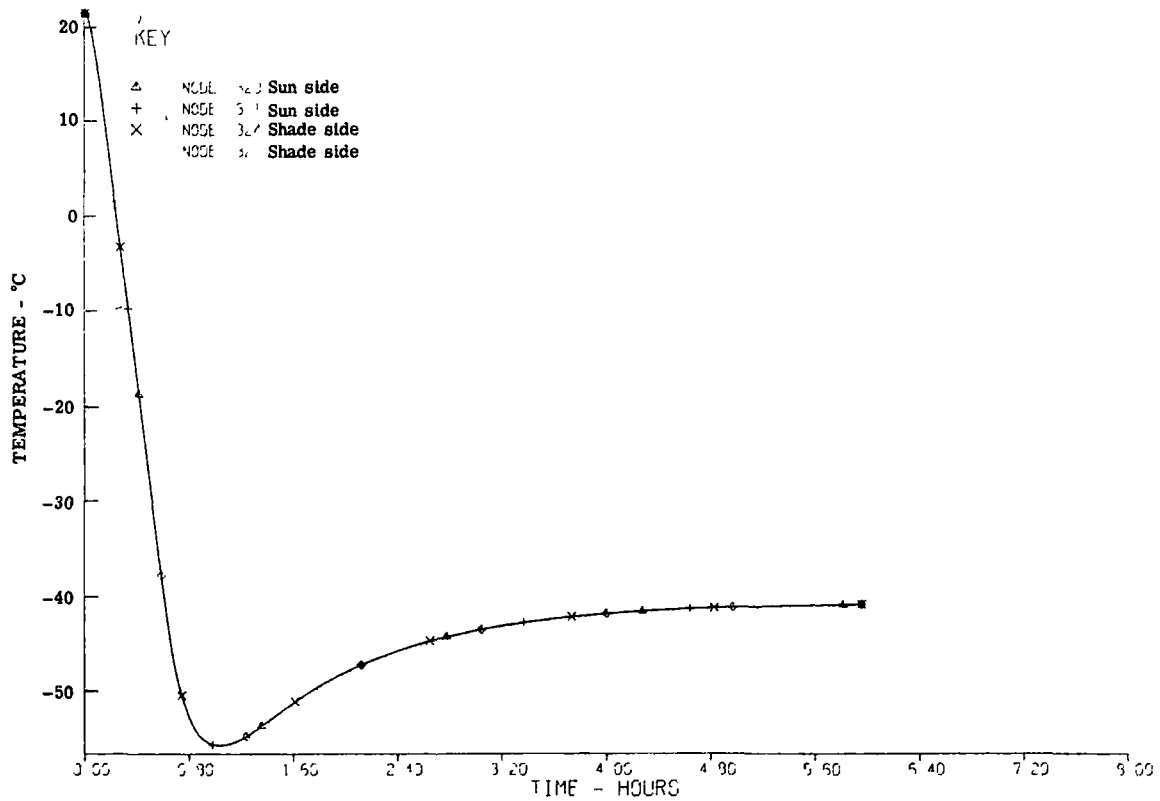

Fig. 4-30 — Temperature history for gondola—launch transient

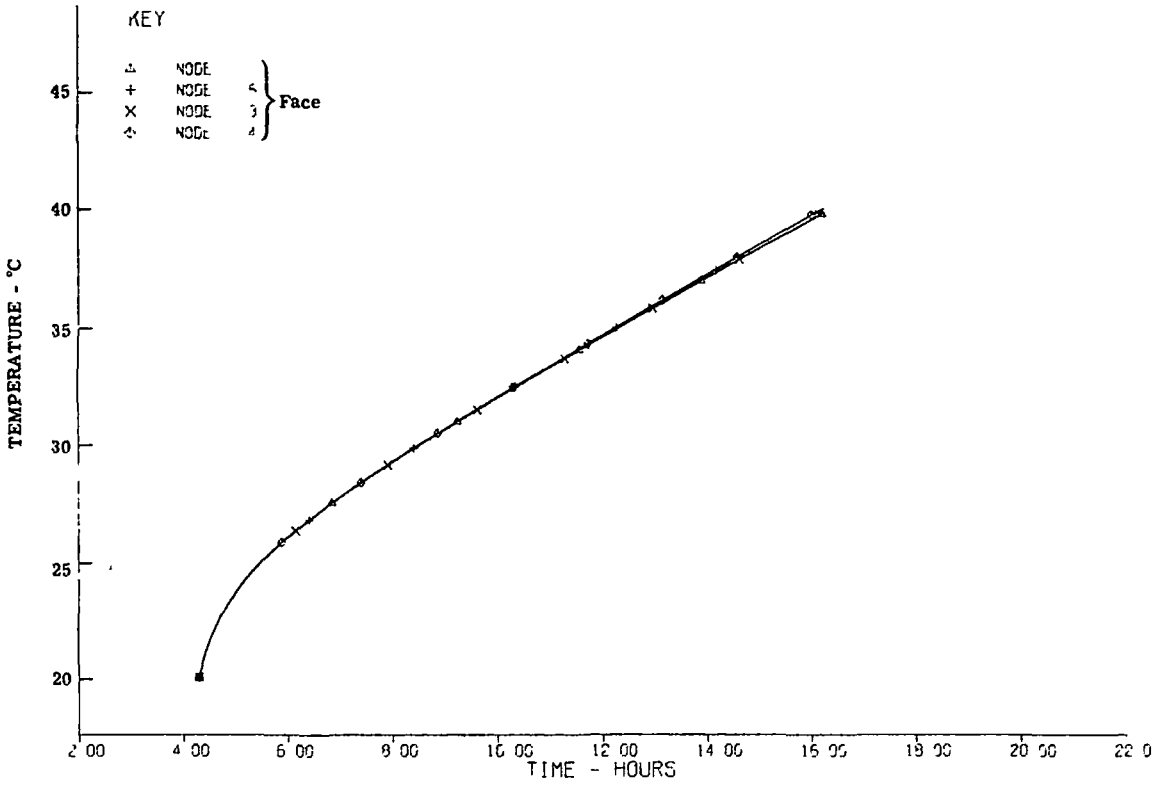

Fig. 4-31 — Temperature history for primary mirror—flight transient

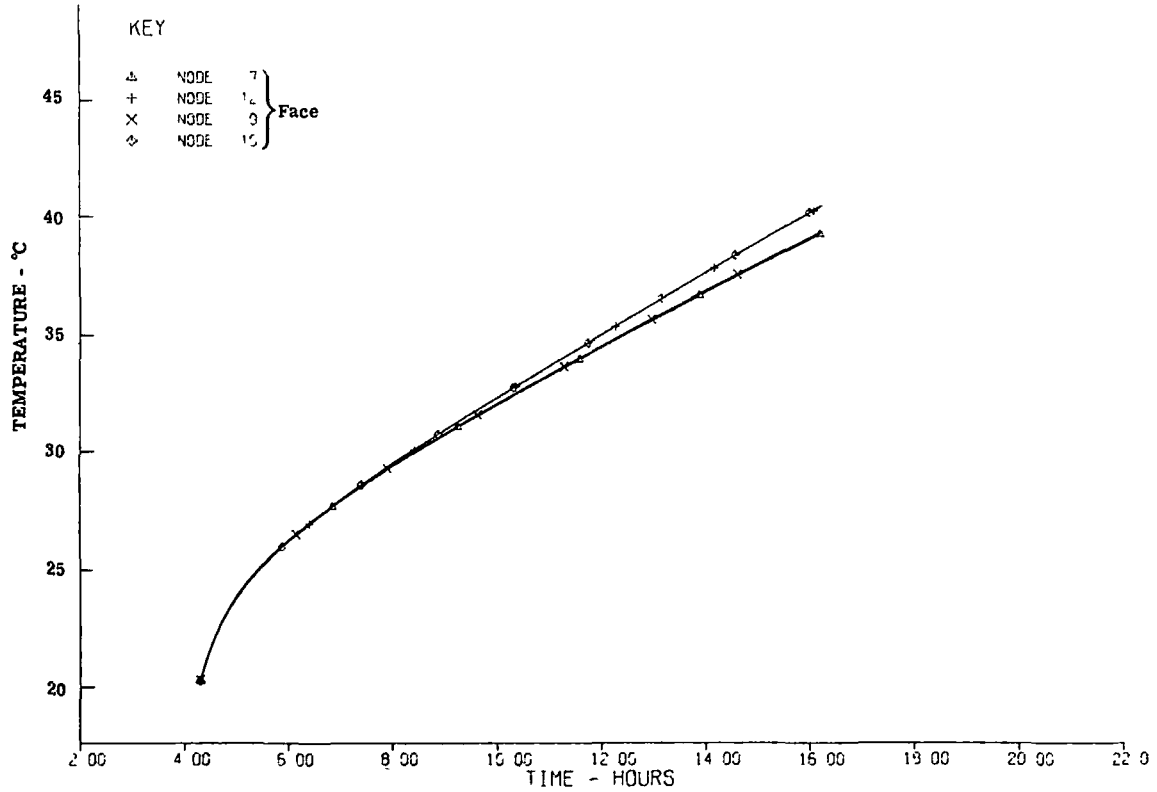

Fig. 4-32 — Temperature history for primary mirror—flight transient

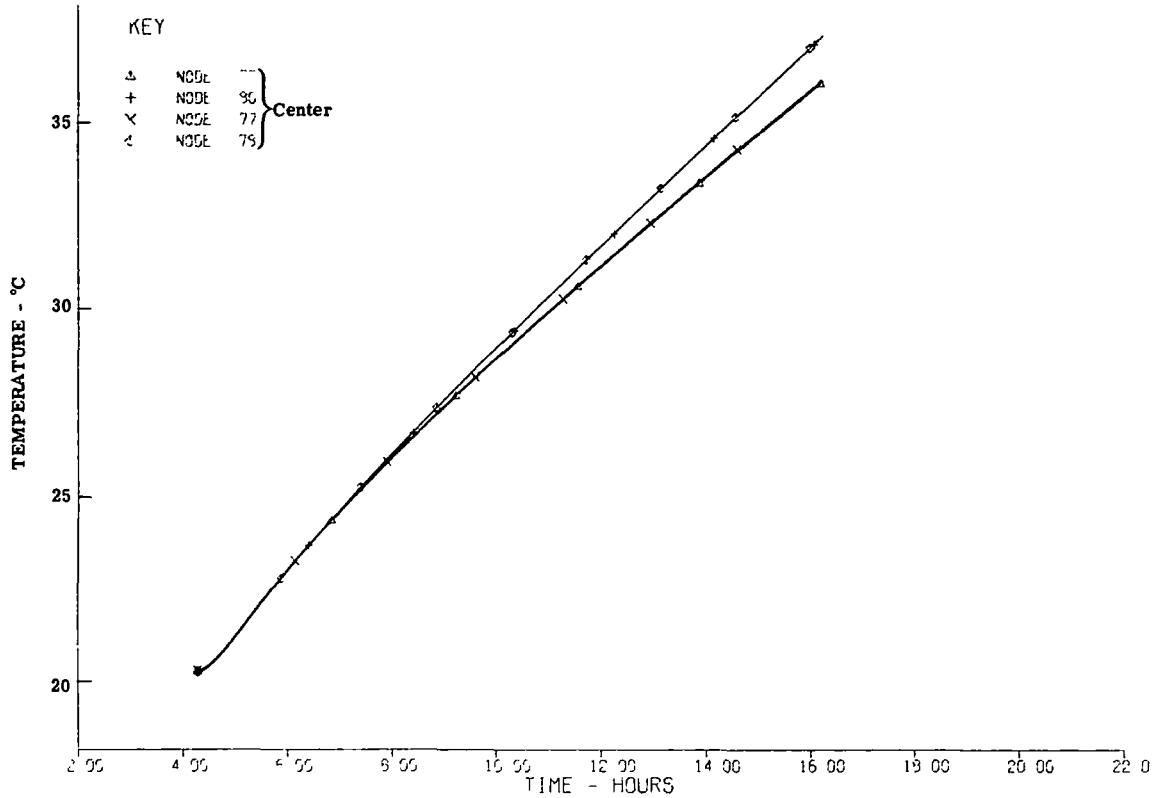

Fig. 4-33 — Temperature history for primary mirror—flight transient

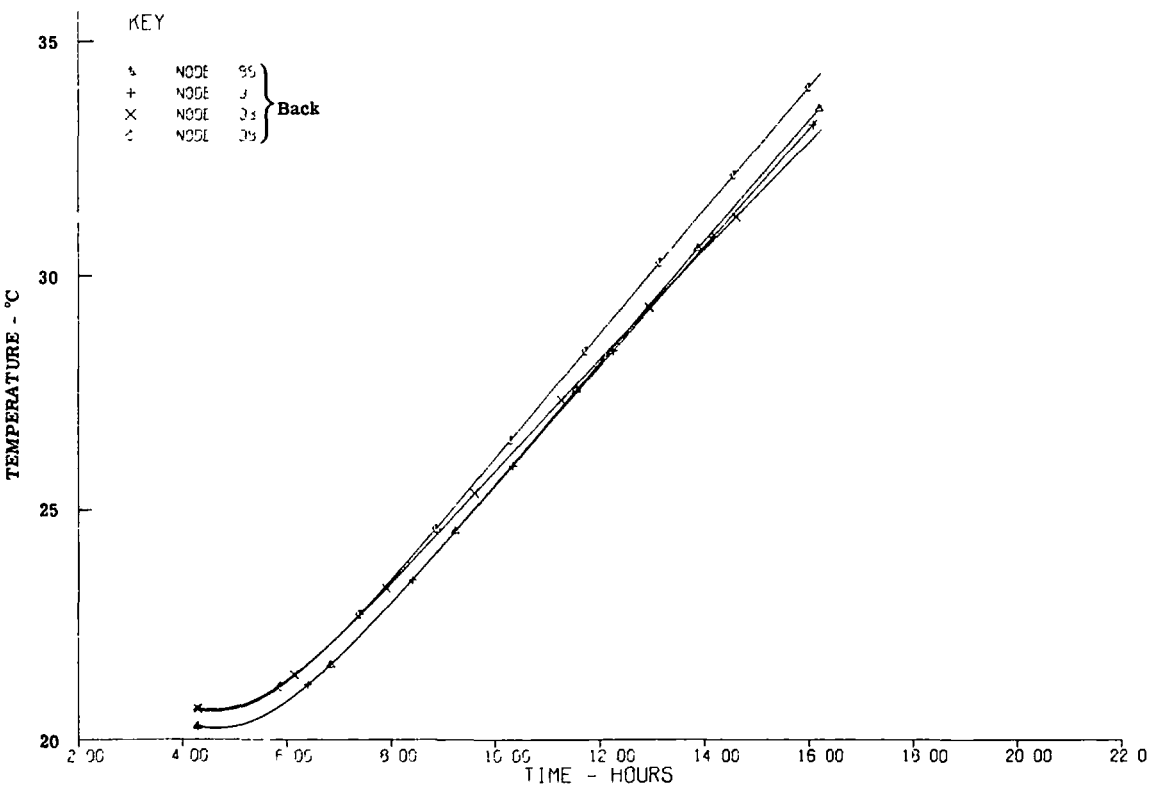

Fig. 4-34 — Temperature history for primary mirror—flight transient

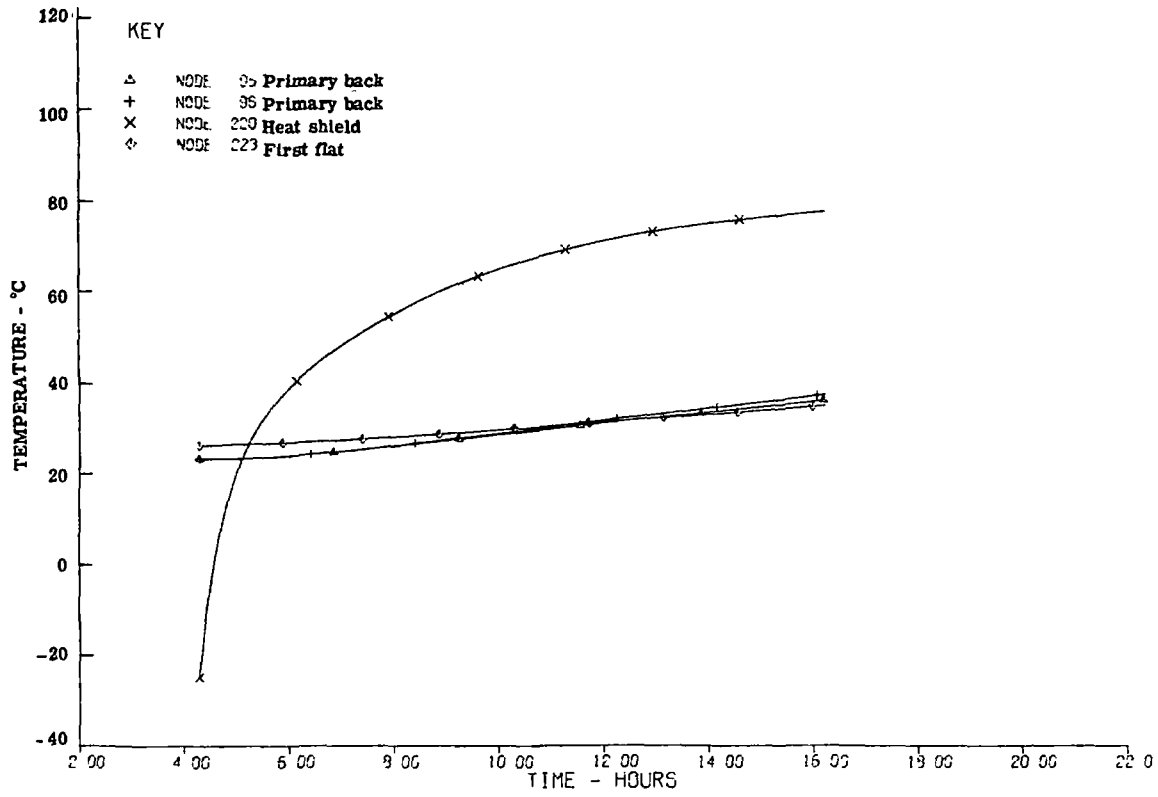

Fig. 4-35 — Temperature history for primary, heat shield, and first relay mirrors—flight transient

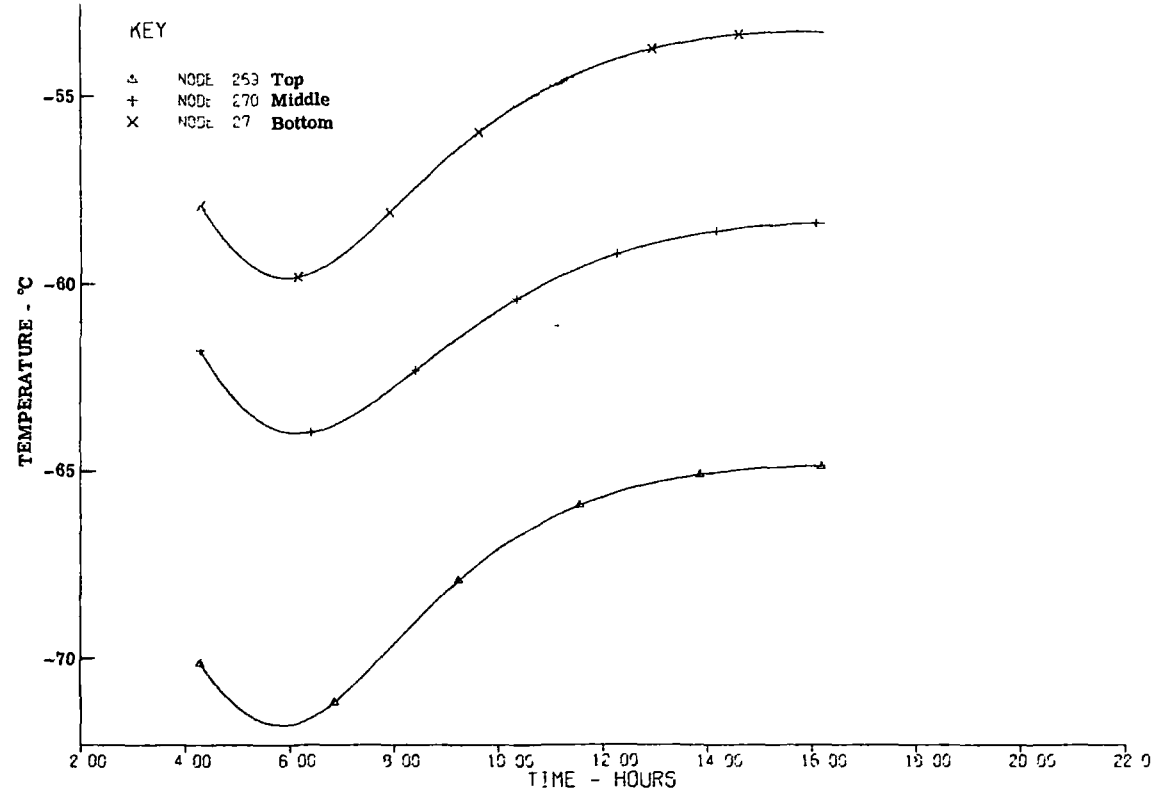

Fig. 4-36 — Temperature history for truss structure primary bay—flight transient

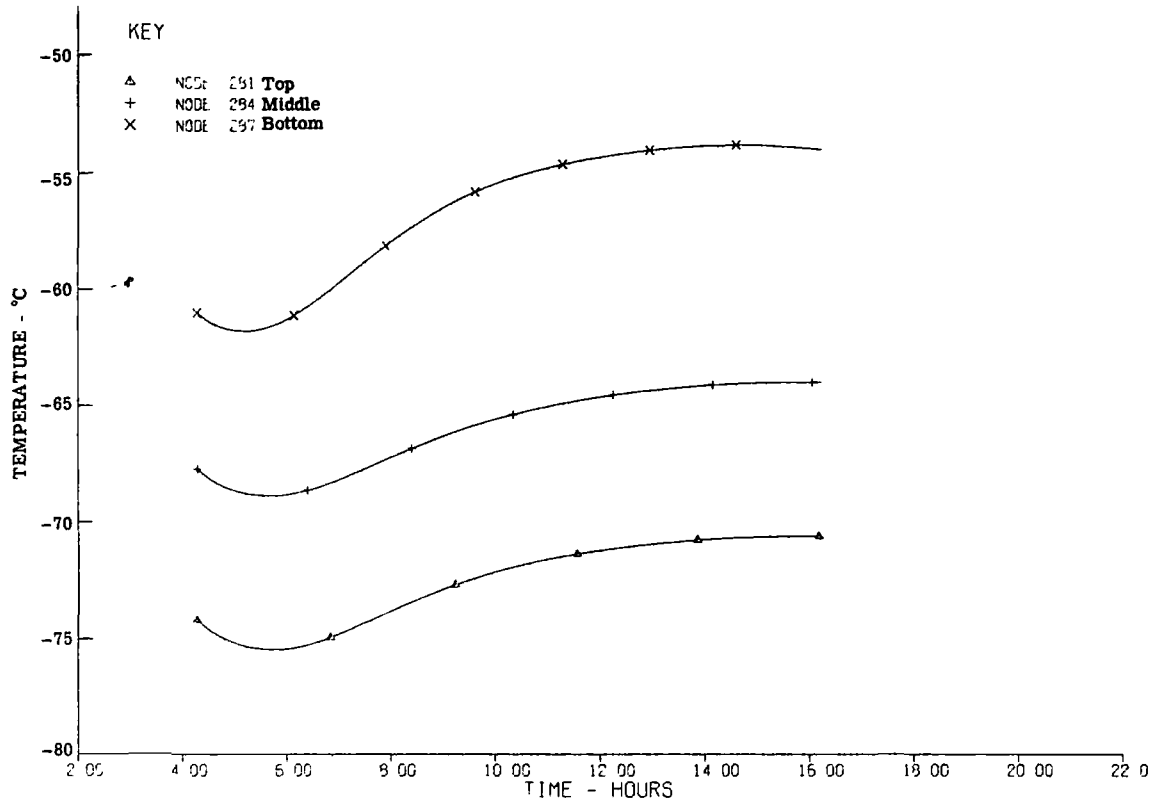

Fig. 4-37 — Temperature history for truss structure secondary bay—flight transient

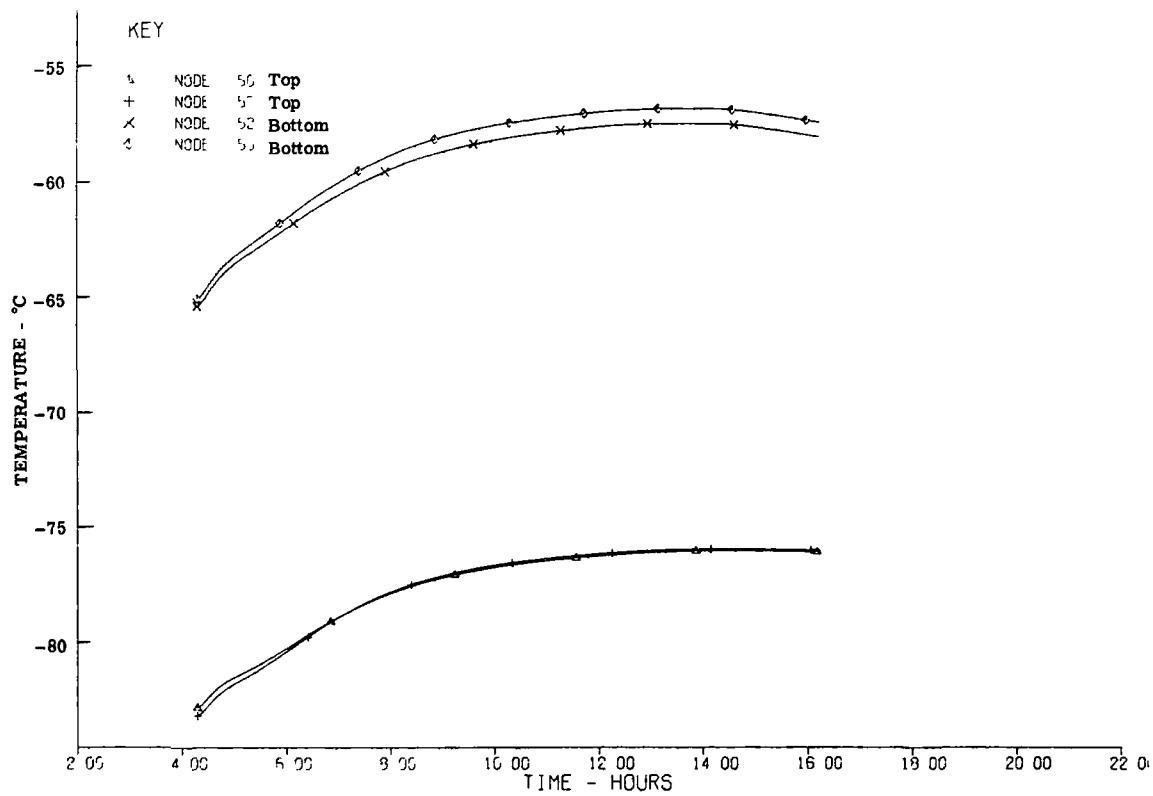

Fig. 4-38 — Temperature history for outer shell—flight transient

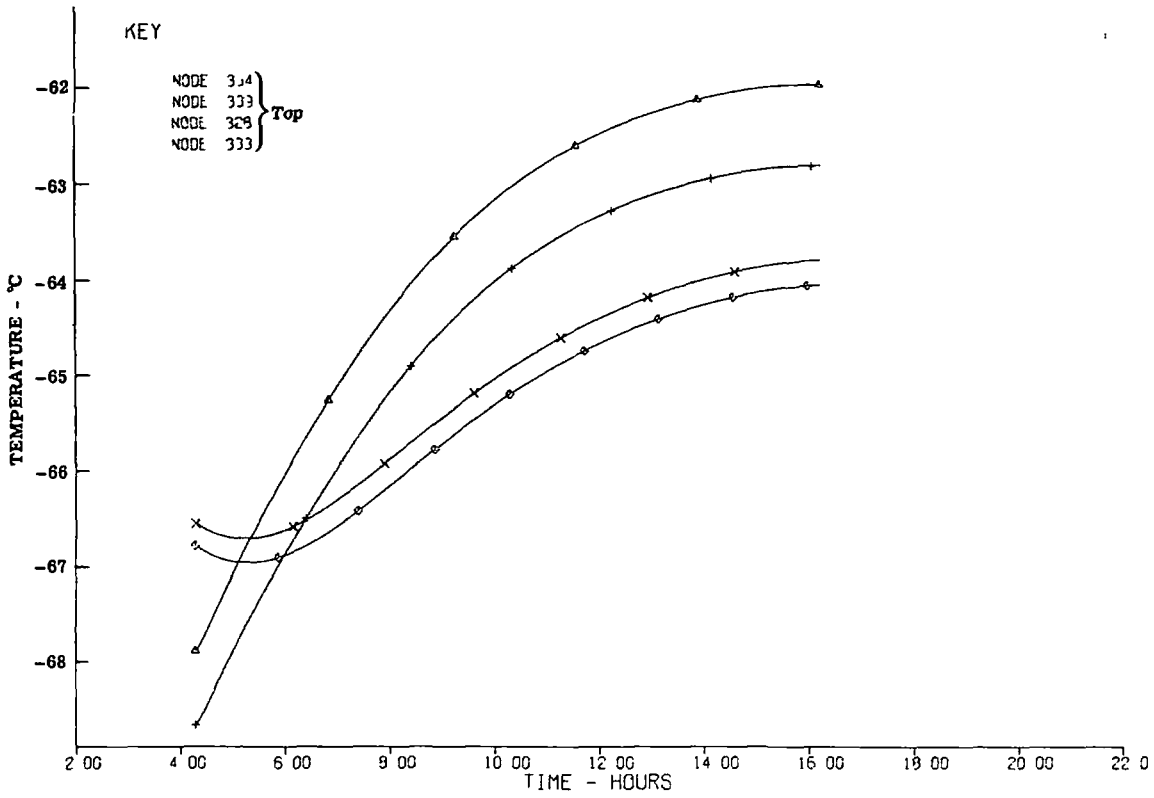

Fig. 4-39 — Temperature history for window—flight transient

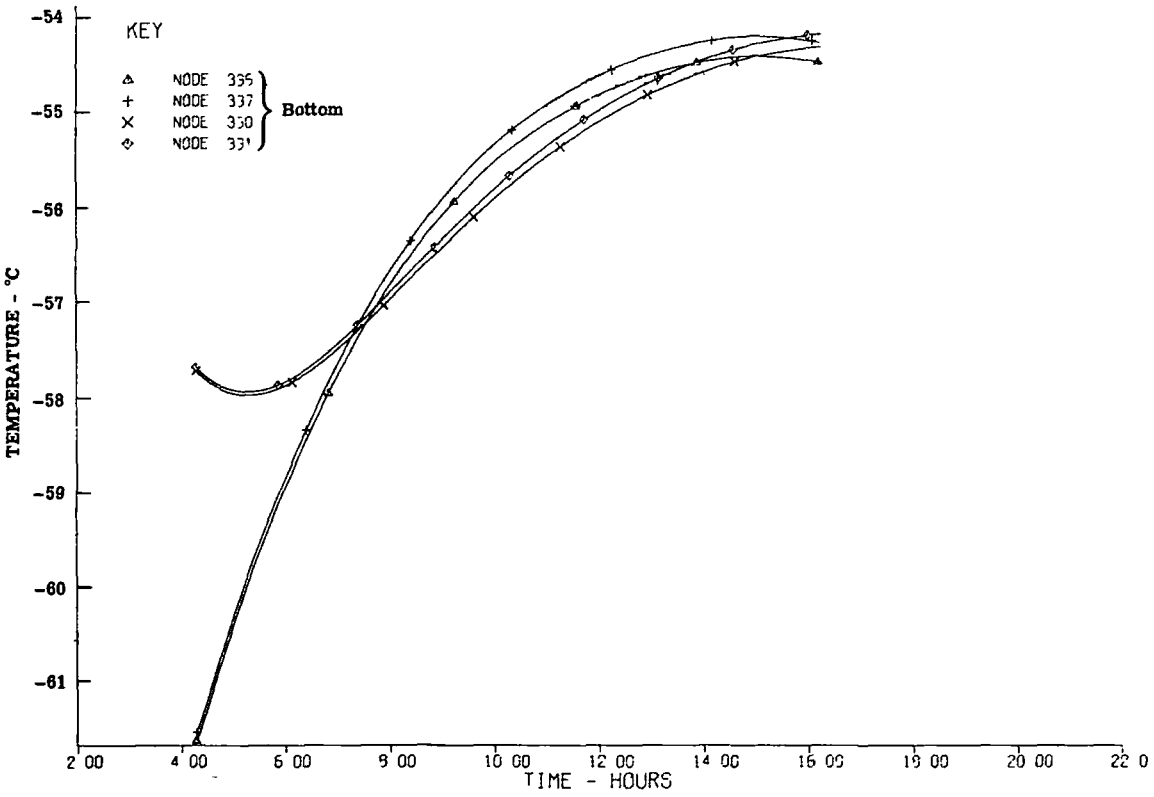

Fig. 4-40 — Temperature history for window—flight transient

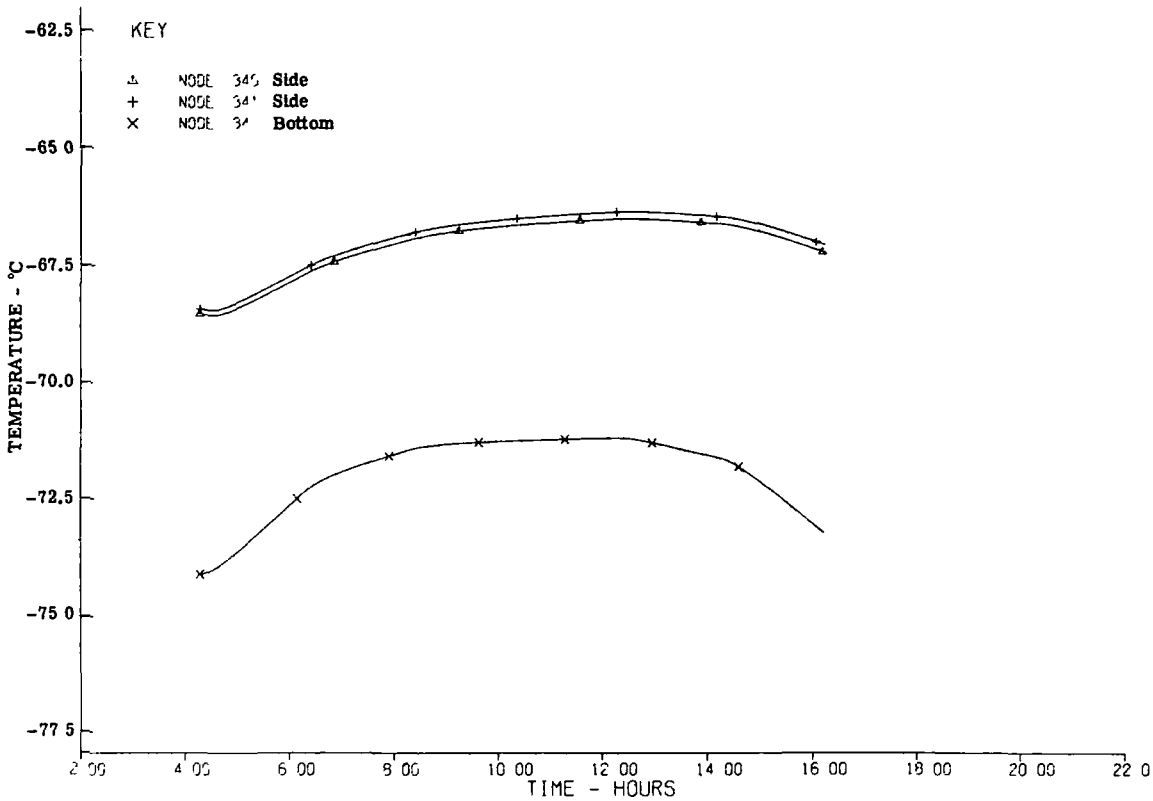

Fig. 4-41 — Temperature history for earth shade—flight transient

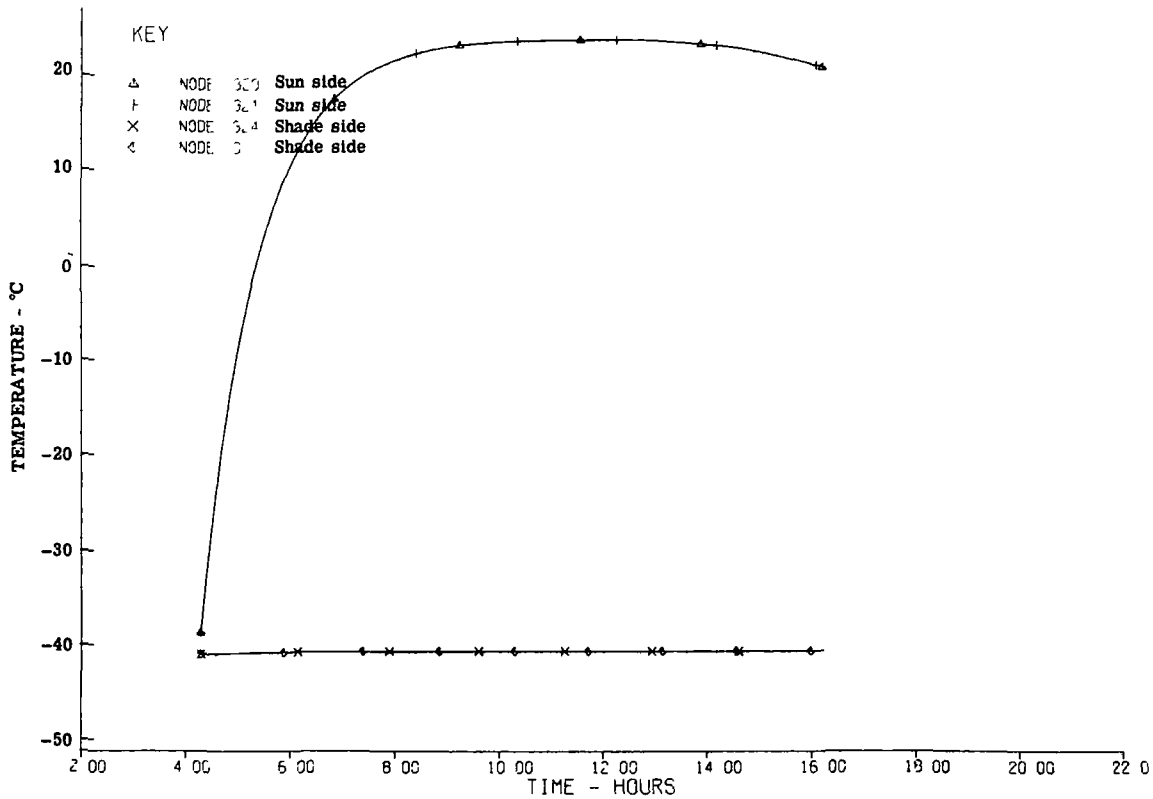

Fig. 4-42 — Temperature history for gondola—flight transient

5. PHOTOHELIOGRAPH TEST PLANS

5.1 TEST CONCEPTS

A logical series of test plans has been developed to support the Photoheliograph Thermal Concepts Study. These plans include breadboard testing to verify design concepts for both the Shuttle mission and the balloon mission, subsystem test of "flight" hardware to confirm as-built performance, and a "full-up" system thermal test of the fully assembled telescope.

The specific tests are described in greater detail in Sections 5.2, 5.3, and 5.4 for breadboard, subsystem, and system, respectively. The breadboard tests include:

1. Primary mirror specular core
2. Vidicon camera −17.8 °C cooling
3. Primary mirror heat rejection system
4. Heat shield mirror heat rejection system
5. Phase change material
6. Thermal pluming.

Subsystem tests of flight configuration hardware include:

1. Instrument structure
2. Primary mirror heat rejection system
3. Heat shield mirror heat rejection system.

Although each test is treated separately, certain tests and/or pieces of test support equipment are common to more than one experiment. Thus, certain items such as temperature recorders, auxiliary coolers, and vacuum tanks are costed against each experiment where they are used.

Not included in these test plans is a description and discussion of the primary mirror thermal design breadboard. This test program is intended to verify primary mirror operating characteristics, both thermal and optical, under simulated solar loading conditions. As such, it is a key element in the overall Photoheliograph Thermal Concepts Study. Work on this test program was conducted as part of the Photoheliograph Definition Study and the reader is directed to the final report of that program* for a complete discussion of the primary mirror breadboard.

The use of heat pipes for the primary mirror and heat shield mirror heat rejection systems results in a significant design constraint in regard to system and subsystems testing. It is an established fact that heat pipe performance is strongly dependent on orientation in a 1-g field,

---

* Photoheliograph Definition Study, Volume II, Book III, Advanced Technology and Project Planning, Itek Report 73-8212-5 (8 Jan 1973).

and thus, unless the original design accounts for and configures the heat rejection systems accordingly, subsystem and system testing will not be possible.

For the purposes of this effort, we must assume that the design of the system accommodates the 1-g field by configuring the heat pipes in horizontal planes such that gravity effects are minimal. With this stipulation or implied design constraint, we can postulate the performance of the following tests.

1. Primary mirror heat rejection system test
2. Heat shield mirror heat rejection system test
3. Final system thermal test.

The test plans described in the following sections have been developed in a straightforward fashion employing the logical progression indicated below:

1. Identify key items requiring testing.
2. Define the objectives or goals of the test program.
3. Identify the boundary conditions for the test.
4. Develop a test block diagram for all subsystems required.
5. Identify, compare, evaluate, and select the required subsystem components.
6. Develop a preliminary test procedure.
7. Develop a hardware and labor cost estimate for the proposed test program.

5.2 BREADBOARD TESTS

5.2.1 Primary Mirror Specular Core (Fig. 5-1)

This breadboard will be used to investigate the thermal performance of a specular core mirror and to compare it with the analytical predictions of heat transfer and temperature gradients in cored mirrors. The critical nature of this breadboard is obvious in terms of the final design of the photoheliograph system.

Boundary conditions are based on primary mirror absorbtance of 0.0165 watt/cm^2 at a temperature of approximately 29.4 to 37.8 °C. Variation in sink temperature will be the primary parameter to be investigated.

Concept Evaluation

The proposed test will require a specular core test specimen for concept evaluation. No other equipment or support facility is considered critical or significant in terms of performance or evaluation of this program. Our concept evaluation will be directed toward the specification of the specular core test specimen.

Ideally, this test should be performed with a specular core, lightweight mirror. This approach presents a number of problems including handling, development of final techniques for fabricating specular walls and diffuse ends, and availability of the proper internal geometric arrangement. It is obvious that this approach presents a high cost, complex, low flexibility approach to the problem.

A more flexible and rational approach to the test specimen problem would be to develop a simple test specimen representation of the specular core concept. This can be done in at least two ways (1) using flat pieces of glass to build up a typical cell configuration (hexagonal or square), and (2) using a cylindrical glass pipe to represent the cell configuration. By using a single cell model, we will be able to experimentally determine core heat transfer and thermal gradients for a simple system in an efficient manner while reducing experimental uncertainties and complexities inherent in larger test articles.

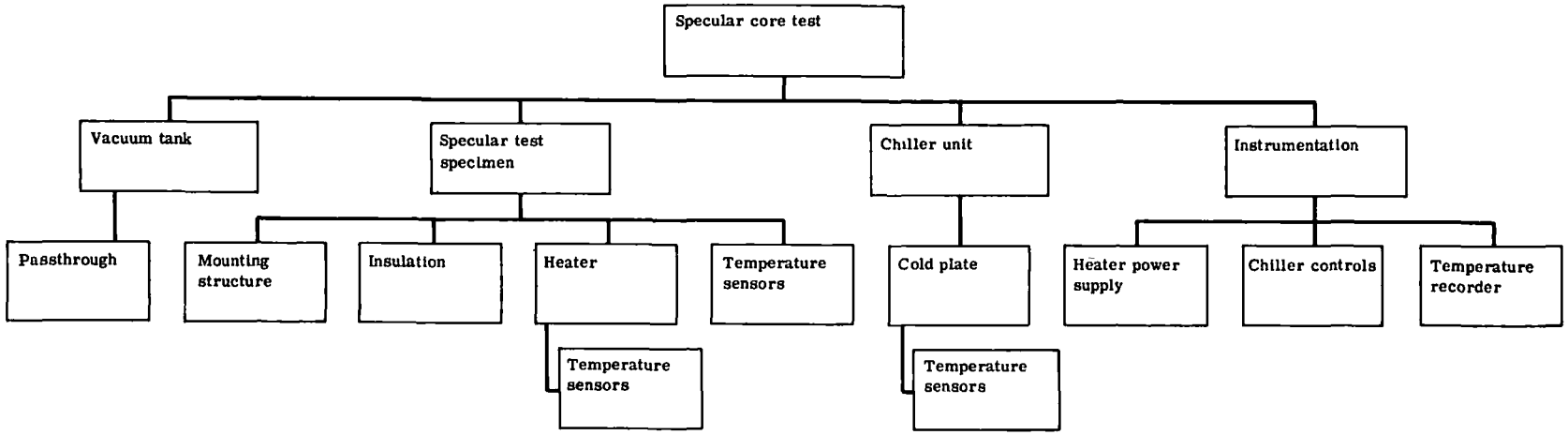

Fig. 5-1 — Primary mirror specular core breadboard test

Test Procedure

The test procedure will be as follows·

1. Set up test specimen in vacuum tank, check out all equipment, and verify general system operation.
2. Operate heater at design heat load with cold plate at 21.1 °C. Record temperature distributions.
3. Reduce cold plate temperature to 10 °C and allow system to come to new steady state temperature distribution. Record temperature data.
4. Repeat step 3 at 11.1 °C increments to at least −23.3 °C.
5. While at a cold plate temperature of −23.3 °C, increase heater output by 25 percent. Allow temperatures to stabilize and record data.
6. Raise cold plate temperature in 11.1 °C increments (at new power level) and record temperature distributions until room temperature is reached.

Required test equipment includes

1. Test specimens with fixed L/D ratio
2. Heater, fixed power output ($q \approx 0.0165$ watt/cm^2)
3. Cold plate and chiller unit
4. Temperature sensors
5. Recorder
6. Vacuum facility with 1.33×10^{-3} newton/meter^2 capability
7. Electric power supply.

Preliminary Cost Estimate

Hardware

Facility	Available
Facility modifications	$ 750
Test specimen	500
Cooler unit	4,000
Instrumentation	2,500
	$7,750

Labor by task

Analysis	40 hours
Design	80
Hardware specifications	20
Fabrication	32
Assembly and installation	60
Testing	40
Data reduction and report	80
	352 hours

5.2.2 Vidicon Camera −17.8 °C Cooling (Fig. 5-2)

This breadboard is intended to demonstrate the temperature distributions and heat flows from an operating vidicon camera that is thermally controlled at −17.8 °C (tube temperature).

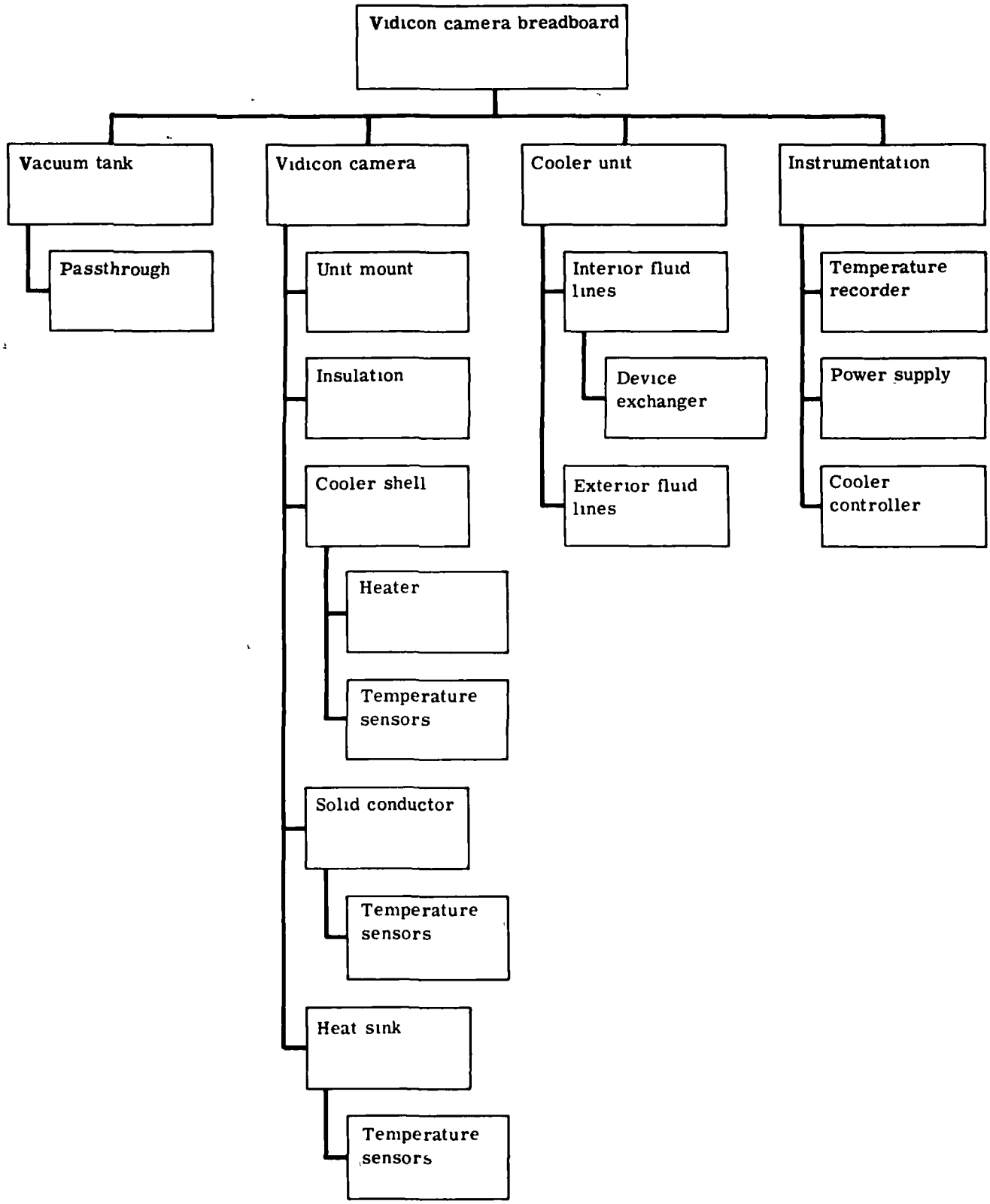

Fig. 5-2 — Vidicon camera cooling breadboard test

The boundary conditions for this breadboard are based on the assumed power dissipation within the cooler shell of approximately 2 watts and a heat sink (vehicle wall) varying between −48.4 °C and −26.1 °C sinusoidal with a 1.5-hour time period.

Concept Evaluation

Verification of camera cooling performance requires a camera tube or simulator for test operation. Clearly, the use of a camera tube with associated focusing coils is not warranted (from a cost and availability standpoint), and the breadboard effort will be based on simulation of the cooler shell geometry and operation.

This may be accomplished by simulation of the camera enclosure and the use of spot electric heaters to simulate the anticipated thermal loads. The solid conductor may be developed exactly as in the basic design. The only remaining portion of the test setup that requires evaluation is the camera heat sink coupling from the solid conductor. The baseline design is based on the use of the vehicle wall as the heat sink. Since the vehicle wall experiences a 22.2 °C temperature swing during orbital operation (from −26.1 °C to −48.4 °C), a representative breadboard simulation must take this into account.

Two possibilities exist: one is to radiatively couple the heat sink to a second radiator operating from the external cooler unit, and the second is to modulate the heat sink temperature to simulate the skin temperature variation. Using a modulated heat sink approach seems to be the more favorable concept, since it results in a simpler system that does not require the design of a coupled radiator. Both concepts imply some control of the cooler system, either directly or by means of a backup heater.

Test Procedure

The test procedure will be as follows

1. Install test specimen in chamber, check out all equipment, and verify performance of data acquisition equipment.

2. Lower heat sink temperature to −26.1 °C and monitor cooler shell and solid conductor temperature decrease until steady-state temperatures are reached. Verify performance against analytical predictions.

3. Maintaining −26.1 °C at heat sink, turn on camera power simulators and monitor temperature response of cooler shell and solid conductor. Verify performance against analytical predictions.

4. Perform transient run by varying heat sink temperature from −26.1 °C to −48.4 °C to simulate orbital period. Maintain constant power output from camera simulator. Record temperature response of cooler shell and solid conductor. Transient run should consist of at least four cycles. Compare data for all cycles to ensure that system is operating as predicted and that quasi-steady-state condition has been achieved.

5. Increase camera simulator power by 100 percent and repeat transient run to demonstrate design capability of basic system.

Required test equipment includes:

1. Cooler shell
2. Solid conductor
3. Heat sink
4. Chiller unit
5. Temperature sensors
6. Recorder
7. Vacuum facility.

Preliminary Cost Estimate

Hardware

Facility	Available
Facility modifications	$ 750
Test specimen	2,500
Cooler unit	4,000
Instrumentation	2,500
	$9,750

Labor by Task

Analysis	80 hours
Design	100
Hardware specifications	40
Fabrication	60
Assembly and installation	100
Testing	100
Data reduction and report	120
	600 hours

5.2.3 Primary Mirror Heat Rejection System (Fig. 5-3)

This breadboard will be used to determine the performance of the heat rejection system of the primary mirror. The experimental performance of the system will be compared with analytical predictions to verify the adequacy of our design.

The breadboard will be configured to duplicate the primary mirror heat rejection system temperature distribution and power loading for the 100-centimeter Shuttle system (power ≈132 watts, cold plate temperature ≈−20.6 °C, radiator temperature ≈−33.3 °C).

It will be necessary to account for the 1-g gravity field in developing boundary conditions for this test.

Concept Evaluation

The primary mirror heat rejection system consists of three basic components and a number of support elements. The three basic components are the mirror cold plate, the connecting heat pipe, and the heat sink (radiator). For this arrangement we must consider not only demonstration of system performance but also the effect of the 1-g field on heat pipe performance.

Heat Pipe

Since our basic heat removal concept is based on the use of heat pipes, we must develop a concept that eliminates gravity vectors as a performance variable. Although it introduces some complexity, we must design the breadboard so that the heat pipe is operated horizontally and all bends (if used) are in the horizontal plane. If we cannot develop such a breadboard design, independent testing of the heat pipe as a separate entity will be required prior to the design and testing of the heat rejection system. In any case, the heat pipe must be representative of the geometric configuration of the flight article.

Mirror Cold Plate

In the operating photoheliograph, the mirror cold plate is uniformly loaded (thermally) from the primary mirror. Possible loading techniques include radiation coupling to a hotter plate

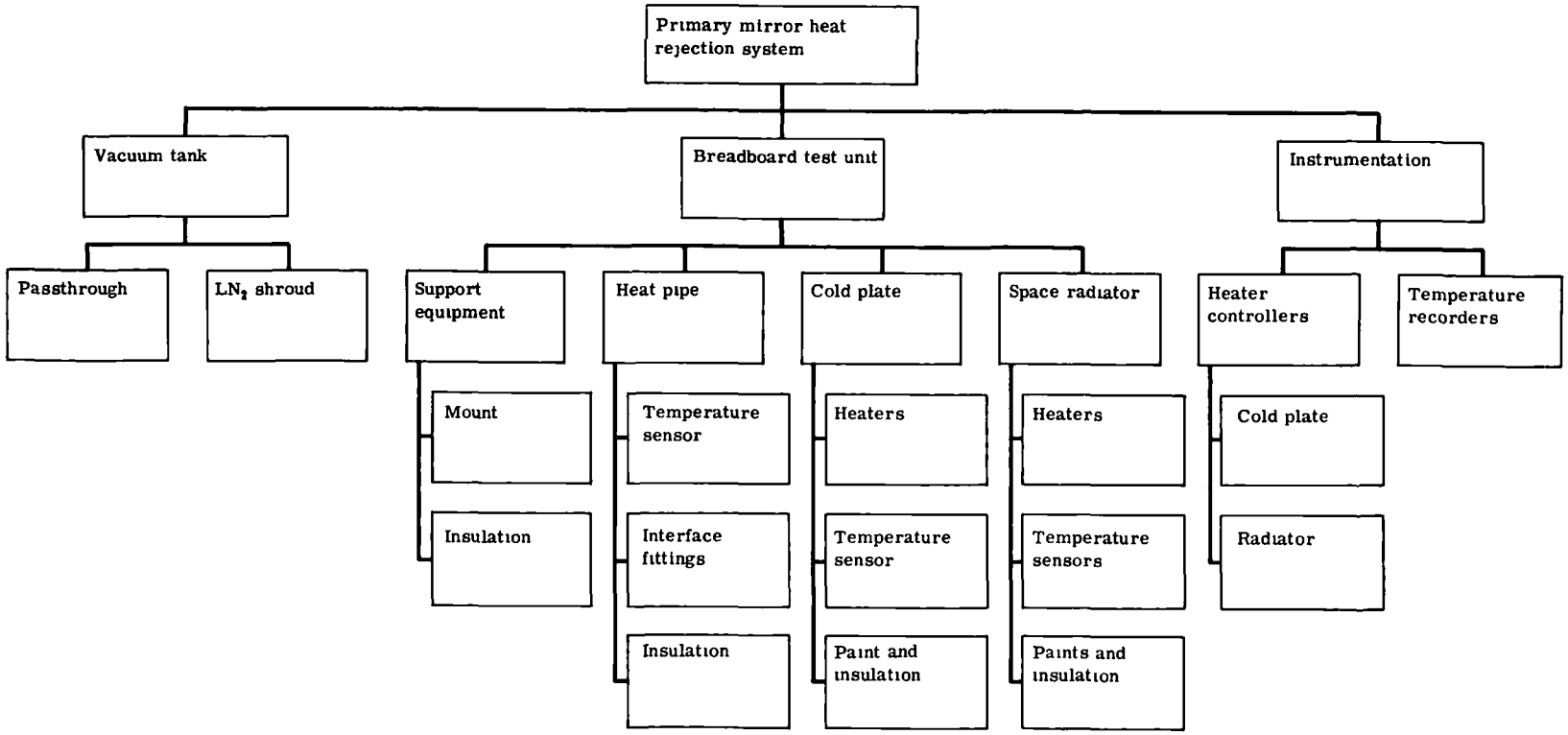

Fig. 5-3 — Primary mirror heat rejection system breadboard test

simulating the mirror, or direct electric heaters bonded to the cold plate. It is obvious that the indirect heating approach more closely simulates the real condition and offers an approach that can account for the variations (admittedly small) in heat source temperature.

The use of electric heaters bonded directly to the cold plate is a less complex approach to the temperature distribution problem. There is a sacrifice in similarity to the real condition. However, since the basic goal of this test program is the performance of the heat rejection system, the comparative ease of boundary condition simulation (Q input) indicates that this is the preferred approach.

Heat Sink

The system heat sink for the operating photoheliograph is a space radiator. Simulation of a space radiator is not possible without introducing additional test complexities, since the mission profile indicates that both earthshine and albedo are incident on the radiator during a typical orbit.

A less complex simulation of the space radiator may be accomplished by allowing the breadboard model to "see" only the cryogenic walls of the test chamber. Partial input flux simulation may be accomplished with electric heaters programmed to the nominal orbit.

An even less complex heat sink can be postulated using an external cooler unit that serves to convectively cool a heat sink. The obvious drawback to this approach is the total lack of system simulation, since it is clearly required that the problems associated with the transfer and distribution of thermal energy from the heat pipe to the radiator be solved experimentally using this breadboard.

Concept Selection

The primary mirror heat rejection breadboard will be designed so that the heat pipe is operated horizontally with any bends made in-plane. The mirror cold plate will use bonded electrical heaters to simulate the normal absorbed thermal loading. The breadboard system will use a space radiator configured to distribute the input thermal energy from the heat pipe. The radiator will have provisions for the input of external thermal loads simulating analytically predicted albedo and earthshine.

The use of the space radiator concept implies that a cryogenic wall vacuum facility is required for the performance of this test program.

Test Procedure

The following test procedure will be used·

1. Install system in vacuum tank, check out equipment, and establish vacuum.
2. Set up initial conditions on cold plate and average flux inputs to space radiator. Start cryogenic cooling.
3. Monitor all system temperatures as cold plate drops to −20.6 °C with design heat load input to cold plate.
4. With cold plate at −20.6 °C, determine temperature distributions on all system components while radiator heaters are at an average orbital value.
5. With system at quasi-steady-state and with cold plate heaters at nominal thermal load, initiate normal orbital flux variation by adjusting radiator heaters.
6. Monitor system temperature variation over at least five orbital flux cycles.
7. Return system to quasi-steady-state condition.

8. Increase cold plate heater input by 25 percent and determine new quasi-steady-state temperature distributions.
9. Repeat steps 5 and 6 to determine orbital temperature variations under the increased heat loading.

Required test equipment includes:

1. Cold plate
2. Heat pipe
3. Heat sink (radiator?)
4. Heater (source)
5. Temperature sensors
6. Temperature recorder
7. Vacuum facility with 1.33×10^{-3} newton/meter^2 capability
8. Power supply (for heater)
9. Liquid nitrogen shroud
10. Heat sink temperature controller.

Preliminary Cost Estimate

Hardware

Facility	Available
Facility modifications	$ 750
Test specimen	16,050
Instrumentation (includes 250-channel DAS)	44,000
	$60,800

Labor by Task

Analysis	400 hours
Design	320
Hardware specifications	80
Fabrication	300
Assembly and integration	300
Testing	400
Data reduction and report	240
	2,040 hours

5.2.4 Heat Shield Mirror Heat Rejection System (Fig. 5-4)

The primary purpose of this breadboard is to demonstrate the performance of the proposed mirror/heat pipe/radiator-sink heat rejection system for the photoheliograph and to compare the analytically predicted performance with the breadboard.

The boundary conditions for this breadboard are based on a heat input of 48 watts at a temperature of 22.8 °C at the mirror and −29 °C at the heat sink. It will be necessary to account for the 1-g gravity field in developing boundary conditions for this test.

Concept Evaluation

The simulation of a heat shield heat rejection system requires that the major portions of the system be breadboarded, i.e., heat shield mirror, heat pipe, and space radiator. The 1-g design constraint discussed previously for the primary mirror breadboard heat removal system

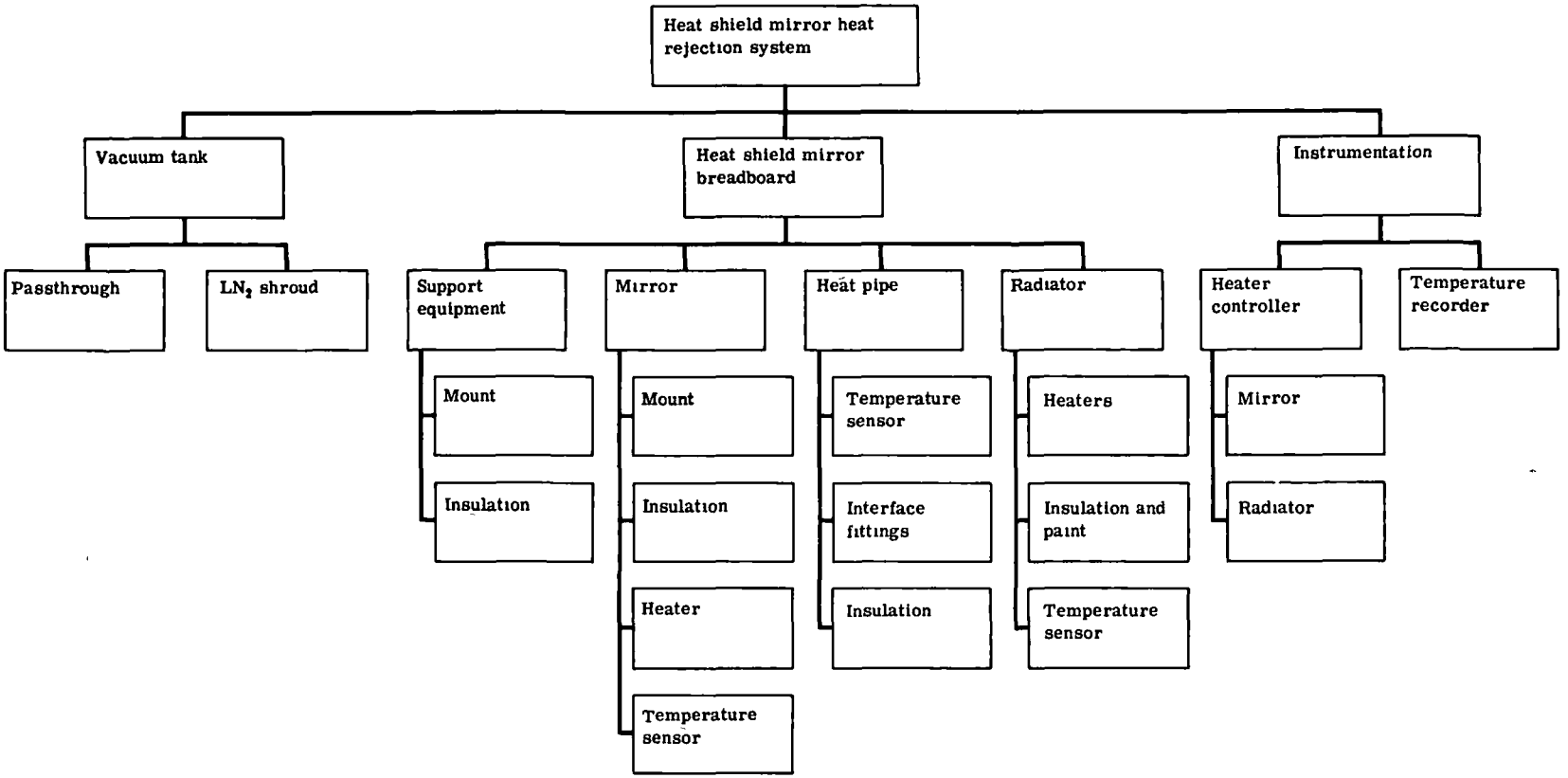

Fig. 5-4 — Heat shield mirror heat rejection system breadboard test

is also applicable to this concept. Since the constraints associated with the heat pipe and the space radiator have been discussed previously (see Section 5.2.3), only the concepts associated with the heat shield mirror are considered below.

The operating photoheliograph will use a silver-coated aluminum mirror with a central hole to reflect most of the excess solar energy out of the system. Only that portion of the solar loading that is absorbed must be handled by the heat rejection system. The singular problem associated with this approach is the concentrated nature of the absorbed solar loading (the solar energy is concentrated over a disc less than 5.08 centimeters in diameter).

For this system we will use an aluminum simulated mirror and apply the required heat loading over the 5.08-centimeter diameter central region. The required thermal load will be applied with an electric heater bonded to the mirror surface. The advantage of this approach is that we can control the amount and location of input energy in a simple manner. No other method offers this advantage.

The heat shield heat rejection breadboard will be designed so that the heat pipe is operated horizontally with any required bends made in-plane. The heat sink will be a space radiator configured to distribute the input energy from the heat pipe. The radiator will have provisions for the input of external thermal loads simulating analytically predicted albedo and earthshine. The heat shield mirror will have an electric heater bonded to the surface to simulate the absorbed thermal loading and will be connected conductively to the heat pipe on the rear surface.

Test Procedure

The test procedure will be as follows

1. Install system in vacuum tank and check out equipment and instrumentation.
2. Monitor temperatures to ensure that system is isothermal.
3. Start cryogenic cooling and simulated solar loading of heat shield mirror. Apply only 1/4 power to the mirror heater and verify system operation.
4. Gradually increase heater power to 100 percent of design value while monitoring system temperature distributions. Space radiator heaters are set at the average orbital value.
5. Maintain the power setting until quasi-steady-state is reached and held for 4 hours. Continue data recording.
6. Perform transient run by adjusting radiator heaters to simulate normal orbital variation. Run for at least five orbits.
7. Return system to quasi-steady-state condition.
8. Increase heater power to 125 percent of design value and monitor system response. Maintain system at new steady-state value for at least 4 hours.
9. Repeat step 6 for the higher power condition.

Required test equipment includes the following

1. Mirror simulator
2. Mirror mount
3. Heat pipe
4. Heat sink (radiator)
5. Heater (source)
6. Temperature sensors
7. Temperature recorder

8. Vacuum facility
9. Power supply (for heater)
10. Liquid nitrogen shroud
11. Temperature controller for radiator.

Preliminary Cost Estimate

Hardware

Facility	Available
Facility modifications	$ 750
Test specimen	10,600
Instrumentation (includes 250-channel DAS)	42,900
	$54,250

Labor by Task

Analysis	200 hours
Design	200
Hardware specifications	40
Fabrication	100
Assembly and integration	240
Testing	400
Data reduction and report	240
	1,420 hours

5.2.5 Phase Change Material (Fig. 5-5)

The purpose of this breadboard is to demonstrate the performance of phase change materials as a means of maintaining the heat shield mirror at an acceptable temperature level during a balloon mission. This breadboard would also demonstrate that the secondary problems (configuration, low k of the phase change material, containment, and compatibility) have been solved.

The basic boundary conditions for this breadboard are the heat shield mirror heat input of 48 watts and the optical geometric constraints of the photoheliograph (i.e., obscuration, optical cone angle, heat shield/relay flat separation).

Concept Evaluation

The phase change material breadboard will consist of a simulated heat shield mirror and surrounding phase change material container in the form of an annular fin extending toward the primary mirror. There are no significant alternative concepts since the basic design variations are in the selection of the phase change material and the method of conductivity enhancement selected. The simulated heat shield mirror will be thermally loaded with a bonded electrical heater identical to that discussed previously for the heat rejection system breadboard.

The singular feature of the test hardware will be an attempt to design the phase change material container so that it may be easily disassembled and reworked internally.

Test Procedure

The following test procedure will be used.

1. Fill test specimen with required amount of phase change material.
2. Install system in test facility and complete test setup and preliminary checkout.

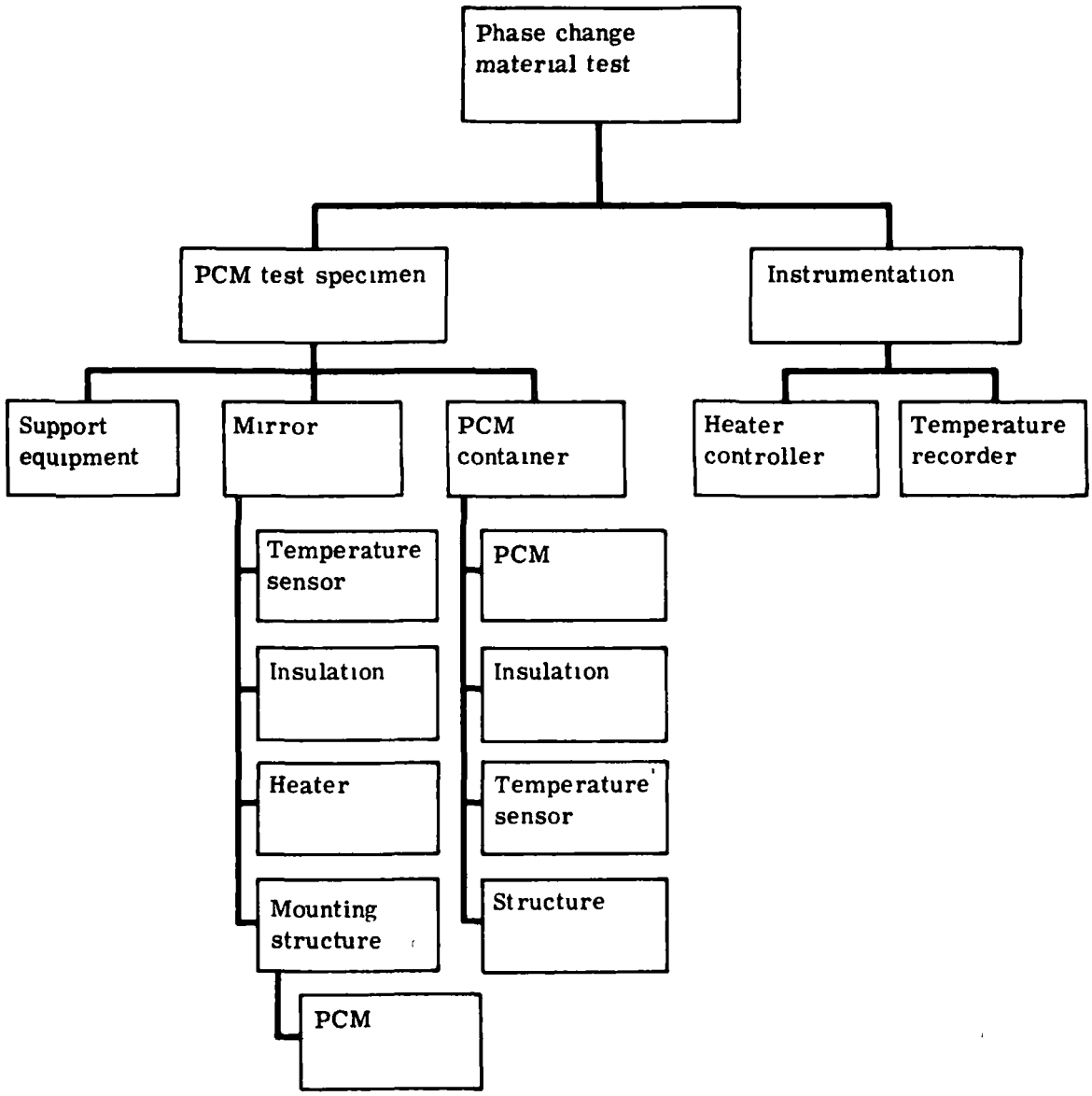

Fig. 5-5 — Phase change material breadboard test

3. Apply simulated solar loading to the heat shield mirror and monitor system temperatures to evaluate phase change material effectiveness as a function of time.
4. Continue test operations for at least 10 hours (estimated mission time).
5. Repeat steps 3 and 4 on successive days to demonstrate system repeatability and overall mission compatibility.
6. Repeat entire test program with alternative internal conductance mechanisms or phase change material.

Required test equipment is as follows:

1. Mirror simulator
2. Mirror mount
3. Phase change material container
4. Source heater
5. Temperature sensors
6. Temperature recorder
7. Heater power supply.

Preliminary Cost Estimate

Hardware

Facility	Available
Test specimen	$5,000
Instrumentation	2,900
	$7,900

Labor by Task

Analysis	100 hours
Design	80
Hardware specifications	40
Fabrication	80
Assembly	100
Testing	200
Data reduction and report	160
	760 hours

5.2.6 Thermal Pluming (Fig. 5-6)

The objective of the thermal pluming breadboard is to experimentally verify the existence of atmospheric turbulence effects and to quantify their relationship to balloon-borne photoheliograph performance. The effects of the aperture window will be of prime concern.

The boundary conditions required for the performance of this test are based on the temperatures of the aperture window, the shell, the earth shield, and the surrounding environment. The nominal operating level for the proposed balloon mission is approximately -56.5 °C.

Concept Evaluation

The goal of this breadboard program is the experimental determination of the onset of thermal pluming or other convective phenomena as a function of temperature gradients and window orientation. Conversely, we will also be determining the thermally stable operating region for the balloon mission.

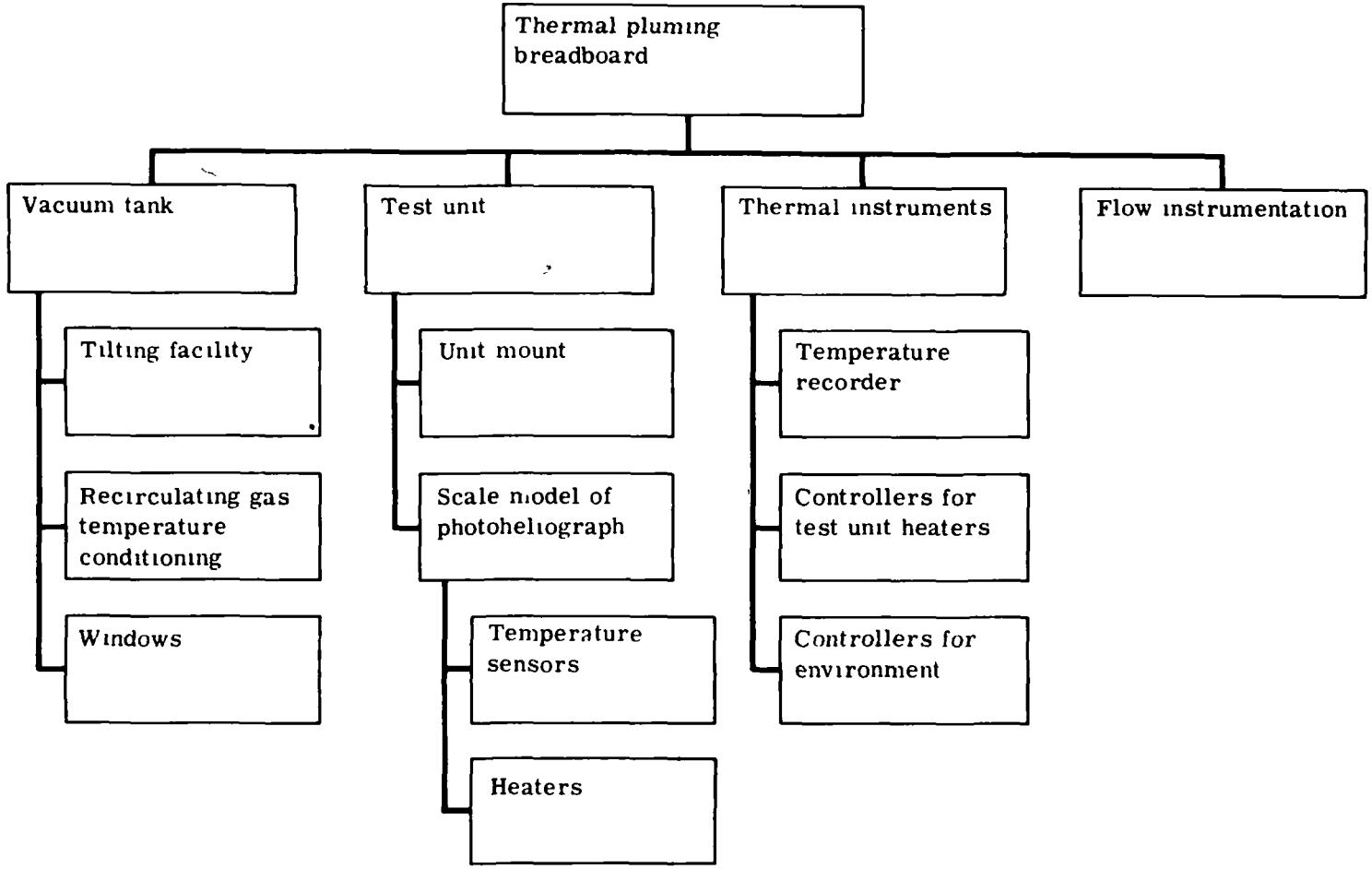

Fig. 5-6 — Thermal pluming breadboard test

Let us first consider the evaluation technique required. There are several methods of flow phenomena visualization available. However, since we are concerned with an optical wavefront, the simplest approach is to use interferometric techniques based on the aperture window. By establishing an unperturbed baseline, we can evaluate the degradation of the perturbed system as the thermal conditions are made more severe. The development of pluming can be detected as a complete breakup of the interferogram.

In order to evaluate the effects of orientation, we must rotate the window (mission simulation requires window orientations from vertical to within 20 degrees of horizontal). This may be done within a large chamber; however, relocation of the interferometer will also be required. A much simpler approach is to utilize a chamber that is itself rotatable and thus the interferometer/window relationship remains fixed. Also, this approach requires a much smaller facility since the photoheliograph does not rotate within the chamber.

Since the thermal pluming phenomenon is induced by temperature gradients and in particular is a function of the Grashof modulus, we must simulate the modulus value that determines the onset of pluming. The Grashof modulus is a function of temperature gradients, characteristic lengths, and coefficient of thermal expansion (bouyancy forces), and thus we have the possibility of scaling any or all of these parameters to yield a similar modulus value. Our approach is to reduce the characteristic length by making a half-scale model. This not only allows us more variability in the gradient and bouyancy terms but also reduces the system cost. Now, by variations of the system pressure within the chamber, we can vary the bouyancy force to maintain a constant window to ambient air temperature gradient of several degrees.

This concept eliminates the need for precise temperature and gradient control.

Test Procedure

The test procedure shown below will be used·

1. Install photoheliograph model in test chamber with window horizontal and check out all equipment.
2. Evacuate chamber to required low pressure.
3. Monitor ambient and test specimen temperatures to confirm isothermal condition.
4. Take baseline interferograms and confirm system operation performance.
5. Operate model heaters to establish a temperature gradient. Do not exceed critical Grashof modulus value.
6. Repeat interferogram data acquisition.
7. Increase temperature gradient with heaters to exceed initial Grashof modulus values.
8. Take interferogram and confirm thermal pluming.
9. Reduce chamber pressure in a number of steps to reduce Grashof modulus below critical value.
10. After each pressure reduction, determine thermal pluming characteristics by interferometric analysis.
11. Repeat steps 2 through 10 at a minimum of four window orientations, concluding with the window vertical.

The proposed test hardware required for the performance of this test program would include:

1. Vacuum tank
2. Small model of photoheliograph (1/2 scale)
3. Temperature sensors
4. Heaters
5. Temperature recorder
6. Power supply for heaters
7. Flow visualization equipment
8. Tank environmental control unit.

Preliminary Cost Estimate

Hardware

Facility	Available
Test specimen	$5,000
Instrumentation	1,000
	$6,000

Labor by task

Analysis	120 hours
Design	240
Hardware specifications	80
Fabrication	100
Assembly and integration	160
Testing	400
Data reduction and report	360
	1,460 hours

5.3 SUBSYSTEM TESTS

5.3.1 Instrument Structure Test (Fig. 5-7)

The objective of this test is to demonstrate that the instrument support structure truss will not degrade instrument performance due to internally or externally induced thermal motions.

The general boundary conditions for this structure are those calculated for the external meteoroid shell and the power dissipations of the various truss-mounted instruments.

Concept Evaluation

The purpose of this test is to determine thermally induced deflections of the instrument structure. The two driving forces for thermal loads are the external orbital environment and the internal power sources of the scientific instruments. Both of these driving forces will be examined during the course of this test program.

The testing concept is based on the performance of three types of thermal test, as follows:

1. Thermal soak
2. Orbital gradient
3. Operating heat load.

In order to perform these tests, an external shroud capable of variations in temperature will be required. This shroud would surround the individual instrument structure elements to

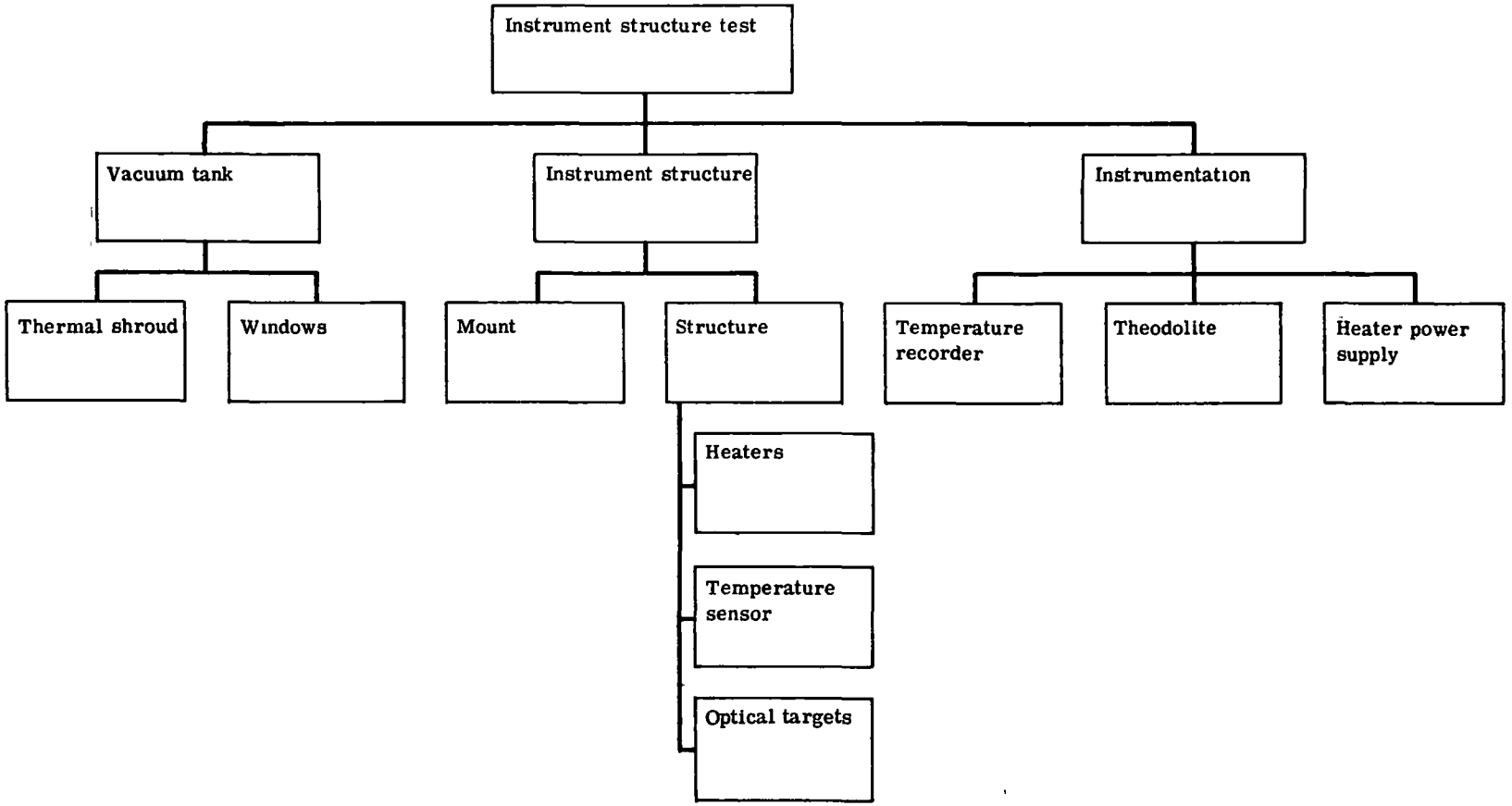

Fig. 5-7 — Instrument structure subsystem test

provide both the thermal soak environment and the orbital gradient environment. This can be accomplished by having a shroud with multizone electrical heaters bonded to its surface. Rather than utilizing a shroud that surrounds individual elements, we would provide a shroud that would enclose the entire structure. This approach is applicable directly to the performance of thermal soak tests. Its use for the performance of orbital gradient testing, however, is questionable due to the nature of the enclosure, which tends to provide an isothermal background even if the heat is applied nonuniformly.

In addition to the thermal shroud, spot heaters will be suitably mounted at the instrument attachment locations. These heaters will be sized to simulate the instrument heat loads into the structure. Since these heaters can be independently controlled, we can simulate operating sequences as required.

The remaining constraint that requires definition is the method of determining thermal deflections. The proposed method is optical measurement of target motion. It is proposed that suitable optical targets be mounted on the instrument structure at significant locations. The baseline locations will be determined and target motion during test will be optically monitored by a theodolite mounted external to the vacuum tank. The transient motion measurement may present some problem. However, suitable tracking of the target is possible.

Other techniques such as the use of displacement transducers imply internal mounting at or immediately adjacent to the instrument structure. Since the mount will experience comparable thermal loading for the soak and gradient cases, it does not appear likely that we will be able to differentiate between structure and mount motions.

Thus, the optical measurement technique discussed previously is recommended.

Test Procedure

The test procedure will be as outlined below:

1. Set up test specimen in vacuum tank, perform ambient equipment checkout, and establish vacuum.
2. Monitor temperatures and verify that structure is isothermal. Using optical targets, establish baseline position of structure.
3. Increase shroud temperature to 26.7 °C and establish new steady-state temperature of structure. Perform optical measurements to determine structural position changes.
4. Repeat step 3 in 5.5 °C increments to 48.8 °C
5. Adjust shroud element temperatures to duplicate orbital gradient and monitor structure temperature distribution.
6. When structure assumes calculated orbital gradient values, perform optical measurements to determine position changes.
7. Perform orbital transient test by varying shroud temperatures to simulate orbital temperature cycle. Repeat for five cycles.
8. During the last two orbital cycles, make optical measurements every 15 minutes to determine structure response characteristics.
9. Reestablish 21.1 °C isothermal condition of structure. Repeat optical baseline measurement.
10. Operate instrument simulation heaters, monitor structural temperatures, and perform simultaneous optical measurements.

The required test equipment will consist of the following:

1. Vacuum tank
2. Instrument truss
3. Temperature sensors
4. Temperature recorder
5. Heaters
6. Power supply
7. Thermal shroud
8. Optical targets
9. Theodolite(s).

Preliminary Cost Estimate

Hardware

Vacuum tank	Available
Vacuum tank modifications	$ 2,500
Test specimen	4,000
Thermal shroud	10,000
Instrumentation (does not include DAS)	12,500
	$29,000

Labor by Task

Analysis	120 hours
Design	240
Hardware specifications	20
Fabrication	60
Assembly and integration	100
Testing	1,000
Data reduction and report	320
	1,860 hours

5.3.2 Primary Mirror Heat Rejection System

The objective of this test is to verify the performance of the primary mirror heat rejection system prior to final assembly of the flight system.

The boundary conditions are identical with the prior breadboard unit, as is the required test equipment (see Section 5.2.3). The exception to the above will be a special mount required for simulation of the flight configuration design.

The approach selected for this system test program is identical with that used previously in the breadboard program. The prior concept evaluation and selection criteria apply as does the testing program, which is intended to not only demonstrate design performance but also over-design capability.

Preliminary Cost Estimate

Hardware

Facility	Available
Facility modifications	Available

Test specimen	$5,000
Instrumentation*	4,000
	$9,000

Labor by Task

Analysis	40 hours
Design	120
Hardware specifications	20
Fabrication	100
Assembly and integration	320
Testing	1,000
Data reduction and report	240
	1,840 hours

5.3.3 Heat Shield Mirror Heat Rejection System

The purpose of this subsystem test is to confirm the performance of the heat rejection system associated with the heat shield mirror.

The boundary conditions of this system are identical with the breadboard unit previously described (see Section 5.2.4).

Concept Evaluation

The fundamental problem associated with the performance of a thermal test of the heat shield system in the final configuration is the application of the appropriate thermal load over the small area as discussed previously. Since the heat shield mirror will be polished and silvered at this time, direct heat application is not feasible. The approach to be used will be based on a focused or spot infrared lamp device capable of inputing sufficient energy to simulate an equivalent solar loading.

All other aspects of the test unit will be identical to that of the original breadboard test unit.

Test Procedure

The unit test procedure will be identical with that for the breadboard unit.

The required test equipment for this test includes

1. Heat shield mirror
2. Heat shield mirror mount
3. Heat pipe
4. Space radiator
5. Solar heat simulator
6. Temperature sensors
7. Temperature recorder
8. Vacuum facility with liquid nitrogen shroud
9. Temperature controller for radiator
10. Heaters for radiator
11. Reflective heat sink.

---

*Assumes that test hardware is supplied and the DAS is available.

Preliminary Cost Estimate

Hardware

Facility	Available
Facility modifications	$2,500
Test specimen	2,000
Instrumentation*	2,900
	$7,400

Labor by Task

Analysis	100 hours
Design	120
Hardware specifications	20
Fabrication	80
Assembly and integration	160
Testing	1,000
Data reduction and report	240
	1,720 hours

5.4 SYSTEM THERMAL TEST

The purpose of this test (see Fig. 5-8) is to verify that the entire thermal control system of the flight model photoheliograph performs as designed.

The expected boundary conditions of this test include direct solar loading of the main optical elements and earthshine and albedo thermal loads to the exterior walls of the photoheliograph in a typical orbital attitude.

Since we are now considering a test of the entire thermal control system of the photoheliograph, it is clear that the only method possible for the generation of system thermal loads is through solar simulation in a cryogenic space chamber. Full system test capability will also require simulation of albedo and earthshine. This may be accomplished by the use of contact heaters or an array of infrared lamps surrounding the photoheliograph. By proper sequencing and power level, the normal orbital flux variations may be simulated. The test setup is shown in Fig. 5-9.

The required test equipment will include:

1. Vacuum chamber having liquid nitrogen shrouded walls and solar simulation
2. Flight model photoheliograph
3. Flight instrumentation readout (thermal only)
4. Temperature sensors and recorders
5. Contact heaters to simulate albedo and earthshine thermal loads.

Preliminary Cost Estimate

The complex nature of this test results in only an ROM estimate for the entire program. It is assumed that a suitable facility having the required solar simulation capability and a flight model photoheliograph are available at no cost.

Hardware	$50,000
Labor	7,640 hours

*Assumes that test hardware and DAS are available.

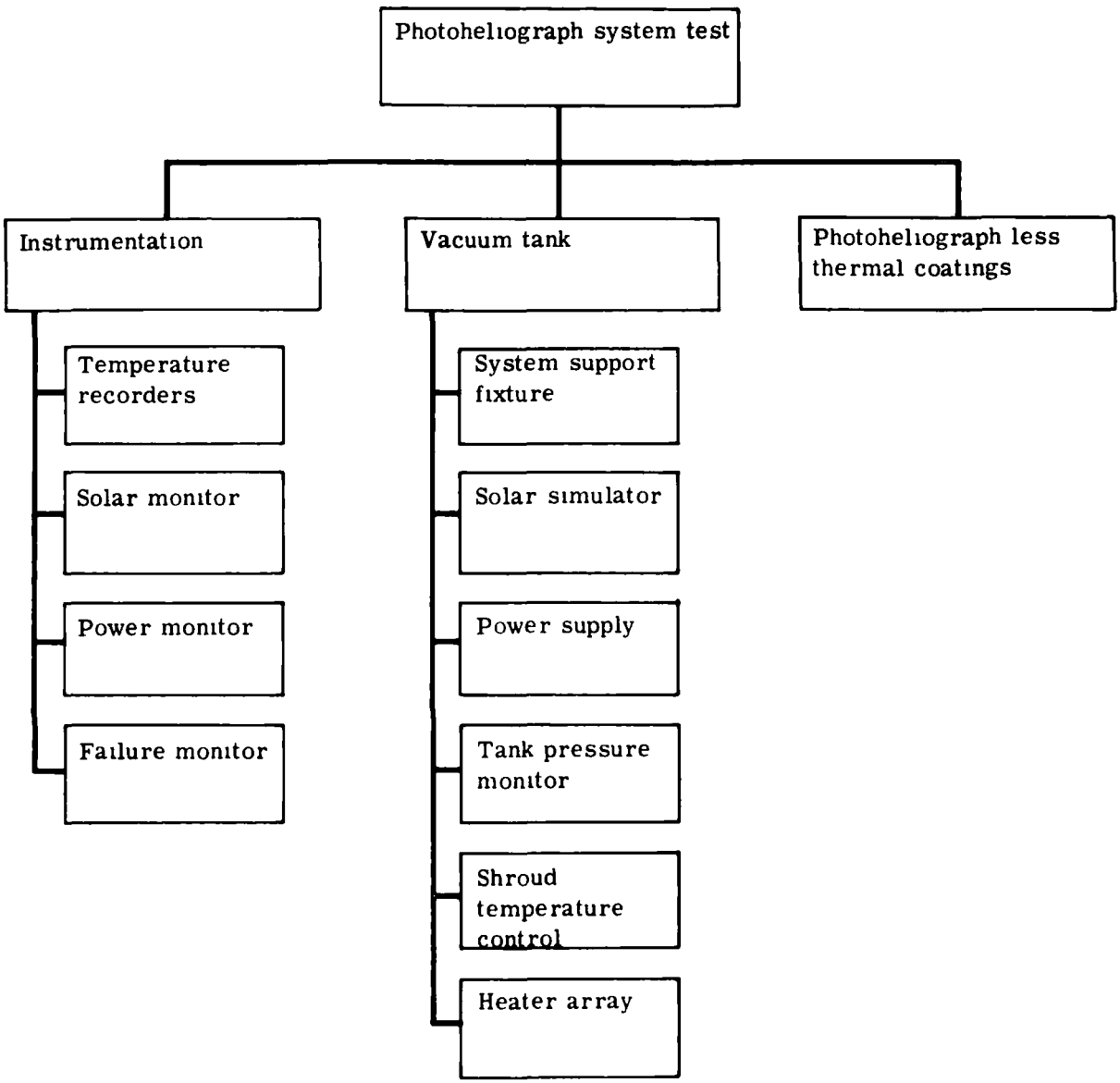

Fig. 5-8 — Photoheliograph system thermal test

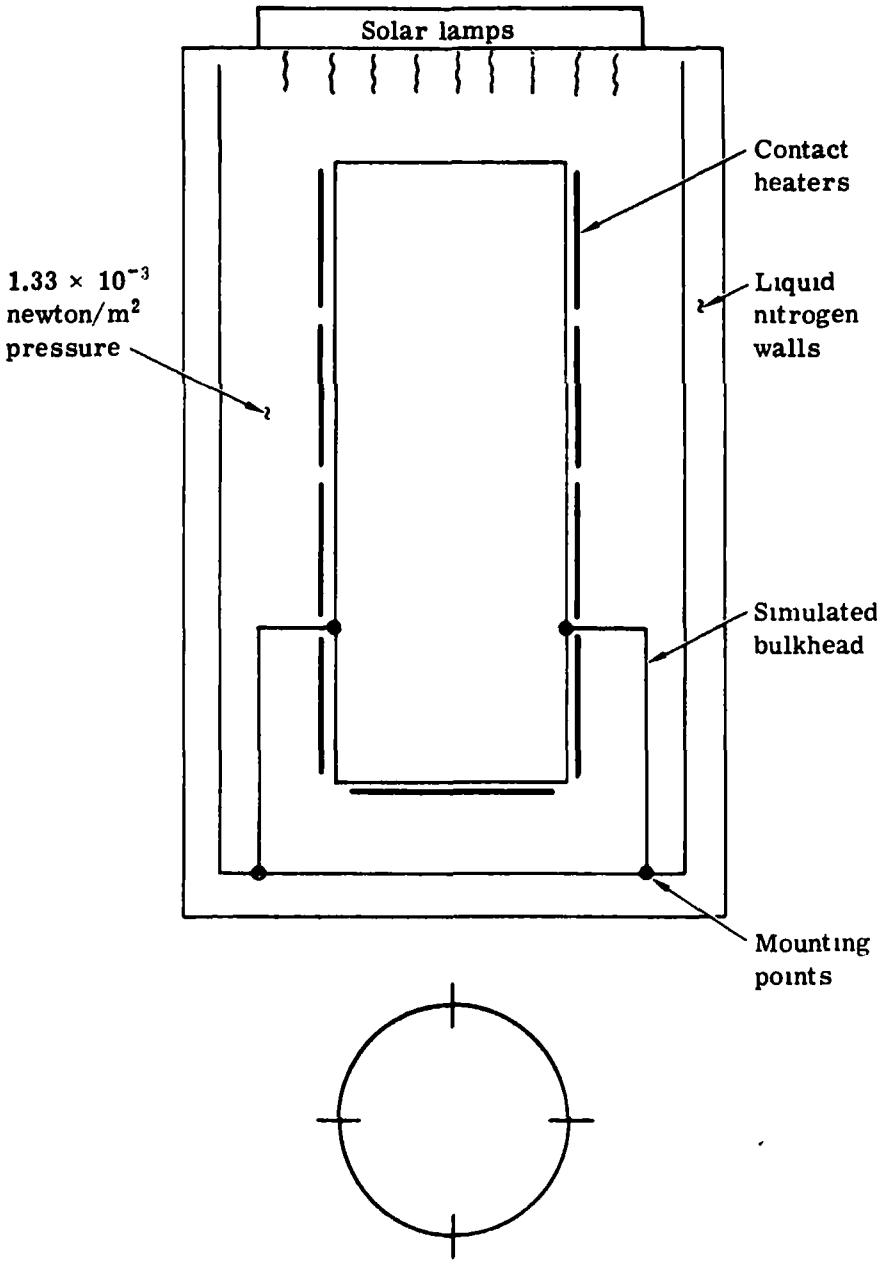

Fig. 5-9 — Photoheliograph system thermal test setup

6. SUGGESTED ADDITIONAL EFFORT

The end result of the Photoheliograph Thermal Concepts Study is the development of baseline thermal control concepts for each of the three photoheliograph designs that account for the unique mission characteristics of each design. In the course of this study program, we identified certain areas worthy of future study. These studies, which are discussed below, will serve to supplement the effort initiated herein. The acquisition of additional experimental data will help to further the goal of design definition.

6.1 100-CENTIMETER BALLOON PROGRAM ANALYSIS

Our efforts in the balloon-borne photoheliograph study have resulted in the definition of a baseline concept. Within this baseline concept, certain areas have been identified as warranting further analytical studies.

6.1.1 Heat Shield Mirror (Balloon Program)

The analysis of heat shield mirrors, cooled or controlled by phase change material, requires the development of methods for improving the poor conductivity of the phase change material in order to effectively utilize the minimum mass of materials. A number of potential methods (aluminum honeycomb, wire mesh, metallic inserts) for improving conductivity are available, and these alternatives should be investigated in sufficient depth to select the best design concept. The analysis should evaluate the proposed methods, develop a system tradeoff matrix, and produce a detailed design of the heat shield mirror thermal control system. We will utilize our past experience in the design of a heat sink system for the Apollo Lunar Camera Program.

6.1.2 Window (Balloon Program)

Preliminary analysis of the aperture window indicates that thermal gradients may present a problem during observation. Additional analysis of the transient behavior of the window, with and without the use of active thermal control, is required to establish the performance of this component.

6.2 BREADBOARD TESTING

The acquisition of experimental data from key breadboard tests will result in the confirmation of our analytical efforts in a direct fashion. Those breadboard tests that are key efforts, significantly affecting the overall photoheliograph design, are enumerated below.

6.2.1 Specular Core Primary Mirror (LSO Program)

The confirmation of the thermal performance of a specular core mirror is a key effort in the design of the photoheliograph, since the primary mirror design affects the system in so many ways. Experimental verification of our analytical predictions of heat transfer and thermal gradients is required prior to the commencement of the final design.

6.2.2 Primary Mirror Thermal Design (All Programs)

Just as the specular core breadboard will confirm the analytic prediction of mirror core heat transfer, the primary mirror thermal design breadboard will confirm the optical performance of the primary mirror under anticipated thermal loads. We have developed a test program that accomplishes this objective in a straightforward manner utilizing existing facilities and equipment to the maximum possible extent (see Fig. 6-1).

6.2.3 Thermal Pluming (Balloon Program)

While thermal pluming or other natural convection phenomena may be predicted analytically for a number of simple geometries, demonstration of the onset of this condition for a complex geometric shape such as the photoheliograph must be confirmed by experimental methods. The thermal pluming test program, which utilizes an existing facility (Fig. 6-2) capable of deploying a scaled photoheliograph in any orientation, is designed to provide such data by means of window interferograms. The establishment of system limits that influence thermal pluming at the photoheliograph aperture is a key element in the design of the 100-centimeter balloon-borne photoheliograph.

6.2.4 Phase Change Material (Balloon Program)

Breadboard confirmation of the predicted phase change material control concept for the heat shield mirror is required prior to the final design of the 100-centimeter balloon-borne photoheliograph. This breadboard effort will be based on the analytical effort discussed in Section 6.1.1 as well as past experience in breadboarding a phase change heat sink designed for the Apollo Lunar Camera.

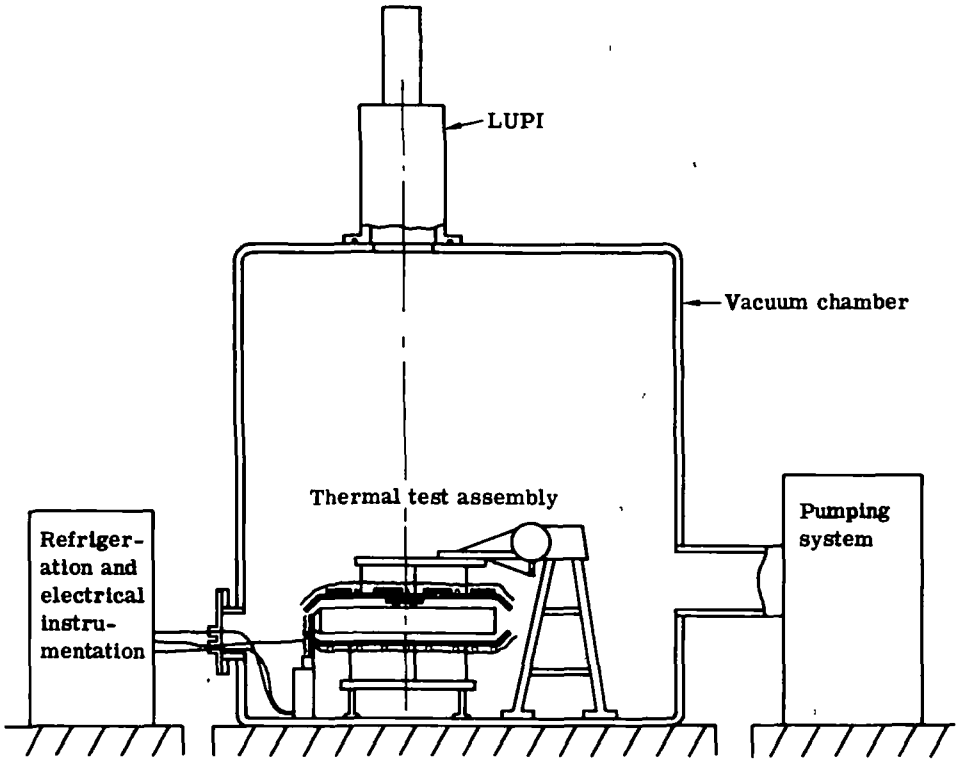

(a) Overall setup

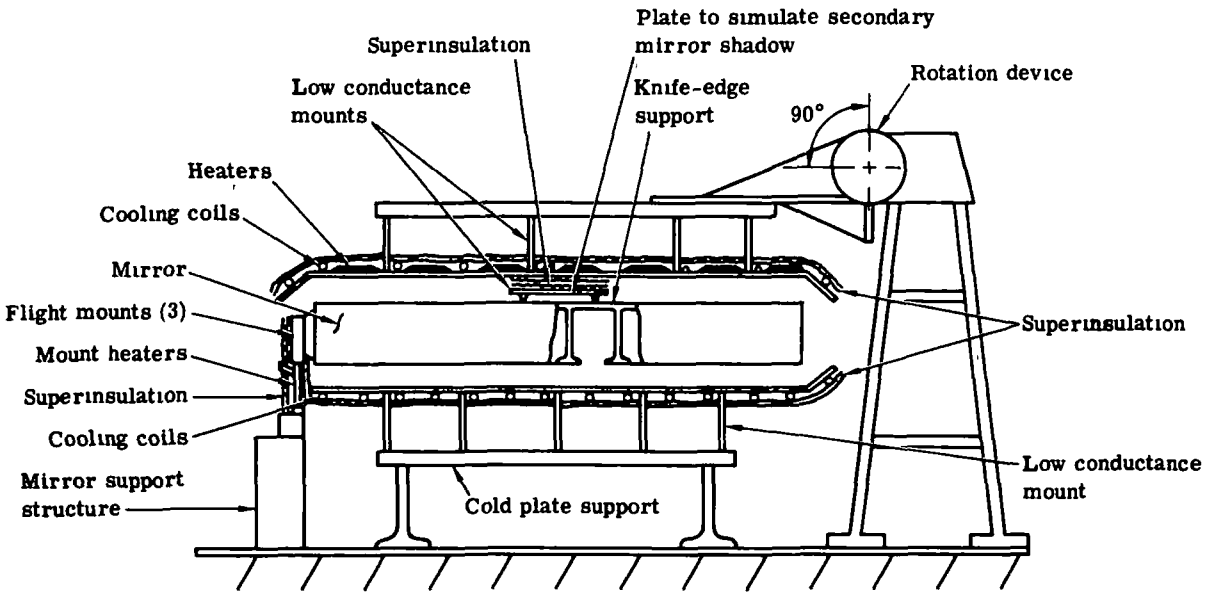

(b) Thermal test assembly

Fig. 6-1 — Thermal test system

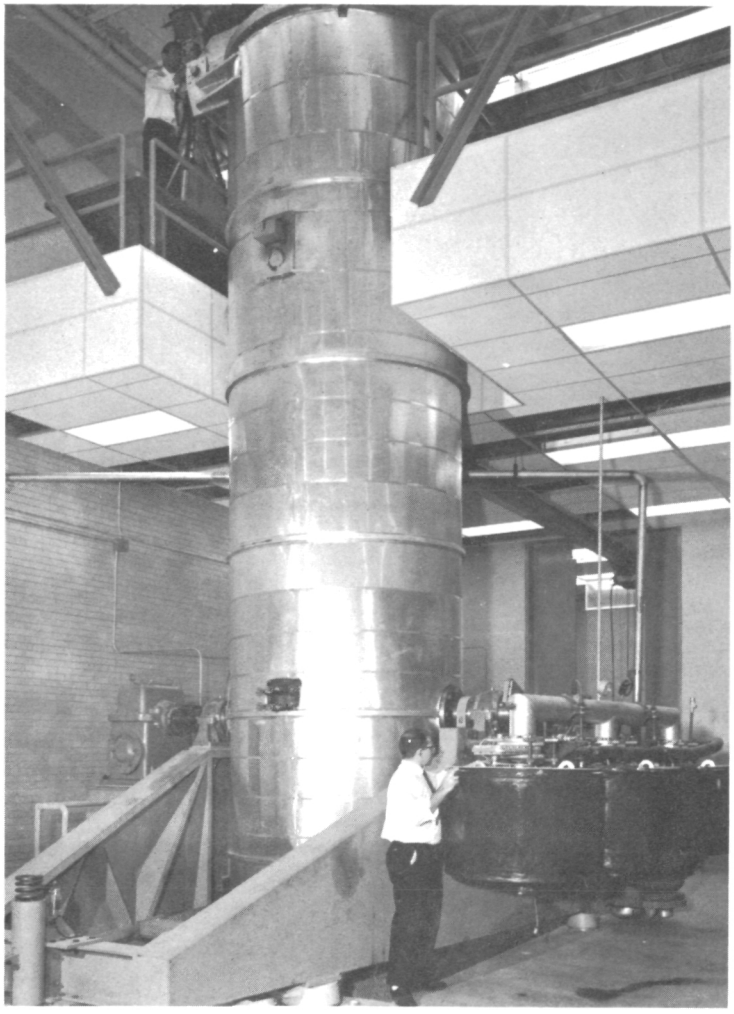

Fig. 6-2 — Thermal pluming test facility